USING CHROMATOGRAPHIC AND MASS SPECTROMETRY TOOLS TO PROBE ALBUMIN AND ITS CARGOS: IN SEARCH OF UNDERSTANDING TYPE II DIABETES

by

Jared Newell Bowden

A dissertation submitted in partial fulfillment
of the requirements for the degree

of

Doctor of Philosophy

in

Biochemistry

MONTANA STATE UNIVERSITY
Bozeman, Montana

April, 2011

APPROVAL

of a dissertation submitted by

Jared Newell Bowden

This dissertation has been read by each member of the dissertation committee and has been found to be satisfactory regarding content, English usage, format, citation, bibliographic style, and consistency and is ready for submission to The Graduate School.

Dr. Edward A. Dratz

Approved for the Department of Chemistry & Biochemistry

Dr. David J. Singel

Approved for The Graduate School

Dr. Carl A. Fox

STATEMENT OF PERMISSION TO USE

In presenting this dissertation in partial fulfillment of the requirements for a doctoral degree at Montana State University, I agree that the Library shall make it available to borrowers under rules of the Library. I further agree that copying of this dissertation is allowable only for scholarly purposes, consistent with "fair use" as prescribed in the U.S. Copyright Law. Requests for extensive copying or reproduction of this dissertation should be referred to ProQuest Information and Learning, 300 North Zeeb Road, Ann Arbor, Michigan 48106, to whom I have granted "the exclusive right to reproduce and distribute my dissertation in and from microform along with the non-exclusive right to reproduce and distribute my abstract in any format in whole or in part."

Jared Newell Bowden

April, 2011

DEDICATION

To my wife, Lorae Bowden, who has encouraged and supported me, as I have pursued my dreams.

To my children, Sarah, Miriam, Rachel, Daniel, Eve, Ruth, and Rebekah, who have given me reason to reach higher, stretch further, and attain more than I thought possible.

TABLE OF CONTENTS

LIST OF TABLES

Table Page

LIST OF FIGURES

Figure Page

LIST OF FIGURES-CONTINUED

Figure Page

LIST OF FIGURES-CONTINUED

Figure Page

LIST OF FIGURES-CONTINUED

Figure Page

LIST OF FIGURES-CONTINUED

Figure Page

LIST OF FIGURES-CONTINUED

Figure Page

LIST OF FIGURES-CONTINUED

Figure Page

GLOSSARY

ACN	Acetonitrile
ACOD	Acetyl CoA oxidase
ACS	Acetyl CoA synthetase
ANS	1-anilinononaphthalene-8-sulfonic acid
Apo-A1	Apolipoprotein A1
ATP	Adenosine triphosphate
BCA	Bicinchoninic acid
BCAA	Branched chain amino acids
BHT	Butylated hydroxytoluene
BLAST	Basic local alignment search tool
BMI	Body mass index
BSA	Bovine serum albumin
C14:0	Myristic Acid
CD	Compact disc
CFHR-5	Complement factor H-related protein-5
CoA	Coenzyme A
CRISP-3	Cysteine-rich secreted protein-3
DCM	Dichloromethane
DIA	Diisopropylamine
DMF	Dimethyl formide

GLOSSARY-CONTINUED

DSC	Differential scanning calorimetry
DTT	dithiothreitol
EDTA	Ethylenediaminetetraacetic acid
EI	Electron ionization
ESI	Electrospray ionization
FA	Formic acid
FPLC	Fast protein liquid chromatography
FRET	Fluorescence resonance energy transfer
FTICR	Fourier transform ion cyclotron resonance
FXR	Farnesoid X receptor
GC	Gas Chromatography
GCMS	Gas Chromatography mass spectrometry
GLP	Glucagon-like peptide
GPCho	Glycerol phosphocholine
H2O2	Hydrogen peroxide
HBA1c	Glycoslylated hemoglobin
HC	Healthy controls
HDL	High density lipoproteins
HPLC	High pressure liquid chromatography
Hpt	Haptoglobin

GLOSSARY-CONTINUED

HRG	Histidine-rich glycoprotein
HSA	Human serum albumin
IAA	Iodoacetimide
ICAT	Isotope-coded affinity tagging
ICP-MS	Inductively coupled plasma mass spectrometer
IRB	Institutional review board
It	Fluorescence intensity
kD	Dissociation constant
kDA	Kilodalton
LD	Lyme disease
LDL	Low density lipoproteins
LMW	Low molecular weight
m/z	Mass to charge
MALDI	Matrix assisted laser desorption ionization
MEHA	3-methyl-n-ethyl- (β-hydroxyethyl)-analine
MeOH	Methanol
MPP	Mass profiler professional
MS	Mass Spectrometry
MWCO	Molecular weight cut off
N	Theoretical plates

GLOSSARY-CONTINUED

n	Peak capacity
N/A	Not available
NCBI	National center for biotechnology information
NCI	Negative ionization
NEFA	Non-esterified free fatty acids
NHS	N-hydroxysuccinimide
NIH	National institute of health
PBS	Phosphate buffered saline
PC	Phosphatidylcholine
PE	Phosphatidylethanol amine
PFB	Pentafluorobenzyl
POD	Presence of peroxide
PWHM	Peak width at half maxium
QTOF	Quadrupole time of flight
RA	Rheumatoid arthritis
RP	Reverse Phase
Rt	Retention time
SAA1	Serum amyloid A (1 pre-protein) isoform
SCX	Strong cation exchange
SEC	Size exclusion chromatography

GLOSSARY-CONTINUED

SLE	Systemic lupus erythematosus
STD	Standard deviation
t1	First eluted peak
T2D	Type II diabetes
TCA	Trichloroacetic acid
TCEP	Tris (2-carboxyethyl) phosphine
TFA	Trifluoroacetic acid
tn	Last retained peak
VDR	Vitamin D receptor
ZAG	Zinc-α-glycoprotein
τ	Fluorescence lifetime

ABSTRACT

We measured molecules carried as cargos on the abundant blood protein human serum albumin (*1*) in patients with newly diagnosed, untreated type II diabetes (T2D) compared to healthy controls (HC). The HSA cargos measured included lipids, minerals, peptides, and metabolites. Differences in these cargos associated with T2D were measured, using chromatography and mass spectrometry, seeking to identify biological markers that may enhance early diagnosis of T2D. An extrinsic fluorescent probe of binding sites on HSA, ANS, revealed that there were distinct differences in loading of hydrophobic cargo between HC and systemic lupus erythematosus, T2D, and Lyme disease plasma samples. A decrease in mineral levels on HSA was also measured in T2D plasma compared to healthy control plasma, using ICP-MS. Zinc ions showed the largest changes and were reduced three fold in T2D. The hydrophobic cargo of HSA revealed a decrease in HSA-associated fatty acids in T2D, measured by GCMS using negative chemical ionization. In this same GCMS study new classes of glycine-containing compounds bound to HSA were found to be increased by two fold in T2D in the hydrophobic extract of HSA. A metabolomic study using RP-uHPLC QTOF MS in both positive and negative ionization modes examined differences in the hydrophobic extract of whole plasma in T2D compared to healthy controls. Increased levels of branched chain amino acids were found in T2D compared to HC. Decreased levels of phosphatidylcholines, phosphatidylethanol amines, and vitamin D3 metabolites were found in T2D compared to HC. The results suggests that the HSA cargo in T2D, SLE, and other disease states, may provide new diagnostic markers and lead to deeper understanding of the mechanisms of disease in humans.

PREFACE

When I was a boy, I was curious as young boys often are. I found that one of the best ways to find out how something worked was by taking it apart and examining its components. This curiosity led me dismantle my portable battery-powered electronic basketball game, when it began to malfunction, to examine what component had worn out, what needed to be fixed, and how it truly worked. Though I was able to reassemble the device, I was not able to correct the damaged circuit board. At the time, I had not yet learned the tools of the trade. For example, it would have helped enormously to have a knowledge of electronics, a schematic of the circuit board, a meter to measure resistance and current, and a good soldering tool. Learning by exploration about the parts of a system can be more then common curiosity. Investigating the parts of a system has the potential to focus the mind into reasoning about the purpose of each component of a system, and to seek to learn the workings of the whole. Understanding the function and purpose of each part can assist in repairing things that do not work properly, as well as prevent damage.

My young son had an elementary school teacher who understood this very concept. She provided a curiosity box for her class that contained discarded and broken electronic equipment. I watched my son's understanding of the world around him increase, as he dismantled flashlights, computer compact disk (CD) drives, and many other devices.

Similarly, my own quest for understanding how things work and why they break has led me to follow evidence that the behavior of human serum albumin, as a carrier protein, plays an important role in Type II Diabetes (T2D). Therefore I have studied HSA by isolating, dismantling, and probing its cargo contents and their roles in T2D. This disease is growing to epidemic proportions, and has already affected my friends and family. Due to the growing prevalence of T2D, it will likely affect many more of those around me in the future. I will describe the findings of my research and how I have dismantled this abundant blood protein and probed its cargos in hopes of developing a deeper understanding of the growing epidemic of T2D and perhaps how to better reduce the prevalence of T2D.

INTRODUCTION

Type II Diabetes

Experts forecast doom and gloom, predicting that 1 in 3 born after the year 2000 in the US will eventually exhibit symptoms of Type II Diabetes (T2D) (*2*). As of 2010, this epidemic of T2D affects 9.4% of the US population (*2, 3*). Some contend that 5% of the current population are still undiagnosed, because the tests currently employed are expensive and can be unreliable (*2, 4*). Medical practitioners are widely requesting improved methods of diagnosis that are more convenient and reliable (*4-6*). A poor understanding of the cause and biological mechanisms of T2D has led to difficulties in developing more effective early diagnostic tests for T2D, and designing effective strategies to prevent the development of T2D.

Medical practitioners have been aware of this disease since physician Hesy-Ra first described the symptoms in 1552 B.C (*7*). It wasn't until 1869, however, that Paul Laugerhans, a German medical student, was successful in linking diabetes to the malfunctioning pancreas islets (*7*). Then in 1921 Fredrick Banting made the key discovery of insulin in the pancreas islets (*7*). Differentiation of two major types of diabetes, type I (insulin-dependent) and type II (non-insulin dependent), was established in 1959 (*7*). Type I Diabetes is much less common then T2D (*8*), and Type I is thought to be due to an auto immune mechanism (*8*). The root cause of the increasingly common T2D, and how to best prevent it, is still unknown. Why has the understanding of T2D

and developing effective prevention strategies taken so long? What is it about T2D that eludes us?

The number of newly diagnosed cases of diabetes has accelerated in the last decade, and T2D accounts for 90 – 95% of all cases of diabetes (*9*). In 1997 there were 0.813 million new cases in the US (*9*). In 2007 there were 1.605 million new cases in the US (*9*). The new cases in that decade increased the total number of diagnosed cases in the US from 9.4 million to 17.4 million (*9*). The disease is not limited to industrialized nations. In 2006 there were 171 million suffering from T2D in the world, and this number is expected to double by the year 2030 (*10*). It is estimated that there were 5.7 million undiagnosed cases of diabetes and 41 million individuals considered pre-diabetic in the US in 2007 (*9*).

Some factors which contribute to the increasing incidence of diabetes, include longer life expectancy than previous decades and increased sugar intake by the population. Sugar consumption has increased from an average of 37 lbs annually per person in 1900 to 151 lbs annually in 2000 (*11, 12*). Fructose consumption is correlated with increased fatty liver (*13*), which is very strongly correlated with insulin resistance (*14*). If more effective methods of early detection and the accuracy of detection of risk could be improved, it might motivate people to avoid the onset of disease by adopting dietary changes to alleviate the debilitating effects of T2D. More specific biomarkers of insulin resistance and T2D might also provide insight into molecular mechanisms, and thereby guide recommendations for more affective diet and lifestyle changes, as well as the design of new drugs that could reverse T2D.

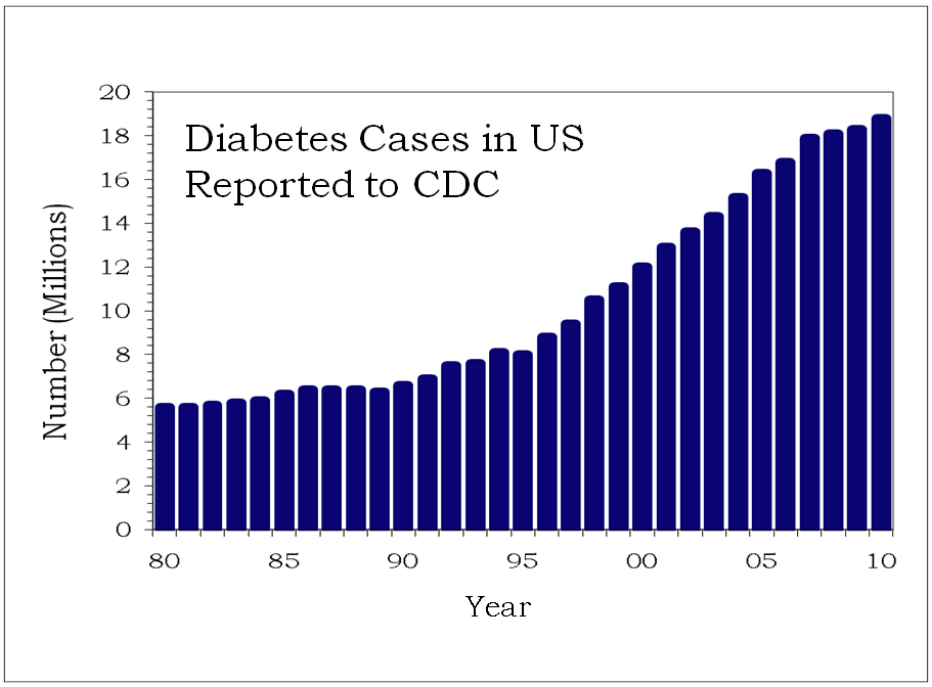

Figure 1.1: Diabetes cases in the US reported by the CDC 1980 – 2010 (*3*).

Many associate T2D with obesity. However, this correlation does not always hold true. In 2009, 34% of the US population was obese, but only 19% of these obese people were diagnosed with T2D (8% of population). On the flip side, 17.3% of those diagnosed with T2D were found to be at their ideal body mass index (weight). Most type II diabetics are merely overweight, as is 68% of the US population (*9*). It may shock many that well known people of normal weight like Halle Berry, Albert Eistein, and Thomas Edison were diagnosed with T2D (*15*). However, this does not remove the fact that 83% of those with T2D are overweight or obese (*9*). Thus there is some correlation between diabetes and weight that seems strong, but correlation does not prove causation.

Type II diabetics who undergo gastric bypass surgery experience major improvements in blood glucose and insulin thus alleviating T2D symptoms levels before there is any significant weight loss (*16, 17*). There is an increase in insulin sensitivity and hormonal responses as well as a decrease in inflammatory markers within a few days after gastric bypass surgery (*16, 17*). Gastric bypass surgery not only resolves T2D directly it also reduces chances of death caused by T2D by 90%. Gastric bypass surgery is, however, an extreme procedure, and is not offered to type II diabetics unless they are morbidly obese (*16, 17*). Improved nutrition and exercise are believed to provide keys to unlocking the metabolic imbalance that causes T2D (*18*).

T2D does run in families (*19, 20*). In fact, currently the highest risk factor for developing T2D is that one or both parents had T2D (*19, 20*). If one parent had T2D there is a 40% risk, while if both parents had T2D there is a 70% risk (*20*). However, surveying the entire human genome for specific genes that would indicate a strong propensity for T2D, only a few genes have been identified, as are listed in table 1.1 (*20*). Unfortunately, all of these genes combined explain only an extremely tiny fraction of those with T2D (0.3%) (*20*). Many with these genetic risk factors easily beat the disease with lifestyle changes, and the tendency of T2D in families appears to result from learned diet and lifestyle factors (*18, 19*).

Table 1.1: Genes associated with T2D: PPARG, peroxisome proliferator-activated receptor gamma; CALN10, calpain 10; KCNJ11, potassium inwardly rectifying channel, subfamily J, member 11; TCF7L2, transcription factor 7-like 2; CDKAL1, CdK5 regulatory subunit associated protein 1-like 1; CDKN2A/B, cyclin-dependent kinase inhibitor 2A/B; HHEX, haematopoietically expressed homeobox; IDE, insulin-degrading enzyme, SLC3OA8, solute carrier family 30 member 8; IFF2BP2, insulin-like growth factor, 2 mRNA binding protein 2; FTO, fat mass and obesity associated; MC4R, melanocortin 4 receptor; NOTCH2, Notch homolog 2 Drosophila; ADAMTS9, ADAM metallopeptidase with thormbospondin type 1 motif, 9; THADA, thryroid adenoma associated; TSPAN8, tetra spanin 8; LGR5, leucine-rich repeat-containing G protein coupled receptor 5; CDC123, cell division cycle 123 homolog; CAMK1D, calcium/calmodulin-dependent protein kinase ID; JAZF1, juxtaposed with another zinc finger gene 1; KCNQ1, potassium voltage-gated channel, KQT-like subfamily, member 1 (*20*); TRPM6 and TRPM7, transient receptor potential membrane melastatin (*21*); ADCY5, adenylate cyclase 5 (*22*); MADD, mitogen-activated protein kinase activating death domain (*22*); ADRA2Aα 2A, adrenergic receptor (*22*); FADS1, encodes fatty acid desaturase 1 (*22*) ; BMAL1, brain and muscle aryl hydrocarbon receptor nuclear translocator-like (*23*);

Date	Gene suggested	Disease mechanism
2000	PPARG	Insulin sensitivity
2003	CAPN10	Glucose transport
2003	KCNJ11	Beta-cell dysfunction
2006	TCF7L2	Beta-cell dysfunction
2007	CDKAL1	Beta-cell dysfunction
2007	CDKN2A/2B	Beta-cell dysfunction
2007	HHEX/IDE	Beta-cell dysfunction
2007	SLC30A8	Beta-cell dysfunction
2007	IGF2BP2	Beta-cell dysfunction
2007	WFS1	Unknown
2007	TCFS	Unknown
2007	FTO	Obesity
2008	MC4R	Obesity
2008	NOTCH2	Unknown
2008	ADAMTS9	Unknown
2008	THADA	Unknown
2008	TSPAN8/LGR5	Unknown
2008	CDC123/CAMK1D	Unknown
2008	JAZF1	Unknown
2008	KCNQ1	Beta-cell dysfunction
2009	TRPM6/TRPM7	Ion channel receptor
2010	ADCY5	Insulin secretion
2010	MADD	Insulin secretion
2010	ADRA2A	Glucose homeostasis
2010	CRY2	Fasting Glucose Regulation
2010	FADS1	Effects triglyceride levels
2011	BMAL1	Temporal Core Clock

Physicians use values of blood glucose levels ≥126 mg/dL after an 8 hour fast, measured on at least two separate occasions, to suggest a tentative diagnosis of T2D (*3*), whereas, healthy blood glucose levels are classified as < 110 mg/dL (*10*). T2D is characterized most reliably by a reduced recovery rate of the glucose level, and an elevated blood glucose level after a large oral glucose challenge (*3, 10*). In 2009, a high level of glycoslylated hemoglobin (HbA1c) in the blood (*24, 25*), has been added to the list of diagnostic biomarkers for T2D (*26*). Testing HbA1c levels is not in widespread use worldwide, due to the difficulty in performing this test, and the relatively small differences in between healthy and T2D levels (*26, 27*). HbA1c levels <5.9% (38 mM) are considered healthy while ≥6.5% (48 mM) are considered T2D (*26*). The gold standard glucose tolerance assays are inconvenient, time consuming, and have not proven effective for screening (*5, 6, 28*).

While the accepted tests are expensive, another reason many type 2 diabetics aren't diagnosed is that they simply are not aware of symptoms that alert them to the probability of T2D (*4*). Early symptoms of T2D include thirst, frequent urination, and fatigue (*29*). Other factors that increase the risk of T2D, include high levels of low density lipoproteins (LDL)(*30*), low levels of high density lipoproteins (HDL)(*30*), and a high body mass index (BMI), but none of these are diagnostic (*31*). When T2D is suspected, doctors will call for a diagnostic test (*29*). The patient must return twice to be screened for fasting glucose, which of course requires the patient to fast for 12 hours before the appointment (*4, 24, 25*). During the second visit the patient also takes a

glucose tolerance test; which requires the patient to drink a large amount of a glucose and be tested for blood glucose at a precise time (2 hours) thereafter (*3, 4, 26*).

Individuals with T2D have developed resistance to the effects of insulin. Advanced insulin resistance leads to chronic high blood glucose levels, which damage both small and large blood vessels and lead to many negative health consequences (*32*). Cells in the body use glucose to provide energy for maintenance, movement, growth, and repair, but excessively high glucose levels are toxic to a multitude of cells (*32-34*). The hormone insulin regulates the level of glucose after a meal (*35, 36*), and the hormone glucagon regulates glucose under fasting conditions, although many factors are involved (*34, 37*).

The abnormally high levels of glucose that characterize advanced T2D eventually can lead to blindness, kidney disease, amputation of limbs, increased risk of stroke, and heart disease if glucose is not controlled (*35*). Expensive kidney dialysis methods and novel drugs have been created to combat the complications and symptoms of T2D, but once the disease has progressed to require dialysis, the prognosis is poor (*38*). When left untreated, the effects of T2D lead to irreversible damage of many tissues, and a reduced life expectancy. T2D increases the probability of chronic heart disease by a factor of 2-3 fold and the overall risk of an early death is increased 2-4 fold (*39*). With an ever-increasing number of T2D cases each year and an estimated 25% – 50% of cases left undiagnosed, there is a clear need to find more facile and effective methods of early detection (*2, 7*).

T2D costs are escalating rapidly because of the increasing incidence rate and lack of effective preventative strategies. Estimated T2D costs in the US alone in 2007 were $174 billion (*9*). The costs associated with screening large groups for the risk of T2D will likely become lower if more specific biomarkers and detection methods can be developed. If early methods of detection become more reliable, and steps to prevention hopefully become more effective, the overall costs and suffering from the disease would also decrease markedly.

Several biomarkers which have been associated with T2D are high blood glucose levels, high C-peptide, high fasting insulin (*30*), high HbA1c (*24, 25*), and an increase in plasma non-esterified free fatty acids (NEFA) (*40*). Since fasting insulin is very expensive to measure only fasting blood glucose and HbA1c (*25, 27, 41*) are considered to be specific enough to be diagnostic for T2D; however these measures are not predictive enough to use effectively as early diagnostics for T2D. With awareness of the large number of individuals currently afflicted, and forecasted increases of T2D, it becomes clear that an early diagnostic to assist in disease prevention, as well as possible insights into mechanisms illuminate more effective preventative strategies and to enhance the search for more effective drug targets, is warranted.

Research done in our lab by Dr. Scott Laffoon, has indicated that the levels of several plasma proteins are altered in newly diagnosed T2D, including zinc-α-glycoprotein (chain B) isoform (ZAG), serum amyloid A (1 pre-protein) isoform (SAA1), histidine-rich glycoprotein (HRG) precursor, cysteine-rich secreted protein-3 (CRISP-3), haptoglobin (Hpt), apolipoprotein A-1 (Apo-A1), and complement factor H-related

protein-5 (CFHR-5) (*42*). These candidate biomarkers still need to be validated by measurements in a larger cohort of patient samples, but the findings suggest several new potential biomarkers. This research was performed using 2D-Gels to measure relative amounts of blood plasma proteins from newly diagnosed T2D patients and HC. Laffoon removed the most abundant plasma proteins, including HSA, by immuno affinity before proteomic analysis. The removal of the abundant proteins allowed him to more clearly see changes in the less abundant plasma proteins. Strikingly, Laffoon observed that six out of the seven candidate biomarkers are known to bind to human serum albumin, even though the albumin was removed prior to analysis (*42*). The implications of these findings are that the binding properties of HSA are substantially changed in T2D. This linkage has led us to investigate the cargo contents of HSA that may affect the binding properties of this abundant plasma protein.

Serum Albumin

HSA is the second most abundant blood protein, behind hemoglobin (*43*). HSA is found in blood plasma at between 30-50 mg/mL, making it the most abundant plasma protein (*43, 44*). Prior studies of HSA and its ability to bind cargos molecules has demonstrated connections between structural changes and variations in carrying capacity of HSA (*45*). These structural and carrying capacity alterations depend on which specific cargos are bound to HSA (*45, 46*). A brief background on HSA will explain further why this protein has been selected for study and how it may relate to biomarker discovery for T2D.

Albumin was one of the very first proteins in the body to be studied. The Greek physician Hippocrates of Cos recorded that foamy urine (presumably from high albumin) indicated chronic kidney disease (*43*). Gürber first attempted crude fractionation of albumin in 1894, using horse plasma. He brought an aqueous blood solution to pH 4.9 the isoelectric point of albumin, and was able to crystallize albumin. This crystalline albumin was not pure, as it co-crystallized with several other proteins and compounds (*43*). Techniques of ultracentrifugation, developed in the 1930's, and electrophoresis, allowed a molecular weight to be determined and a purified product to be produced on a small scale. During World War II, a search for a suitable substitute for blood plasma led E.J. Cohn and colleagues at Harvard University to developed a cold alcohol fractionation procedure that produced purified albumin from plasma (*47*).

Early on, while seeking to provide large amounts of albumin for war victims, bovine serum albumin (BSA) was substituted for HSA, because it was easier to obtain large volumes of bovine serum (*43*). Several volunteers died from intravenous BSA injections before the understanding of species specific proprieties of albumin were understood (*43*). Due to the purification technique developed by E.J. Cohn's group, and readily available quantities of BSA, this protein became widely available to researchers.

Both HSA and BSA differ little in overall sequence and functionality. HSA consists of a single polypeptide chain with 585 amino acid residues, and a unmodified molecular weight of 66,438.41 Da (*43*). HSA contains 17 disulfide bridges and one free cysteine (*43, 48*). Both HSA and BSA possess three hydrophobic binding domains (I, II, III) (*43, 48*). Each of these domains has two sub-domains (A, B) (*43, 48*). These

hydrophobic domains allow for the binding and transport of a large variety of lipids, drugs, metabolites, minerals, bile salts, and peptides (*43, 44, 49-53*). Many proteins are also known to associate in vivo with albumin, as mentioned earlier (*42, 54*). Each of the cargos listed has been demonstrated (in vitro) to be an effector of the binding of other albumin cargos (*49-52*). A crucial role of albumin is thought to be transporting of these various hydrophobic cargos in the bloodstream to their targets, in addition to contributing to maintaining the pH and osmotic pressure of plasma (*43, 55*).

Albumin is also of interest because of its ability to bind and transport drugs. HSA binds many drugs, and each bound drug affects the binding of the other. For example, the cargo of HSA can affect the delivery, circulating lifespan, and toxicity of drugs (*56*). Conversely, drug binding can affect the cargo and carrier function of HSA (*57-59*). Domain I of HSA is sometimes referred to as the warfarin site, and domain II of HSA is referred to as the benzodiazepine site (*56*). Because of the complicated binding site interactions, investigation of drug toxicity performed on healthy humans may not reflect the effects of the drugs on diseased patients (*58, 60*). HSA has the ability to sequester drugs so that they can get past the kidneys, which filter out small molecules in the blood every 20 minutes, therefore allowing drugs to have a longer lifespan and perhaps be more effective overall. HSA has a half-life of 19 days in blood, which in turn translates to an increased lifespan of cargos, that are tightly bound to it (*61*). Researchers also need to understand binding effects on HSA so they can minimize toxic drugs from binding to HSA, allowing the toxic drug to be filtered out of the body (*61*). It has been recognized

that many diseases including diabetes, may cause alterations to the albumin cargo, increasing or reducing a drug's effectiveness (*58, 62-64*)

The crystal structure of albumin was first solved by McClure, et al in 1974 (*15*), and higher resolution structures have been obtained more recently (*48, 65-67*). Figure 1.2 shows the three binding domains of HSA containing six sub-domains (*67*). Seven co-crystallized myristic acids (C14:0) are indicated by the numbers 1-7 and the primary mineral binding site, which is located near the C-terminus is also marked (*67*).

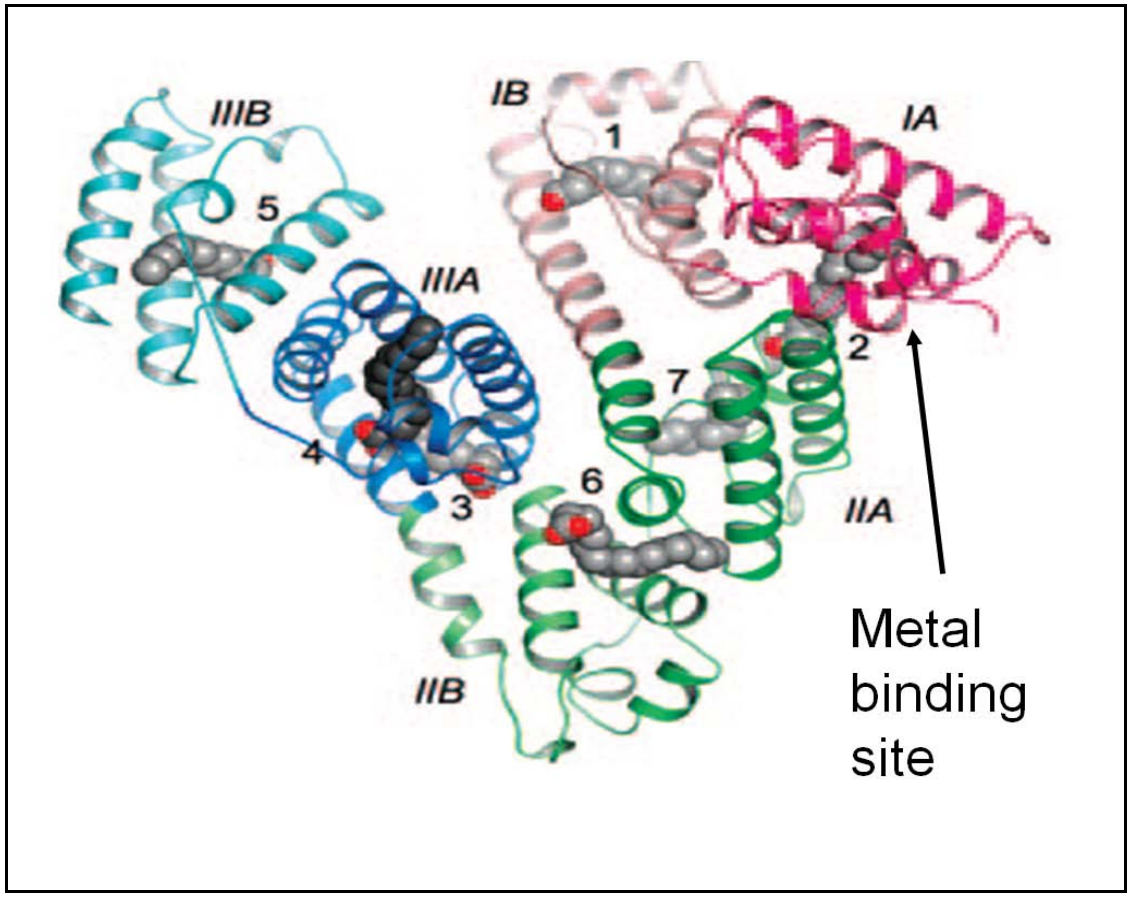

Figure 1.2: X-Ray Crystal structure of HSA (*67*). HSA consists of three binding domains (I, II, II), and each domain is divided into two sub-domains (A, B) (*48*). The numbers 1-7 indicate identified fatty acid binding sites and the metal binding site near the C-terminus is also indicated (*48*).

It has long been known that plasma NEFA are transported on HSA, which carries >99 % of the NEFA in plasma (*68*). HSA has been demonstrated to be capable of loading up to seven NEFA (*69*). In vivo this ratio is observed to be on the order of 0.1 – 2 NEFA per HSA during normal conditions; however when fasting fatty acids are mobilized by glucagon signaling to hormone sensitive lipids in the adipose, and this ratio FA/HSA can increase to 6:1 (*69, 70*). Binding of NEFA also protects polyunsaturated NEFA from oxidation by transporting them inside the hydrophobic binding pockets on albumin (*71*).

Studies on albumin binding have been carried out using fluorescence spectroscopy (*9, 56*). HSA has a single tryptophan at amino acid position 214, while BSA has two tryptophans located at 134 and 212 (*9*). As fluorescent hydrophobic compounds, such as 1-anilinonaphthalene-8-sulfonic acid (ANS), are bound on albumin, and tryptophan is excited fluorescence resonance energy transfer (FRET) occurs from tryptophan to ANS, and tryptophan's fluorescence is quenched (*9, 72, 73*). FRET is the process of transferring electronic excitation energy from one excited molecule to another nearby fluorescent molecule where there is overlap between the emission spectrum of the donor and the excitation spectrum of the acceptor (*72*). Chemical denaturation of HSA, as observed by tryptophan fluorescence, is a two step process, whereas in thermal denaturation, a single step denaturation is observed (*74*). The hydrophobic binding domains I and II are known to unfold in both modes of denaturation (*74*). However, for a complete unraveling of the entire protein, reduction of the 17 disulfide bonds is required (*75*).

Albumin has been implicated as a biomarker in several diseases (*43, 76, 77*). Many diseases are observed to be associated with a decrease in albumin, including viral hepatitis, and rheumatoid arthritis (*43*). Most of the diseases where albumin levels are effected were due to a malfunction in the liver, which is where albumin is produced (*43*). However, the number of diseases in which albumin's relative abundance has been altered is so common, that it is not considered to be valuable as diagnostic biomarker for any specific disease (*43, 76*).

It is known that as T2D progresses, albumin and many proteins < 78kDa are observed to increase in the urine due to breakdown of kidney filtration (*43*). As kidney function decreases in advanced T2D, there is a build-up of many metabolites in the blood, that in turn affects liver function (*43*). Many of these metabolites bind to albumin, which alters the normal binding properties of HSA (*43*).

Hypothesis and Dissertation Research

The possibility of early detection of T2D would be greatly enhanced by identifying more specific biomarkers. Additional biomarkers of insulin resistance and T2D might also provide insight into molecular mechanisms of the disease, thereby guiding improved prevention steps, and may also aid in the design of new drugs that could reverse insulin resistance.

My hypothesis is that the cargo content of HSA is an excellent area for discovery of biomarkers for insulin resistance and T2D. My research work focused on the

investigation of alterations in the cargos of HSA including fatty acids, peptides, minerals, and metabolites in T2D, compared to healthy controls (*44, 49-53, 78*) .

THERMAL DENATURATION OF HSA

Introduction

Jonathan Chaires's group in Louisville, Kentucky reported a striking finding that albumin in human plasma was greatly stabilized against thermal denaturation in patients with three different inflammatory diseases (*78*). This was shown by simple differential scanning calorimetry (*79*) experiments on whole plasma, and by DSC experiments on the albumin fraction (*78*). An explanation offered for the thermal stabilization of the plasma in inflammatory diseases was that increased amounts of small molecules, such as peptides or lipids were bound in the hydrophobic pockets of HSA (*78, 79*). Addition of a small molecule, bromocresol green (BCG), that is known to bind in the hydrophobic binding pocket of HSA, was successful in mimicking thermal stabilization of HSA demonstrated by DSC (*78*). Some of the DSC data reported by Garbett, et al from Chaires group is shown in figure 2.1. The pink trace is a plot of thermograms from the plasma of healthy controls (HC). The blue traces are thermograms of plasma from three specific diseases: systemic lupus erythematosus (SLE) [Figure 2.1 (A)], Lyme disease (LD) [Figure 2.1 (B)], and rheumatoid arthritis (RA) [Figure 2.1 (C)].

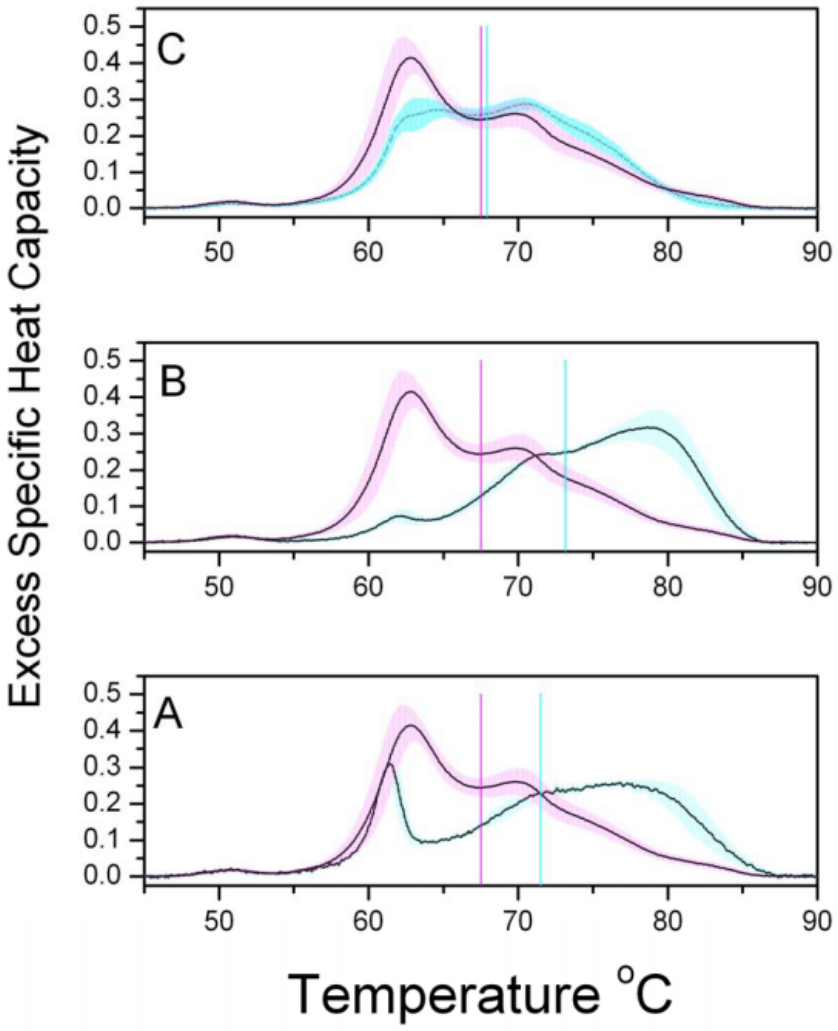

Figure 2.1: Thermograms of plasma from diseased (blue) compared to the plasma of healthy controls (pink). The average thermogram is shown as a solid line, and the shading indicates the standard deviations between multiple samples. (A) Plasma samples from two individuals with lupus were analyzed in duplicate DSC scans and the results averaged. (B) Plasma samples from four individuals with Lyme disease were analyzed in duplicate DSC scans and the results averaged. (C) Plasma samples from five individuals with rheumatoid arthritis were analyzed in duplicate DSC scans and the results averaged (*78*).

One of the most striking features of this data was that all of the diseases showed a marked increase in the temperature where a major portion of the mass of the plasma proteins underwent thermal denaturation. As a protein is exposed to increasing temperature, it reaches a point in which the favorable Van der Waals and hydrophobic interactions began to break apart and the protein unfolds. The midpoint in the thermal denaturation curve is termed the melting point of the protein (*80*). At the temperatures where the DSC plots show an increase in the excess specific heat capacity (Cal/C°·g), an increased amount of energy is taken up by the protein, and the apex of the excess specific heat capacity corresponds to the melting point of the protein.

Garbett, et al proposed that the cause of the increased thermal stability of the plasma in the diseases was due to changes in the cargo bound to HSA (*78*). To test this possibility, they bound the BCG dye to HSA. Binding of this small molecule has long been used as a method of quantification to determine the amount of HSA in whole plasma (*81*). BCG has been reported to bind to site I in HSA (*43*). Binding BCG to albumin was observed to have a stabilizing effect on the whole plasma thermal DSC thermogram of normal controls, and this stabilizing effect was similar to that found in the diseased samples without BCG (*78*). The effect of increasing amounts of BCG in the thermograms of whole plasma and on the thermograms of pure HSA can be observed in figure 2.2. It appears that the major effect on the thermograms of whole plasma is accounted for by the stabilization of HSA.

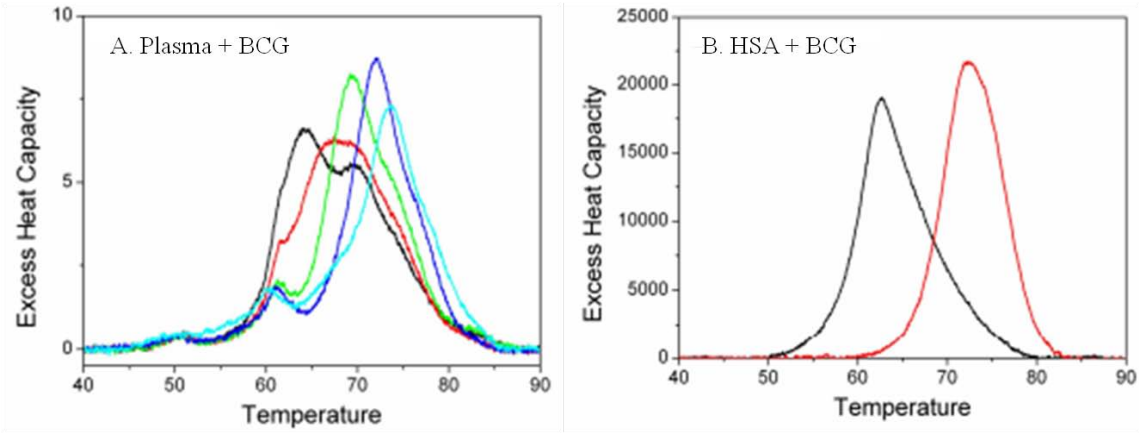

Figure 2.2: Effect of bromoscresol green (BCG) on the thermal denaturation of plasma, as measured by DSC. (A) Normal plasma (black) was compared to normal plasma plus BCG final concentrations of 30uM (red), 148 uM (green), 290 uM (blue), and 686 uM (cyan). (B) BCG was added to pure HSA (black) to a final concentration of 459 uM (red).

Since T2D has been correlated with increased inflammation (*82*), we considered that plasma samples from newly diagnosed T2D, which we had obtained for a proteomics project might exhibit similar thermal stability behavior. We hypothesized that thermal stabilization of HSA in human plasma might be occurring in T2D, and initiated an investigation into the albumin cargo of T2D. In particular, we hypothesized that changes in the level of NEFA may have impact on the thermal stability of plasma protein in inflammatory diseases, and that thermal stabilization could be caused by a higher degree of NEFA bound to albumin in T2D or in other inflammatory diseases, greater than 99% of NEFA in plasma are bound to HSA (*68*). Stabilization of HSA against thermal denaturation by bound lipids has been shown previously (*83-85*).

Shortly after we began our study, additional evidence related to possible changes to HSA in T2D plasma was developed by Scott Laffoon, a colleague in the Dratz lab at

Montana State University (MSU). Laffoon was seeking differences in protein levels in T2D using 2 dimensional gel electrophoresis (2D gels) (*42*). In Laffoon's study, the first step was to remove the fourteen most abundant proteins in plasma, using an immuno-affinity column (MARS14) provided by Agilent (Santa Clara, CA) (*42, 86*). Laffoon was successful in discovering seven distinct proteins and several protein isoforms that fulfilled criteria to be considered as candidate biomarkers for T2D (*42*). Five of the proteins that Laffoon found correlated with T2D were proteins known to bind to HSA in plasma (*42*), however, he had removed the HSA and its bound components at the outset of his study. Thus, changes in the cargo contents within HSA in T2D may change the conformation of HSA, leading to changes in the binding of the five proteins typically associated with HSA.

We hypothesized that an investigation of the cargo of HSA in T2D would provide insights into both Laffoon's and Garbett's findings (*42, 78*). The cargos we considered to be most promising to investigate were peptides (*51, 53*), lipids (*49, 80*), and minerals (*80*). Proteins (*80*), drugs (*51*), and other metabolites (*51*) are also known to associate with HSA, however, in the scope of our investigation, the first three classes of compounds were potentially of the most interest to us, since the proteins had already been investigated by Laffoon (*42*), and we did not have adequate tools at the time to measure the drugs and all the metabolites.

Investigations of Thermal Stability

Our initial work investigated the thermal stability of human plasma by attempting to repeat the findings of Garbett's work on LD and SLE plasma samples (*78*), and we expanded the study to include T2D samples. As we did not possess a differential scanning calorimeter (*79*), we contacted the vendor of DSC MicroCal (Piscataway, NJ) that Garbett, et al had used in their studies (*78*). Microcal was willing to run several test samples to demonstrate the abilities of their instruments.

Samples for our pilot T2D study were purchased from Bioreclamation Inc. (Westbury, New York), who provided a set of five healthy samples and five T2D plasma samples since we did not possess large enough sample volumes of the T2D plasma from NIH for DSC. We also obtained samples of SLE and LD from SeraCare Diagnostics (West Bridgewater, MA), the same source of the samples used by Garbett, et al (*78*). It was advantageous that two of the SLE samples we obtained were from the same lot as was used by Garbett, et al (*78*). A description of these samples, including biometric data that was available, is provided in table 2.1 (A and B).

Table 2.1: (A) Methods used to determine the diagnosis of the patients provided by the commercial lupus and Lyme plasma samples. (B) Biometric data for the commercial T2D and HC plasma samples. Any data not available is listed as N/A. All samples also tested negative for infectious diseases. Samples were provided as blood plasma with ethylenediaminetetraacetic acid (EDTA) anticoagulant as had been used by Garbett, et al (*78*). All sampling was done in accordance with principals of the Declaration of Helsinki and in accordance to Title 45, US Code of Federal Regulations, Part 46, and Protection of Human Subjects, revised November 13, 2001. The patients had signed a form of informed consent that their blood would be used for research purposes.

A

Sample	Disease	Method	Vendor
BM142160	SLE	Immuno-Lex SLE	SeraCare
BM142168	SLE	Immuno-Lex SLE	SeraCare
BM140028	Lyme	Diamedix EIA	SeraCare
BM140031	Lyme	Diamedix EIA	SeraCare
BM146606	Lyme	Mardx EIA	SeraCare
BM217753	Lyme IgM	Wampole EIA	SeraCare
BM217754	Lyme IgM	Wampole EIA	SeraCare

B

Sample	Disease	Age	Gender	Drugs	Vendor
BRH177108	T2D	51	F	Glucophage, Synthroid, Cytomel, Lipitor, Aldactazide	Bioreclamation
BRH177109	T2D	58	F	Glucophage, Zocor, Cytomel	Bioreclamation
BRH177110	T2D	46	F	Metformin, Detrol, Synthroid, Humatrope	Bioreclamation
BRH177111	T2D	57	F	Glucophage	Bioreclamation
BRH177112	T2D	49	M	Glumetza, Lipitor	Bioreclamation
BRH177916	HC	49	F	N/A	Bioreclamation
BRH177917	HC	61	F	N/A	Bioreclamation
BRH177918	HC	38	M	N/A	Bioreclamation
BRH177919	HC	47	M	N/A	Bioreclamation
BRH177920	HC	29	M	N/A	Bioreclamation

As a pilot study on this investigation, three samples were sent to MicroCal: healthy plasma, SLE, and T2D, as three samples are all that they agreed to run. Samples were prepared according to the methodology described by Garbett, et al (*78*). Samples were thawed on ice, and a 150uL aliquot was removed and placed into a 3500 dalton molecular weight cut off dialysis slide analyzer (Pierce, Rockford, IL). The dialysis slide was submerged in 75mL (500 fold excess) of a cold 4º C solution sodium citrate

phosphate buffered saline (PBS) (10mM K2HPO4, 150 mM NaCl, 0.38% (w/v) NaCitrate, pH 7.5). The outer solution was kept stirring at 4º C for the duration of dialysis. The dialysis buffer was exchanged at 3 hours, 7 hours, and 11 hours. Dialysis was completed at 24 hours and samples were removed. Samples were placed into microfuge tubes sealed with parafilm and shipped along with NaCitrate PBS buffer for a blank. Results obtained by MicroCal are shown in figure 2.3.

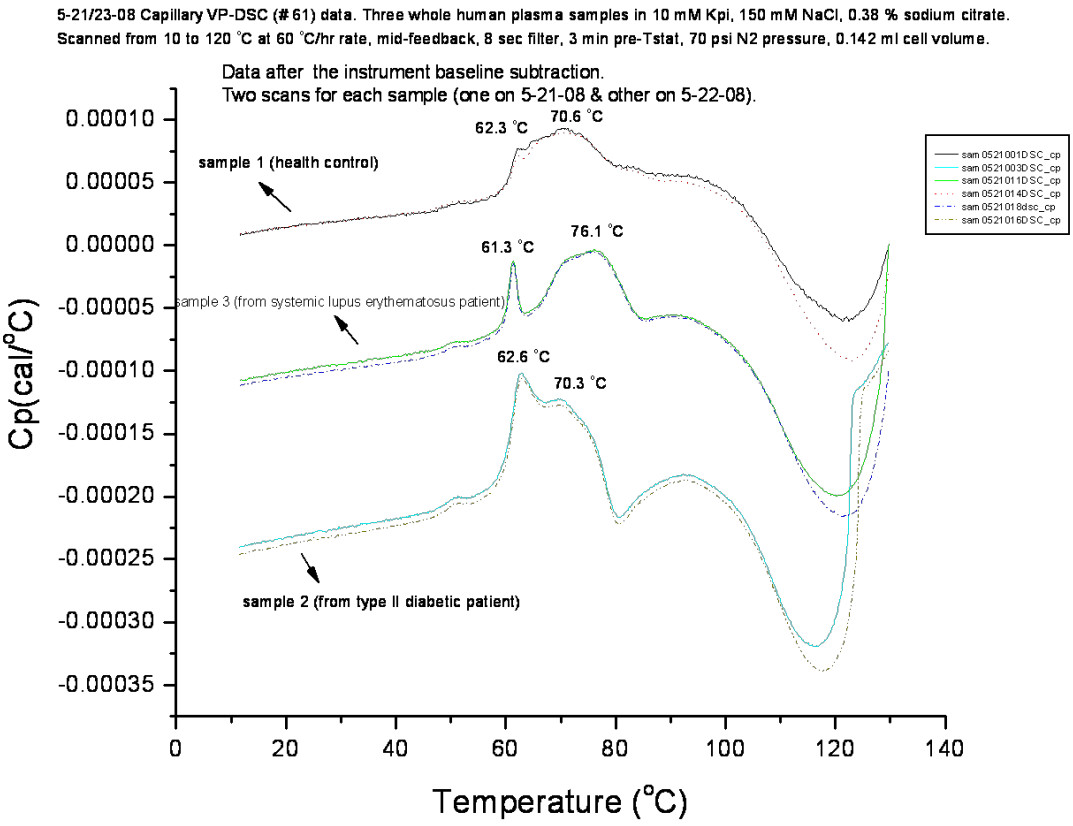

Figure 2.3: Differential scanning calorimetry on sample of HC (BRH177919), lupus (BM142168), and T2D (BRH177112) whole plasma by MicroCal. Each sample was measured twice as shown by the solid and dased line.

Both MicroCal and Garbett, used scan rates of 1º C/min and the instrumentation and methodology were identical. The SLE DSC profile appeared to match the published results of Garbett, et al (*78*). However, the DSC profile of our healthy plasma did not match the Garbett, et al (*78*) healthy plasma data. Additionally, our T2D plasma DSC matched the healthy plasma sample DSC from Garbett, et al (*78*) fairly closely. This raised some concern as to the sample handling. Were the samples received properly marked from Bioreclamation, or did we or MicroCal, mix up the samples prior to analysis? We were able to get MicroCal to repeat the study with the same results on freshly prepared aliquots of the same T2D and HC samples, so we were satisfied that MicroCal did not mix up the samples.

It has been noted that the samples provided from Bioreclamation may not have been drawn or handled in the same fashion as the samples from SeraCare. Additionally, each of the T2D samples we received from Bioreclamation were on medications for T2D and for high cholesterol. Drugs given to the patient used in our study, such as Lipitor, which binds to albumin (and has antioxidant effects) (*87*), and Glumetza, which changes the susceptibility of the free thiol on albumin to be oxidized (*88*), may lead to distinctly different plasma behavior then what would be observed in newly diagnosed individuals without such medications. Many drugs are known to bind to HSA in the hydrophobic binding domains (*57-59, 87*) , which may well effect DSC analysis. These drugs may also alter the levels of lipids, cholesterol, and other lipophilic compounds known to associate with T2D, as well as levels of oxidized HSA (*87, 88*). There were small differences in the T2D samples versus the healthy plasma. The T2D had a maximum

stabilization temperature at 70.3º C compared to the 70.6º C in the HC. The shape of these DSC scans also appeared to be somewhat different. However, we were left with considerable uncertainty about the value of continuing this line of study.

Fluorescence Lifetime

We switched to another more accessible method of monitoring the thermal stability and denaturation of proteins in the healthy and diseased plasma. Working with Ben Krajacich, a talented undergraduate researcher at MSU, we began to investigate the possibility of monitoring thermal denaturation of HSA using the fluorescence of the single tryptophan in HSA. This single tryptophan at position 214 is buried in one of the three binding domains of HSA (*67*). As the HSA protein unfolds during the thermal denaturation, the tryptophan changes from a hydrophobic environment to a hydrophilic environment, which greatly decreases the tryptophan fluorescence. Monitoring the whole plasma fluorescence during thermal denaturation was problematic because of changes in light scattering when the thermally denatured proteins aggregated. However, we found that we could monitor the changes in the environment of the tryptophan in HSA using the fluorescence lifetime, which was not sensitive to changes in turbidity of the solution. The fluorescence lifetimes get shorter when the fluorescence intensity drops. We hypothesized that we would observe a change in fluorescent lifetime if the HSA cargo was altered in disease states compared to healthy controls.

Knowing that our samples of SLE, LD, and healthy plasma should, according to Garbett, et al (*78*), exhibit differences in thermal stability, we investigated these samples

and also included samples of T2D. Fluorescence lifetime studies were done with the help of Fluorescence Innovations, a local company (Bozeman, MT), which develops fluorescence lifetime instrumentation.

Lifetimes are calculated using the following formula (*89*):

$I_t = I_0 \exp(-t/\tau)$

In this formula:

I_t = Fluorescence Intensity at Time (t)

I_0 = Fluorescence Intensity at Time (0)

t = Time

τ = Fluorescence Lifetime

This formula can be rearranged by taking the natural log (ln).

$\ln I_t = \ln I_0 + (-t/\tau)$

This equation describes a line when $\ln I_t$ is plotted against t.

$y = mx + B$

With slope (m) .

$m = -(1/\tau)$

Thus, the fluorescence lifetime is the negative inverse of the slope of the natural log of the fluorescence intensity plotted versus time after a flash excitation.

$\tau = -(1/m)$

Samples were prepared in the same fashion as for the DSC experiments (*78*), described previously. Samples were then diluted 1 to 25 in order to avoid inner filter effects with too high a concentration of protein in solution (*90*). This dilution also allows

measurements of the fluorescence without saturating the detector. The samples were measured in a 2 mm cuvette to keep the total absorbance down and to minimize outer filter effects. A UV/Vis scan was taken of each sample to measure the overall protein concentration. Each sample was then measured for fluorescence lifetime in a 2 mm quartz cuvette, while mixing with a stir bar while heating at scheduled increasing temperature set points of 5º C increments every 10 minutes. The temperature increase was relatively linear as a function of time. After thermal denaturation runs, the cuvettes were carefully cleaned with nitric and sulfuric acid, since the protein tended to cook (aggregate) on the cuvette surfaces.

Examples of lifetime data can be seen in figures 2.4 and 2.5 for the LD and SLE samples plotted with the HC data. These data were considered to be a practice sample set. After collecting this data, it was determined that the differences in lifetime measurements between control and experimental samples were very small. In the SLE sample it was noted, however, that a difference could be easily measured below 50º C. This change in thermal denaturation did not correlate to the changes that Garbett, et al (*78*) had seen around 62º C. We concluded that the tryptophan was being exposed to the aqueous environment early on in the denaturation process and did not appear to be a good marker for the major macro-unfolding of the bulk of the protein. In addition we were unable to detect significant differences between the LD and the HC samples.

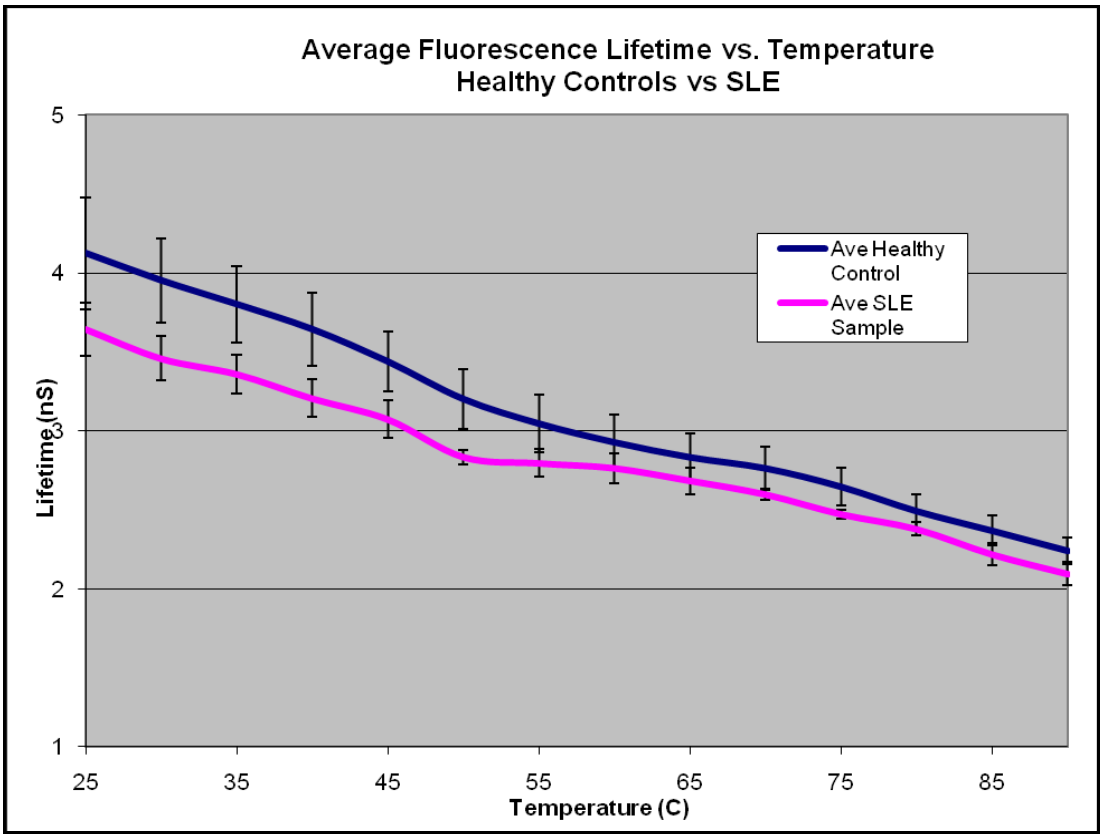

Figure 2.4: Lupus plasma and HC plasma fluorescence lifetimes were measured every 5º C as the sample was exposed to a stepwise increase in temperature every 10 minutes with constant stirring in the cuvette. These plots show that the lupus sample had significantly lower fluorescence lifetimes than the HC at the lower temperature and this difference persisted until about 55º C. Thus, the lupus sample appears to be more unfolded then the HC between 25º to 55º C in strong variance with the Garbett, et al findings (*78*).

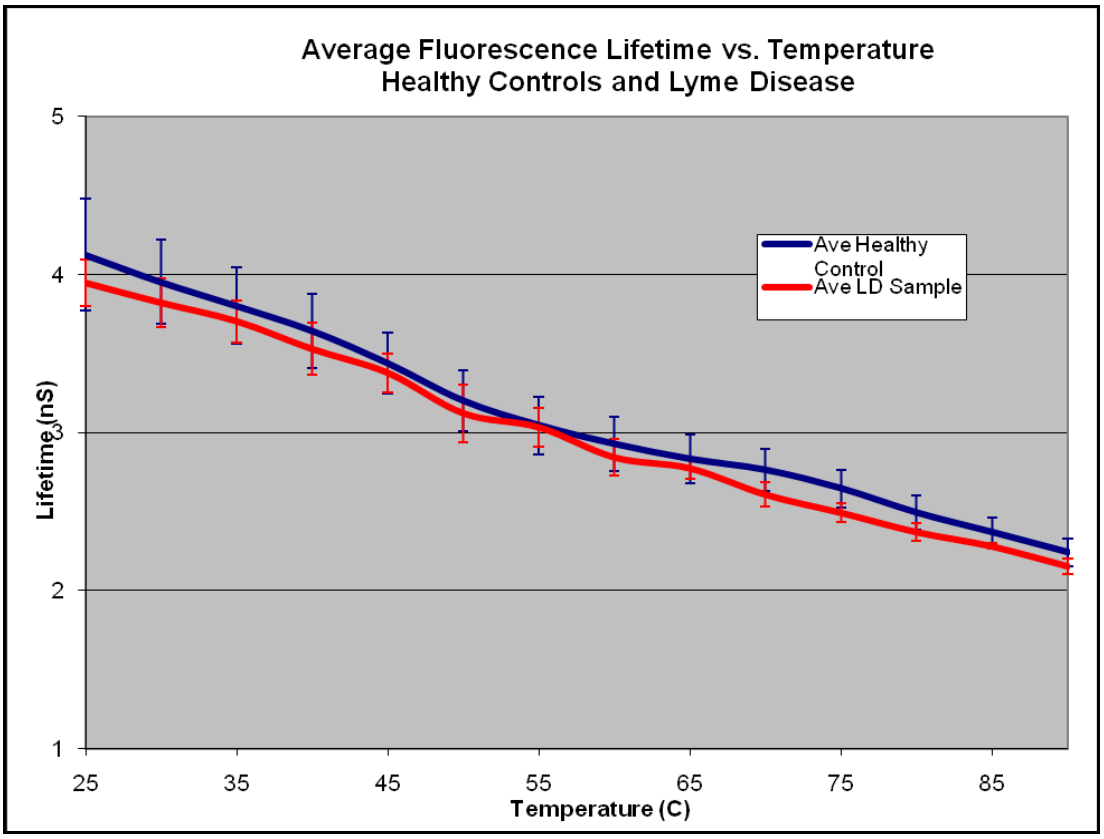

Figure 2.5: Lyme disease plasma and HC plasma fluorescence lifetimes were measured every 5º C as the sample was exposed to a stepwise increase in temperature every 10 minutes with constant stirring in the cuvette. These plots showed no significant differences between the two samples.

Fluorescent Lifetime with Extrinsic Probe

We decided to use an extrinsic fluorescent probe to monitor the unfolding of the hydrophobic pockets in the HSA protein that might better reflect the global unfolding. 1-anilinonaphthalene-8-sulfonic acid (ANS) was selected as a probe that fluoresces poorly in an aqueous environment, but the fluorescence increases dramatically when bound into the hydrophobic pockets of HSA (*72*). Importantly, the ANS probe does not displace NEFA that may be bound to HSA (*49, 73*). This is important, because we wanted to

minimize the disturbance of the binding of disease specific cargos on HSA that might cause changes to the HSA thermal denaturation. As the hydrophobic pocket is unfolded and exposed to the aqueous environment, the fluorescence signal of ANS will decrease markedly, which will also be reflected in the fluorescence lifetime.

To make these measurements, the amount of protein in each sample is normalized, and then the probe is added in equal amounts to each sample. Using the same preparation as described previously, the dialyzed whole plasma, diluted 1 part plasma to 25 parts PBS solution, was further slightly diluted in order to match the protein 280 nm absorbance of the control sample. An aliquot of 40uL of 5 mM ANS was added to each 2 mL of dialyzed diluted plasma sample to give a final concentration 100uM ANS. The protein signals, measured by UV/Vis, are shown in figure 2.6 before and after adding ANS to samples of healthy control plasma and SLE plasma. This is a typical spectrum before and after ANS is added and is similar to experiments done with T2D and LD samples, which were prepared in similar fashion.

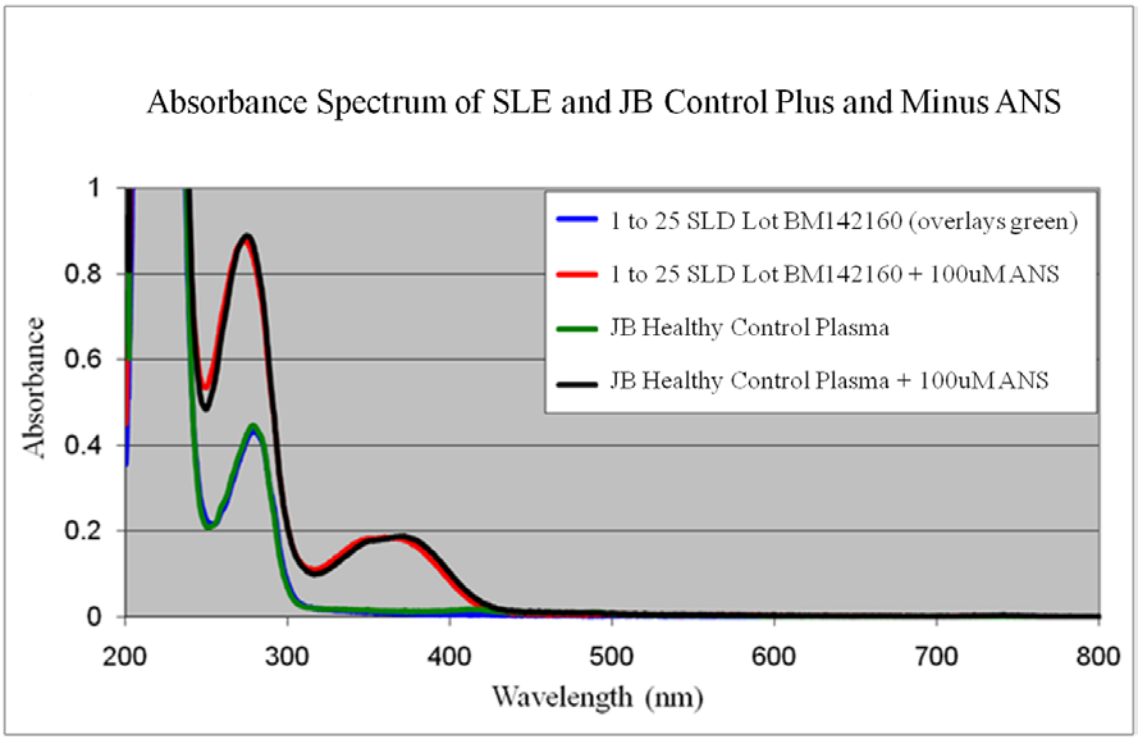

Figure 2.6: Absorbance spectra of HC control sample JB normalized to lupus disease (Lot BM142160) plasma sample by matching 280 nm protein signals. An aliquot of 40 uL of 5 mM ANS was then added to both samples and the ANS signal addition was measured at 380 nm. The UV/Vis signal reflected identical ANS added to both the samples. This is a representative plot of what T2D and LD would also look like.

The fluorescence was measured while exciting the samples at 295 nm. Excitation at 295 nm favors the excitation of the single tryptophan in HSA, which transfers this energy to the ANS, that emits fluorescence at 477 nm by a FRET mechanism (*72*). The decrease in tryptophan fluorescence signal at 336 nm, as ANS concentration increases due to quenching of the tryptophan fluorescence due to FRET is shown in figure 2.7. There is a clear difference in the fluorescence intensity between samples that is a reflection of the difference in the extent of bound ANS, as is shown in figure 2.8(a)(b). The quenching of the tryptophan fluorescence as ANS concentration increases and FRET

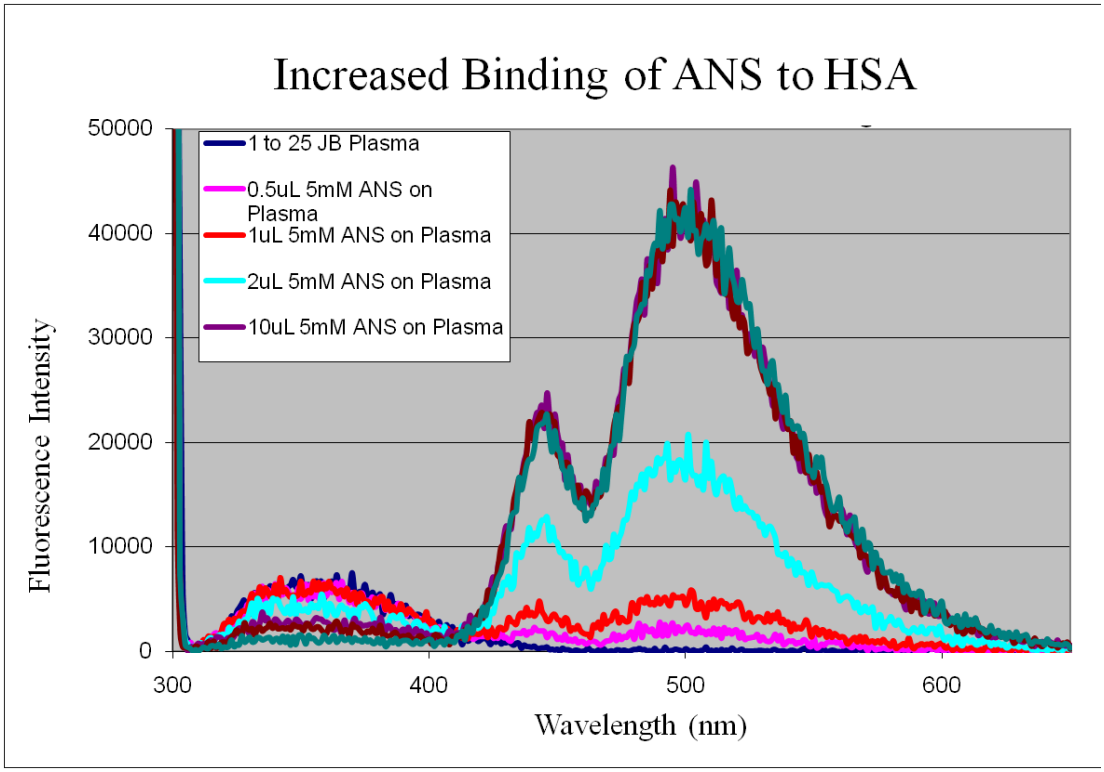

Figure 2.7: ANS fluorescence bound to HC samples is markedly different at 25°C with increasing ANS concentration. Excitation at 295nm induces tryptophan excitation at 336nm and FRET ANS fluorescence at 477nm. As the ANS concentration increases the tryptophan 336nm emission is reduced and the 477nm emission is increased.

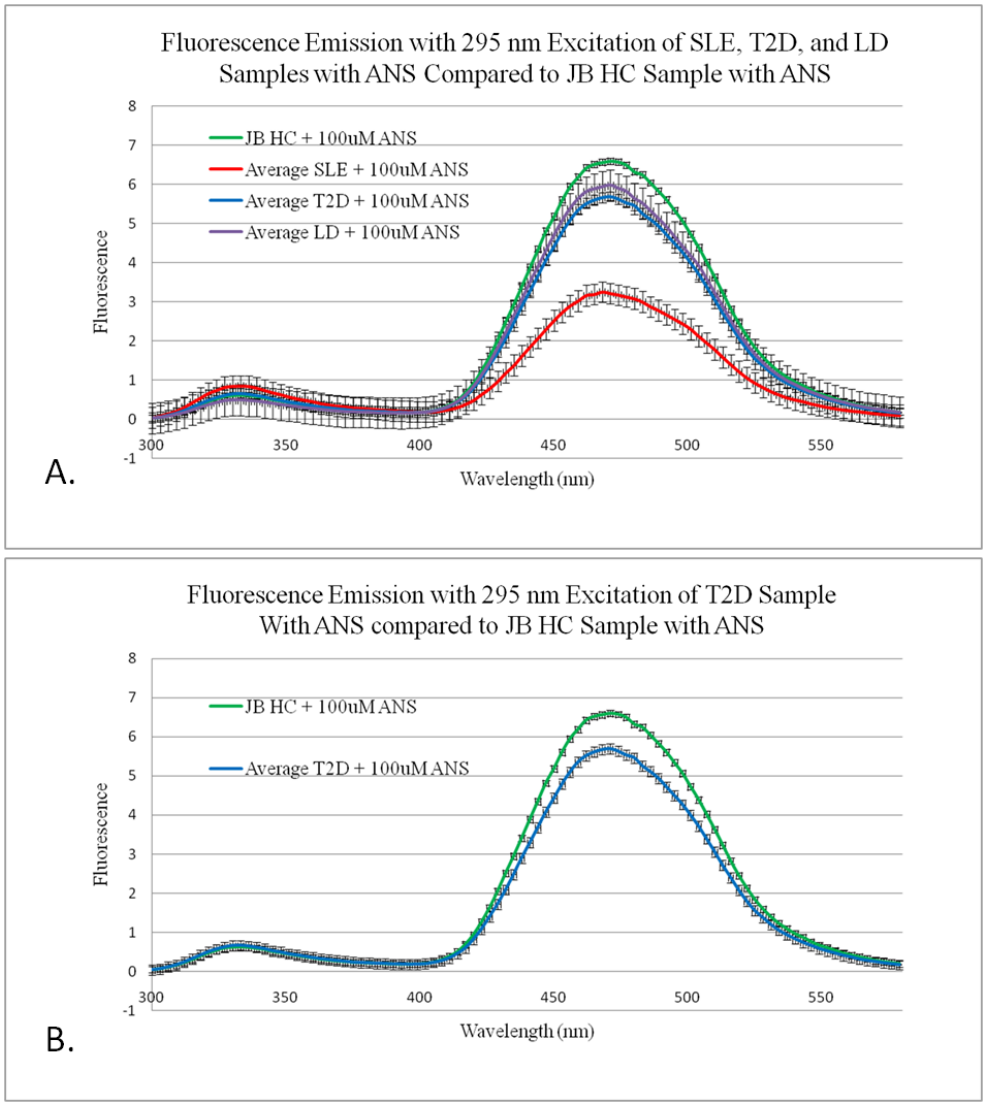

Figure 2.8 (A.): ANS fluorescence bound to replicate SLE, T2D, LD, and HC samples is markedly different at 25°C with tryptophan excitation. Each sample was run in duplicate and the average spectrum intensity is shown and standard deviations for the fluorescence of each sample are shown as error bars. The overall fluorescence intensity is not a result of differences in amounts of either protein or ANS. The differences are believed to be a result of the binding pockets in HSA disease samples being partially filled with some hydrophobic molecule that inhibits the binding of ANS. (B.) ANS fluorescence bound to replicate T2D and HC samples is markedly different at 25°C with tryptophan excitation. Each sample was run in duplicate and the average spectrum intensity is shown. Standard deviations for the fluorescence from each sample are shown as error bars. The overall fluorescence intensity is not a result of differences in amounts of either protein or ANS. The difference is believed to be a result of the binding pockets in HSA disease samples being partially filled with some hydrophobic molecule that inhibits the binding of ANS.

As noted previously, ANS is known not to displace lipids bound to HSA (*49, 73*). This makes differences in the amounts of lipids and other hydrophobic compounds interesting targets as an explanation to why ANS binds HSA to a lesser extent in the diseased samples. This observation could be consistent with Garbett et al's DSC result on SLE, LD, and control plasma, if the materials bound to the disease samples also stabilized the HSA against denaturation (*78*). The overall difference between total fluorescence SLE compared to HC is 50% +/- 4%, T2D compared to HC is 14% +/- 2%, and LD compared to HC is 10% +/- 6%.

It is clear that the HC has considerably more hydrophobic binding pocket sites to bind ANS. We propose that the disease samples have additional cargo bound in the hydrophobic binding pockets that are not then accessible to binding ANS. The fluorescence lifetime measurements plotted between the most dramatic SLE and HC samples with ANS are shown in Figure 2.9. Since ANS may act as a small molecule to stabilize HSA during thermal denaturation, difference in ANS fluorescent lifetimes between the disease and HC samples, as found in figure 2.9, are likely reflecting the level of bound ANS probe combined with hydrophobic cargos already found in the sample prior to ANS binding.

It would be desirable to measure ANS fluorescence and FRET from typtophan in a wider range of control and diseased human blood samples to rapidly assess differences in HSA cargo amounts between healthy and diseased samples. Therefore, investigating the hydrophobic cargo responsible for filling the HSA hydrophobic binding pocket is clearly an area of great interest that will require further investigation.

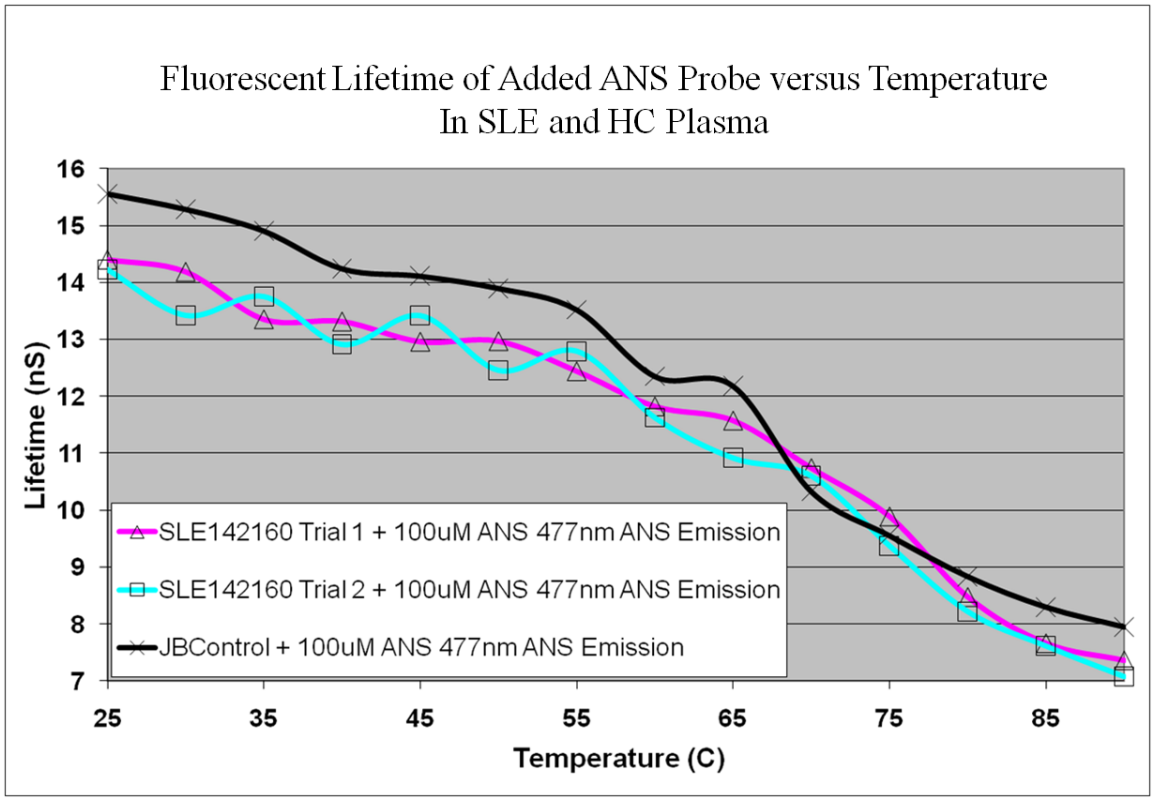

Figure 2.9: Fluorescent lifetimes of the same two samples of dialyzed plasma from an SLE patient with added ANS taken every 5º C as shown in Figure 2.7, compared to a sample of dialyzed HC plasma with added ANS.

At this point, we made a decision to switch our efforts to measuring the cargo contents of the HSA directly, seeking to determine the molecules responsible for filling the hydrophobic binding pockets on HSA that appeared to prevent the ANS binding in the diseased samples. In this way we hoped to prove a mechanistic explanation for both Garbett, et al (*78*) and Laffoon's observations (*42*). Note, however, that we have not been able to support the findings reported by Garbett, et al (*78*) either by direct DSC or by fluorescence, since the fluorescent lifetime of the ANS in the diseased samples was either shorter than the control (less stable protein) or essentially the same as the control.

INVESTIGATING THE MINERAL CARGO OF HSA

HSA is known to have multiple metal binding sites (*91*). A talented summer undergraduate researcher, Rezma Shrestha, assisted in measuring the minerals bound to HSA in T2D and HC samples. The primary site of metal binding in HSA located at the N-terminus has been well characterized and includes an N-terminal (asp, ala, his) sequence (*91*). Three additional metal binding sites are also known: cys 34, where Au+ in anti-arthritic drugs binds (thiolate sulfur); site A his 67, where Cd (II) has been shown to bind; and site B, which has not yet been localized (*92*). Site A interacts with Cd (II), Zn (II), and fatty acids (*93*). However, when the A site is occupied by fatty acids, Zn (II) cannot be bound at this location (*93*). Zn is found normally in blood at concentrations near 19 uM, and most of the Zn (II) in plasma is bound to HSA (*92, 94*). Antagonistic binding of the Zn (II) and fatty acid is of substantial interest, since low blood levels of Zn, and higher levels of NEFA have been implicated in T2D (*40, 92, 94*).

To measure the minerals bound to HSA, samples of the purchased diseased plasmas and the normal controls were each loaded onto an Agilent HSP7 immuno-affinity column (a MARS7 column prototype). This column removes the seven most abundant proteins in plasma, by binding them to antibodies in the column (*95*). An absorbance trace of the immuno-depletion of plasma, using the HSP7 column is shown in figure 3.1. The retained proteins, including HSA, are removed from the column by exposing them to Agilent buffer B. This buffer is a proprietary solution, containing a low concentration of urea in PBS, estimated to be approximately 2 M urea. Three immuno

affinity column versions were utilized throughout work. First, an HSP 7 column was used, which depletes the seven most abundant proteins in plasma. Second, a MARS14 column was used, which depletes the 14 most abundant proteins in plasma. Lastly, a polyclonal anti-HSA column was used, which depletes only the HSA from the plasma. Chromatography conditions were the same for all immuno-depletions, and the visual appearance of the chromatograms were nearly identical.

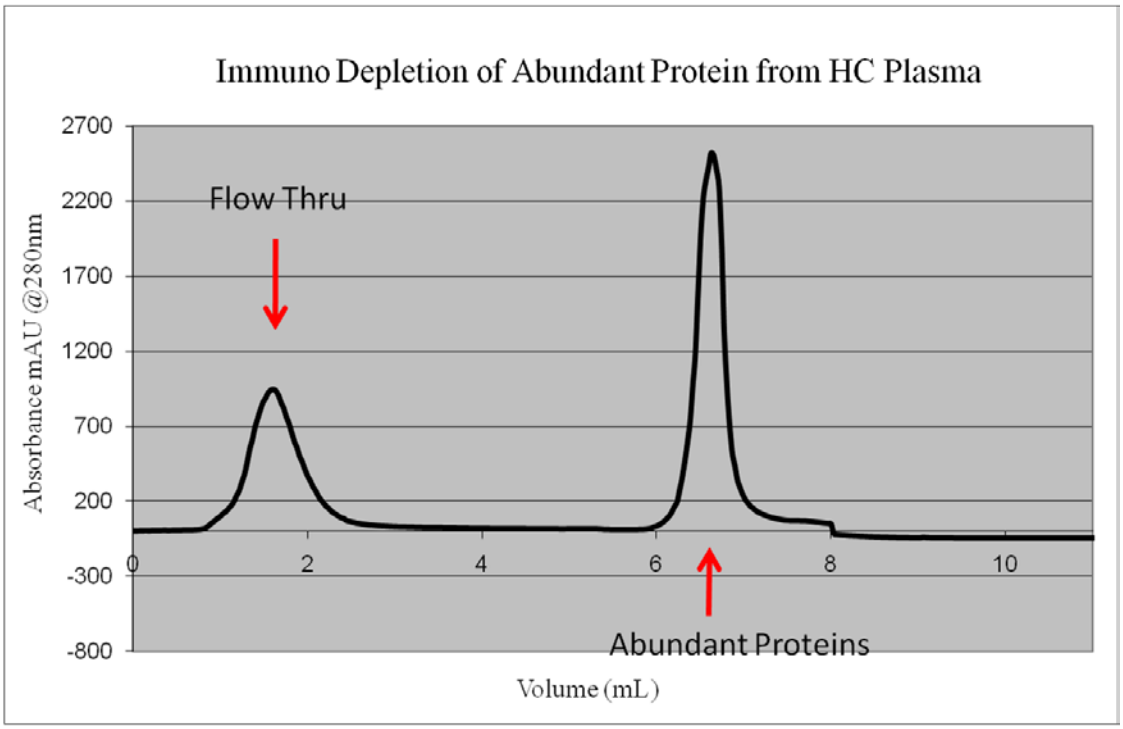

Figure 3.1: Immuno-depletion of abundant proteins from human plasma using an Agilent immuno-affinity column. The abundant protein peak saturates the absorbance detector so that the signal does not reflect the amount of the protein present

Samples were prepared as follows. 100uL of plasma was diluted, with Agilent buffer A (a proprietary PBS solution), to 500uL total volume. These samples were stored on ice until ready for injection. 480 uL of a sample (the column loading capacity) was

injected onto the column. We performed the affinity separation using a GE (Fairfield, CT) Pharmacia Fast Protein Liquid Chromatography (FPLC), AKTA system. Elution conditions were 100% Agilent buffer A, with a flow rate of 0.5 mL/min. At 4.5 minutes this flow rate was increased to 1.0 mL/min. At 6.5 minutes the elution solvent was switched to 100% Agilent buffer B. The fraction containing the HSA peak was collected from 7.6 minutes – 9.0 minutes. The abundant protein fraction containing HSA was collected, frozen, and lyophilized for further analysis. At 13.5 minutes the gradient was switched to 100% Agilent buffer A until 25 minutes, which ended the run and the reinitialized the column.

The additional proteins extracted with the HSP7 or MARS14 columns were not found to be significant carriers of minerals, compared to the HSA depletion. The background sodium (Na), potassium (K), and chloride (Cl) in the buffers added considerable noise, due to the high levels of these minerals in the Agilent elution buffer B used in the sample preparation. Samples were manually collected over a 1.4 minute elution time. Variations in the Na, K, and Cl levels in the data can likely be attributed to minor variations in the collected volume of Agilent buffer B.

Lyophilized abundant protein samples were digested using 2 mL of a 5% nitric acid (w/v) solution for 3 hours at room temperature. The proteins were effectively digested under these conditions, and the minerals were all solublized to an ionic state. The digested mixtures were submitted to Robin Gerlach, a professor at Montana State University, who ran these samples on an Agilent 7500CE Inductively Coupled Plasma Mass Spectrometer (ICP-MS). The levels of the metals in our samples were calculated,

based on signals obtained from commercial mineral standards for ICP-MS. The results of this analysis are shown in figure 3.2.

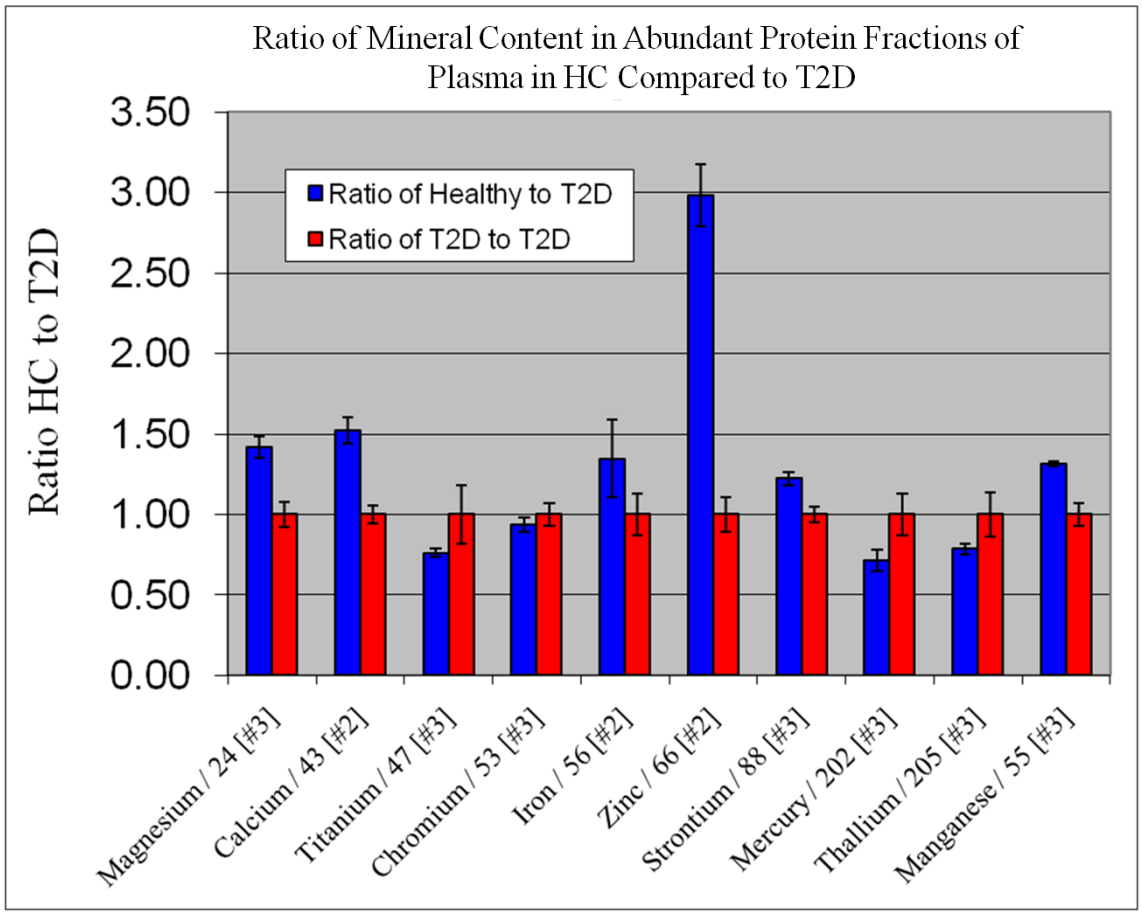

Figure 3.2: Ratio of the levels of minerals detected in the acid digested abundant protein fraction obtained from T2D and HC immune-depletion of plasma. The ratios of minerals found in 5 samples of T2D compared to 5 sample of HC (obtained from Bioreclamation) are shown. The levels of the different minerals varied greatly so the signals are normalized to the levels of T2D in the samples for ease of visual comparison. An Agilent HSP 7 immuno-depletion column was used to collect this data. Since the elution buffer contained large amounts of sodium and potassium, these minerals were excluded from the study. Zinc exhibited the largest difference, with a 3 fold reduction in T2D. Other minerals showed smaller differences, but many of the differences were statistically significant (Ca, Mg, Fe, Sr, Hg, and Mn).

A decrease in the levels of many minerals in T2D plasma has been previously reported in the literature (*94, 96*). The most striking difference was the zinc, reduced by almost 3 fold in our T2D samples. Previous studies of whole blood serum reports a 40% decrease of zinc in T2D and if calculated in the same fashion our results correspond to a 66% decrease in zinc (*94*). As most of the Zn is reported to be bound to HSA in healthy blood, a 3 fold decrease of Zn associated with T2D suggests a significant alteration in Zn binding capacity of HSA, compared to the other values reported in the literature (*92, 94*).

When we made efforts to expand this study, the results got very noisy. We then realized that despite the good match of the initial results to the current literature, our study had a deficiency. Plasma always must be collected with a chelating agent to inhibit blood clotting. EDTA was used in the purchased samples, and sodium citrate was used in the NIH newly diagnosed T2D samples. EDTA binds minerals much stronger then citrate, but both have the capacity to strip a percentage of bound minerals from proteins (*97*). In previous literature reports using human plasma, the entire samples, and not just the abundant proteins (chiefly HSA), are digested in acid to measure the mineral content. Thus, even though the findings shown in Figure 3.2 are likely to be correct, this study warrants repeating with serum free of anticoagulant rather than using plasma. Plasma requires anticoagulants, which have an unknown affect on the mineral analysis. Serum does have active proteases during the clotting, but there are no chelating agents present in serum collection to disturb the HSA bound minerals.

INVESTIGATING THE PEPTIDE CARGO IN HUMAN PLASMA

Peptides are another prominent cargo of HSA. Our study was designed to measure differences low molecular peptides in T2D in whole plasma compared to HC. Some prior work in the plasma peptidomics field has been done by Tammen et al (*98-103*), Villenuvia et al (*104, 105*), Lopez et al (*53, 106*) and others (*107-125*). Tammen's and Villenuvia's studies were focused on characterizing the peptides found in whole human plasma and did not attempt to localize peptides bound to HSA. Lopez et al did focus on carrier protein bound mass signatures in Alzheimer's disease and ovarian cancer (*53, 106*). In the ovarian cancer study Lopez et al were successful in identifying several candidate biomarkers bound to HSA, such as complement casein kinase 2 and trangelin, and diamino oxidase (*53*).

Molecular Weight Cut Off Filters

Previous work has largely utilized molecular weight cut off (MWCO) filters to collect the low molecular weight (LMW) peptide fraction from plasma (*98, 100, 104, 117*). In these studies a 50 or 30 kDa MWCO filter was used to separate the abundant proteins, such as albumin, from the LMW peptide fraction. Only a few groups used denaturation of albumin to remove the native peptides bound to HSA (*53, 106, 115*); however, this denaturation seem crucial, as albumin has been reported to carry >90% of the peptides available in plasma (*102, 108*).

A major issue in utilizing the small peptide fraction of the peptidome for biomarker studies lies in the short life span of molecules of this size in the blood stream. The glomeruli in the kidneys act as a filter for the blood stream, and removes protein below 40 kDa during their passage into the proximal renal tubes (*126*). Most small proteins and peptides are removed from circulation within only a few hours unless they are bound to a sufficiently larger carrier (*126*). Concentrations of small proteins and peptides that are free in the blood are dilute, and are found in nanomolar to femtomolar concentrations in the whole blood (*99, 108*) Because small proteins and peptides are quickly filtered out, this also means that the peptide signal is relatively noisy, as it reflects only a short time snapshot.

Offsetting this loss of peptides by the kidney filtration is the fact that serum albumin and other carrier proteins bind and retain many members of the peptidome in the plasma. The half-life of albumin is 19 days in the circulatory system (*108, 122, 124, 127, 128*). It is well documented that albumin acts as a carrier protein to many important peptides and protein signaling molecules, like cytokines, hormones, and some lipoproteins (*122*). The loading of peptides on the albumin carrier protein increases the half-life of peptides accordingly. However, removing the abundant proteins with immuno-affinity techniques commonly used today, under mild conditions that do not employ strong denaturation agents, would greatly reduce the available peptide signals remaining on the protein fraction depleted of the of the abundant proteins (*122, 127*). Capturing the carrier protein-bound peptides allows for increase of the peptidome signal 10 to 500 times greater than their free counterparts, based on the production rate and

percent loaded onto the carrier protein (*103, 108*). Therefore, if appropriate denaturation of albumin and other carrier proteins is accomplished, the peptides they carry will be released. This release of bound peptides may allow accumulation of the lowest level peptides to increase from femtomolar to picomolar concentration, bringing many more of these peptides into the realm of the detectable within our study (*103, 108*).

As previously mentioned, most groups currently use a low molecular weight protein fraction from MWCO filters followed by digestion of the fraction that passes this filter with trypsin (*98, 101, 109, 129*) . They then perform reverse phase (RP) high pressure liquid chromatography (HPLC) mass spectrometry (MS)/MS separations (*98, 101, 109, 129*). A common alternative method is to spot ninety-six, one-minute RP fractions onto a matrix assisted laser desorption ionization (MALDI) plate (*98, 101, 104, 105*). The peptide masses are measured and plotted as a heat map with three components: RP fraction, m/z, and intensity. These plots are examined for differences among multiple samples to identify the differences in m/z peaks in experimental versus control samples (*102, 104*).

We decided to alter the approach by quantifying peptides with high sensitivity using fluorescence labels attached to the epsilon amine of lysine on the peptides. We started our study by separating the LMW peptides through a series of MWCO filters. A known weakness of this approach is that minor defects in the MWCO filters allow approximately 1% of the abundant proteins to pass through the filter (*130*). To correct this problem, we designed a series of MWCO filters to sieve our sample. First, a 30 kDa MWCO filter was used; then a 10 kDa; then finally a 5 kDa. In this manner, any larger

proteins that had been shown in prior studies to pass through the MWCO filters would be removed by the following MWCO filter (*130*). This approach should leave us a very crisp LMW peptide fraction for our analysis.

Our initial data, after performing this serial cleanup with MWCO filters, lacked reproducibility. To track down the problem we contacted the supplier of the MWCO filters. The supplier informed us that the filters were being used incorrectly. These filters are designed to work with the retentate, not the flow through. They are best used to collect the large proteins and not the peptidome. They believed that the LMW peptides were binding nonspecifically to the membranes or possibly to the retained proteins. Thus, after passage through three membranes, very little of the overall LMW peptidome was making it through to the end collected fraction.

To test this hypothesis, we designed a spiking recovery experiment. We placed three fluorescently labeled protein spikes [BSA (66 kDa), ovalalbumin (43 kDa), and lysozyme (14 kDa)] into the diluted HC plasma at a concentration to obtain 50 ng of each fluorescently labeled spiked protein in the end solution final volume. This HC plasma spiked with mixed fluorescently labeled proteins was denatured with urea to release bound peptides. We found that the MWCO filters retained our fluorescent spiked proteins. After passing through a single 50 kDa MWCO filter, 95% of all three of the internal spikes were retained. Fluorescently labeled lysozyme (14 kDa) protein spike is not expected to be lost after passing through the MWCO filter, and much of the ovalalbumin was expected to be retained. It was visually apparent that the denatured plasma was aggregating and clogging the MWCO filter, as it turned to an extremely

viscous protein jelly. Varied loading of sample on the MWCO filters resulted in no increase in recovered LMW peptides. 800 uL of denatured plasma did not visually clog the MWCO filter, but recovered less fluorescently labeled lysozyme spike then 10 mL of denatured plasma proteins that did visually clog the MWCO filter. Data from these experiments is shown in Table 4.1, Figure 4.1, and Figure 4.2.

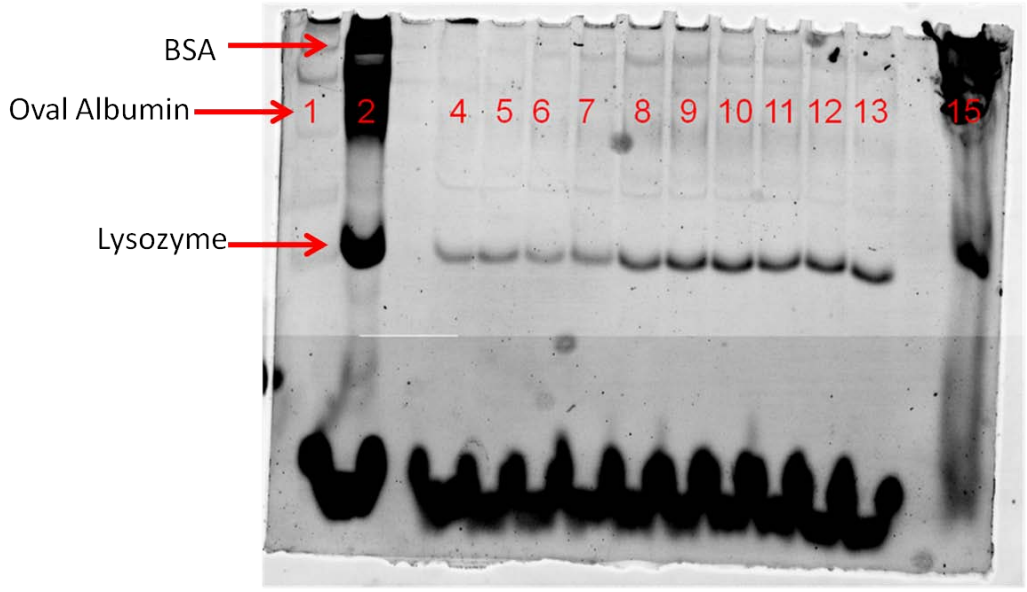

Figure 4.1: Fluorescent dye (ZGB) image of 1D tris-tricine SDS gel showing the LMW peptides and proteins that pass through a 50 kDa MWCO filter. A spike of three fluorescently labeled proteins, BSA (66 kDa), oval albumin (43 kDa), and lysozyme (14 kDa), was added to each sample before filtrate to obtain a final concentration of 50 ng of each fluorescently labeled protein. 15 uL of each sample was added to each lane in the gel. Key to 1D gel lanes: 1- molecular weight ladder (not passed through the filter; 2- fluorescent, ZGB labeled internal spike including BSA, oval albumin, and lysozyme; 3- blank lane (50 ng per protein); 4 & 5- Plasma diluted 1:4 in 8M urea, 800uL total volume; 6 & 7- Plasma diluted 1:4 in 6M urea, 800uL total volume; 8 & 9- Plasma diluted 1:4 in 6M urea, 2 mL total volume; 10 & 11- Plasma diluted 1:4 in 6M urea, 4mL total volume; 12 & 13- Plasma diluted 1:4 in 6M urea, 10mL total volume; 15- Unfiltered plasma diluted 1:4 in 6M urea with internal standard, 100 uL total volume. Only fluorescently labeled proteins are observed in this image. Lanes 4 – 7 have less lysozyme then lanes 8 – 15. If full recovery of the lysozyme were obtained there should have been equal signal from the internal standard that did not pass through a MWCO filter as shown in lane 2.

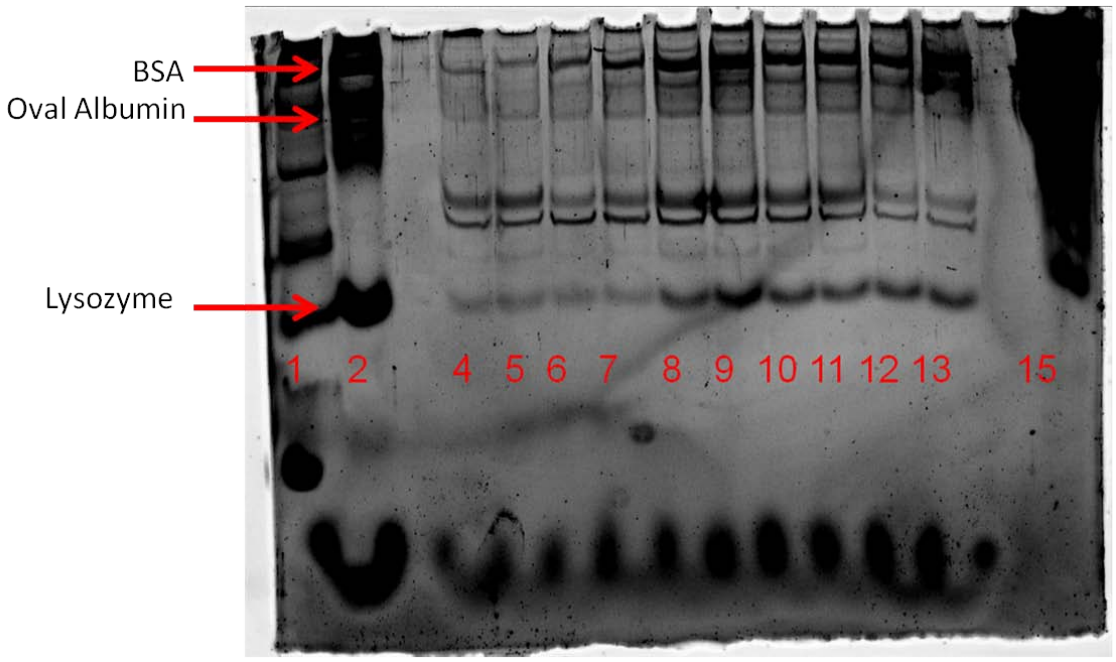

Figure 4.2: Sypro-ruby image of 1D tris-tricine SDS gel LMW peptides passed through a 50 kDa MWCO filter. A spike of three fluorescently labeled proteins, BSA (66 kDa), oval albumin (43 kDa), and lysozyme (14 kDa), was added to each sample before filtrate to obtain a final concentration of 50 ng of each fluorescently labeled protein. 15 uL of each sample was added to each lane in the gel. Key to 1D gel lanes: 1- molecular weight ladder (not passed through the filter; 2- fluorescent, ZGB labeled internal spike including BSA, oval albumin, and lysozime; 3- blank lane (50 ng per protein); 4 & 5- Plasma diluted 1:4 in 8M urea, 800uL total volume; 6 & 7- Plasma diluted 1:4 in 6M urea, 800uL total volume; 8 & 9- Plasma diluted 1:4 in 6M urea, 2 mL total volume; 10 & 11- Plasma diluted 1:4 in 6M urea, 4mL total volume; 12 & 13- Plasma diluted 1:4 in 6M urea, 10mL total volume; 15- Unfiltered plasma diluted 1:4 in 6M urea with internal standard, 100 uL total volume. The Sypro-ruby image labels all of the proteins and peptides placed on the gel.

Table 4.1: Lysozyme spike recovery 1D Gel quantitative analysis. Fluorescence signal was measured for each lysozyme band in the lane. A background from below the lysozyme in the same lane was subtracted from each reading. The average signals with background subtracted for each sample volume were divided by the original lysozyme band signal that had not passed through the MWCO filter. Percent loss of each spike is listed in the right column. It appears that 2 – 6% of the lysozyme 14 kDa passed through the 50 kDa MWCO filter. More material was lost in the low volume loadings of 800 uL, which did not plug, then in the high volume 10 mL loading. We hypothesize this is due to binding of the dye labeled proteins to the MWCO filters.

Sample name (15uL of each sample loaded on gel)	Lysozyme Band Signal - Background	Average	% Lost from Original Spike
Lane 2 (fluorescent, ZGB labeled internal spike including BSA, oval albumin, and lysozyme) [no MWCO filter]	387,606	387,606	0%
Lane 4 (Plasma diluted 1:4 in 8M urea, 800uL total volume) [passed through MWCO filter]	8,808	9,500	98%
Lane 5 (Plasma diluted 1:4 in 8M urea, 800uL total volume) [passed through MWCO filter]	10,192		
Lane 6 (Plasma diluted 1:4 in 6M urea, 800uL total volume) [passed through MWCO filter]	7,421	9,060	98%
Lane 7 (Plasma diluted 1:4 in 6M urea, 800uL total volume) [passed through MWCO filter]	10,700		
Lane 8 (Plasma diluted 1:4 in 6M urea, 2 mL total volume) [passed through MWCO filter]	18,003	20,307	95%
Lane 9 (Plasma diluted 1:4 in 6M urea, 2 mL total volume) [passed through MWCO filter]	22,610		
Lane 10 (Plasma diluted 1:4 in 6M urea, 4mL total volume) [passed through MWCO filter]	24,170	22,986	94%
Lane 11 (Plasma diluted 1:4 in 6M urea, 4mL total volume) [passed through MWCO filter]	21,801		
Lane 12 (Plasma diluted 1:4 in 6M urea, 10mL total volume) [passed through MWCO filter]	23,530	23,652	94%
Lane 13 (Plasma diluted 1:4 in 6M urea, 10mL total volume) [passed through MWCO filter]	23,774		
Lane 15 (Unfiltered plasma diluted 1:4 in 6M urea with internal standard, 100 uL total volume) [no MWCO filter]	79,238	79,238	80%

Size Exclusion Chromatography

Given the poor yield and lack of reproducibility of LMW peptides after passage through the MWCO filter, another way to separate LMW peptides was pursued. Many methods have been used by other groups to isolate LMW peptides: Cibachron blue dye

affinity (*53*), acetonitrile (ACN) denaturation and precipitation (*107*), solid phase extraction cartridges (*107*), multiple sieving using hollow fiber based serum pre-fractionation (like a kidney dialysis machine)(*131*), selective extraction of peptitides with porous silica nanoparticles (*120*), enrichment of peptides using multi-walled carbon nanotubes (*113*), as well as MWCO filters (which we have shown have low recovery and poor reproducibility) (*107*). We found that size exclusion chromatography (SEC) (*132*) had been used successfully by Horn in 2006 to isolate LMW peptides (*133*), but their SEC work used PBS and no denaturant, and so the HSA bound peptides that we desired to obtain would not have been isolated (*133*).

We selected SEC because of its reproducibility and high recovery, qualities that the MWCO filters lacked. This method also allowed us to utilize a strong denaturant on the whole plasma to aid in isolating the LMW peptidome fraction. There tends to be no specific binding to the SEC stationary phase, but rather a bulk separation of the molecules based on size. Percent recoveries using SEC are typically found to be >99% (*134*). Because of the high recovery values, reproducibility is also excellent.

A column is packed with a stationary phase, such as Sephadex or Sephacryl, which contains large particles with minute channels in them. The minute channels are inaccessible to the larger molecules, and thus the larger molecules move through the column at a much faster rate than smaller molecules that can access the pores. The volume accessible to the larger particles is called the exclusion volume. The smaller molecules have a longer inherent path length when they enter into the tiny channels. At some smaller size limit, the column inclusion volume is obtained, in which the smallest

particles, such as salts, travel. This is the longest path any molecule will take to travel the length of the column. Illustrations of this principle of separation can be seen in figures 4.3 and 4.4.

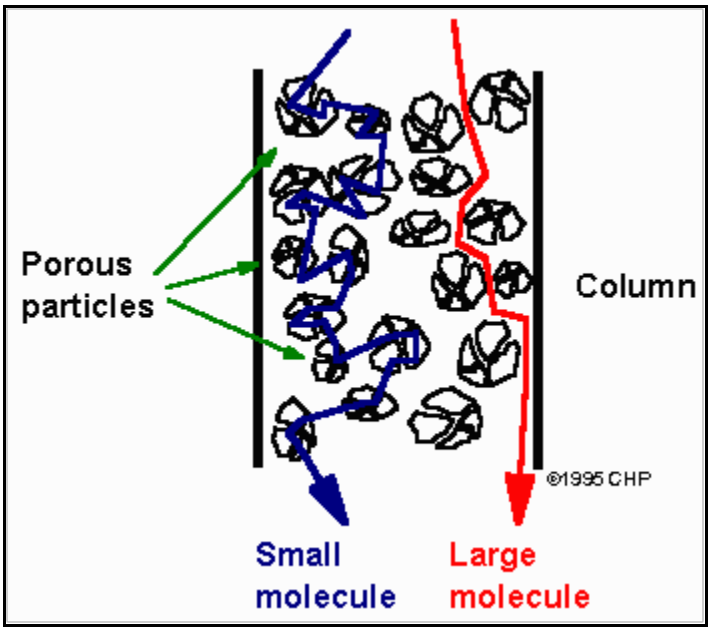

Figure 4.3: A cartoon figure representing the volume accessible to large and small molecules in a SEC column. The particles contain porous channels that allow smaller molecules to pass through while excluding the larger molecules. This gives rise to larger molecules traveling much faster through the column and smaller molecules taking longer (*135*).

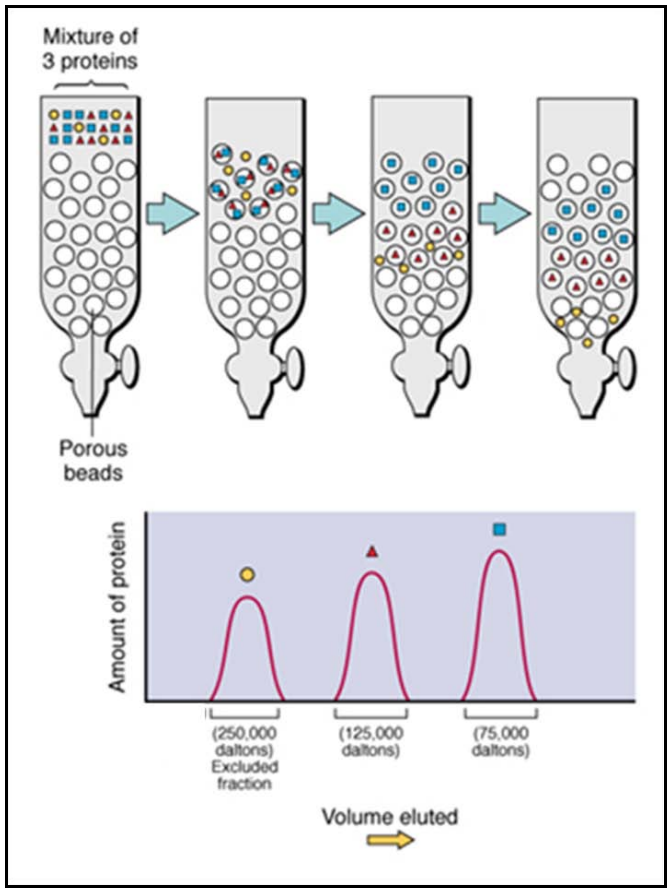

Figure 4.4: An illustration of the elution times of a mixture of three proteins of varying size. The mixture is separated while traveling through the SEC column to produce resolved protein peaks eluting over time. The largest protein elutes first and the smallest last (*135*).

To prepare a sample of LMW peptides, 0.75 mL of plasma was thawed on ice. This sample was denatured by adding 2.25mL of 8M urea with 40 mM Bicine pH 8.5 to the plasma. After 30 minutes, 8.6 mg of tris (2-carboxyethyl) phosphine hydrochloride (TCEP) was added to the 3 mL sample, making a 100 mM solution. TCEP reduces the disulfides in the sample, allowing further denaturation. 30 minutes later, 47.7 uL of 4.4 M 4-vinyl pyridine is added to the sample, making a 700 mM solution. 4-vinyl pyridine is an efficient alkylating agent, which quantitatively blocks the cysteines from

reforming di-sulfides. To quench any excess alkylating agent, an additional 32.4 mg of dithiothreitol (DTT) was added after 30 minutes of alkylation, making the final DTT concentration 700 mM. These high concentrations of reducing and alkylating agents were chosen due to the high concentration of protein in our sample. Excess quenched reducing and alkylating agents are removed in the SCX fractionation.

A 2 mL of this urea denatured, reduced, and alkylated human plasma is loaded onto a GE (Fairfield, CT) Pharmacia Sephacryl S-100 SEC column (10mm x 60 cm). The column is run with isocratic elution in 6 M urea 30 mM bicine pH 8.5. These conditions elute the LMW peptides from the denatured plasma sample. A low molecular weight peptide fraction is collected from 62 minutes to 140 minutes. Characterization of this column to determine when to collect this LMW fraction was performed by injecting a mixture of blue dextran (2,000 kDa), BSA (66 kDa), lysozyme (14 kDa), cytochrome C (12 kDa), and free dye HBO187 (<1 kDa). The results of this procedure can be seen in figures 4.5 (A and B).

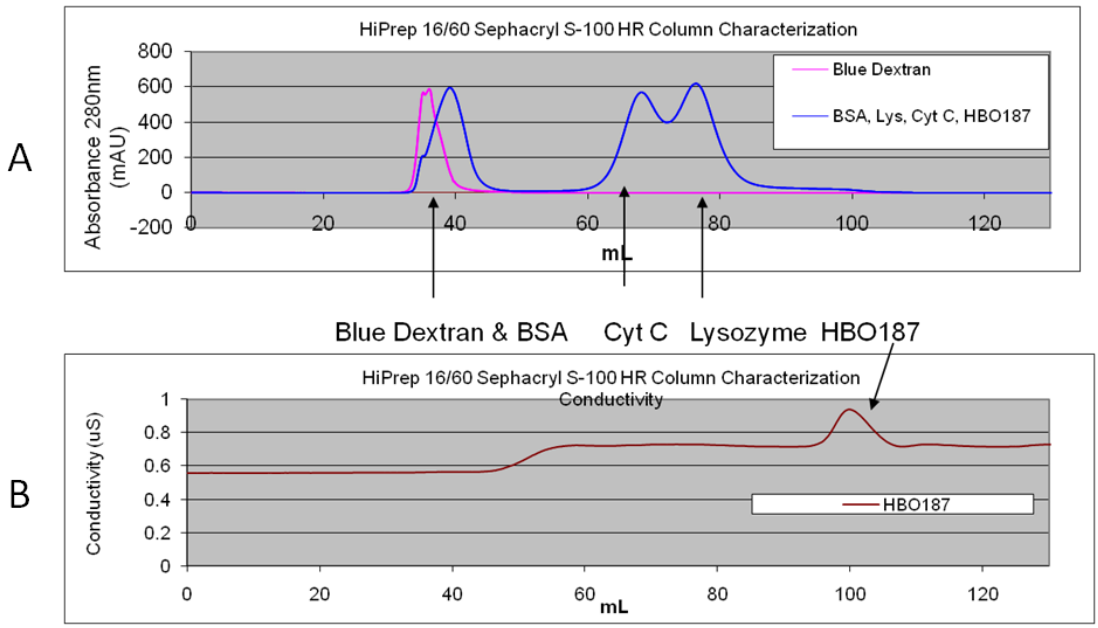

Figure 4.5: (A) The exclusion limit for the Sephacryl S-100 SEC column was determined using blue dextran (2,000 kDa) and BSA (66 kDa). The lysozyme (14 kDa) and cytochrome C (12 kDa) are molecular weight markers that assist in determining the point required to collect a LMW peptide fraction. (B) As part of the characterization of the Sephacryl S-100 SEC column, a sample of low molecular weight HBO187 fluorescent dye (< 1 kDa) was injected. This was not visible at 280 nm in absorbance. However, the conductivity from this small charged particle can be clearly observed eluting at 100 minutes. This allows determination of the end of the column chromatography collection required for eluting the smallest components of a sample prior to the next injection. The smallest components were also observable visually in the transparent column due to the free fluorescent dye present.

After denaturing, reducing, and alkylating the whole plasma sample, a LMW fraction was collected between 62 minutes and 140 minutes. These fractions were run on tris-tricine SDS gels and the peptides were desalted on a RP C12 column, concentrated by lyophilization, and dissolved in dimethyl formide (DMF) to solublize the LMW peptides.

Fractions C and D in figure 4.6 contain < 0.004% HSA. The samples do contain 27% of the LMW peptide signal approximately 6.5 kDa and smaller, although a large

fraction of the LMW peptides were found to be contained in fraction B. A relatively large amount of LMW peptides found in fraction B suggest the LMW peptides still have affinity for the denatured HSA in 6M urea at pH 8.5. The 280nm trace of denatured plasma collected on the SEC column is extremely reproducible.

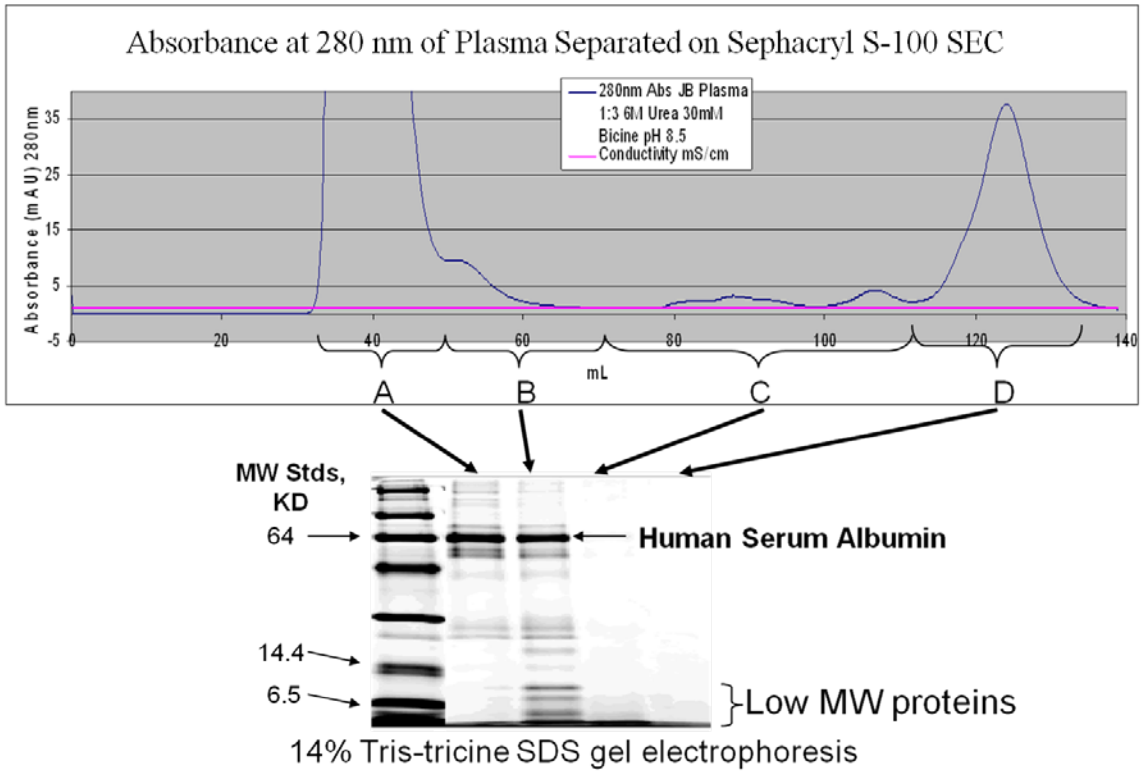

Figure 4.6: Analysis of a ½ mL of denatured, reduced, and alkylated human plasma fractionated on the Sephacryl S-100 SEC column. Fractions marked A-D were collected and run on a 14% tri-tricine SDS 1D-gel. It is clear that fractions C and D have the abundant HSA removed, and contain a substantial fraction of the LMW peptides used for future peptidomics studies.

We decided to compare our denatured SEC method to a method using MWCO filters described by Tammen, et al (*99*). We used the same plasma sample, and ran both methods side by side, to find out which produced more LMW peptides.

Tammen, et al's method used a 50 kDa MWCO filter and 1.3 mL of plasma. This was diluted to 3.9 mL with 8 M guanidium hydrochloride to denature the protein and release LMW peptides from binding to the high molecular weight proteins (*99*). The filtrate was separated by RP using an elution gradient beginning with 96% buffer A [0.1% trifluoroacetic acid (TFA), 100% water] and 4% buffer B [0.1% TFA, 100% ACN] (*99*). The proportion was then increased to 40% of buffer B over 96 minutes. One minute fractions were taken through the entire 96 minute gradient following Tammen et al's procedure (*99*). Tammen, et al reported finding approximately 4000 peptide signals detected by MALDI in each sample (*99*).

We chose to utilize our SEC method with ½ mL plasma diluted to 2 mL with urea denaturant, due to the loading capacity limitation of our SEC column. Denaturation was performed by diluting the sample to 2 mL total volume with 8 M urea, making the end urea concentration 6 M. Reduction and alkylation was omitted so that the 214 nm amide bond signal could be observed without interference from the 4-vinyl pyridine which absorbs at this 214 nm wavelength. After desalting the SEC fractions by HPLC using a RP C12 column, the samples were solubilized in 5% DMF, 95% (0.1% TFA, water), and separated by RP using the same elution gradient that Tammen, et al reported (*99*).

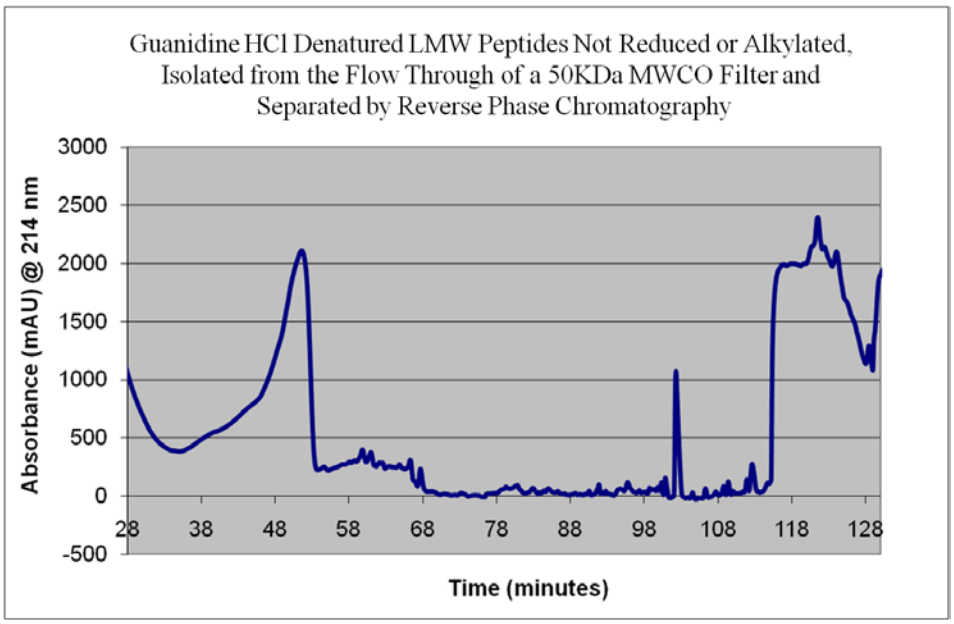

Figure 4.7: 1.3 mL of plasma was denatured with 8 M guandine hydrochloride and passed through a 50 kDa MWCO filter. The filtrate was separated by RP with a 4-40% ACN solvent gradient over 96 minutes. This chromatogram represents the absorbance signal from the sample monitored at 214nm.

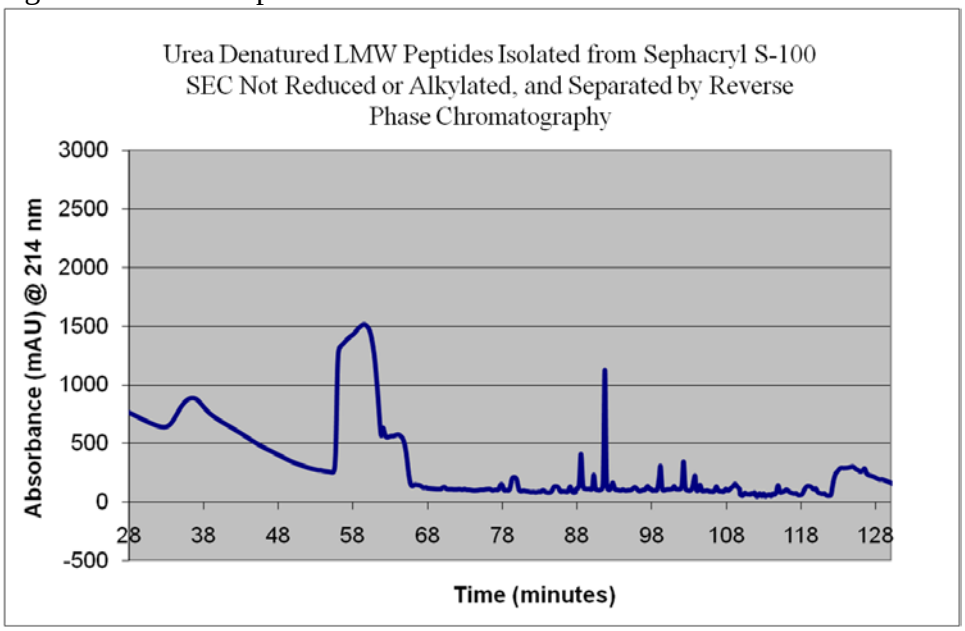

Figure 4.8: 0.5 mL of plasma was denatured with 6 M urea and separated by SEC, collecting the < 5 kDa LMW fraction. The filtrate was separated by RP with a 4-40% ACN solvent gradient over 96 minutes. This chromatogram shows the absorbance signal from the sample monitored at 214 nm.

The chromatograms are shown in Figures 4.7 and 4.8. Note the SEC fraction only represents 38% as much plasma as was used in the MWCO filter method. Guanidine hydrochloride and urea does not contribute to the LMW peptide signal monitored on RP, since they were found to elute in the first three minutes of the chromatogram. One-minute fractions collected from both runs were analyzed with a Bruker (Billerica, MA) BiFlex III MALDI-TOF. Each mass signal over 700 m/z was considered a mass that may have enough information for peptide identification. A Venn diagram comparing these findings is shown in figure 4.9. 24% more LMW peptide signals were found in the urea denaturing SEC method even though only 38% as much starting plasma was used. It was striking that little commonality was found between the peptides isolated by the two methods.

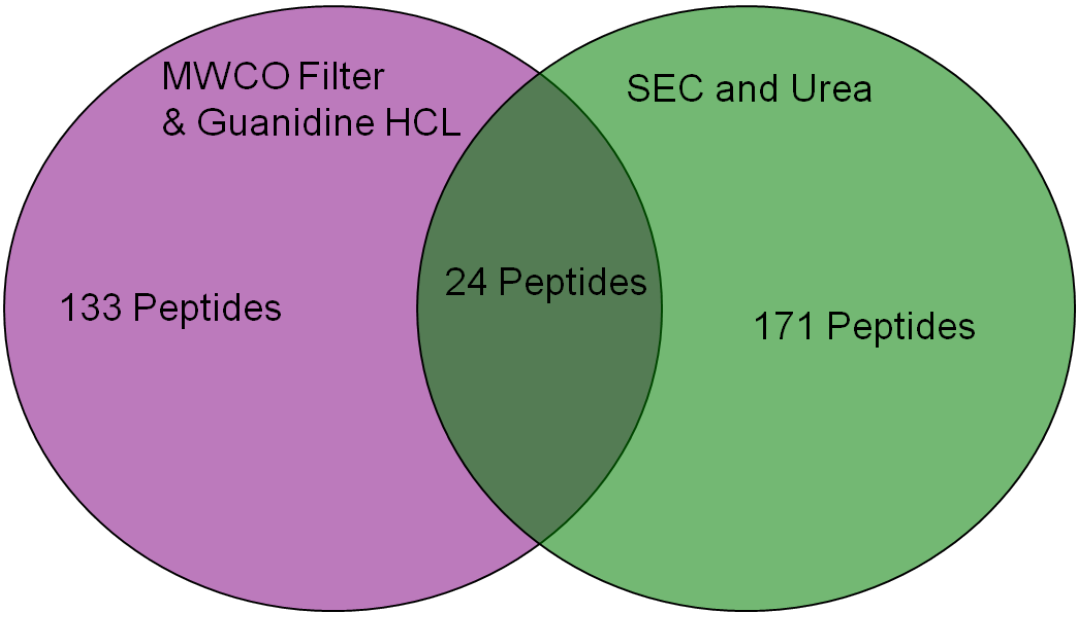

Figure 4.9: Comparison of the number of LMW peptides detected by the SEC method in urea vs. Tammen, et al's 50 kDa MWCO filter with the guanidine hydrochloride method (*99*). 24% more peptides were identified in SEC method even though only ~1/3 of the plasma was utilized.

Fluorescent Dye Labeling

With low molecular peptide fractions in hand, methods were explored to covalently attach a fluorescent dye to each peptide. Each free amine from the lysine group or N-terminus can be labeled with a fluorescent dye bearing an amine reactive N-hydroxysuccinimide (*136*) ester. A single peptide can have between zero and perhaps up to about four free amine labeling sites, since we are not using trypsin digest of peptides, and this allows different possibilities for dye attachment. Any permutation of labeling of these free amines that does not saturate all of these potentially reactive sites completely creates the possibility that this peptide will elute in multiple peaks.

Therefore, saturation labeling of all available lysine groups and the N-terminus was a requirement, so that peptides would not be heterogeneously labeled. If saturation labeling is not obtained, the signal for some of the partially loaded peptides may be so low that they cannot be observed. This is due to splitting the labeled peptide signal into multiple peaks, causing a decrease in the overall sensitivity. Multiple peaks for each peptide would also create a chromatogram that is extremely difficult to interpret. It would be hard to identify which peaks belong to which peptide and to resolve each and every peak from each other so that one can interpret which peptides are changing between T2D and HC. An example of a peptide with 3 potential amine labeling sites is illustrated in Figure 4.11.

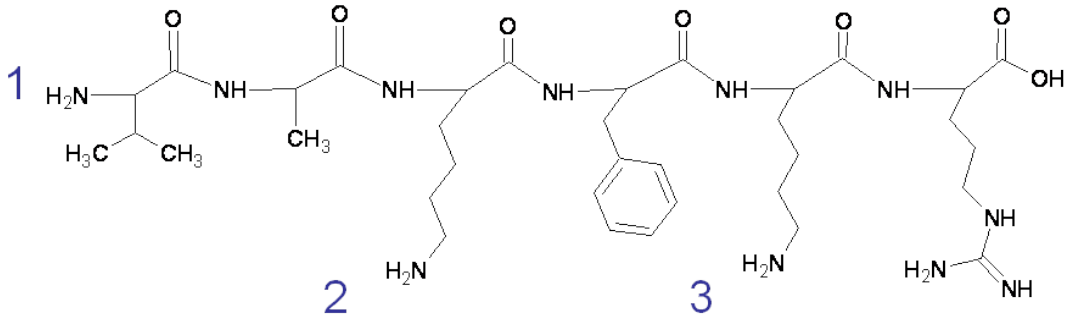

Figure 4.10: An example of a peptide containing two lysines and an N-terminus that has the capacity to label with fluorescent dye at position 1, 2, and 3. Dyes might be attached at all three positions 1 or 2 or 3. Additionally, combinations of labeling of sites 2 and 3 or 1 and 3 or 1 and 2 are all possible permutations along with single site labeling. Each of these labeling combinations will tend to lead to different retention times when using reverse phase chromatography to separate dye labeled peptides.

To accomplish saturation labeling, 12 nmoles of a model peptide, β-amyloid (which has one lysine group and an N-terminus), was labeled with 144 nmoles of fluorescent dye ZGB obtained in collaboration with the Grieco group at MSU (Bozeman, MT). 6 fold molar excess fluorescent dye, per labeling site, was used in 20 uL anhydrous DMF and 10 uL of anhydrous diisopropylethalamine (DIEA) was added to elevate the pH of the reaction. Labeling was allowed to proceed at room temperature overnight in the dark under argon. A diagram of this reaction scheme is shown in Figure 4.11. Results of this peptide labeling are shown in figure 4.12.

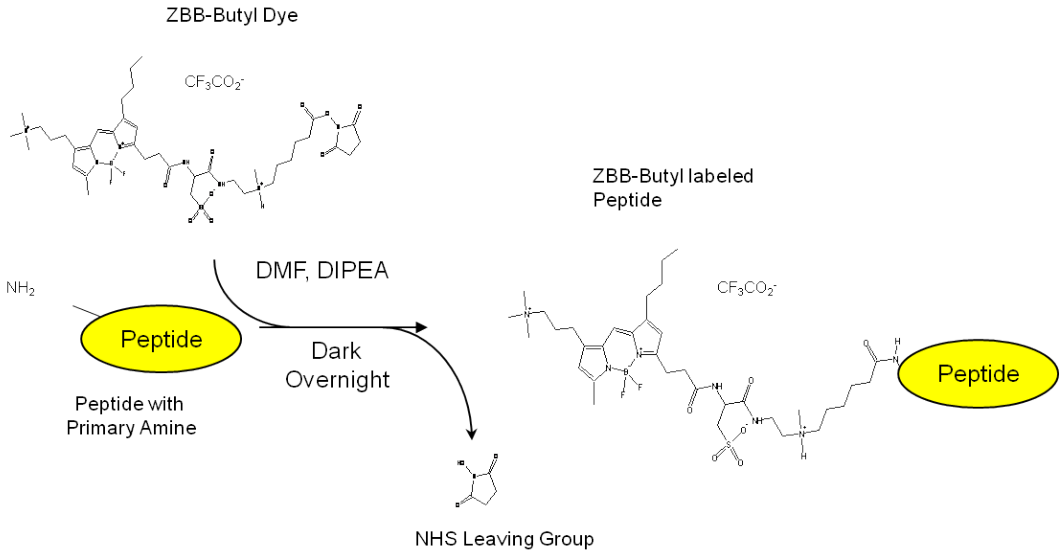

Figure 4.11: Reaction of Zdyes with NHS ester group with an N-terminal alpha amine or epsilon amine from a lysine in a peptide.

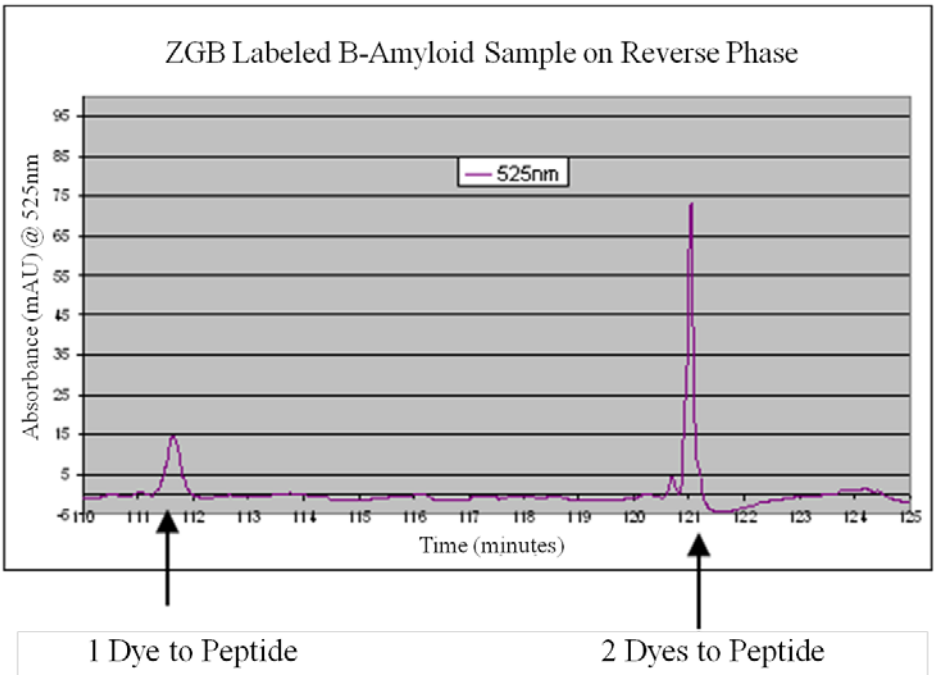

Figure 4.12: β-amyloid (10-20) contains a free N-terminus and a single lysine as potential labeling sites. When saturation labeling was attempted in triplicate, only 67% of the peptide was saturated with two dyes. The other 33% of the peptide was labeled with one dye. No un-reacted peptide was detected. These peaks were identified by mass spectrometry.

Testing of labeling efficiency concluded that we were labeling 67% +/- 5.8% under the maximum labeling conditions that seemed practical. This lack of saturation in labeling was not going to work effectively and pushing the labeling harder would require very large amounts of fluorescent dye.

An alternative approach, blocking the lysine groups by first converting all the lysines to homoarginines was pursued. Reactions with o-methyl isourea have been used to block lysine groups against labeling with the NHS ester linkage, when using tandem mass tag (TMT) reagents for mudpit-style proteomics mass spectrometry experiments (*137, 138*). This lysine guanidinylation procedure has an added bonus in mass spectrometry. The guanidine moiety used to modify lysines to homoarginines, increases the ionization of the peptides that have been modified in both MALDI and electrospray ionization (ESI) (*139, 140*). This modification is readily identifiable in MS as being different then the arginine molecular weight, and thus can readily be determined as originally being a lysine (*139, 140*).

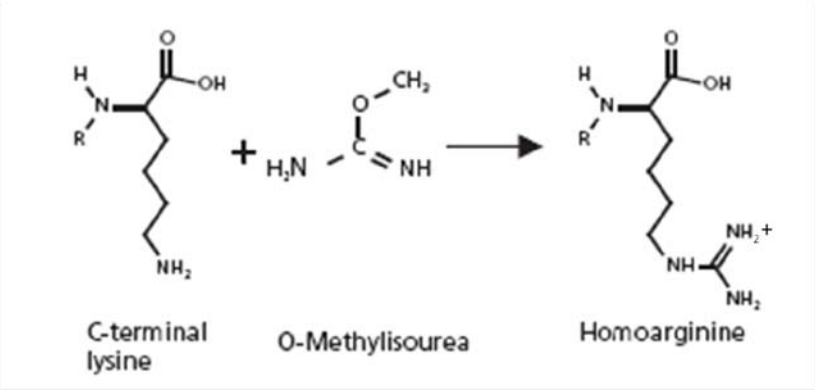

Figure 4.13: Reaction for conversion of a lysine to a homoarginine by reacting with o-methyl isourea under basic conditions. This reaction does not appear to modify the N-terminal amine in practice, with the exception of proline (*141*). The guanidine moiety adds an additional 42 daltons peptide for each lysine modified.

The conversion of peptide lysine groups to homoarginine was carried out as follows. First the peptides were solublized in 10 - 50 uL of DMF. To this solution 1mL of 0.5 M o-methyl isourea pH 10.5, adjusted with sodium hydroxide, were added. The reaction was performed overnight at room temperature. The sample was then desalted on a RP C12 column and the peptide fraction was collected, frozen, and lyophilized to dryness.

This reaction was tested on the model peptides β-amyloid (10-20) (MW = 1446.7), apelin 12 (MW = 1422.7), and = angiotensin II (MW = 1046.2). The first two contained a single lysine group as well as an N-terminal amine. Angiotensin II has no free lysine and contains only the N-terminus as a possible site for a guanidylation reaction site. The expected mass shift is 42 daltons if only one guanidine moiety is added, and guanidinylation should only occur on the lysine groups (*141*).

Figures 4.14 and 4.15 were measured to determine the completion of the reaction using MALDI.

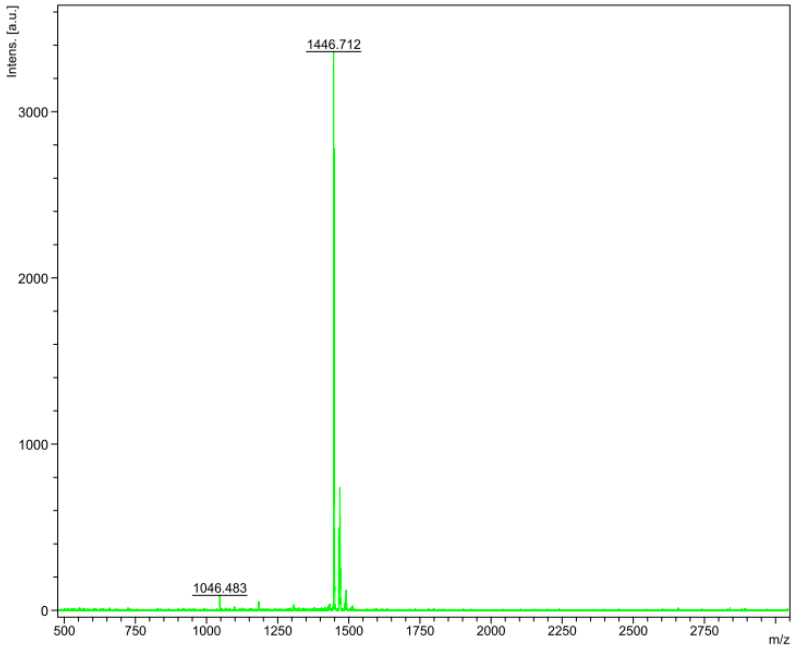

Figure 4.14: A MALDI analysis of unmodified β-amyloid and angiotensin II peptides. Mass 1046.2 m/z is angiotensin II and 1446.7 is the β-amyloid. Angiotensin II has been added at 10% the concentration. The mass error on the MALDI calibration is <0.3 daltons in this data.

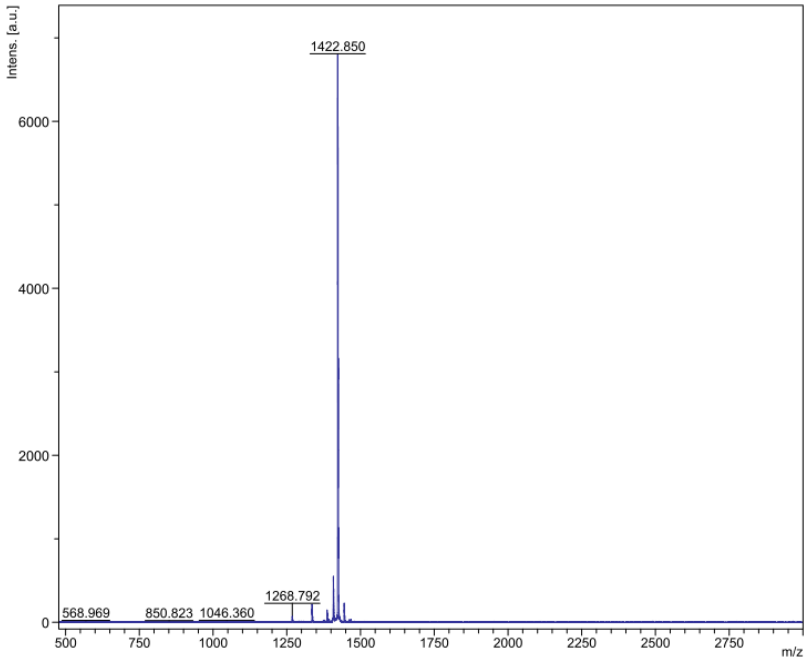

Figure 4.15: MALDI analysis of unmodified apelin 12 and angiotensin II. Mass 1046.2 m/z is the angiotensin II. Angiotensin II has been added at 10% the concentration. Mass 1422.7 m/z is the apelin 12. The mass error on this data is <0.2 daltons.

After the homoarginine reaction the peptides were analyzed by MALDI-TOF as shown in figures 4.16-4.19.

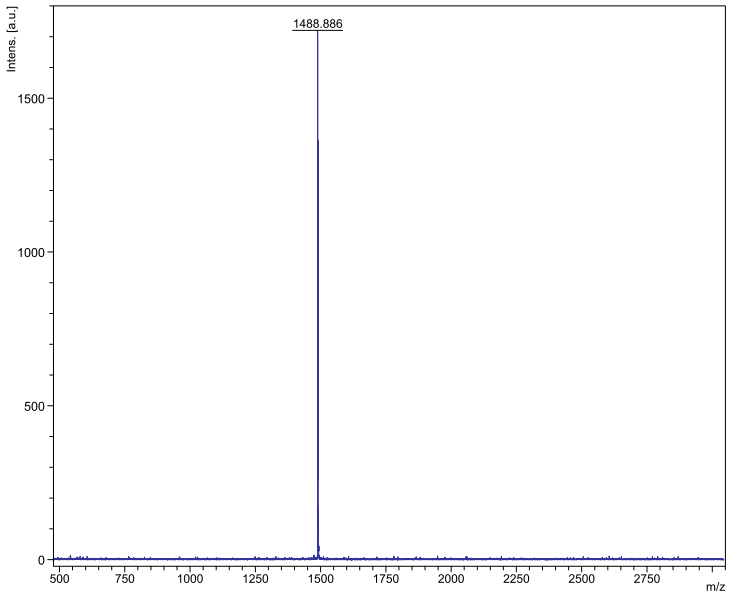

Figure 4.16: MALDI analysis of a mixture of β-amyloid and Angiotensin II after guanidylation. The β-amyloid homoarginine was measured by MALDI at the 1488.7 m/z. No residual unmodified 1446.7 m/z peak was found. The peak of the angiotensin II, present in the sample, was not visible on this zoom setting. Since it was not modified by the treatment and the guanidylated peptides fly extremely well.

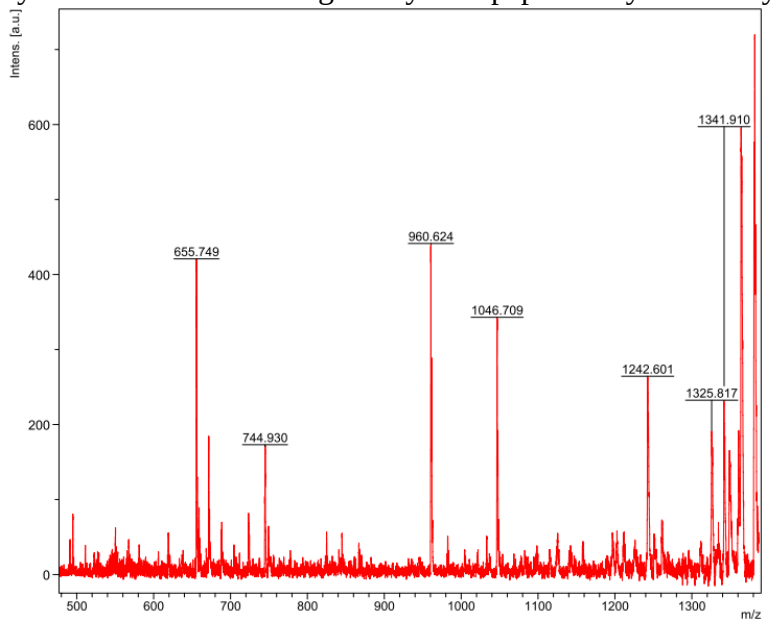

Figure 4.17: MALDI analysis of a mixture of β-amyloid and Angiotensin II after guanidylation. The N-terminus of angiotensin II was not modified, which would be

(Figure 4.17 continued) expected at 1088.7 m/z under the reaction conditions for guanidylation, since only the unmodified peak 1046.7 was found. The relative peak intensity of the angiotensin II dropped substantially after guanidinylation. This was likely because the β-amyloid was ionizing more efficiently due to the guanidine moiety attached. Other peaks are considered to be impurities.

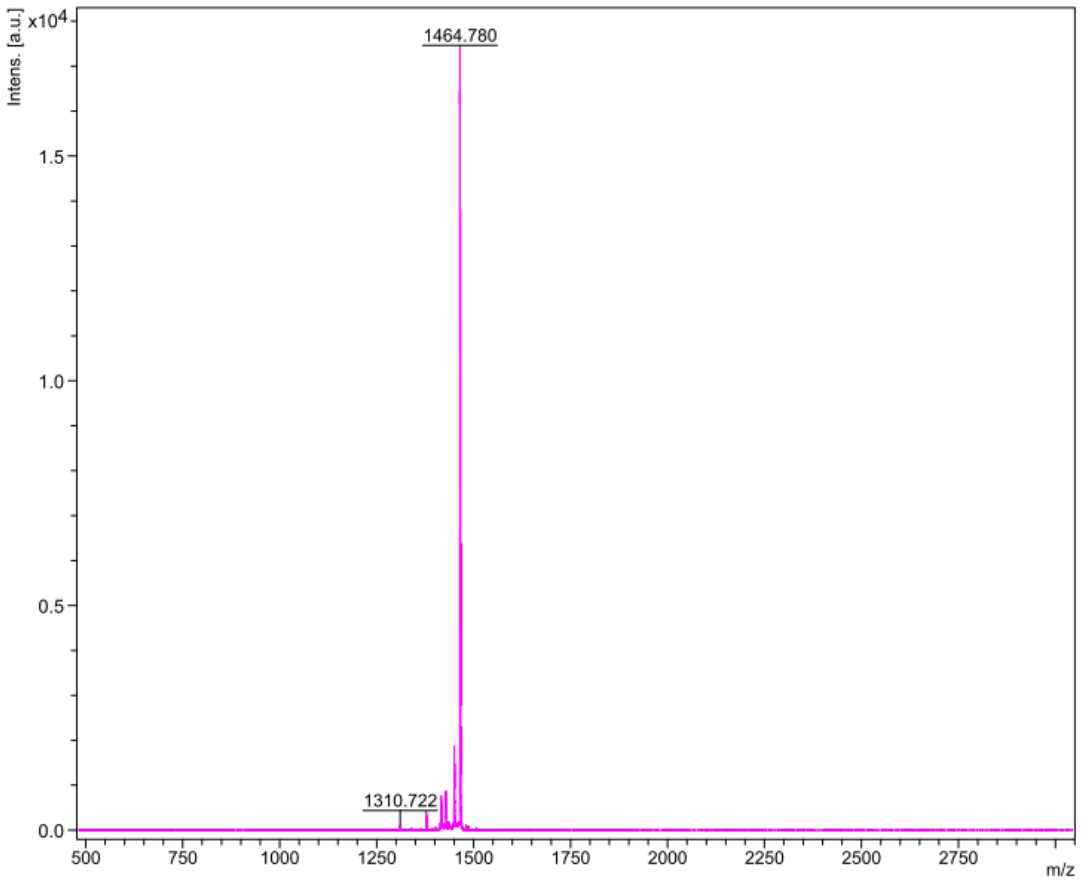

Figure 4.18: MALDI analysis of a mixture of apelin 12 and angiotensin II after guanidylation. The apelin 12 homoarginine was observed by MALDI. No residual unmodified 1422.7 m/z peak was found while the expected homoarginine modified peak was found at 1464.7 m/z. The angiotensin II, present in the sample, was not visible at this zoom setting due to the strong signal from the guanidylated apelin 12.

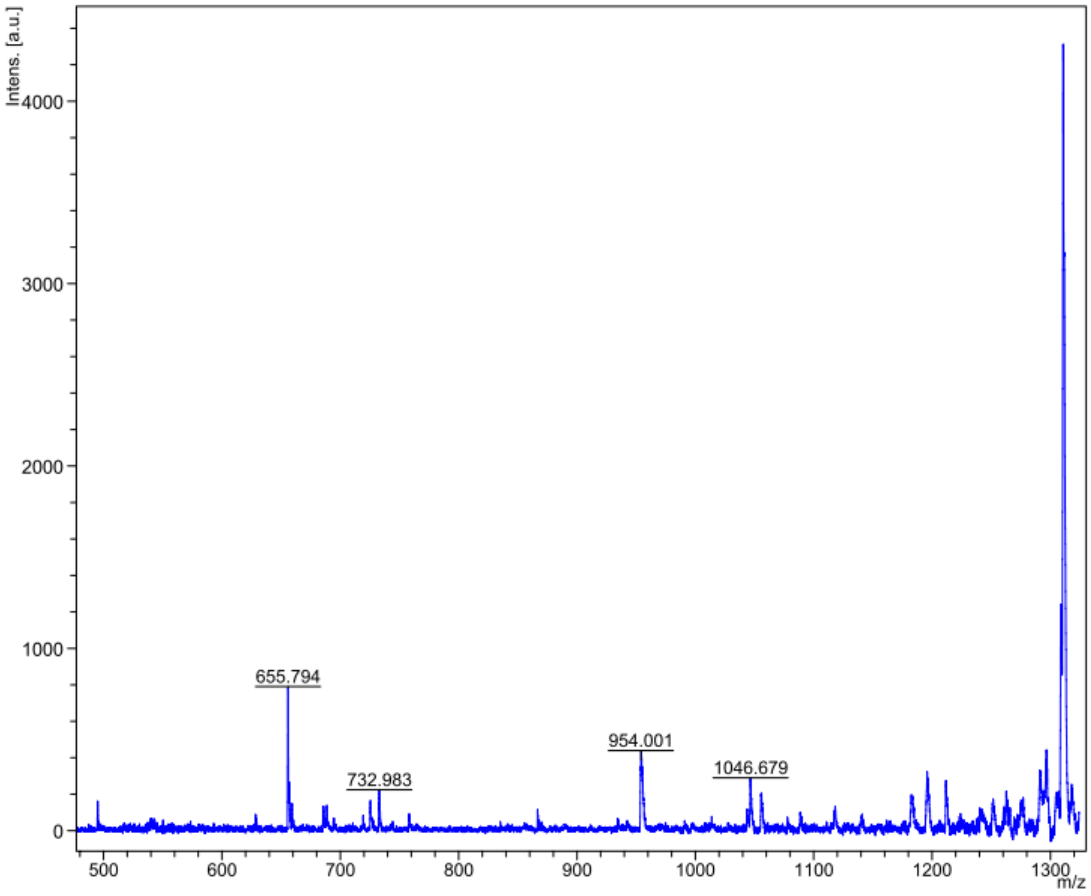

Figure 4.19: MALDI analysis of a mixture of apelin 12 and angiotensin II after guanidylation. The N-terminus of angiotensin II was not modified, which would be expected at 1088.7 m/z under the reaction conditions for guanidylation, since only the unmodified peak 1046.7 was found. Angiotensin II peak intensity dropped substantially. This was likely because the apelin 12 was ionizing more efficiently due to the guanidine moiety attached. Other peaks are considered to be impurities.

After modifying the lysines on these model peptides to homoarginine, they were then reacted on their N-terminus with a fluorescent dye, ZB-Butyl from the Greico group, as previously described, and the products separated by RP HPLC. It was expected that only one dye labeled peak for each homoarginine model peptide would be observed by fluorescence. One main peak of β-amyloid homoarginine with a bound ZB-Butyl dye

was detected, as can be seen in figure 4.20. This peak was collected from the HPLC and analyzed on the Bruker AutoFlex III MALDI TOF/TOF. The MS shown in figure 4.21 was 2224.9 m/z as expected. This MS/MS in the Autoflex III was able to sequence the peptide backbone as shown in figure 4.22. A National Center for Biotechnology Information (NCBI) basic local alignment search tool (BLAST) was able to correctly identify this MS/MS fragmentation as β-amyloid, using the partial amino acid sequence found from the MALDI MS/MS as shown in figure 4.23.

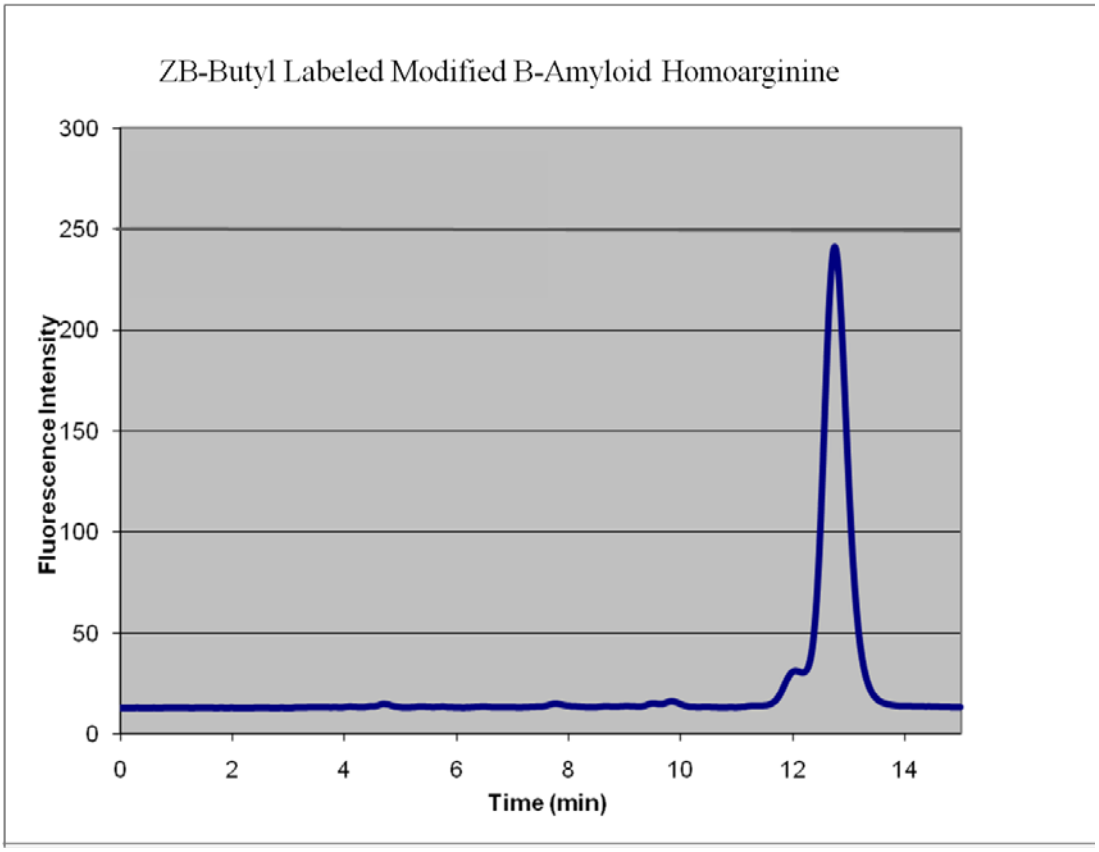

Figure 4.20: HPLC trace of ZB-Butyl labeled homoarginine modified β-amyloid run on RP -C12. Fluorescence excitation for detecting the ZB-Butyl used 512nm excitation and 520nm emission.

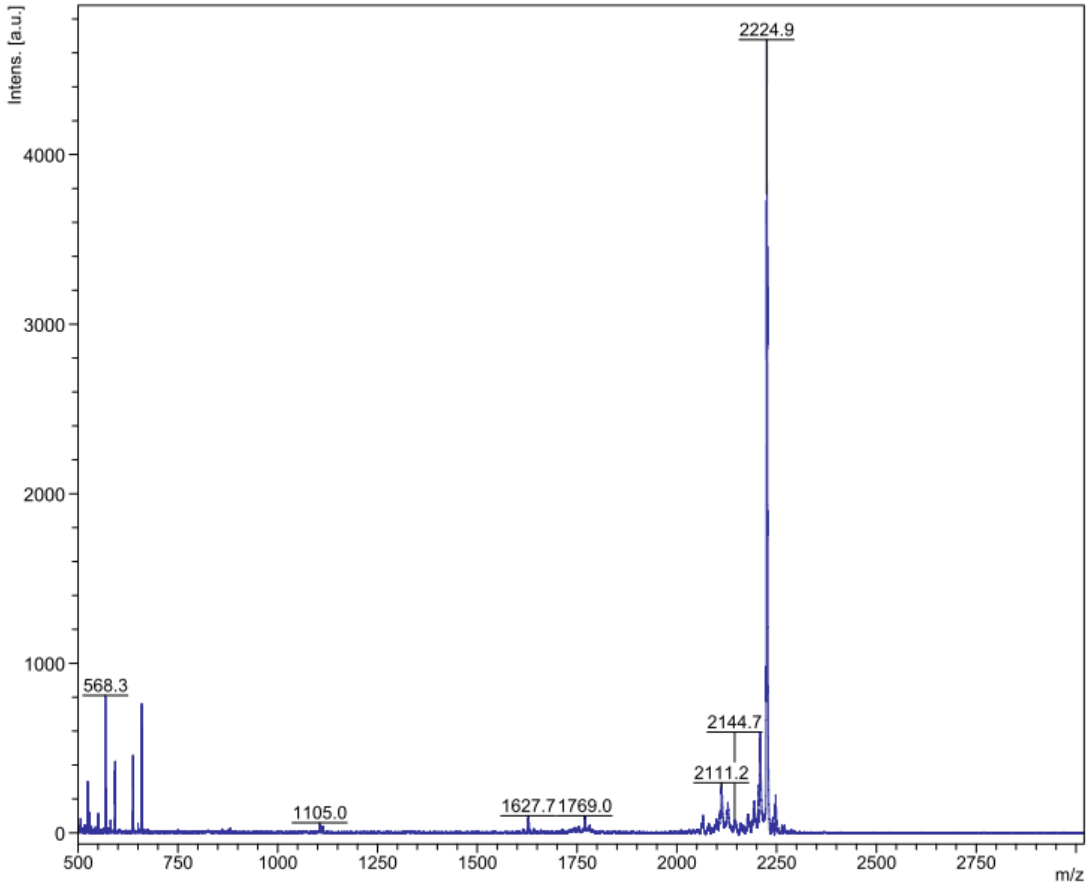

Figure 4.21: MALDI-TOF analysis of ZB-Butyl labeled homoarginine of the modified β-amyloid isolated from RP-C12. The mass of 2224.9 m/z matches that expected for a single ZB-Butyl attached to the N-terminus of the homoarginine modified β-amyloid peptide.

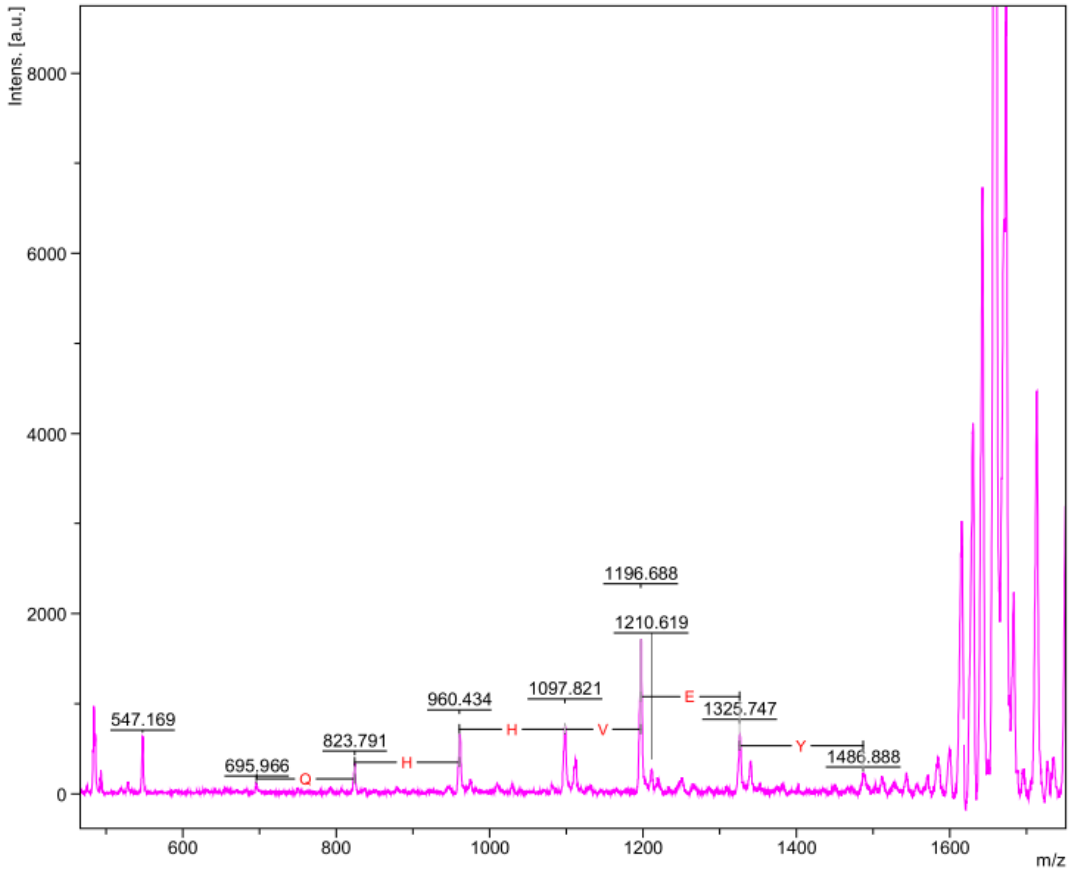

Figure 4.22: The 2224.9 m/z parent peak of the ZB-Butyl labeled homoarginine modified β-amyloid peak as fragmented in the Bruker Autoflex III MALDI TOF/TOF. The sequence information that can be read off the mass fragments is YEVHHQ and identifies this peptide as the β-amyloid starting material.

Figure 4.23: NCBI protein BLAST search of the amino acid sequence YEVHHQ derived from the ZB-Butyl labeled homoarginine modified β-amyloid MALDI TOF/TOF data. All of the scores for matches to this sequence were equivalent. Many of the hits were for very similar amyloid peptides. Several hits on an unnamed protein were also identified. These alternate identities illustrate the difficulty of absolute identification of a single peptide with only short partial amino acid sequence coverage.

Using the combination of the techniques we have described allows the identification of a LMW peptide in the < 5kDa peptidome fraction, although measures would have to be taken to obtain longer peptide sequences, perhaps by electron transfer disassociation (ETD) analysis. The lysines in the peptides are first converted to a homoarginine and the free N-terminus of the peptides are labeled with a fluorescent NHS dye, where we were able to obtain an acceptable 67% labeling on the N-terminus of the peptide. These peptide MS peaks can then be identified using the MALDI-TOF/TOF and a BLAST search, although additional MS analysis may be needed for firm identifications.

Coeluting Dye – Strong Cation Exchange Fraction

The principal aim of our study was to use two different colored fluorescent dyes to label peptides and measure differences between T2D and HC samples in a two-dimensional (2D) HPLC approach. This meant we needed to identify or design two different colored dyes that elute identically in the first dimension [strong cation exchange (SCX)] as well as the second dimension RP separation.

In this approach the cationic character of the molecule interacts with the SCX anionic resin (*142*). The molecule is then eluted using a stronger cationic buffer (*142*), which is usually a salt. Because salt solutions, when evaporated, require liquid to resolublize the salts as well as the sample, it is advantageous to select volatile salts for a study such as this. In this way, the amount of liquid required to resolublize the sample

before moving to the next dimension of separation RP is minimal. We selected ammonium formate as our volatile cationic salt.

A concern we encountered early on was that the free net neutral dye was retaining on the SCX column. The SCX packing material has some hydrophobic character with which the somewhat hydrophobic dye was interacting. This interpretation seemed clear because when we increased the ACN this interaction of the free dye with the SCX support was eliminated. The dye molecule prefers the organic phase to the column's slightly hydrophobic stationary phase. The cationic peptides with bound dye were still attracted to the anionic stationary phase.

The SCX buffers selected for eluting the fluorescent dye labeled peptides were optimized with organic salts and varying percents of ACN to achieve desirable elution charcteristic. These results can be seen in figures 4.24-4.27. At 15% ACN, the column did not interact with the net neutral free dye, which flowed straight through, but allowed the dye labeled cationic LMW peptides to be retained on the column. Buffer B, containing ammonium formate salt, eluted the dye labeled peptides. Figure 4.28 demonstrates separation of a digest of a small protein, aprotin, which was labeled with the fluorescent dye.

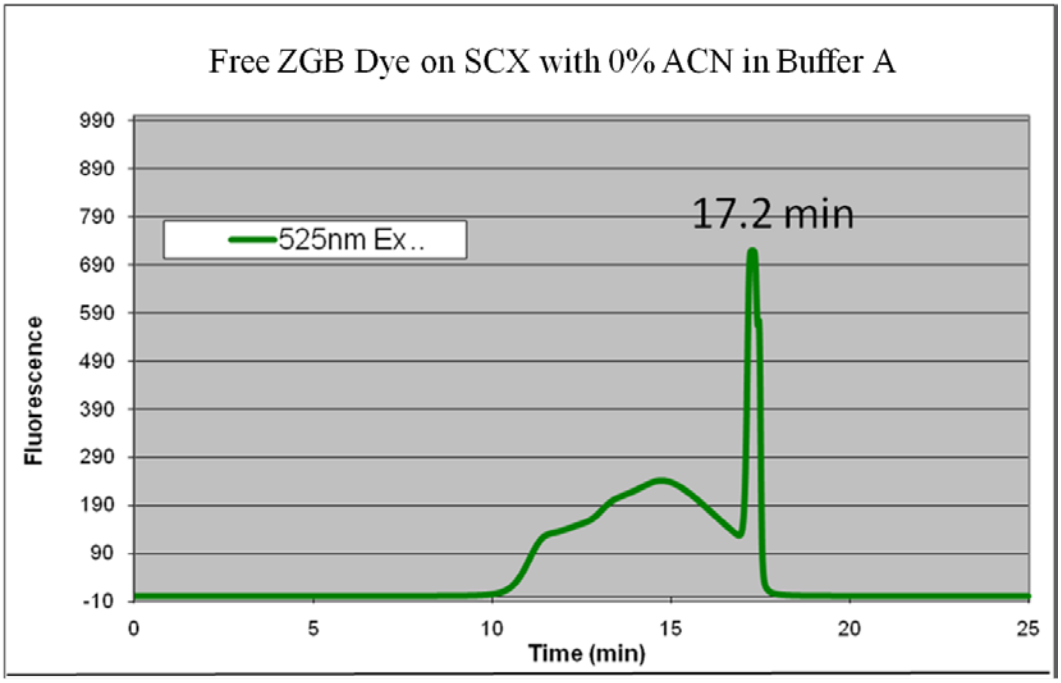

Figure 4.24: Free ZGB is attracted to the stationary phase of the SCX column at 0% ACN in buffer A.

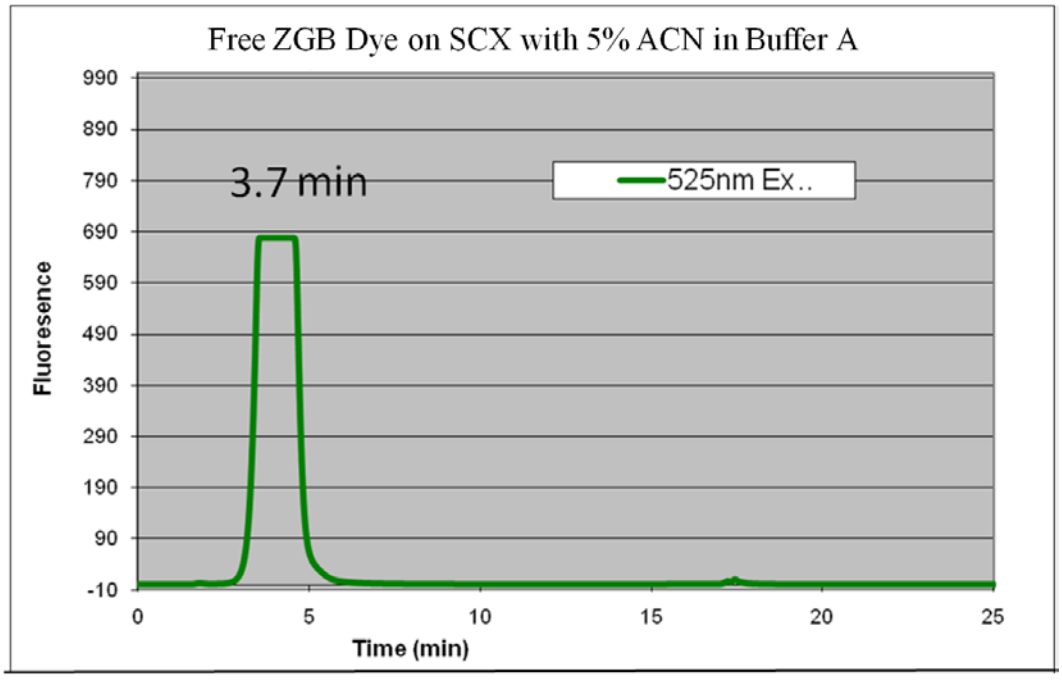

Figure 4.25: Free ZGB is barely attacted to the stationary phase of the SCX column with 5% ACN in buffer A.

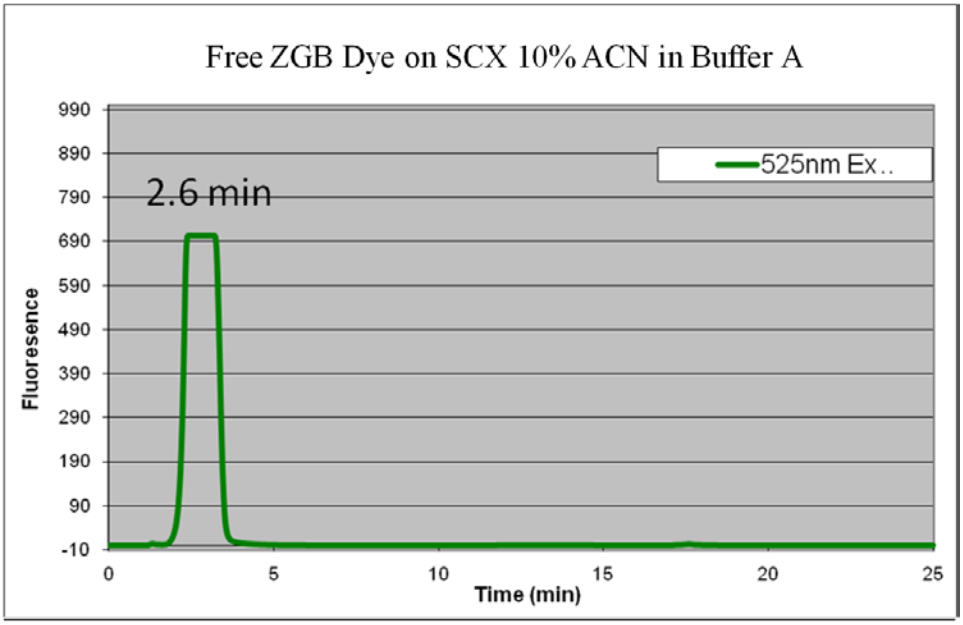

Figure 4.26: A very weak interaction of the free ZGB with SCX column can be seen in buffer A with 10% ACN. This elution time appears close to the void volume of the column

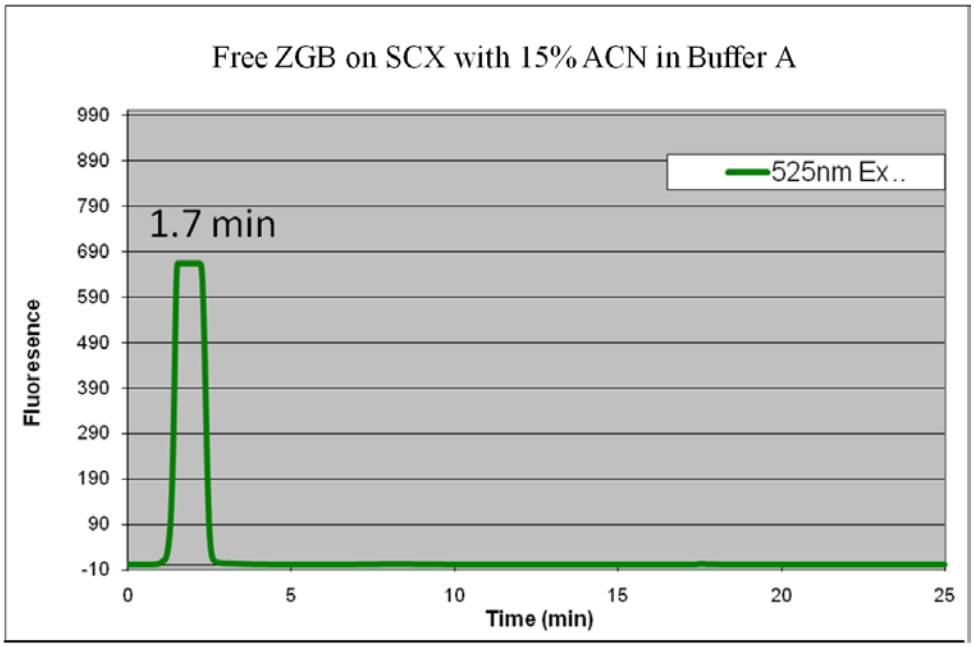

Figure 4.27: At 15% ACN the free ZGB is not interacting with the SCX column. The retention time corresponds to the void volume for the column.

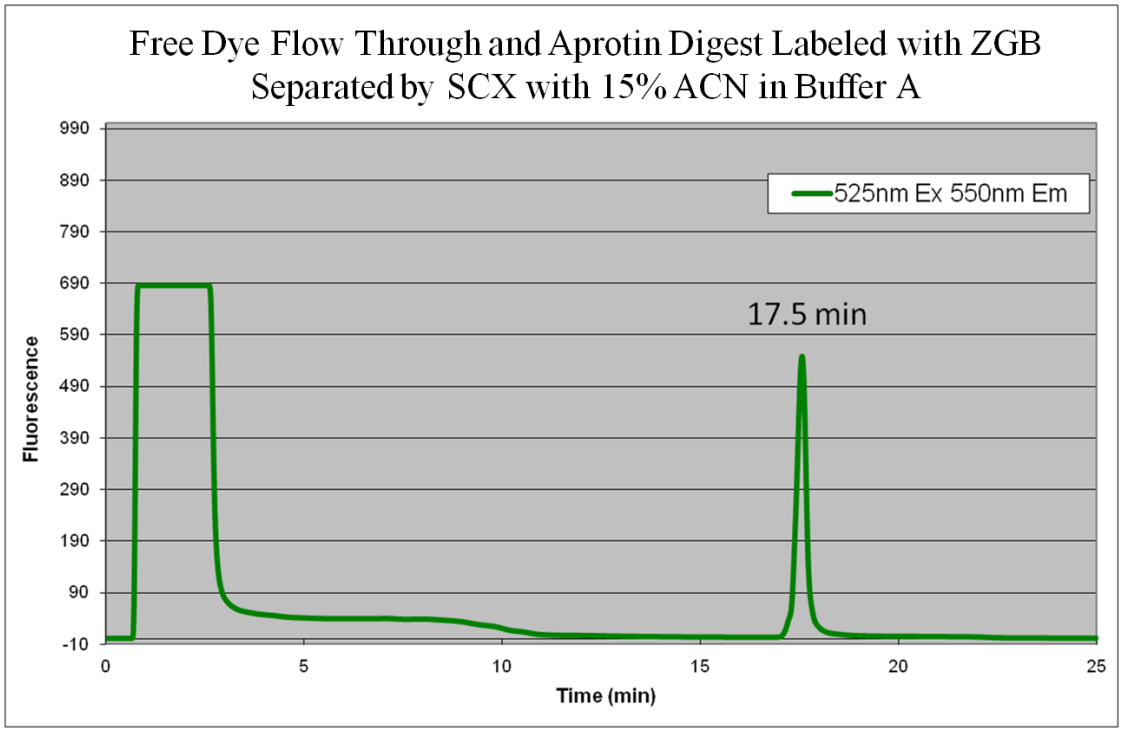

Figure 4.28: The ZGB labeled peptides from the aprotin digest are retaining much later then the eluting free dye on SCX in 15% ACN. The retention time for the first large peak containing the free Zdye corresponds to the void volume for the column.

Coeluting Dyes on SCX and Reverse Phase

Optimization in the RP dimension for a two color differential fluorescent dye labeling study requires selecting two dyes with different fluorescent emission wavelengths that elute at the same time. Two ideal fluorescent dyes would also be excited efficiently by the same wavelength, but emit light in significantly different regions of the color spectrum. Previous work using this general approach has been reported with several different fluorophores in the Imai lab (*143*).

Samples of various Zdyes were examined on reverse phase as shown in figure 4.29.

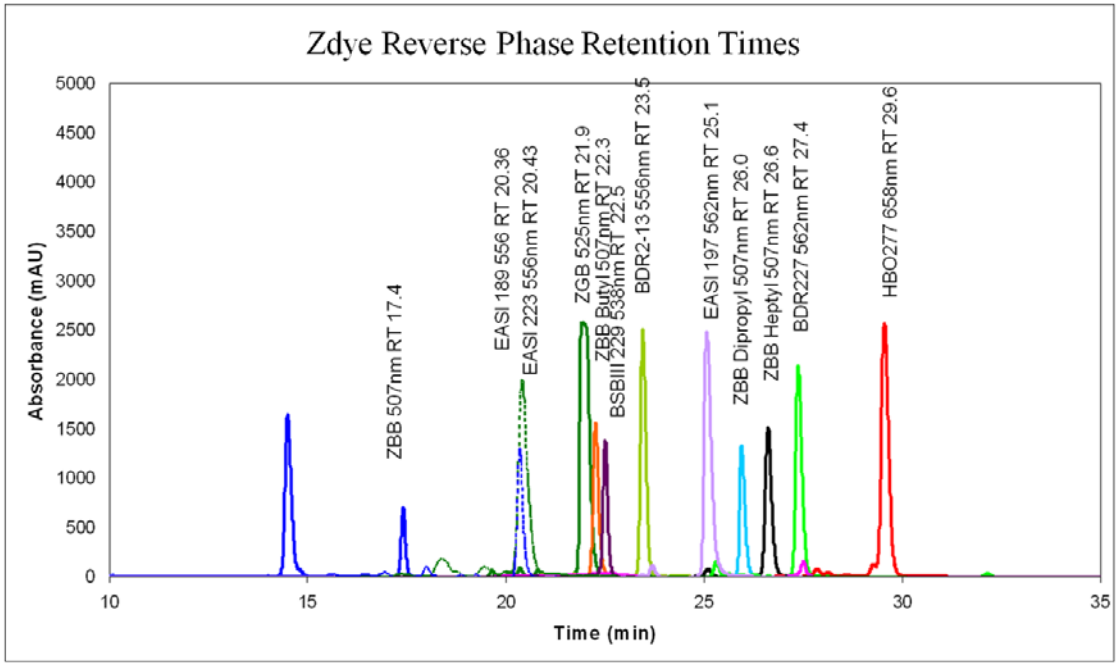

Figure 4.29: RP separations of candidate free Zdyes. The best candidate dyes for this study, based on similar retention time, overlapping excitation, and well separated emission spectra, are ZBB-Butyl (red) and BSBIII-229 (black). Both ZBB-Butyl and BSBIII-229 fluorescent dyes were created by the Grieco lab at MSU. The structures of these Zdyes are shown in figure 4.30 (a, b).

A

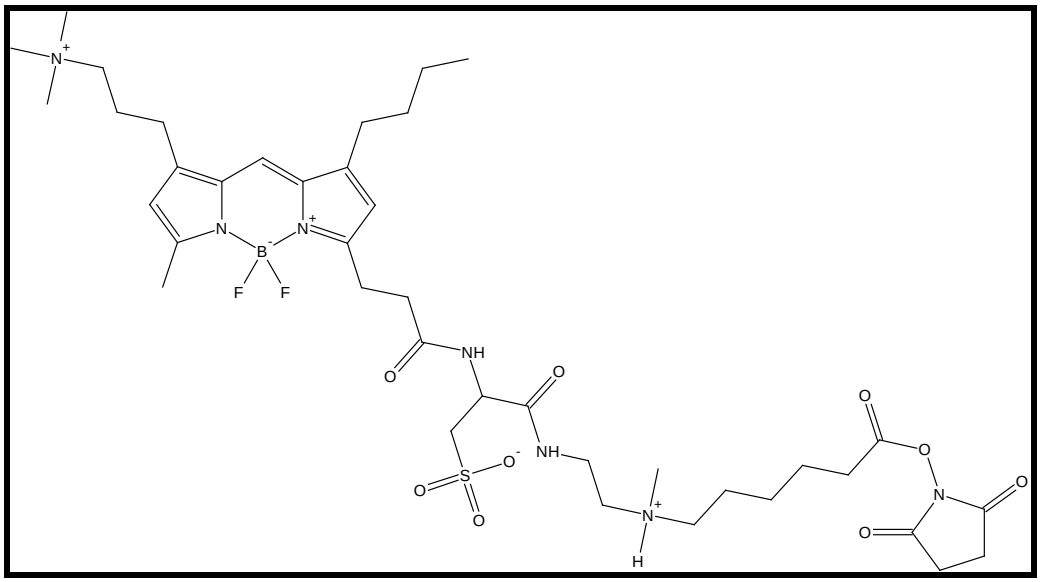

B

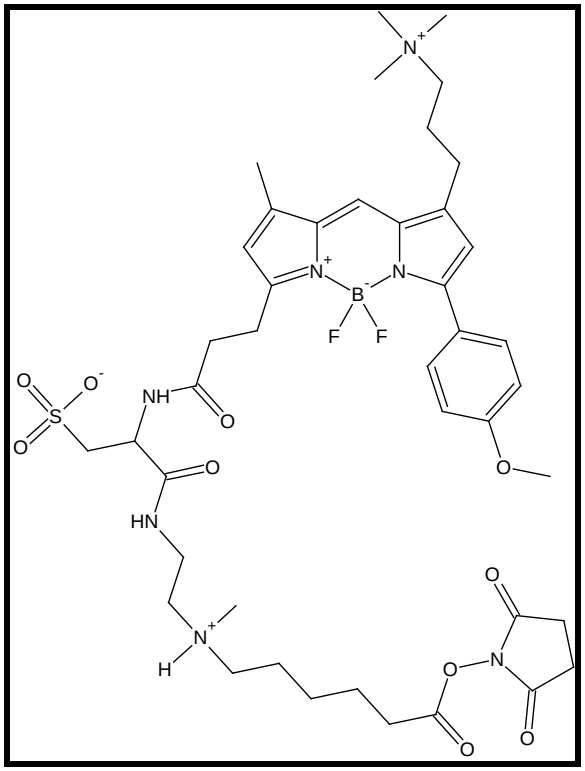

Figure 4.30: (a) Structure of ZB-Butyl which has a maximum excitation 507nm and emission 520 nm (b) Structure of BSBIII-229 which has maximum excitation 536nm and emission 564nm. The two dyes can be co-excitated at 512 nm with a 3% cross talk in the fluorescence emission signals.

When these two dyes were attached to the N-terminus of a homoarginine modified model pepitide and eluted in isocratic conditions, they were separated by 0.6 minutes. Figure 4.31.

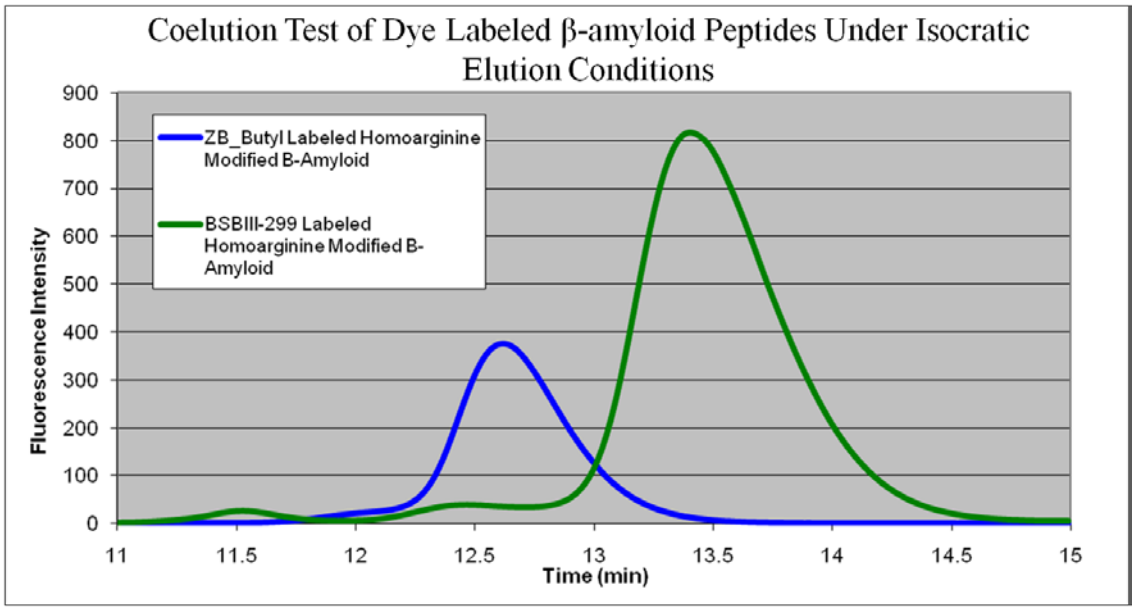

Figure 4.31: β-amyloid labeled with BSBIII-229 or ZB-Butyl are closely matched in elution time under maximum resolution isocratic conditions. The retention time is 0.6 minutes apart from peak maxima to maxima. In practical applications, the elution of a complex peptide mixture will be performed under gradient conditions. With a solvent gradient applied in the chromatography, the retention times of the dye labeled peptides are much closer.

With a peptidomic labeling strategy in place, the separtion of the LMW peptidome by SCX and RP was optimized by adjusting the chromatographic elution solvent to obtain as many resolved peptide peaks as possible. A sample of LMW peptide standards was prepared as follows. A sample of 0.75 mL of plasma was thawed on ice and denatured by adding 2.25mL of 8M urea in 40 mM Bicine pH 8.5. After 30 minutes, 8.6 mg of tris (2-carboxyethyl) phosphine hydrochloride (TCEP) was added to the 3 mL

sample, making a 100 mM TCEP solution. TCEP reduces the disulfides in the sample, allowing further denaturation. 30 minutes later, 47.7 uL of 4.4 M 4-vinyl pyridine was added to the sample, to yield a 700 mM solution. 4-vinyl pyridine is a highly effective alkylating agent, which blocks cysteines from reforming di-sulfides. An additional 32.4 mg of dithiothreitol (DTT) was added 30 minutes after addition of 4-vinyl pyridine to quench the excess alkylating agent, making the final concentration 700 mM of DTT. These high concentrations of reducing and alkylating agents were chosen due to the high concentration of proteins in our samples. Excess quenched reducing and alkylating agents were removed in the SCX fractionation.

Two mL of the sample processed as above, which is dervived from a ½ mL of whole plasma, was injected into a Sephacryl S-100 SEC column, using the method previously described. The LMW fraction was collected between 62 mL and 140 mL. The GE AKTA FPLC employed has an automated fraction collector, which allows for sample collection into 2 mL microfuge tubes. An example of the elution trace was shown in figure 4.6, as described earlier.

The entire LMW peptidome, 78 mL total volume at this stage, was collected in 39 two mL microfuge tubes. To minimize problems with ammonium cyanate formation from urea, fresh, high grade cyanate free urea was used for preparation of the 6M Urea 30 mM pH 8.5 buffer for SEC elution (*144*). After the LMW peptide fractions were collected, the urea was removed from each fraction by RP chromatography in less than 24 hours. Carbamylation of the amino termini of peptides will eventually occur to some extent if the urea is not removed (*144*). Since our down-stream fluorescence

derivatization reaction is aimed at the free N-terminal amine groups, avoiding the carbamylation side reaction is important for sample reproducibility.

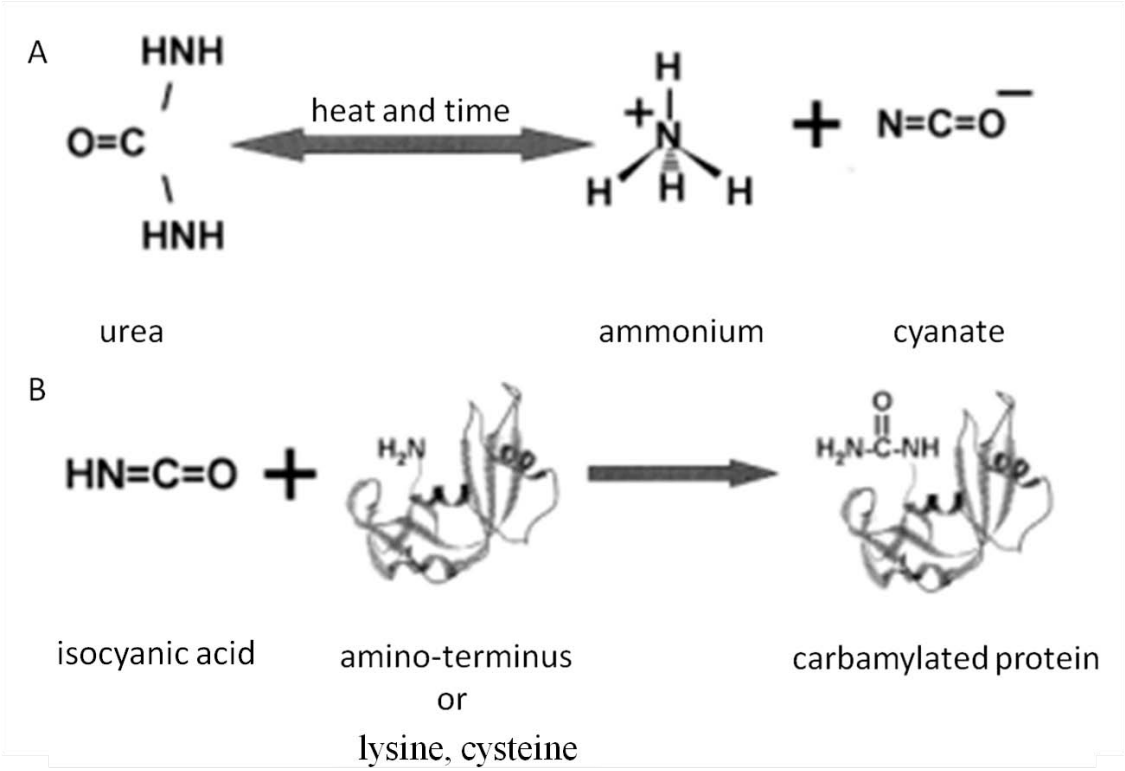

Figure 4.32: Description of the degradation of urea and the resulting carbamylation reaction on proteins. (a) The degradation path of urea is favored by increased temperature, time and high pH; (b) The attack of isocyanic acid on reactive nucleophilic groups in proteins or peptides (*144*).

In order to remove the 6 M urea and salts from each of the LMW peptide fractions, a semiprep RP column (Jupiter 4u Proteo 90 Å, 250 mm x 10 mm) was used. The size of this column allows for high flow rates (2 mL/min), and has a sufficiently high capacity to retain all of the LMW peptides loaded onto it from each fraction.

An Agilent 1100 HPLC system with a manual 3 mL injection loop was used to remove the urea and salts from the SEC fractions. The solvent gradient conditions are

listed in Table 4.2. Buffer A contained 0.1% TFA in water. Buffer B contained 0.1% TFA in ACN. 5 two mL fractions could be loaded onto the RP column in series prior to beginning solvent gradient elution. Fractions of bound LMW peptides from all five injections were found to elute together between 31-35 minutes after the start of the gradient, and were collected in a 15 mL falcon tube. These tubes were frozen and lyopholized to dryness. Thus in 8 consecutive HPLC runs, the urea could be removed from all of the fractions containing the LMW sample.

Table 4.2: The RP method used for removing urea from LMW peptide SEC fractions on HPLC. A Jupiter 4u Proteo 90A, 250mm x 10mm RP C12 column was used.

Time (minutes)	% Buffer B (0.1% TFA ACN)
0	0
15	0
15.01	5
19.5	5
24.5	30
24.51	30
29	100
32	100
37	0

These urea stripped samples were then guanidylated to convert the lysine side chains to homoarginines, as previously described, followed by labeling at the N-terminus with 6 molar excess NHS ester fluorescent dye. Peptide quantification with common protein assays was determined to be problematic. Protein assay methods supplied by Pierce, Thermo Scientific (Rockford, IL) bicinchoninic acid (BCA) (*145*), and Bradford protein assays (*146*) reacted with other metabolite compounds and free amino acids,

over-estimating the apparent peptide concentration value. Amido black uses precipitation to determine the protein concentration (*147*). The precipitation reaction does not precipitate all of the LMW peptides and is thus not quantitative. Attempts to quantify the peptides using the absorbances of the 214 nm amide bond or 280 nm aromatic amino acid signal were uninformative, because of interference from the 4-vinyl pyridine alkylating agent attached to the peptides. The excess alklyating agent, which is not removed until after the SCX fractionation step, also absorbs strongly at 214nm and 280nm. Dye labeling is performed prior to SCX.

To estimate the molar concentration of the LMW peptides, we chose to follow a procedure that several other peptidomics papers had used, based on the hypothesis that 1% of the protein in plasma consists of LMW peptides (*122*). Thus ½ mL plasma, which contains approximately 70 mg of protein/mL (*148*), would have 350ug of LMW peptides. An approximate average weight of 4 kDa for the mass of the peptide translates to approximately 90 nMoles of peptide per sample. We found that only 1/10th of the LMW peptide fraction was needed for sufficient signal to visualize chromatograms for the fractionated peptidome using fluorescence detection. Thus 10 nMoles of the LMW peptidome required 60 nMoles of dye to approach saturation labeling of the N-terminal sites.

To prevent the boron from popping out of the Bodipy-bound Zdye structures, which stops fluorescence, it was discovered, that after labeling was completed in mild base, addition of 200 uL of 20% formic acid changed the pH rapidly enough to avoid this

problem. A 220 uL homoarginine capped and N-terminal fluorescently labeled LMW peptide sample was prepared as described for separation and fractionation by SCX.

Many methods of chromatographic separation were tested, and the best separations of the LMW peptidome will be discussed.

A polysulfoethyl A column, 4.6mm x 50mm, 5u, 200A from the Nest Group (Southborough, MA), was used for all SCX trials. The most clearly resolved SCX gradient conditions were a gradient lasting 110 minutes, as shown in table 4.3. A guanidylated sample of LMW peptides that had been split in ½ and each ½ N-terminally labeled with ZB-Butyl and BSBIII-229, was combined, and run on SCX, as shown in figure 4.33. This level of SCX fractionation produced RP traces shown for each SCX fraction in Figures 4.35-4.44. A total of 409 fluorescent peaks were found using this method. By examining these traces, it can be observed that plots of labeled LMW peptides appear to follow the same chromatographic peak features in SCX and RP with few exceptions. However, baseline resolution, between peaks that would be required to quantify differences in specific peaks, was not obtained.

The resolution of peaks in the RP was so limited, it is questionable that specific peptides in the peaks could be indentified as changing between T2D and HC samples. We estimate that there are approximately 12 peptides per peak, if the previously published 5000 peptides in the human peptidome is a reasonable estimate (*101, 149*). If we collected 1 minute fractions throughout the run, the average fraction would contain 6 peptides. This assumes that every peptide was separating equally across the elution regions, which is clearly not correct from the appearance of the profile. Some of the

peaks are expected to contain many more peptides then the average. To estimate the number of peptides in the peaks we carried out MALDI analysis on several peaks. Figure 4.45 shows an example of a MALDI spectrum that assesses the peptide composition of a typical RP fraction, and which makes it clear that the peak complexity in each RP fraction was too rich to utilize this method to quantify differences of individual peptides between T2D and HC.

Another sample of LMW peptides that had been guanidylated was split into two aliquots, and each aliquot was labeled separately with ZB-Butyl and BSBIII-229. The two colored labeled fractions were combined, and run on SCX using and extended step gradient shown in figure 4.34. The gradient conditions are shown in table 4.4. It is readily apparent that the isocratic solvent steps were not sufficient to allow these SCX fractions to resolve to baseline. In fact, the same features that had been observed in the shorter SCX run in figure 4.33, are found to be broader, using the gradient. The separation in figure 4.34 will not translate into better resolved peaks in the RP, and will just produce more fractions to run.

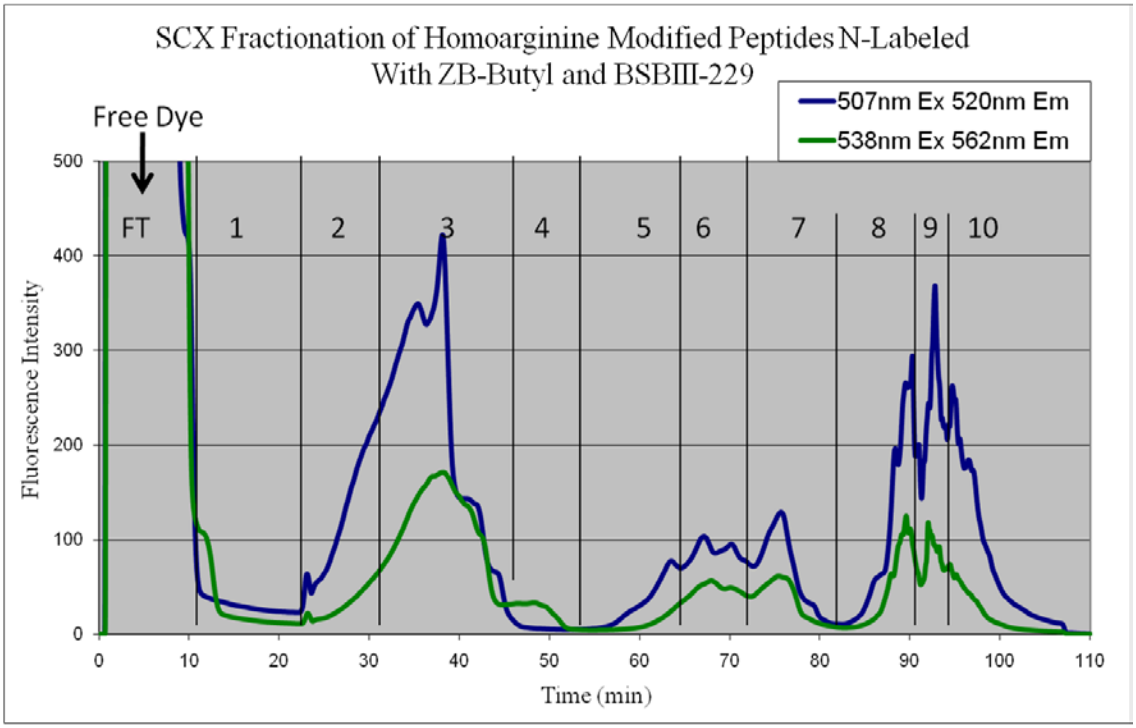

Figure 4.33: SCX separation of homoarginine modified HC LMW peptides labeled with ZB-Butyl and BSBIII-229. Ten fractions were taken for analysis by RP-HPLC.

Table 4.3: The SCX gradient that produced the most clearly resolved LMW peptides. Solvent A is 0.1% Formic Acid and 15% ACN. Solvent B is 0.8 M ammonium formate pH 3.0 with 25% ACN.

SCX Gradient	
Flow	1 mL/min
Time	%B
0	0
20	0
20.01	2
70	12
85	25
95	100
105	100
105.1	0
110	0

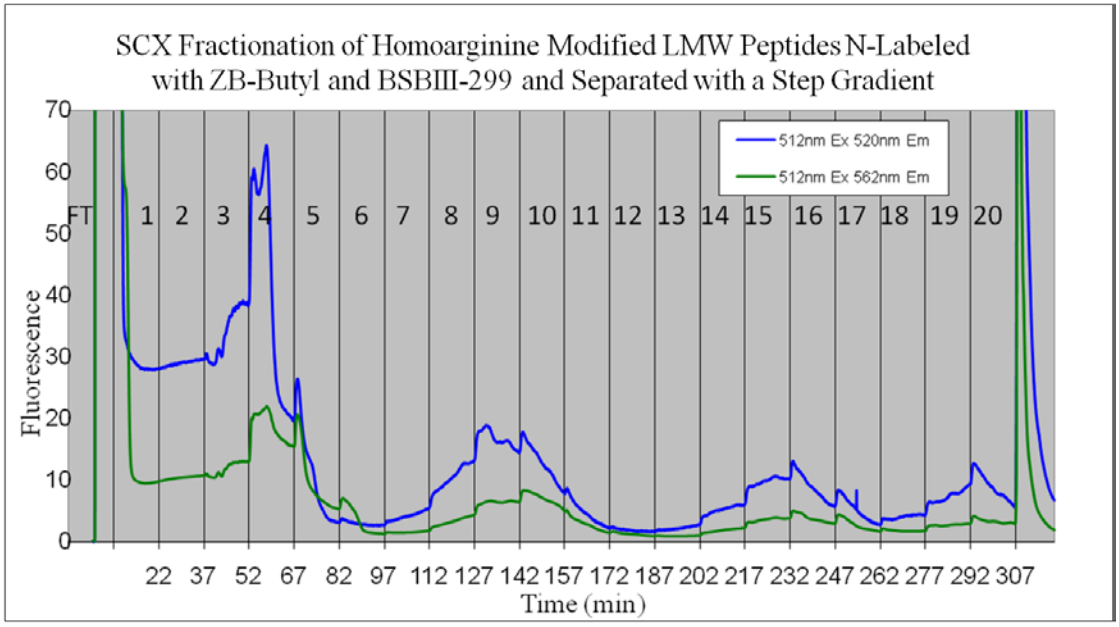

Figure 4.34: SCX separation of homoarginine modified LMW peptides from HC labeled with ZB-Butyl and BSBIII-229. Twenty fractions were taken for analysis by RP-HPLC. It is clear that the gradient could have usefully been extended, because fraction 20 contains an abrupt transition, which eluted a great deal of material that presumably could have been separated further.

Table 4.4: SCX gradient extended from conditions used in table 4.3 to utilize a step gradient with much finer steps and longer dwell times at each step. Though individual fractions did not resolve each peak to baseline, as shown in Figure 4.34, cuts were taken every 15 minutes. Solvent A is 0.1% Formic Acid and 15% ACN. Solvent B is 0.8 M ammonium formate pH 3.0 with 25% ACN.

Grad Conditions			Grad Conditions (continued)		
Frac	/Time	% B	Frac	/Time	%B
FT	/0	0			
1	/20	1	11	/170	11
2	/35	2	12	/185	12
3	/50	3	13	/200	14
4	/65	4	14	/215	16
5	/80	5	15	/230	18
6	/95	6	16	/245	21
7	/110	7	17	/260	24
8	/125	8	18	/275	27
9	/140	9	19	/290	30
10	/155	10	20	/305	100

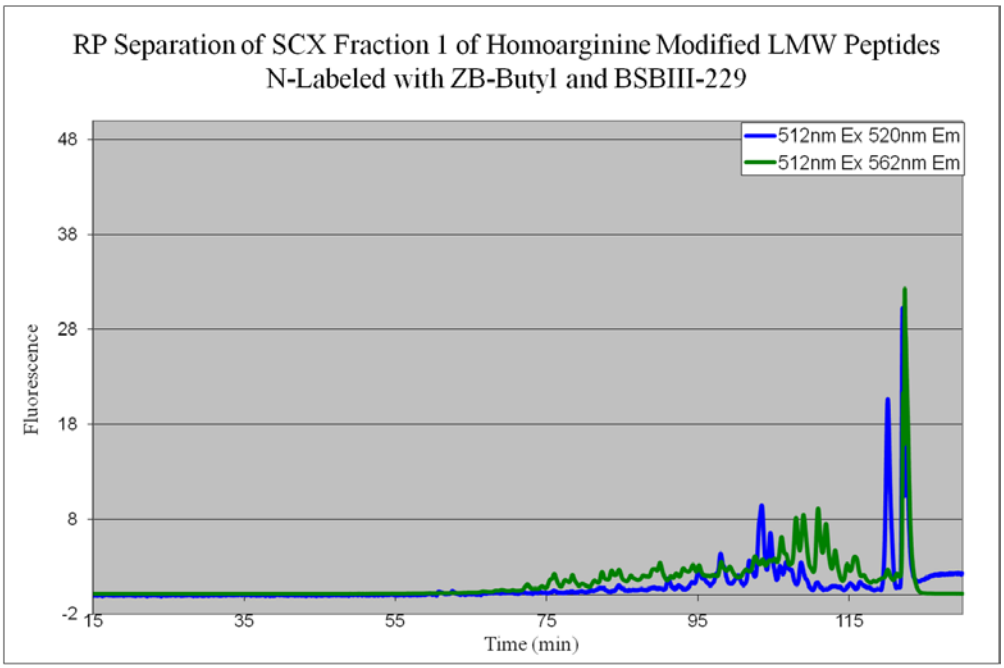

Figure 4.35: RP analysis of SCX fraction 1 shown in figure 4.33 from homoarginine modified LMW peptides from HC samples N-labeled with ZB-Butyl and BSBIII-229. 31 peaks were identified.

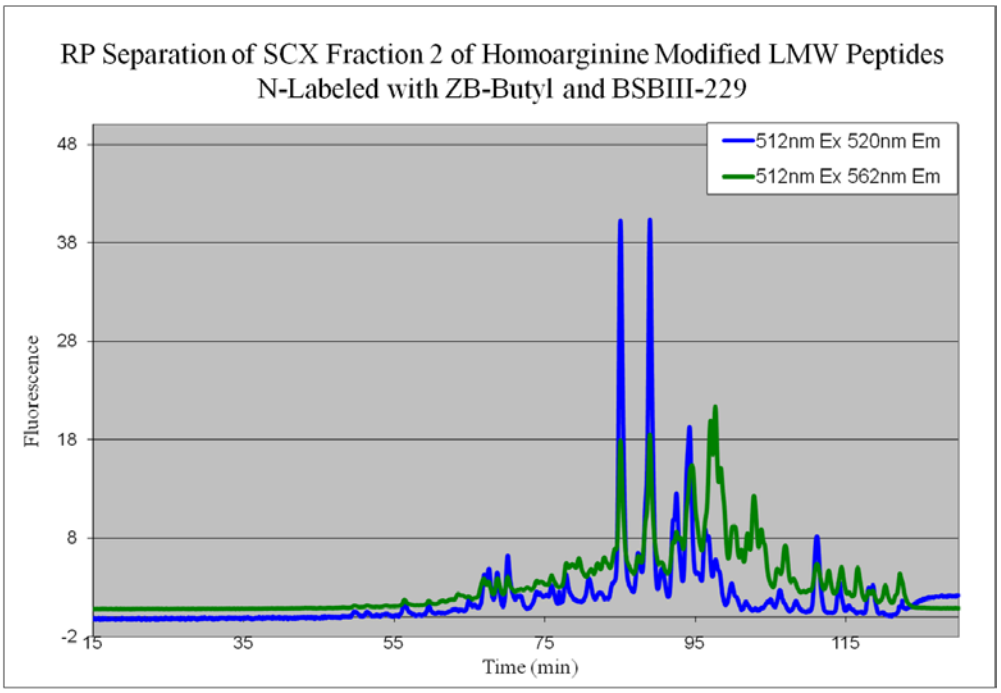

Figure 4.36: RP analysis of SCX fraction 2 shown in figure 4.33 from homoarginine modified LMW peptides from HC samples N-labeled with ZB-Butyl and BSBIII-229. 38 peaks were identified.

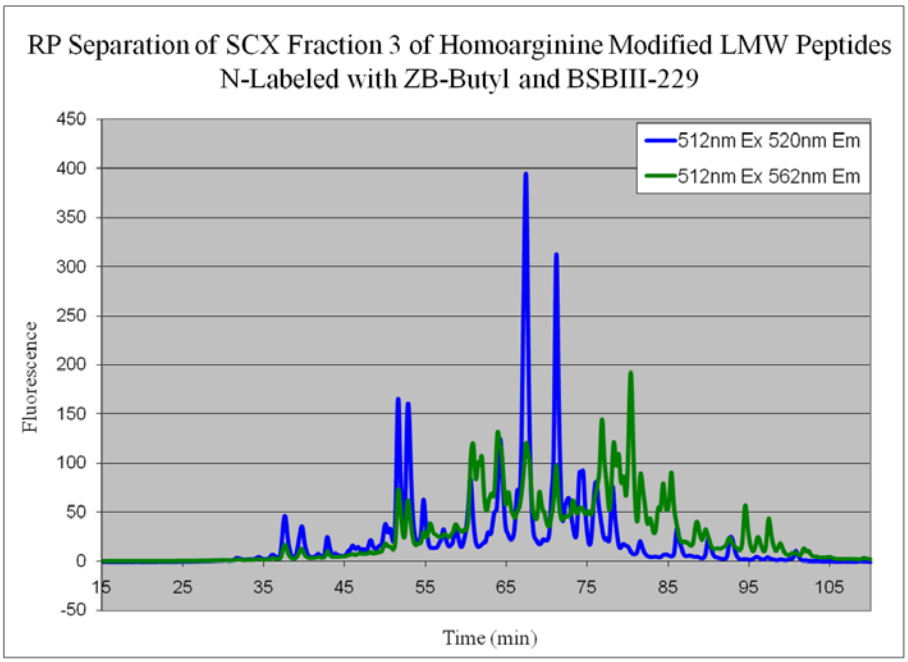

Figure 4.37: RP analysis of SCX fraction 3 shown in figure 4.33 from homoarginine modified LMW peptides from HC samples N-labeled with ZB-Butyl and BSBIII-229. 34 peaks were identified.

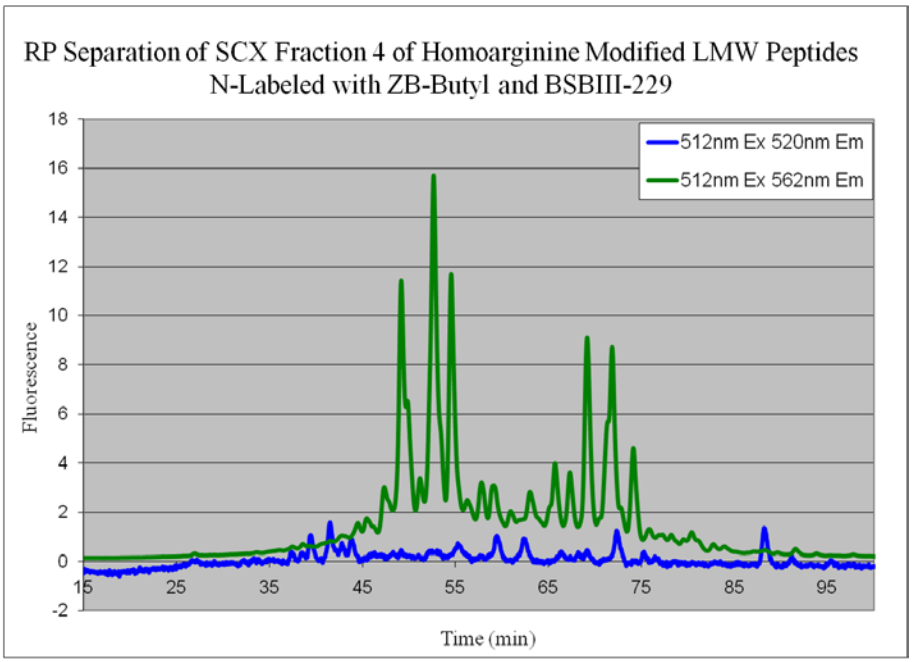

Figure 4.38: RP analysis of SCX fraction 4 shown in figure 4.33 from homoarginine modified LMW peptides from HC samples N-labeled with ZB-Butyl and BSBIII-229. 32 peaks were identified.

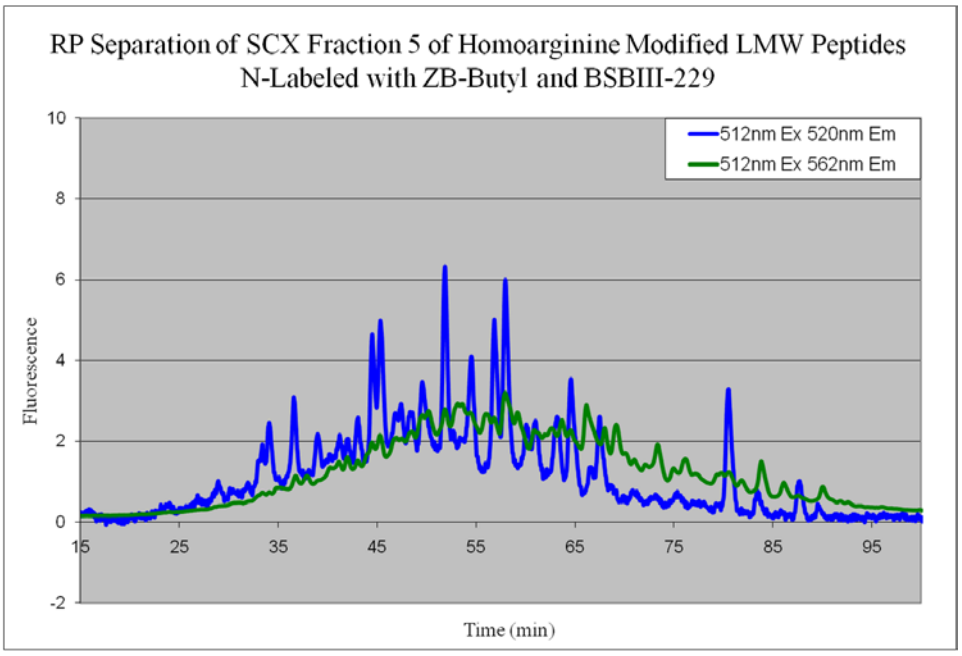

Figure 4.39: RP analysis of SCX fraction 5 shown in figure 4.33 from homoarginine modified LMW peptides from HC samples N-labeled with ZB-Butyl and BSBIII-229. 41 peaks were identified.

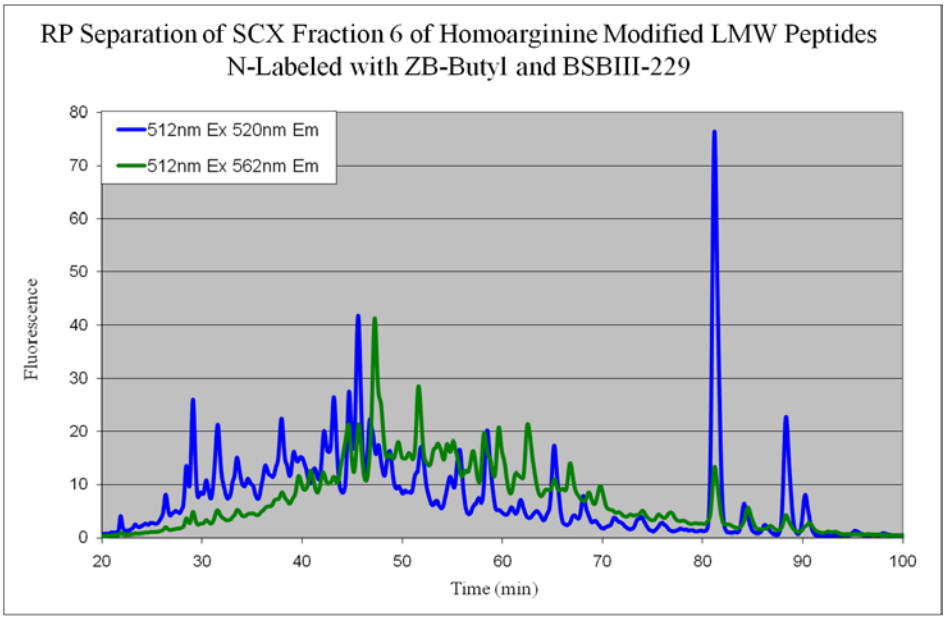

Figure 4.40: RP analysis of SCX fraction 6 shown in figure 4.33 from homoarginine modified LMW peptides from HC samples N-labeled with ZB-Butyl and BSBIII-229. 53 peaks were identified.

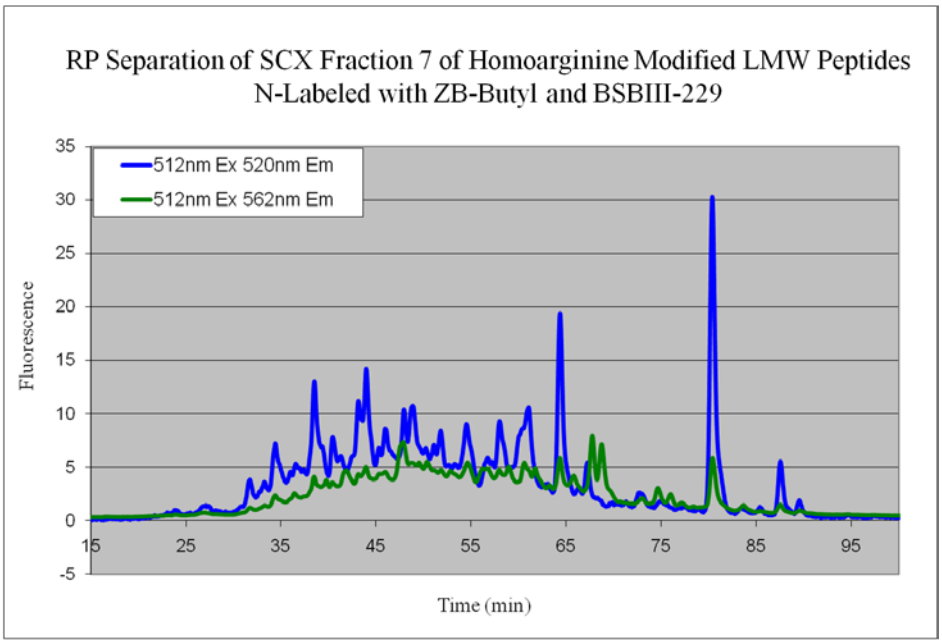

Figure 4.41: RP analysis of SCX fraction 7 shown in figure 4.33 from homoarginine modified LMW peptides from HC samples N-labeled with ZB-Butyl and BSBIII-229. 50 peaks were identified.

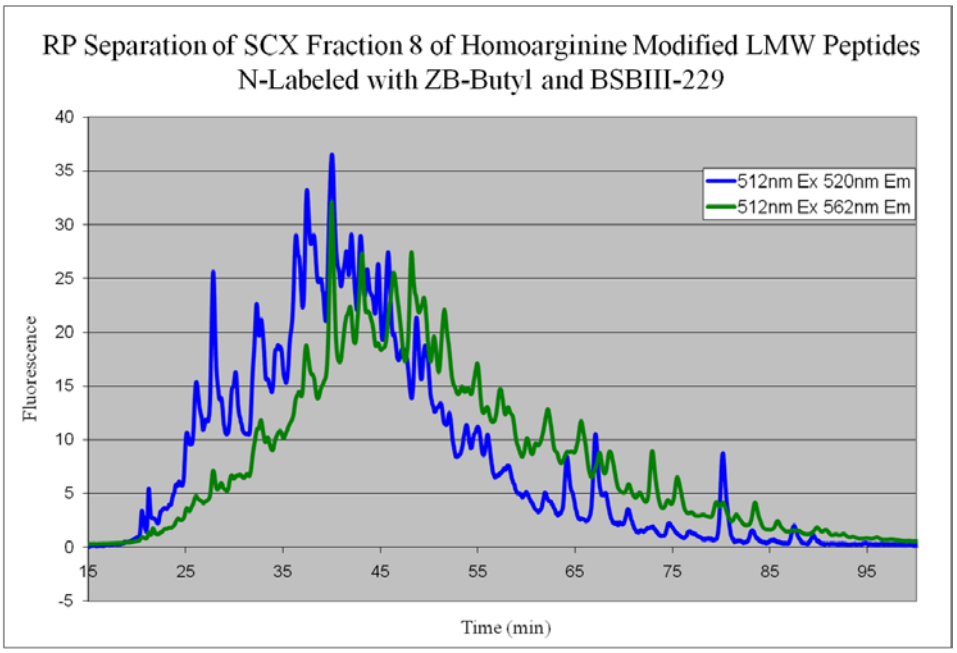

Figure 4.42: RP analysis of SCX fraction 8 shown in figure 4.33 from homoarginine modified LMW peptides from HC samples N-labeled with ZB-Butyl and BSBIII-229. 58 peaks were identified.

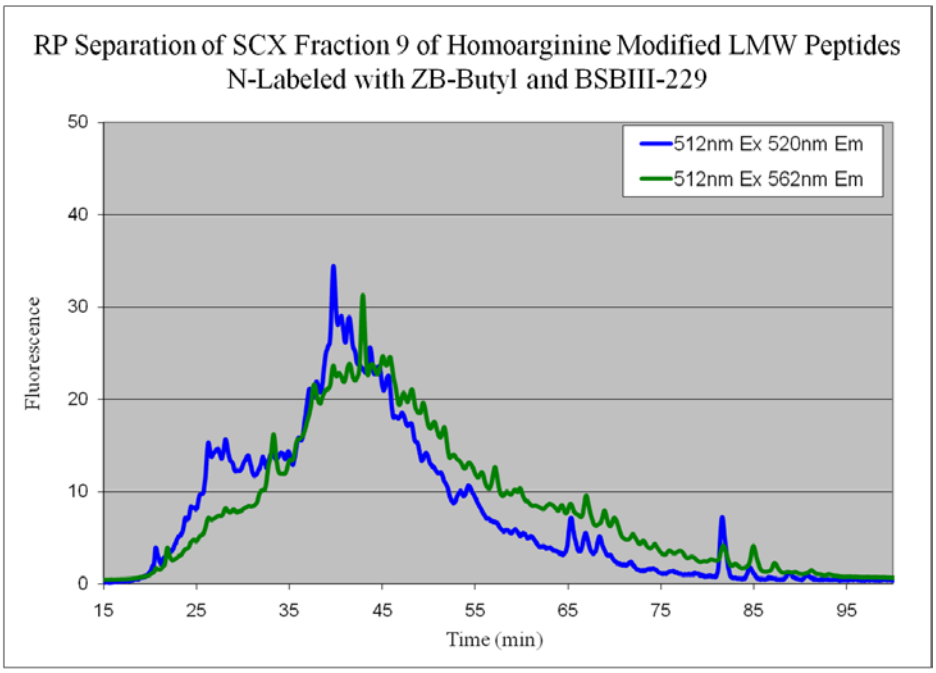

Figure 4.43: RP analysis of SCX fraction 9 shown in figure 4.33 from homoarginine modified LMW peptides from HC samples N-labeled with ZB-Butyl and BSBIII-229. 48 peaks were identified.

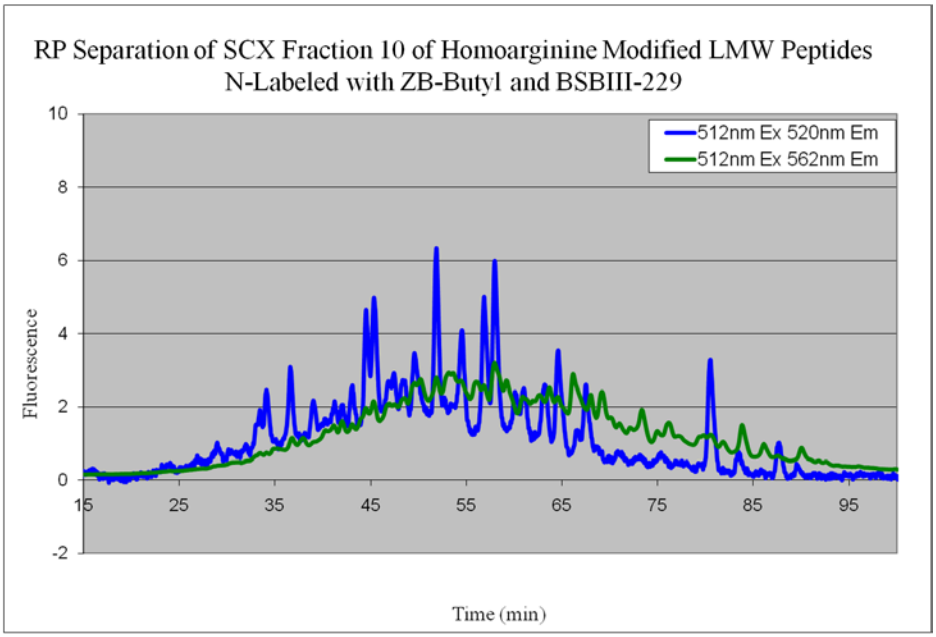

Figure 4.44: RP analysis of SCX fraction 10 shown in figure 4.33 from homoarginine modified LMW peptides from HC samples N-labeled with ZB-Butyl and BSBIII-229. 24 peaks were indentified.

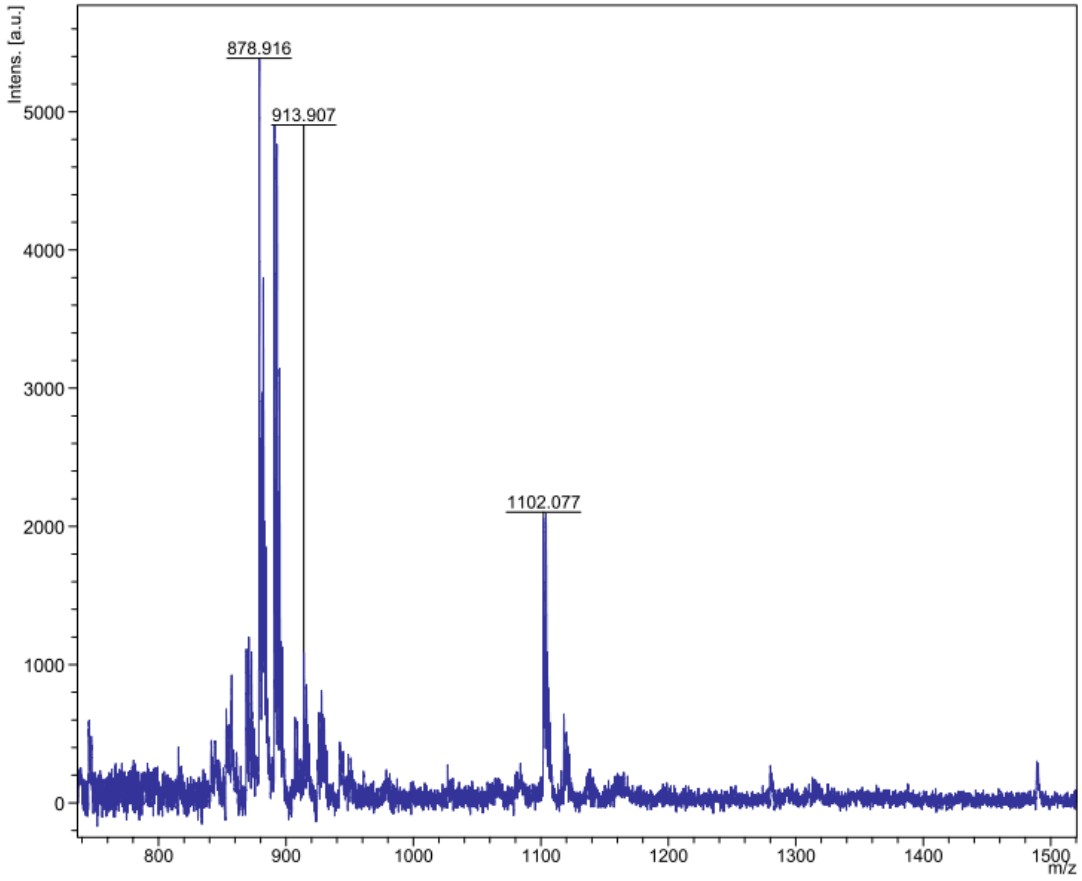

Figure 4.45: MALDI analysis of one fraction of LMW peptide following SCX and RP. LMW peptidome fractions yielded several rather simliar MALDI spectra. The most prominent peak masses were too low to include the mass of a covalently bound dye. There are clearly mutltiple peptide peaks per fraction, as expected.

Though RP-HPLC is a mature and well defined field of chromatography, the readership may be unfamiliar with this separation technique. Before 1900, chemists used separation techniques such as paper chromatography to perform separations of compounds that were based on interactions of the molecule with either the stationary phase or the solvent.

In 1901 Mikhail Tswett, who is often hailed as the father of chromatography, envisioned that by packing calcium carbonate into a column as a stationary phase, and

flowing an eluting solvent over the column, this same principle could be applied (*150, 151*). Tswett seperated colored plant pigments and this gave rise to the term "chromatography" (*150, 151*). Later developments improved resolution by achieving more consistent packing of the stationary phase in smaller particle sizes and required the used of higher pressure pumping systems. Thus high pressure liquid chromatography (HPLC) was born in the mid 1960's (*151, 152*).

More recently, research groups have continued to improve upon high pressure liquid chromatography technology. In 1999 higher pressure pumping systems were introduced that could use smaller particles to achieve improved separations and still deliver a steady flow and incremental adjustments to the gradient conditions (*153*). This new technology, ultra-HPLC (uHPLC or UPLC), has become more widely used, and most major HPLC vendors now sell a system for ultra high pressure separations. As the packing particle size decreased and the pressure required for the separations increased, the number of theoretical plates of separation and resolution increased. HPLC columns such as the Jupiter 4u Proteo RP 90A 150mm x 2mm column, that we used for the RP separations in figures 4.35-4.44, have a theoretical plate capacity of approximately 174,000. The number of theoretical plates is calculated using formula 1 below (*154*). Values for Rt = 480 mm and PWHM = 1.15 mm.

Formula 1: N= (Rt/PWHM)^2

N= Theoretical plates of separation

Rt = Retention time at peak max (expressed in millimeters)

PWHM = Peak width at half maxium (expressed in millimeters)

Using this of Nvalue one can calculate the peak capacity of the column using formula 2 below (*154*).

Formula 2: $n= 1+ [(\sqrt{N})/4]*\ln(t_n/t_1)$

n = peak capacity

t_n = last retained peak

t_1 = first eluted peak

The peak capacity for the Jupiter Proteo, using 214 nm absorbance data for peptidomic study with t_1 = 3 minutes and t_n = 92.5 minutes, is found to be 717. This means that within a gaussian distribution of compound hydrophobicities, approximately 717 compounds can be reasonably separated. The dye labeled peptides, however, did not distribute over this entire region of the elution gradient, rather they eluted over a time span from 27 to 67 minutes, a range which would be expected to be capable of resolving about 320 compounds. If this RP separation is then applied to 10 SCX fractions, one may estimate that 3200 compounds may reasonably be separated (*155*). As the molecules become more and more similiar in functional groups, length, and structure, the narrow range of hydrophobic properties of the compounds make separating the complex mixture more difficult. The [1] alklyation of all cysteines, [2] guanidinylation of all lysines, [3] the often short amino acid chain length, and [4] the chromatographic properties of a single fluorescent dye dominating the N-terminal amine of each of these peptides, created a population of LMW plasma peptides that in its functionalized state, was extremely difficult, and essentially impossible to separate to baseline.

With this above information, it was decided that further attempts at developing a peptidomics method using N-terminal labeling with fluorescent dyes as a quantification and difference detection tool was not promising for application to the low molecular weight peptidome from whole plasma. Estimates of approximately 5000 peptides in the LMW peptidome presented too difficult a separation challenge for this method (*101, 105*). The procedure developed would likely be a plausible method for separating samples with fewer peptides.

Comparison of the digest of Intact BSA to Oxidized BSA

It is clear that the HSA in the human T2D plasma has been altered in some substatial way compared to healthy control samples. Increased inflammation and oxidative stress have been associated with T2D (*156-158*). Therefore, in the present work we modeled possible changes in HSA by performing a peptide separation on a BSA trypsin digest and compared this to a trypsin digest of oxidized BSA (*158*). We performed a theoretical digest on BSA using the protein cutter tool on the ExPASy proteomics server (*159*). 194 peptides were created from this theoretical digestion, with masses between 750 to 4000 daltons and allowing for one missed trypsin cleavage. The 194 peptides included theoretical post translational modications of oxidation to methionine and phosphorylation of serine, theorine, and tyrosine (*160*). The list of peptide masses generated is shown in Table 4.5. This level of peptide diversity is simple enough that the separation and detection method we have outlined previously in this chapter should be suitable.

Table 4.5: A theoretical trypsin digest of BSA was performed of EXPASY, allowing for 1 missed cleavage, and examining masses between 750 – 4000 daltons. The protein was reduced and alkylated with iodoacetimide (IAA) in silico, and known protein modifications of oxidation and phosphorylation were allowed. This list includes peptide masses that may be detectable by mass spectrometry using MALDI or QTOF.

Theoretical EXPASY Trypsin Digest of BSA Reduced and Alkylated with Iodoacetimide Allowing One Missed Cleavage, Oxidatation, and Phosphorylation and Masses Between 750-4000 Daltons

3636.877	2574.125	2301.082	2004.846	1850.899	1633.662	1466.709	1347.712	1107.514	927.4934
3617.614	2529.219	2298.118	2003.778	1844.848	1627.8	1466.587	1331.717	1083.595	922.488
3579.856	2506.25	2277.158	1964.867	1823.9	1616.749	1465.689	1308.727	1072.509	922.4662
3503.571	2498.191	2247.943	1962.948	1814.83	1595.927	1463.589	1305.716	1068.442	918.5189
3447.704	2494.159	2220.137	1955.96	1795.832	1579.732	1445.758	1294.704	1052.45	906.4713
3390.683	2492.264	2219.977	1946.016	1756.734	1578.598	1443.642	1291.602	1050.492	898.4815
3038.249	2490.255	2215.095	1942.82	1751.742	1576.768	1439.812	1283.711	1034.472	886.4152
3009.451	2487.11	2199.1	1941.922	1749.663	1567.743	1429.512	1254.578	1024.455	847.5036
3000.401	2472.198	2174.029	1927.798	1747.705	1554.653	1419.694	1249.621	1015.488	841.46
2952.429	2471.191	2136.974	1907.921	1738.811	1546.895	1418.738	1197.557	1014.619	820.4675
2872.31	2458.181	2121.929	1906.798	1724.835	1539.82	1415.688	1195.589	1011.42	818.4254
2867.184	2444.165	2117.821	1901.87	1723.844	1532.781	1399.693	1193.602	1002.583	817.489
2864.265	2441.169	2113.885	1900.008	1707.766	1519.746	1388.739	1177.559	1001.589	789.4716
2829.337	2435.243	2105.934	1897.075	1700.787	1511.843	1388.571	1166.493	988.5673	752.3573
2773.167	2414.17	2091.079	1890.803	1692.942	1504.921	1386.621	1163.631	987.5694	
2717.24	2401.159	2076.878	1888.995	1684.821	1502.614	1380.475	1153.694	987.537	
2701.245	2387.144	2045.028	1888.927	1683.808	1497.631	1364.48	1145.643	977.4509	
2693.2	2355.14	2034.058	1884.901	1673.77	1482.798	1362.672	1142.714	975.5404	
2608.202	2345.093	2019.969	1880.921	1667.813	1479.795	1352.666	1138.567	974.4577	
2604.298	2316.046	2019.773	1879.837	1639.938	1478.523	1349.546	1138.498	960.5472	

BSA has been well studied over the years due to its availability and many similar characteristics to HSA (*43*). Essentially the same cargos carried on HSA are also carried on BSA (*43*). BSA has two tryptophanes rather than one as in HSA. However, the sequence and structural homology is very high, including the conserved hydrophobic binding domains (*43*).

In their native forms, both BSA and HSA have two modifications that affect their capacity to transport cargo and to serve as a carrier for peptides, drugs, and minerals.

These two modifications include glycation and oxidation (*161, 162*). Glycation is a nonenzymatic addition of a sugar molecule to amino groups in proteins (*163*). Glycation occurs on many proteins, particularly in the presence of high blood glucose, such as is found in diabetes (*162, 163*). Glycation is thus an important modification to search for, since it reflects the recent history of the glucose levels that the protein and thus the patient has been exposed to (*163*). Under oxidative stresss conditions this modification is termed glycoxidation (*163*).

The increased oxidation of proteins occurs when free radicals are present in the environment. Increased free radicals are indicative of oxidative stress, aging, and accompany disease (*164*). Oxidative stress may increase due to poor omega-3/omega 6 fatty acid nutrition, excessive exercise, magnesium deficiency, ozone, cigarette smoking, x-radiation, or chronic alcohol consumption (*164*). As the aging process and oxidative damage occurs, inactive or less active forms of numerous enzymes accumulate (*164*). Such processes occur in both young and old animals that are exposed to sources of oxidative stress, such as x-radiation or hydrogen peroxide (H_2O_2) (*164, 165*). Oxidative stress results in an increase in the carbonyl content of proteins that have been found to occur, especially in certain key tissues: brain, eye lens, red blood cells to name a few (*164, 165*). It has been noted that reduced caloric diets in rats, mice, and flies, increase life span as well as decrease the protein carbonyl content (*164, 165*).

Key diseases already known to have a strong link to increased oxidative damage of proteins are Alzheimer's Disease, respiratory distress syndrome, muscular dystrophy, cataractogenesis, and rheumatoid arthritis (*164, 165*). There is evidence that the

oxidative damage is also occurring in other diseases, such as diabetes, Parkinson's disease, and cystic fibrosis (*157, 158, 160, 164, 165*).

With HSA's high abundance in blood and its susceptilbility to oxidative stress, the chances of oxidation occuring on this protein in diabetics seems high. Several reasons for increased oxidative stress include increased blood glucose, increased weight, and poor diet, all of which can lead to an increase in free radicals (*158, 160, 163, 164*). Thus, it is useful to study BSA, as a model for HSA, under control conditions, compared to oxidative stress conditions. We also considered the digest of native BSA and oxidized BSA to be useful models for our evaluation of peptidomic analysis methodology.

We used 150 uL of BioRad (Hercules, CA) 2 mg/mL BSA standard solution. To oxidize BSA, we added 800 uL of 50 mM tris HCl buffer, pH 7.8, 0.5 ug of horse radish peroxidase enzyme, and 2.3 uL of 8.8 M hydrogen peroxide (H_2O_2), and this mixture was incubated at 37ºC for 20 hours.

Trichloroacetic acid (TCA) precipation was performed to isolate the protein with minimal carryover of oxidative reagents. To 1mL sample, 250 uL of 100% (w/v) TCA was added, and the sample was cooled to 4ºC (on ice) for 10 minutes in 1.5mL microfuge tubes. The sample was spun down at 14K rpm for 5 minutes and the supernatant removed. The protein pellet was washed with 200 uL aliquots of cold acetone, and spun down in the centrifuge. This process was repeated two more times and the acetone residual was dried off in a heat block. The oxidized protein pellet was resuspended and digested by trypsin overnight at 37º C. The protein was solublized in 25 mM ammonium hydroxide

(NH4OH), pH 8.5 and a ratio of 1 part trypsin to 20 parts BSA was used to digest the protein.

To prepare non-oxidized control BSA, a 150 uL aliquot of 2 mg/mL BioRad BSA standard solution was reduced by addition of 10 uL of 200 uM DTT in 100 mM NH_4OH , pH 8.5, and allowed to react for 45minutes. Alkylation was performed by adding 8 uL of 1 M IAA in 100mM NH_4OH, pH 8.5, and allowing the sample to react for 45 minutes. Excess IAA was quenched by adding 20 uL of 200 mM DTT in 100 mM NH_4OH, pH 8.5, and incubating for 45 minutes. This mixture was digested overnight at 37˚ C, using a 1:20 trypsin to BSA protein in 25mM NH_4OH, pH 8.5.

After the protein mixtures were digested, the pH was adjusted to pH 10.5, and the samples were guanidylated by doubling the sample volume with 0.5M o-methyl isourea, and reacting overnight. Excess o-methyl isourea was removed using the sample desalting method described earlier to remove urea as described in table 4.2. These samples were analyzed by MS using an Agilent 6538 QTOF, with the results shown in figures 4.46 and 4.47. The fragmented peptides were identified with a combined mammals genome data base search, using Mascot (*166*).

Mascot Search Results

Protein View

Match to: **gi|1351907** Score: **571**
Serum albumin precursor (Allergen Bos d 6) (BSA)
Found in search of 20100927_03.mgf

Nominal mass (M_r): **71770**; Calculated pI value: **5.82**
NCBI BLAST search of gi|1351907 against nr
Unformatted sequence string for pasting into other applications
Links to retrieve other entries containing this sequence from NCBI Entrez:
gi|1351907 from Bos taurus

Fixed modifications: Guanidinyl (K)
Variable modifications: Carbamidomethyl (C),Deamidated (NQ),Oxidation (M)
Cleavage by Trypsin: cuts C-term side of KR unless next residue is P
Sequence Coverage: **27%**

Matched peptides shown in **Bold Red**

```
   1 MKWVTFISLL LLFSSAYSRG VFRRDTHKSE IAHRFKDLGE EHFKGLVLIA
  51 FSQYLQQCPF DEHVKLVNEL TEFAKTCVAD ESHAGCEKSL HTLFGDELCK
 101 VASLRETYGD MADCCEKQEP ERNECFLSHK DDSPDLPKLK PDPNTLCDEF
 151 KADEKKFWGK YLYEIARRHP YFYAPELLYY ANKYNGVFQE CCQAEDKGAC
 201 LLPKIETMRE KVLASSARQR LRCASIQKFG ERALKAWSVA RLSQKFPKAE
 251 FVEVTKLVTD LTKVHKECCH GDLLECADDR ADLAKYICDN QDTISSKLKE
 301 CCDKPLLEKS HCIAEVEKDA IPENLPPLTA DFAEDKDVCK NYQEAKDAFL
 351 GSFLYEYSRR HPEYAVSVLL RLAKEYEATL EECCAKDDPH ACYSTVFDKL
 401 KHLVDEPQNL IKQNCDQFEK LGEYGFQNAL IVRYTRKVPQ VSTPTLVEVS
 451 RSLGKVGTRC CTKPESERMP CTEDYLSLIL NRLCVLHEKT PVSEKVTKCC
 501 TESLVNRRPC FSALTPDETY VPKAFDEKLF TFHADICTLP DTEKQIKKQT
 551 ALVELLKHKP KATEEQLKTV MENFVAFVDK CCAADDKEAC FAVEGPKLVV
 601 STQTALA
```

Figure 4.46: Reduced, alkylated, and trypsin digested homoarginine modified BSA peptides were examined on an Agilent 6538 QTOF and the results were analyzed with Mascot. 27% sequence coverage of the protein was obtained and the peptides that were identified are shown in red.

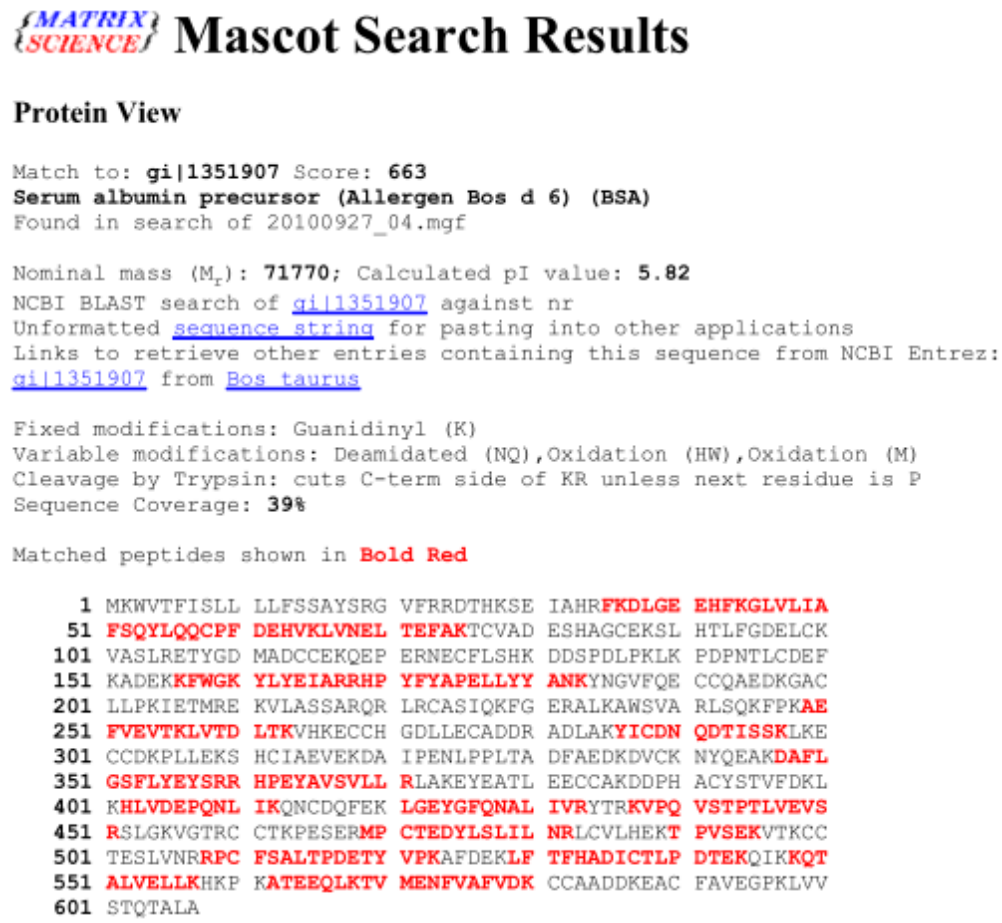

MATRIX SCIENCE Mascot Search Results

Protein View

Match to: gi|1351907 Score: 663
Serum albumin precursor (Allergen Bos d 6) (BSA)
Found in search of 20100927_04.mgf

Nominal mass (M_r): 71770; Calculated pI value: 5.82
NCBI BLAST search of gi|1351907 against nr
Unformatted sequence string for pasting into other applications
Links to retrieve other entries containing this sequence from NCBI Entrez:
gi|1351907 from Bos taurus

Fixed modifications: Guanidinyl (K)
Variable modifications: Deamidated (NQ),Oxidation (HW),Oxidation (M)
Cleavage by Trypsin: cuts C-term side of KR unless next residue is P
Sequence Coverage: 39%

Matched peptides shown in Bold Red

```
  1 MKWVTFISLL LLFSSAYSRG VFRRDTHKSE IAHRFKDLGE EHFKGLVLIA
 51 FSQYLQQCPF DEHVKLVNEL TEFAKTCVAD ESHAGCEKSL HTLFGDELCK
101 VASLRETYGD MADCCEKQEP ERNECFLSHK DDSPDLPKLK PDPNTLCDEF
151 KADEKKFWGK YLYEIARRHP YFYAPELLYY ANKYNGVFQE CCQAEDKGAC
201 LLPKIETMRE KVLASSARQR LRCASIQKFG ERALKAWSVA RLSQKFPKAE
251 FVEVTKLVTD LTKVHKECCH GDLLECADDR ADLAKYICDN QDTISSKLKE
301 CCDKPLLEKS HCIAEVEKDA IPENLPPLTA DFAEDKDVCK NYQEAKDAFL
351 GSFLYEYSRR HPEYAVSVLL RLAKEYEATL EECCAKDDPH ACYSTVFDKL
401 KHLVDEPQNL IKQNCDQFEK LGEYGFQNAL IVRYTRKVPQ VSTPTLVEVS
451 RSLGKVGTRC CTKPESERMP CTEDYLSLIL NRLCVLHEKT PVSEKVTKCC
501 TESLVNRRPC FSALTPDETY VPKAFDEKLF TFHADICTLP DTEKQIKKQT
551 ALVELLKHKP KATEEQLKTV MENFVAFVDK CCAADDKEAC FAVEGPKLVV
601 STQTALA
```

Figure 4.47: Trypsin digest of oxidized, homarginine modified BSA peptides were examined on an Agilent 6538 QTOF and the results were analyzed by Mascot. 39% sequence coverage of the protein was obtained and the peptides identified are shown in red.

These samples were then labeled with the previously developed fluorescent dye labeling protocols. Samples were then run on the SCX column, as described previously, and produced the results shown in figures 4.48 and 4.49. Using this multiplex approach, major differences were observed in the absorbance signal intensities between 30 - 50 minutes. The 507 nm absorbance represents the ZB-Butyl labeled peptides and the 538 nm absorbance represents the BSBIII-229 labeled peptides. The largest fluorescence

peaks were saturating the detector and are difficult to interpret at this loading. The absorbance peaks were not saturating, and the differrences in absorbance are indicative of differing degrees of labeling on certain pepitdes. Due to the relatively weak signal from the BSBIII-229 channel, we chose to treat future experiments as a single dye study.

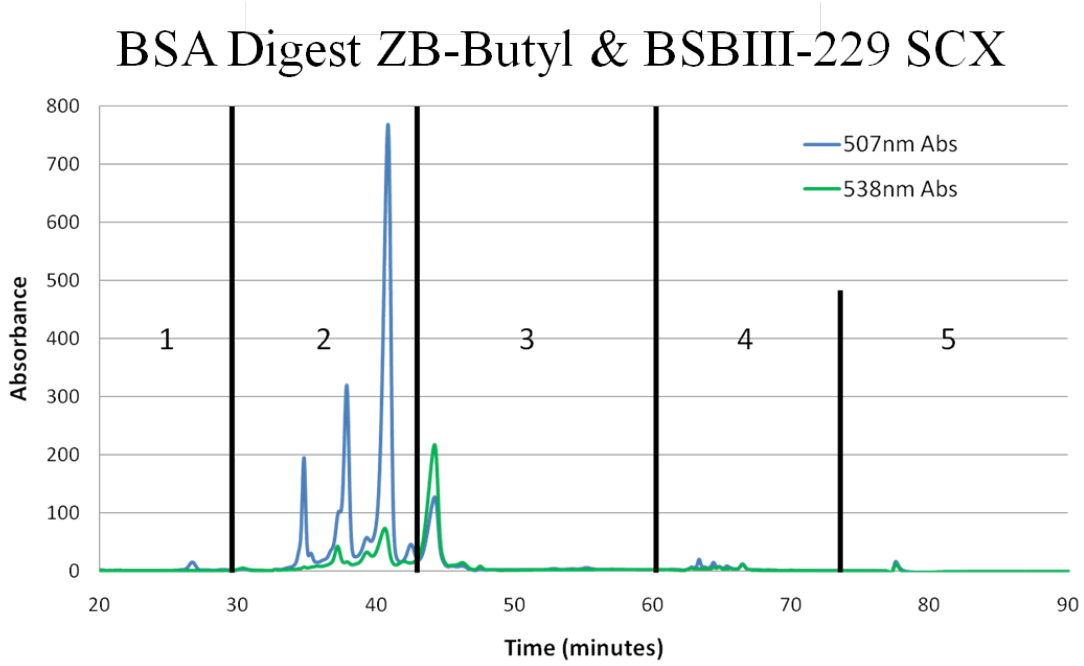

Figure 4.48: SCX trace of a homoarginine modified BSA that has been reduced, alkylated, and digested. Absorbance at 507 nm corresponds to the ZB-Butyl dye, and the 538 nm absorbance corresponds to the BSBIII-229 dye. Fluorescence traces were saturating the detector, and thus examining absorbance differences makes interpetation easier. Differences in absorbance between dyes indicated unexpected highly perferential labeling on many of the peptides. 1 - 5 represent fractions taken for further analysis. Free dye was removed prior to 20 minutes and no signal was found after 90 minutes.

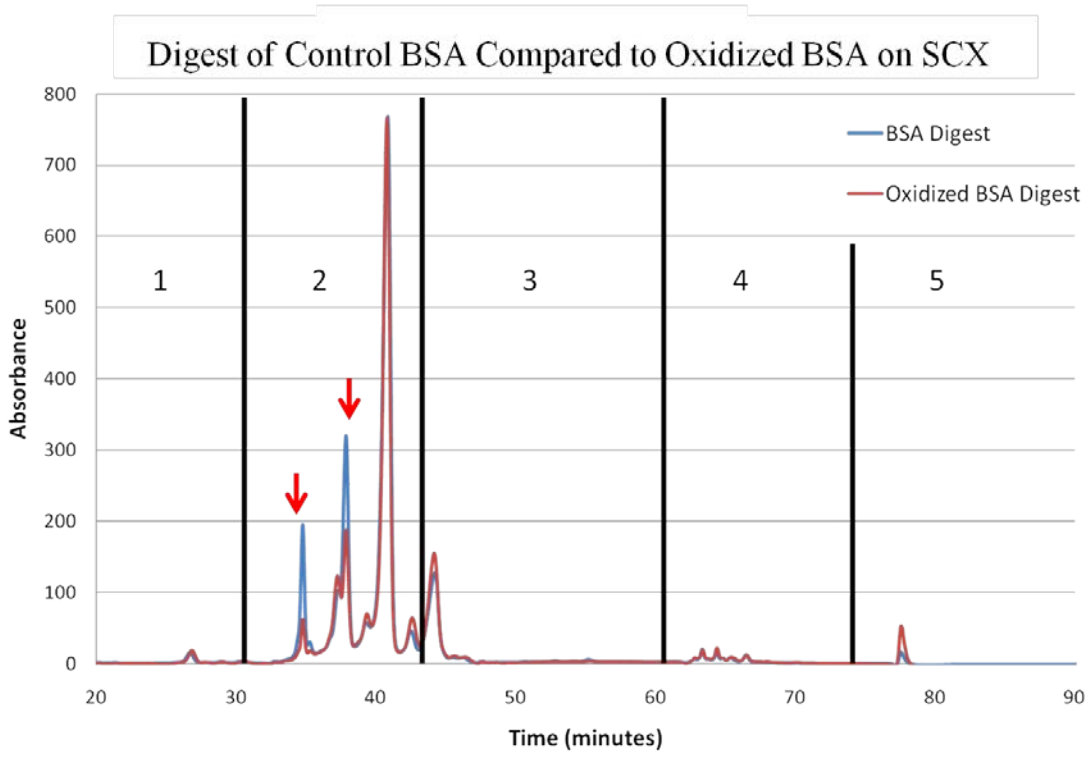

Figure 4.49: SCX trace of reduced, alkylated, and digested homoarginine modified BSA compared to oxidized, digested homoarginine modified digested BSA. The absorbance at 507 nm of ZB-Butyl dye is overlayed from two separate runs and has been normalized to detect differences in individual peak absorbances between the two samples. Fluorescence traces were saturating the detector, and thus using absorbance made it possible to interpet the results. Major differences in peaks at 34.4 and 37.7 minutes have been marked with a red arrows. The other peaks were very similar. The 1 - 5 represent fractions taken.

Samples were separated into five fractions, as shown in figure 4.49, with free dye being removed prior to 20 minutes and no signal observed after 90 minutes. Differences in peaks at 34.4 and 37.7 minutes appeared to correspond to oxidation of some peptide species. These differences were found in the RP fraction 2. Each of the fractions 1 - 5 was collected, frozen, and lyophilized to dryness.

The peptide samples were solublized in 200uL of 10% DMF, and 90% (0.1% TFA water), and each sample was injected onto RP, using the previously optimized RP method. Samples of BSA control digest and oxidized BSA digest SCX fractions 1 – 5 were examined for differences. Figures 4.50-4.59 represent the absorbance and fluorescence of these fractions. Absorbance is measured at 507 nm. Fluorescence is detected with 512 nm excitation and 520 nm emission for the ZB-Butyl peak. The loading of fraction 2 had to be reduced in loading to avoid saturation of fluorescence peaks. Two peaks, visibly marked with a red arrow, were clearly different in both the concentrated as well as the diluted samples.

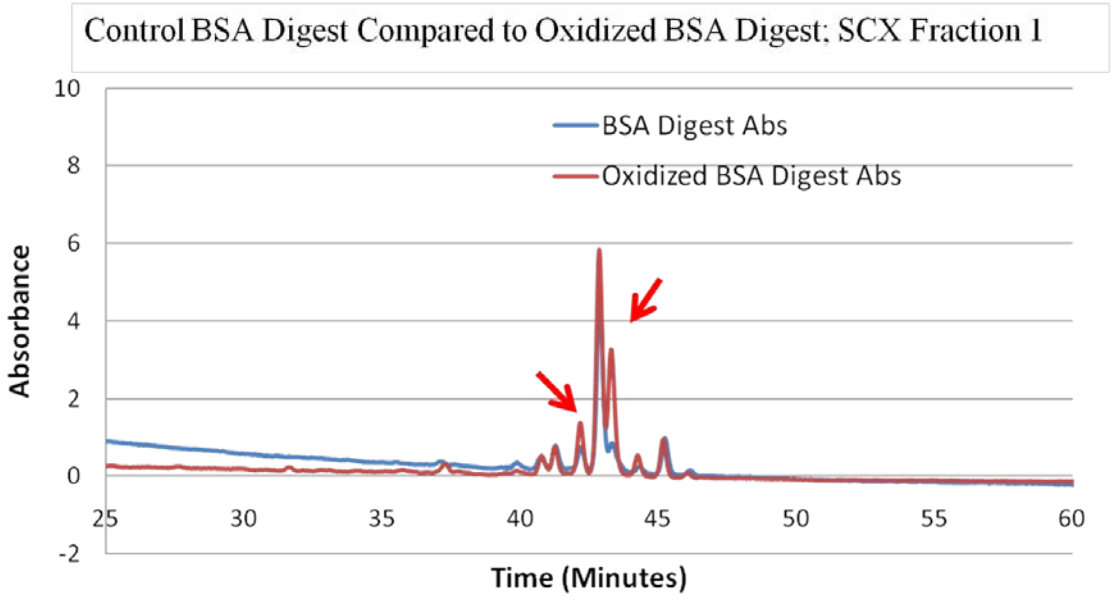

Figure 4.50: Control BSA digest SCX fraction 1 in blue compared to oxidized BSA digest SCX fraction 1 in red. The largest differences in the absorbance peaks are marked with red arrows.

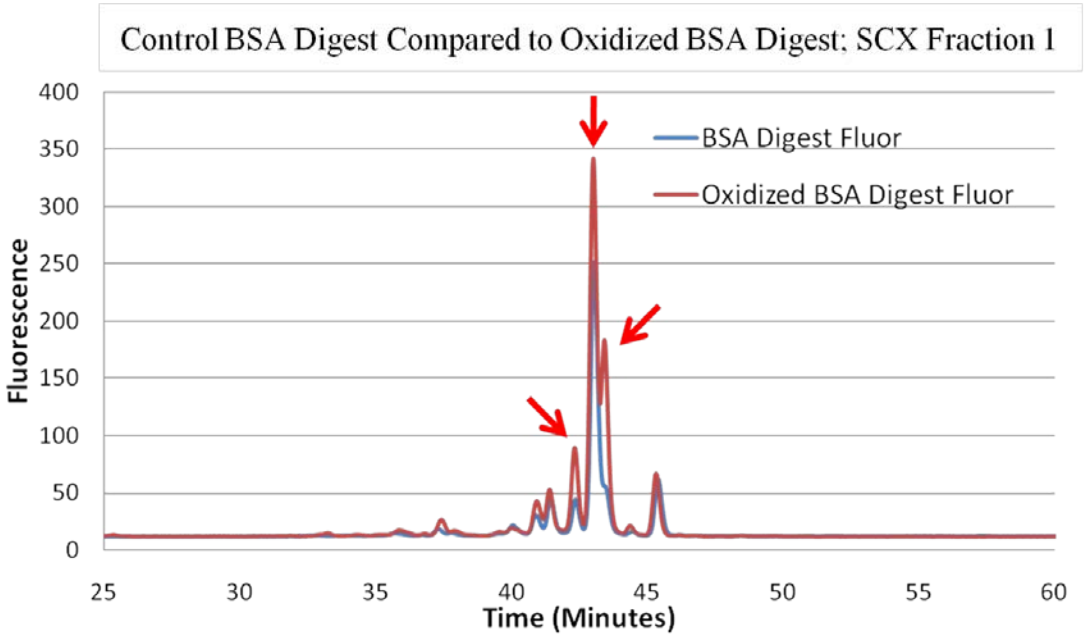

Figure 4.51: Control BSA digest SCX fraction 1 in blue compared to oxidized BSA digest SCX fraction 1 in red. The largest differences in the fluorescence peaks are marked with red arrows.

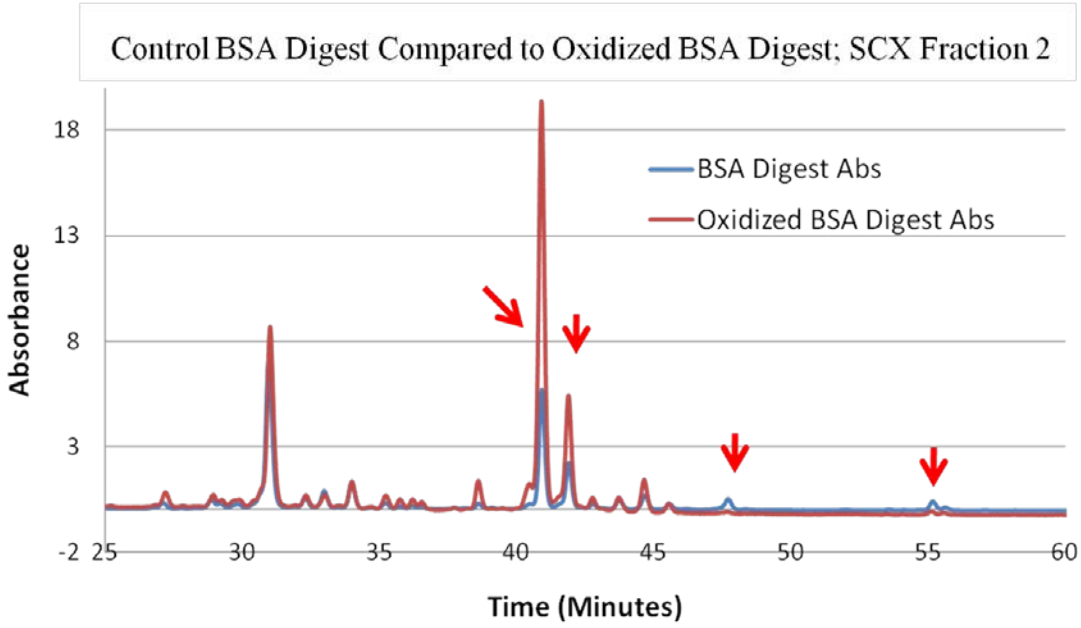

Figure 4.52: Control BSA digest SCX fraction 2 in blue compared to oxidized BSA digest SCX fraction 2 in red. The largest differences in the absorbance peaks are marked with red arrows.

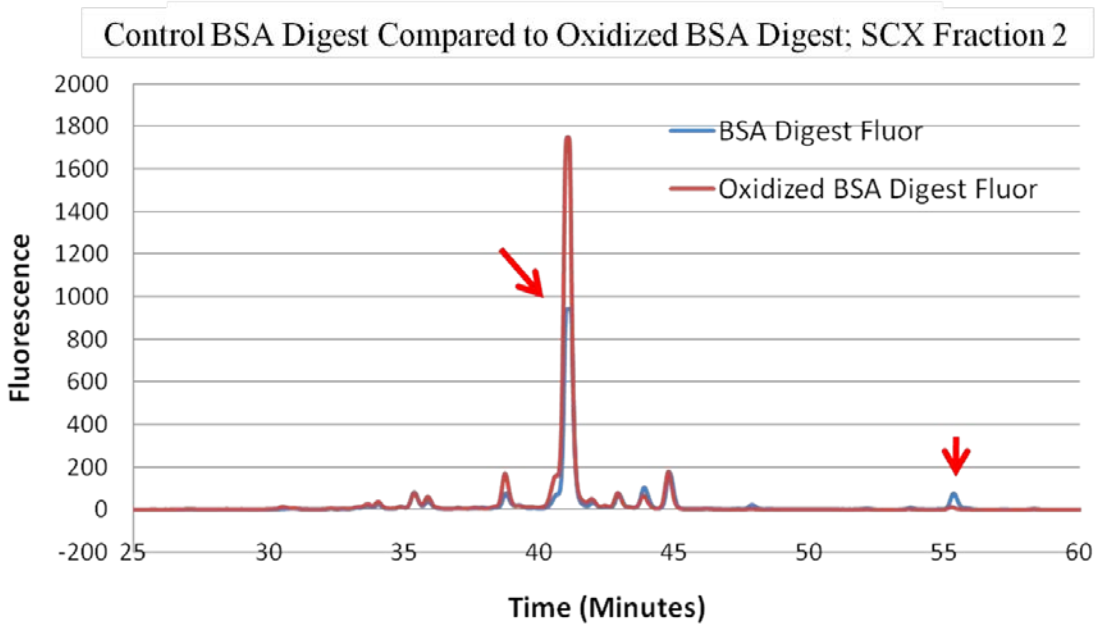

Figure 4.53: Control BSA digest SCX fraction 2 in blue compared to oxidized BSA digest SCX fraction 2 in red. The largest differences in the fluorescence peaks are marked with red arrows.

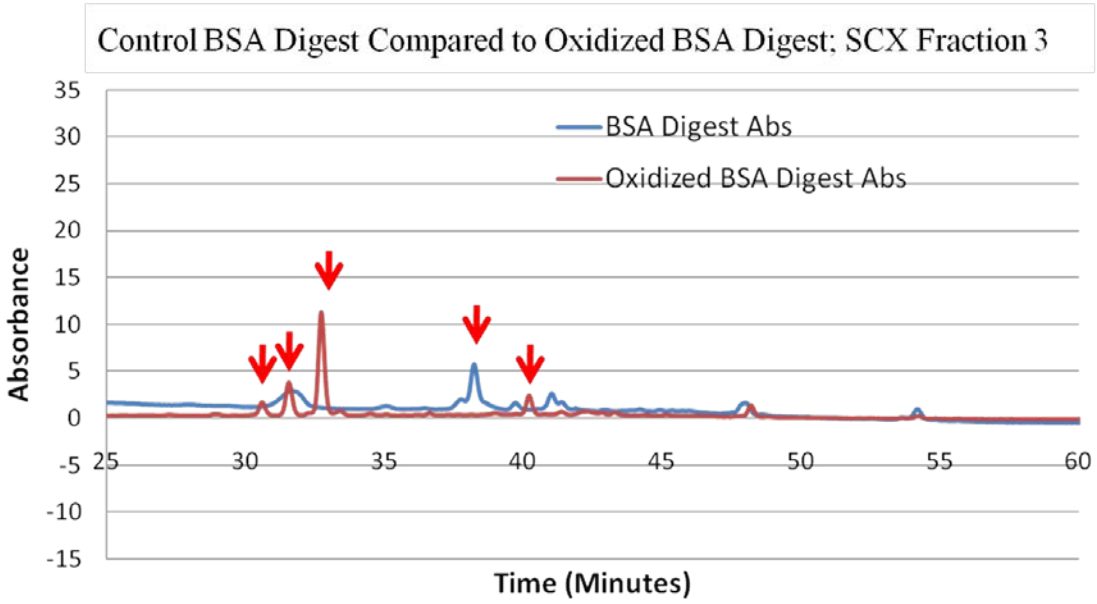

Figure 4.54: Contrl BSA digest SCX fraction 3 in blue compared to oxidized BSA digest SCX fraction 3 in red. The largeset differences in the absorbance peaks are marked with red arrows.

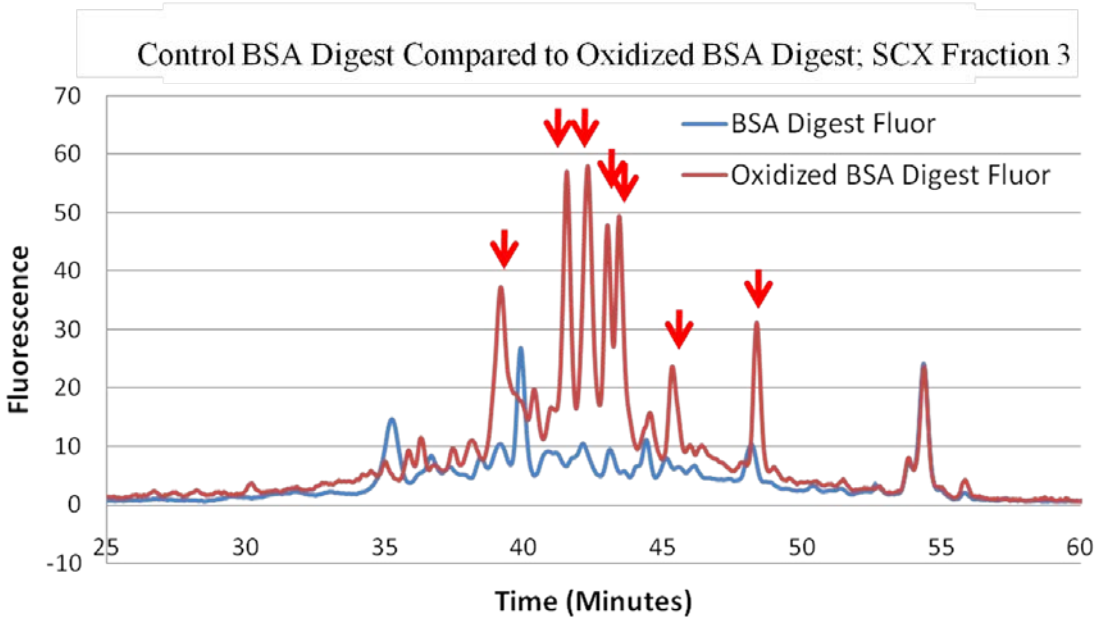

Figure 4.55: Control BSA digest SCX fraction 3 in blue compared to oxidized BSA digest SCX fraction 3 in red. The largest differences in the fluorescence peaks are marked with red arrows.

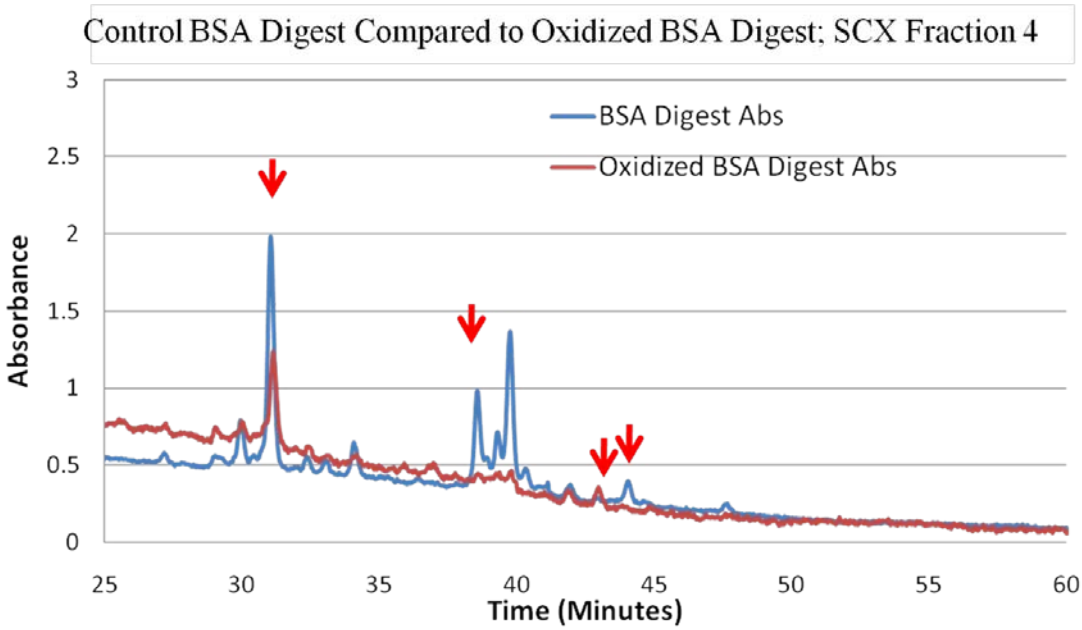

Figure 4.56: Control BSA digest SCX fraction 4 in blue compared to oxidized BSA digest SCX fraction 4 in red. The largest differences in the absorbance peaks are marked with red arrows.

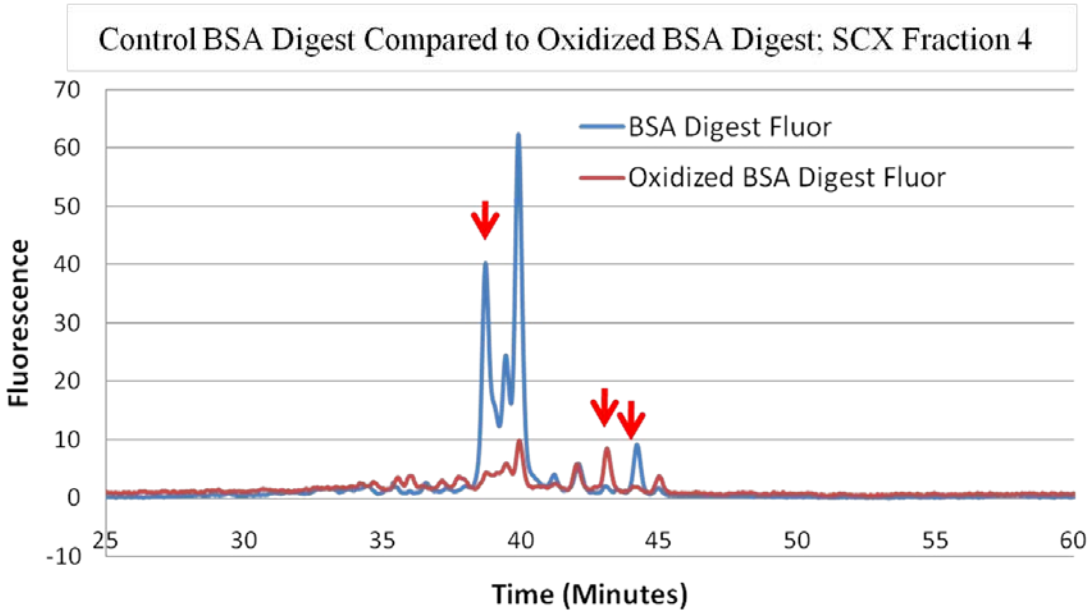

Figure 4.57: Control BSA digest SCX fraction 4 in blue compared to oxidized BSA digest SCX fraction 4 in red. The largest differences in the fluorescence peaks are marked with red arrows.

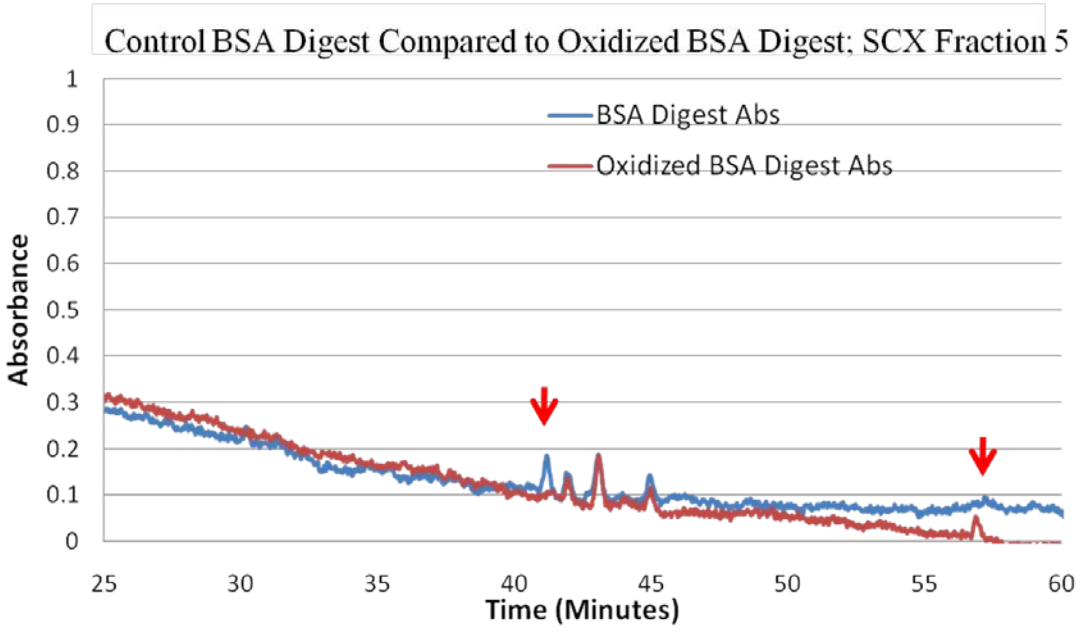

Figure 4.58: Control BSA digest SCX fraction 5 in blue compared to oxidized BSA digest SCX fraction 5 in red. The largest differences in the absorbance peaks are marked with red arrows.

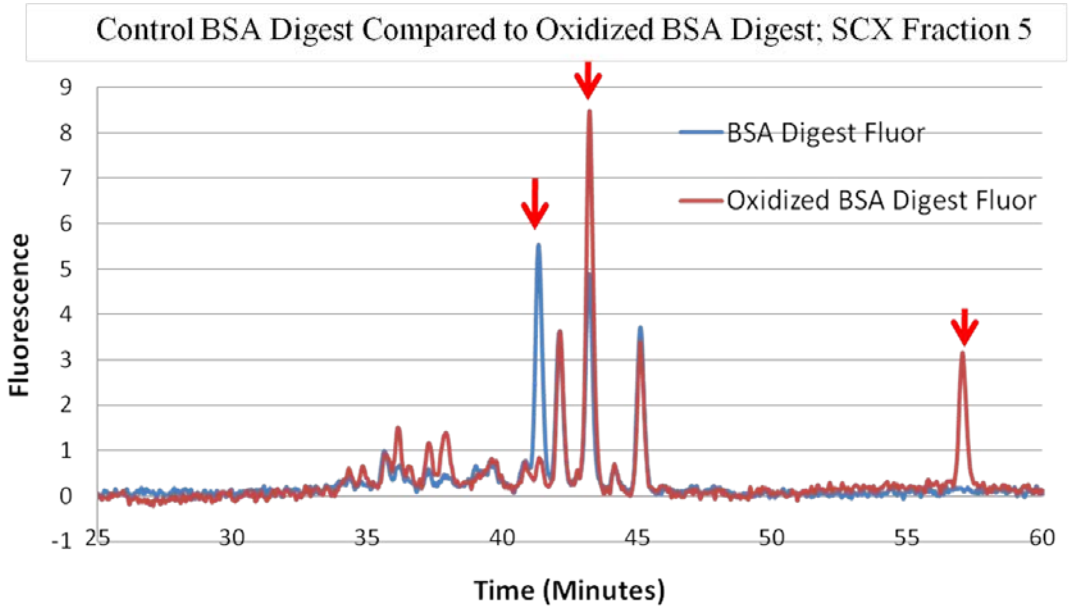

Figure 4.59: Control BSA digest SCX fraction 5 in blue compared to oxidized BSA digest SCX fraction 5 in red. The largest differences in the fluorescence peaks are marked with red arrows.

Fractions of these samples were collected every 1 minute throughout the run. Each fraction was then analyzed by MALDI TOF/TOF to identify the labeled BSA digest peptides. The low concentration of peptides in many of these fractions was inadequate for identification by MALDI. However, several fractionated samples had sufficient dye to visibly observe color on the MALDI plate, and must contain sufficient dye-labeled peptide to observe by MALDI. Serial dilutions of these fractions were unable to identify any dye-labeled peptides, even though our dye-labeled peptides had been observed by MALDI previously.

Our conclusion was that using fluorescently labeled dyes as a sensitive marker to detect modifications on a protein, such as oxidized BSA, is feasible. This may have

practical application in locating and isolating a particular peptide where the modification occurs. More effort using mass spectrometry techniques will likely yield promising results in obtaining identifications for these fluorescent dye-labeled peptides.

INVESTIGATING THE HYDROPHOBIC METABOLITES IN PLASMA

Fatty Acids Cargo Analysis by GCMS

Fatty acids and other ligands have the capability to modify the confirmation of HSA, increasing its thermal stability, and affecting the binding affinity of many molecules (*49*). Therefore, the levels of bound fatty acids are interesting targets of investigation as a potential cause for changes in the stabilization of HSA in inflammatory diseases (*78*), and as a potential cause for changes in binding affinities of proteins associated with HSA (*42*).

Plasma non-esterified fatty acids (NEFA) were shown to be up-regulated by 75% in Pima Indians with T2D (*40*). These finding are particularly interesting as >99% of the NEFA in plasma are known to be bound to HSA (*68*). HSA has three fatty acid binding domains and has been demonstrated in vitro to be capable of binding up to seven NEFA (*69, 167*). In vivo this ratio is observed to be on the order of 0.1 – 2 NEFA per HSA under normal conditions; however when blood sugar is low during fasting fatty acids are mobilized and this ratio FA/HSA can increase to 6:1 (*69*).

Increased dietary omega 3 fatty acids are correlated with reduced insulin resistance in T2D (*168, 169*). Other lipid species have been observed to induce insulin resistance in rats and mice (*170*). Insulin resistance is particularly tied to skeletal muscle lipid metabolism, as insulin levels increase there is increase in fat synthesis and decrease in fat metabolism for energy by the cells (*70, 171, 172*). The regulation of lipids and cholesterol species is greatly distorted in T2D, which is associated with high levels of

triacylglycerides and cholesterol (*31, 173-176*). Polyunsaturated NEFA are easily oxidized in vivo or in vitro to form lipid peroxidases, which are known to cause oxidative damage to tissues (*177, 178*). Despite these observations, increased levels of NEFA in plasma are not considered diagnostic of T2D. The use of classical fasting blood glucose, the oral glucose challenge response and HbA1c are currently recognized as the best diagnostic indicators for the onset of T2D.

Upon completion of his plasma proteomic study of T2D, Laffoon stored the abundant proteins fractions from the immuno-depletion steps of sample processing (*42*). Laffoon carried out plasma immuno-depletion on an Agilent MARS14 column under the same conditions as those we described previously, for use with an Agilent HSP7 immuno-depletion column, as was shown in figure 3.1 (*42*). The abundant plasma protein fractions were collected on ice and stored frozen at -80˚C.

We were able to obtain stored abundant protein fraction samples for 8 T2D and 8 paired HC samples for this lipidomics study from a prior proteomics study in our lab. The plasma samples, obtained from the NIH (*42*), were from newly diagnosed T2D patients which had not been treated for T2D. Each participant provided an NIH institutional review board (*42*) approved informed consent, and the sample collection was performed in accordance with the Declaration of Helsinki principals, in addition to adhering to the guidelines set forth in Title 45, US Code of Federal Regulations. Part 46, Protection of Human Subjects, revised November 13, 2001. A list of biometric data was provided with these samples, and additional biometric data (insulin, blood albumin) were

obtained by Laffoon (*42*). We measured the whole plasma NEFA levels using a WAKO (Richmond, VA) enzymatic analysis kit and the results are shown in table 5.1.

The NEFA test kit from WAKO was developed using Ducombe's research on low level quantitative detection of NEFA in plasma (*179, 180*). Figure 5.1 represents the reaction carried out with the kit (*180*). Acyl coenzyme sythetase, coenzyme A (*181*), and adenosine triphosphate (ATP) react with NEFA to form fatty acyl –CoA esters (*181*). The acyl CoA then reacts with oxygen, in the presence of acyl CoA oxidase (ACOD), to produce H_2O_2. The H_2O_2, reacts with 4-aminoantipyrine, and 3-methyl-n-ethyl-n (β-hydroxyethyl)-aniline (MEHA) in the presence of a peroxidase enzyme to generate a purple pigment that absorbs at 550 nm. Utilizing the enzyme specificity and the sensitivity of the 4-aminoantipyrine and MEHA product, this kit is very specific and sensitive for NEFA detection. The detection limit is on the order of 50 nmoles, which is sensitive enough to detect the NEFA levels in 5uL plasma (*179*).

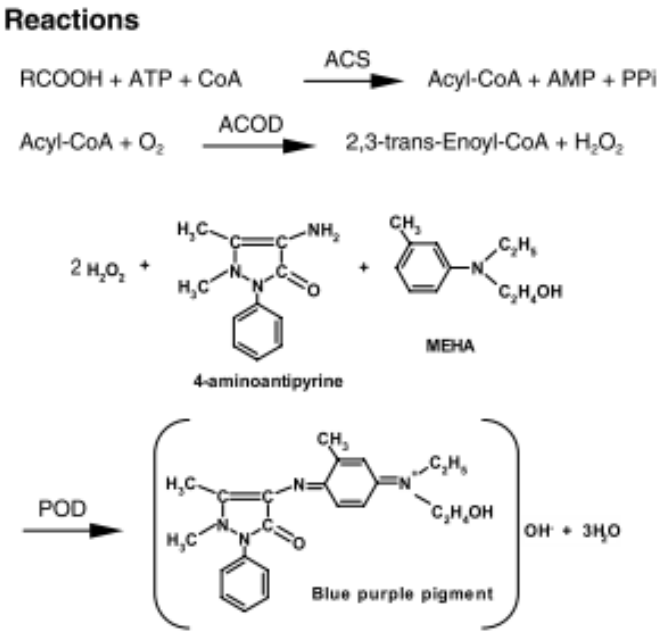

Figure 5.1: Reaction chemistry utilized in the WAKO NEFA kit. Acyl CoA Synthetase = ACS, Acyl CoA Oxidase= ACOD, Peroxidase = POD (*179*, *180*).

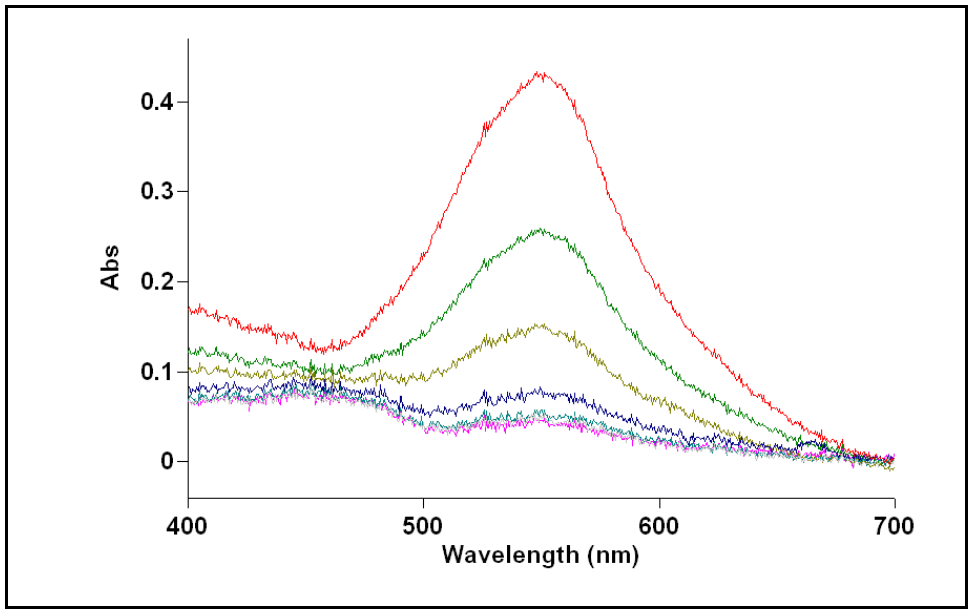

Figure 5.2: Absorbance data for generating an oleic acid standard curve with the WAKO NEFA kit. This data produced a standard curve with a slope value of 0.041, intercept of 0.037 and an R^2 value of 0.992.

Table 5.1: Biometric parameters of the newly diagnosed T2D (impaired glucose tolerance IGT) and normal glucose tolerance (*182*),+/- standard deviation) in study group.

		NGT n = 8	*IGT n = 7*	*Significance p =*
Age	mean	50.9	58.3	0.03
[years]	95% CI	45.6 – 56..2	56.7 – 59.9	
BMI	mean	25	33	0.025
[kg/m^2]	95% CI	23 - 27	28 - 39	
WHR	mean	0.83	0.89	0.207
	95% CI	0.76 – 0.90	0.83 – 0.95	
Blood Parameters				
RR systolic	mean	123	134	0.104
[mmHg]	95% CI	116 - 129	123 -145	
RR diastolic	mean	78	72	0.743
[mmHg]	95% CI	72 - 82	65 - 79	
Triglycerides	mean	60	111	0.028
[mg/dL]	95% CI	38 – 81	78 – 143	
Total cholesterol	mean	178	179	0.987
[mg/dL]	95% CI	151 – 206	149 – 208	
HDL-cholesterol	mean	62	39	0.014
[mg/dL]	95% CI	54 – 70	26 – 52	
LDL-cholesterol	mean	104	118.0	0.014
[mg/dL]	95% CI	84 – 125	160 - 216	
Free fatty acids	mean	0.25	0.45	0.026
[mM]	95% CI	0.16 – 0.36	0.32 – 0.58	
HbA_{1C}	mean	5.0	6.0	0.011
[%]	95% CI	4.8 – 5.2	5.5 – 6.6	
ALT	mean	21	30	0.098
[IU/L]	95% CI	16 - 27	23 - 37	
Glucose Fasting	mean	87	131	0.001
[mg/dL]	95% CI	83 - 90	116 -146	
Glucose 1 Hr	mean	102	277	<0.001
[mg/dL]	95% CI	85.3 -118	243 - 312	
Glucose 2 Hr	mean	78	231	<0.001
[mg/dL]	95% CI	69 - 88	208 - 255	
Insulin	mean	5.9	15.9	0.008
[uIU/mL]	95% CI	4.6 – 6.8	11.3 – 20.6	
C-reactive protein	mean	1.7	7.9	0.014
[mg/L]	95% CI	0.32 – 3.0	4.4 – 11	
Albumin	mean	41	43	0.320
[mg/mL]	95% CI	38 - 44	41 - 45	
Urine Parameters				
Albumin	mean	0.5	1.0	0.069
[mg/L]	95% CI	0.2 – 0.8	0.6 – 1.6	
Creatine	mean	91	131	0.241
[mg/L]	95% CI	35 - 146	99 - 163	
Albumin/Creatine	mean	11	9	0.0241
[ug/mg]	95% CI	4 - 17	6 - 12	

Table 5.2: Determination of NEFA in whole plasma samples from NIH, using the WAKO NEFA kit (*179*). Enough plasma sample remained to run this analysis once with duplicates. Trends match previous literature studies in that T2D plasma has about two fold higher NEFA then HC plasma. Standard deviations (STD) are included, and the p-value for the measured difference between T2D and HC was 0.024.

Sample	Average 550nm Absorbance - Background	Whole Plasma NEFA Concentration (mEq/L)	STD
26800013	0.122	0.42	
26800016	0.086	0.24	
26800017	0.135	0.48	
26800060	0.051	0.07	
26800063	0.072	0.17	
26800079	0.082	0.22	
26800106	0.069	0.15	
26800122	0.081	0.22	
HC Averaged (mEq/L)		0.24	0.14
26800077	0.121	0.41	
26800101	0.124	0.42	
26800134	0.120	0.41	
26800304	0.180	0.70	
26800457	0.175	0.67	
26800552	0.098	0.30	
26800581	0.090	0.26	
26800586	0.106	0.34	
T2D Averaged (mEq/L)		0.44	0.16

Due to the limited amount of sample available, it was decided that the best method of analysis for the fatty acid cargo on the abundant proteins would be GCMS in the negative chemical ionization mode (NCI). Pentafluorobenzyl ester derivatives of fatty acids have been detected at levels as low as 10 femtograms, using the NCI mode in GCMS (*183*, *184*). The NCI mode produces a high percentage of negatively charged fatty acid molecular ions in the presence of the methane reagent gas, and produces only a single carboxylic acid fragment ion peak for each fatty acid species. The masses of the molecular ions are not fully informative for identification of unknown peaks, however, when matched to retention time and mass of PFB fatty acid ester standard peaks, the NCI

method has very high sensitivity for fatty acid species. It was deemed beneficial to utilize the highest degree of sensitivity at our disposal because of limited sample amounts available.

GCMS Sample Preparation from Extracts of Abundant Plasma Proteins

Forty micro-liters of human plasma was diluted with Agilent buffer A, and injected onto an Agilent MARS14 immuno-depletion column. Separations were performed on a GE AKTA FPLC. Elution conditions were 100% Agilent buffer A, with a flow rate of 0.5 mL/minute. At 4.5 minutes the flow was increased to 1.0 mL/minute. At 6.5 minutes, the conditions were changed to 100% Agilent buffer B. The HSA peak was collected from 7.6 – 9.0 minutes. The elution was altered at 13.5 minutes to 100% Agilent buffer A, to regenerate the column, until the end of the run at 25 minutes. The abundant protein fraction containing HSA was collected, frozen, and lyophilized for analysis.

A known amount of an internal standard of pentadecanoic fatty acid (C15:0) was added to each sample after thawing. Hydrophobic molecules were extracted using a modified Folch extraction procedure, which uses an extraction solvent of (2:1) dichloromethane (DCM): methanol (MeOH) (*184, 185*). For this forty micro-liter sample volume, 2 mL of 2:1 DCM: MeOH, and 1 mL 0.88% aqueous potassium chloride (KCl) were added to the lyophilized HSA samples. The hydrophobic compounds, including fatty acids, were extracted into the lower DCM layer, during a two-hour incubation with agitation. The DCM layer was removed and dried under a stream of nitrogen gas. The

dried hydrophobic material was reacted with [1/10/1000][v/v/v] [PFB Br/ diisopropylamine (DIA)/(ACN)] and 0.1% butylated hydroxytoluene (BHT) at 60° C. These conditions form PFB fatty acid esters from esterified and non-esterified fatty acids (*183, 184*). The derivatized sample was dried under a nitrogen gas stream and re-solublized in 200 uL of n-hexane. Samples were analyzed by GCMS using the NCI mode with methane reagent gas. The fatty acids were quantified using fatty acid response curves from even chain fatty acid standards, after normalization to the C15:0 internal standard spike.

The GCMS analysis was carried out on a Shimadzu QP2010 MS (Kyoto, Japan), equipped with a 2010 GC and AOC-20i auto injector. The fatty acid PFB esters, dissolved in hexane, were injected, using splitless injection, onto a 60 m x 0.25 mm i.d., 25 um ZB-FFAP coated Phenomex (Torrance, CA) capillary column interfaced directly to the ion source. The GC oven temperature was programmed to hold for 3 minutes at 120º C after sample injection, and then increased to 200º C at 6.5ºC per minute. The oven temperature was then raised from 200º to 240º C at 5º C per minute, from 240º to 250º C at 20º C per minute, and finally held at 250º C for 30 minutes. The injector and interface temperature were maintained at 250º C, and the ion source temperature was set at 200º C. Methane (99.99%) was used as the reagent ionization gas, and fatty acids were analyzed using the parent mass minus the PFB group for the PFB ester derivatives in NCI mode. Ions from 50 – 450 m/z were scanned at a speed of 2000 scans/second. These same conditions were utilized when analyzing for known and unknown peaks on the Shimadzu QP2010 in the electron ionization (EI) mode.

We prepared a standard curve from a series of saturated fatty acids obtained from Sigma, and a mixture of key unsaturated fatty acids of interest obtained from NuChek (Elysian, MN). All of the standard curves showed a linear response, allowing us to normalize the peak intensities of each sample with respect to the internal reference pentadecanoic acid (C15:0), for quantifying individual fatty acid species.

The fatty acid PFB esters extracted from the hydrophobic extract of the abundant proteins using the MARS14 immuno-depletion column are shown in figure 5.3. In the healthy control pilot runs we were able to visualize many more fatty acids, due to increased sample amounts; however, using the small amounts of the study samples available, only 8 major fatty acid PFB esters are reproducibly detected in each of the samples. After normalization of data to the internal C15:0 standard, the combined total fatty acids reveal a decrease by 24% in total fatty acids in type II diabetics. An unexpected decrease in nonanoic acid (C9:0) was also observed in T2D. Figures 5.4 – 5.6 provide a summary of these findings. The fatty acid PFB ester peaks observed appeared relatively small because of the presence of the larger peak at 254 m/z. The peaks at 254 m/z and 434 m/z did not match any known fatty acids, based on mass and retention time. These unexplained peaks were found in both HC and T2D samples; however the normalized peak area of the unexplained peaks was twice the magnitude in T2D samples compared to HC. See figures 5.7-5.9.

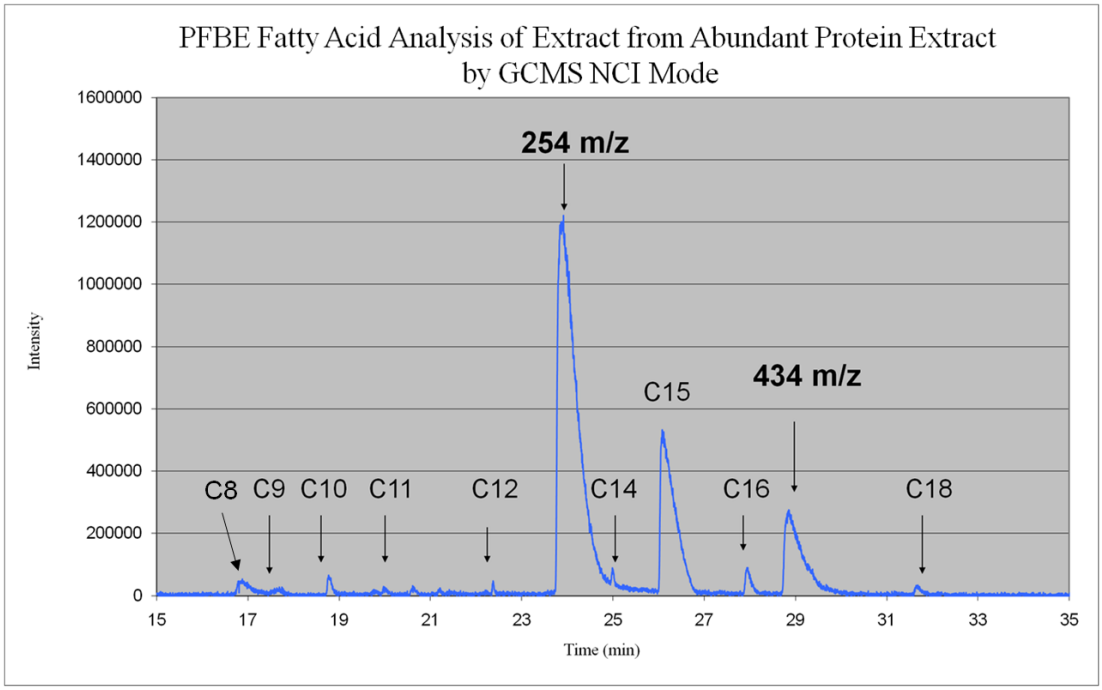

Figure 5.3: PFB Br derivatized hydrophobic extract of the abundant protein fraction from 40uL of human plasma. The GCMS chromatogram was analyzed in the NCI mode with methane reagent gas. The large peaks at 254 and 434 m/z could not be explained by any known fatty acid species.

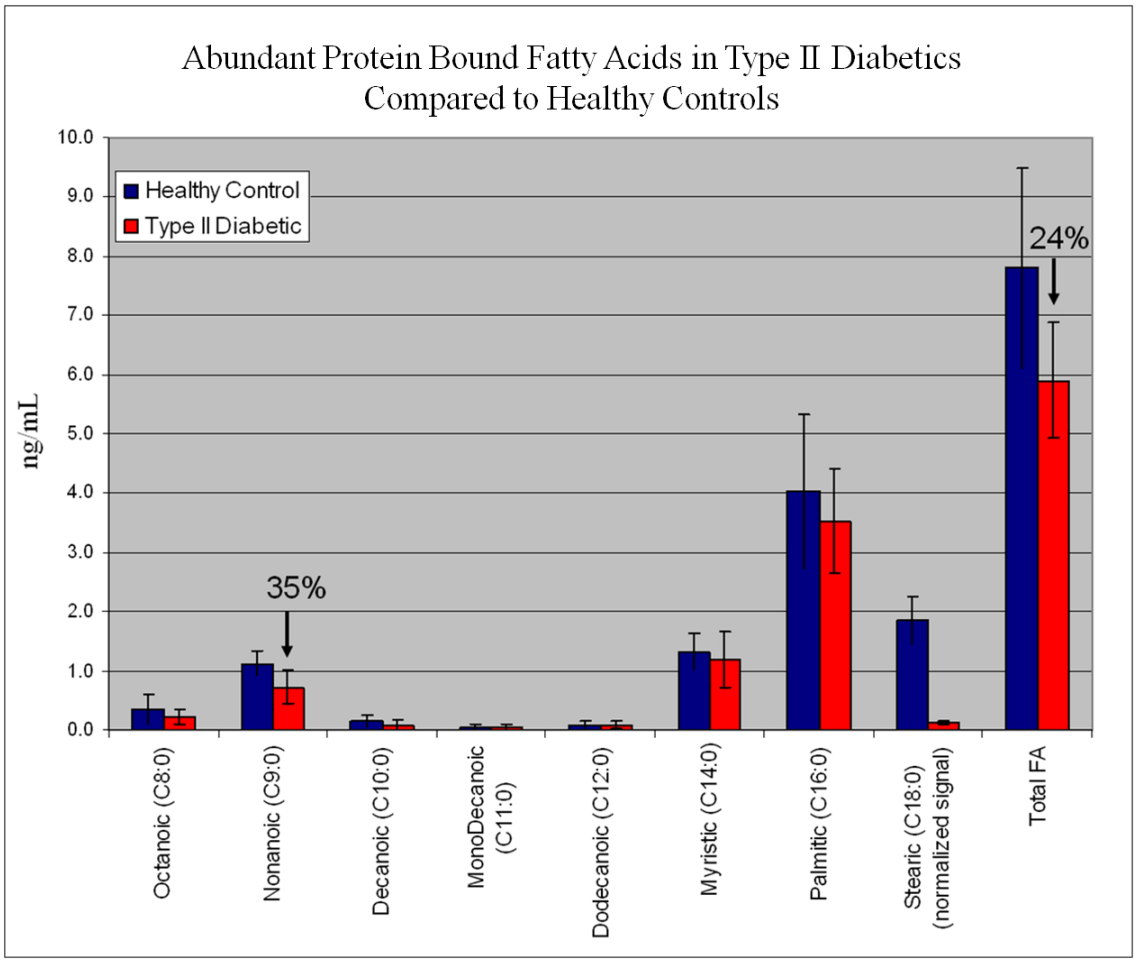

Figure 5.4: Eight saturated fatty acids were extracted from the abundant protein fraction derived from the Agilent MARS14 immuno-depletion column. The hydrophobic extracts were derivatized with PFB Br to form PFB esters and measured by GCMS in the NCI mode. The trend of down regulation of these fatty acid species in diabetic patients is observed in the red bars compared to the values found in the HC in the blue bars.

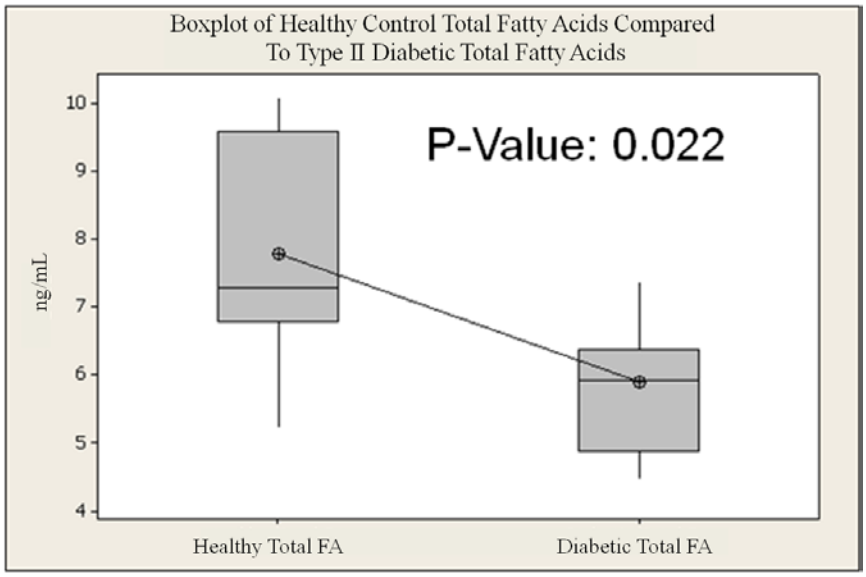

Figure 5.5: Box whisker plot of total fatty acids extracted from type II diabetic and healthy control abundant plasma proteins, as measured by GCMS in the NCI mode.

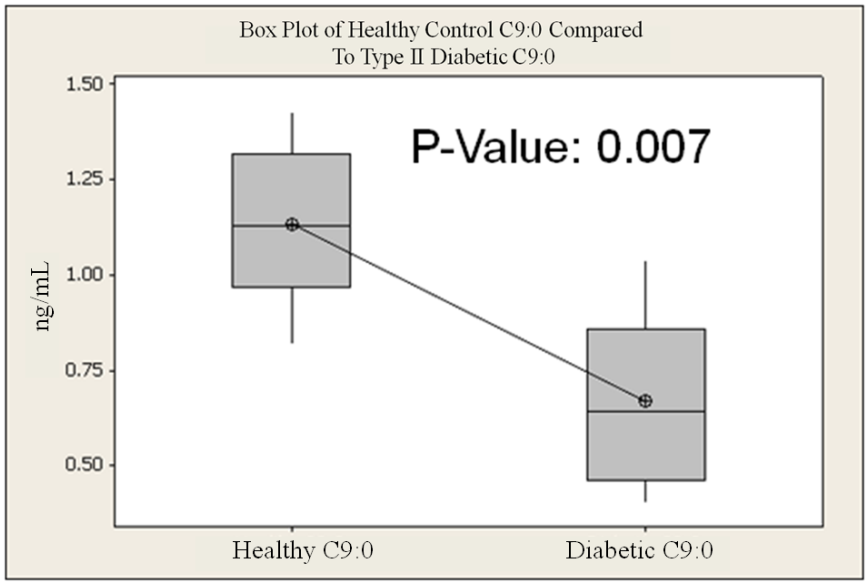

Figure 5.6: Box whisker plot of nonanoic acid (C9:0) levels between type II diabetic and healthy control extracted from the abundant plasma proteins, as measured by GCMS in the NCI mode.

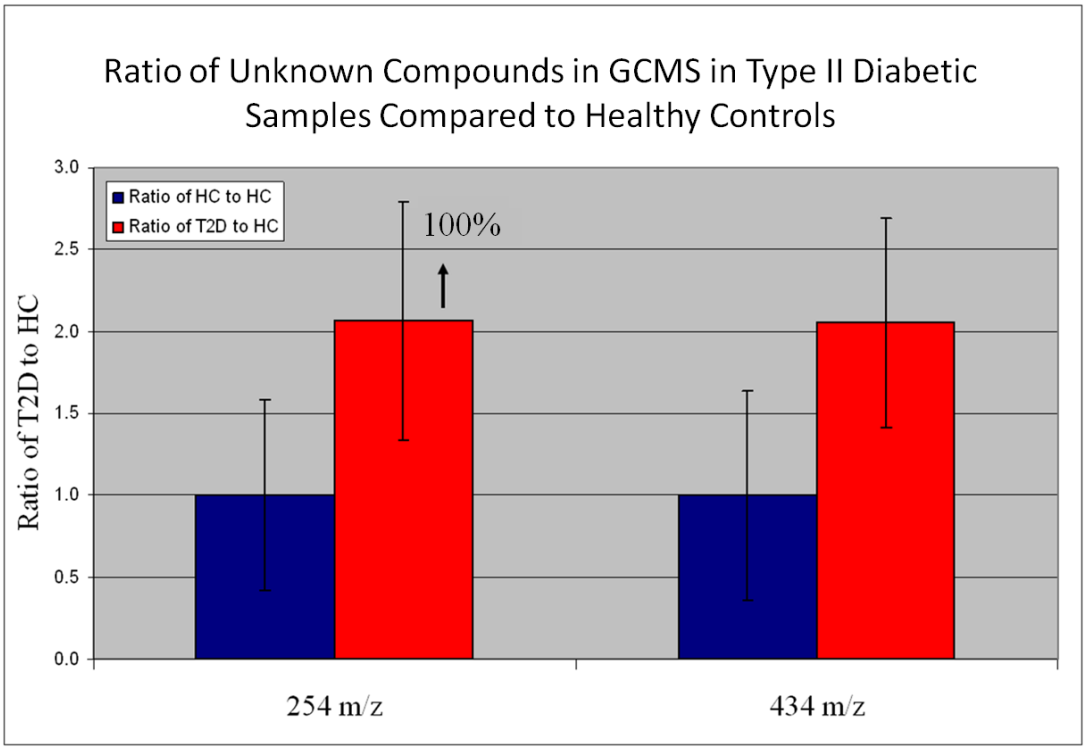

Figure 5.7: The two unknown PFB ester peaks observed in the GCMS in the NCI mode in type II diabetics compared to healthy controls. Both peaks areas increased by 2 fold in type II diabetics, as is shown in red and the variation in the normalized HC is shown in blue.

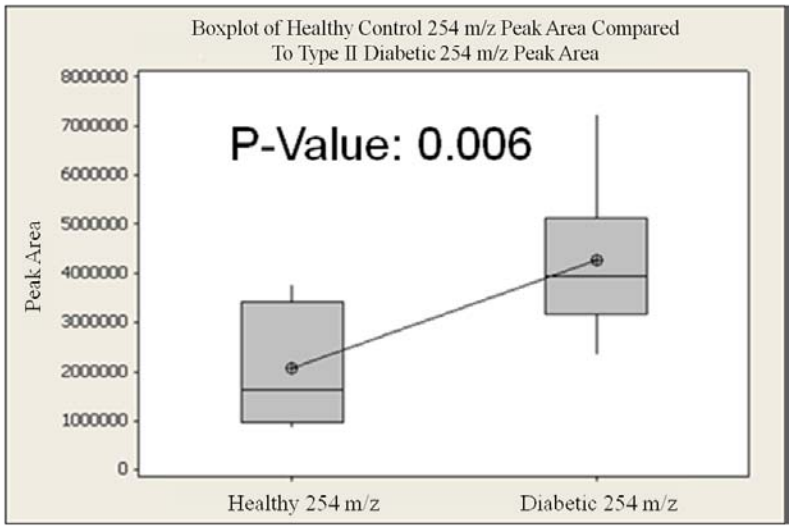

Figure 5.8: Box whisker plot of the peak area at 254 m/z in T2D and HC on GCMS.

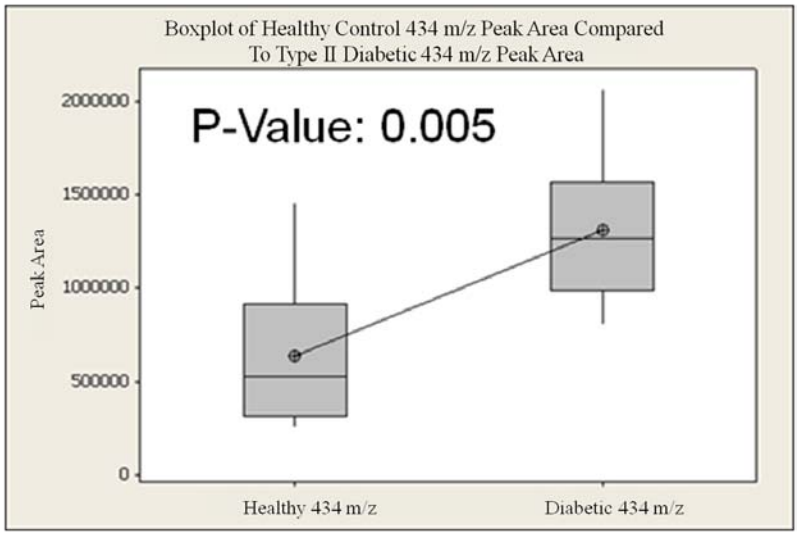

Figure 5.9: Box whisker plot of the peak area at 434 m/z in T2D and HC on GCMS.

Indentifying Unknown PFB Peaks

In an attempt to indentify these unknown hydrophobic peaks, we ran the PFB ester derivatized sample in electron ionization (EI) mode on the GCMS. The fragmentation pattern appeared to contain a PFB, as shown in figures 5.10 and 5.11, by the mass feature at 181, but the full EI fragmentation pattern did not match any compound in the NIST 107 and 121 GCMS EI databases, which contained 163,000 compounds. The hydrophobic extract of abundant plasma proteins that had not been reacted with PFB Br did not reveal these abundant peaks. We then analyzed the PFB derivatized material using ESI in the positive ion mode on a high resolution Bruker MaXis QTOF to gain more information from the accurate mass of the parent compounds and from the accurate masses of the fragments. Exact mass and fragmentation patterns in positive ionization mode revealed the peak at 256 m/z to be a mono-PFB glycine, and the

peak the 436 m/z to be a di-PFB glycine. These two peaks are two mass units larger in ESI positive mode (M+H) than the negative carboxylic acid fragments (RCOO-PFB → $RCOO^-$) formed from the PFB esters measured by NCI GCMS. See figures 5.12-5.13 for explanation of the ESI fragmentation.

Later experiments using the Agilent 6520 QTOF demonstrated that during the electrospray ionization, one PFB ester had been cleaved from both of the 256 m/z and 436 m/z masses in the MS source. The entire PFB ester molecule stayed intact at low voltage ESI, and the parent molecule with one more PFB in an ester linkage could be measured in ESI by adjusting the capillary exit voltage to a lower setting. The parent masses were found to be 436 m/z in ESI, which is a di-PFB glycine, and 616 m/z in ESI, which is a tri-PFB glycine when the lower ESI voltage was used. See figures 5.14 for ESI spectra in the QTOF. The EI fragmentation in the GCMS became clearly interpretable with knowledge of the accurate mass and additional fragmentation information from the QTOF, as is shown in figures 5.10 and 5.11.

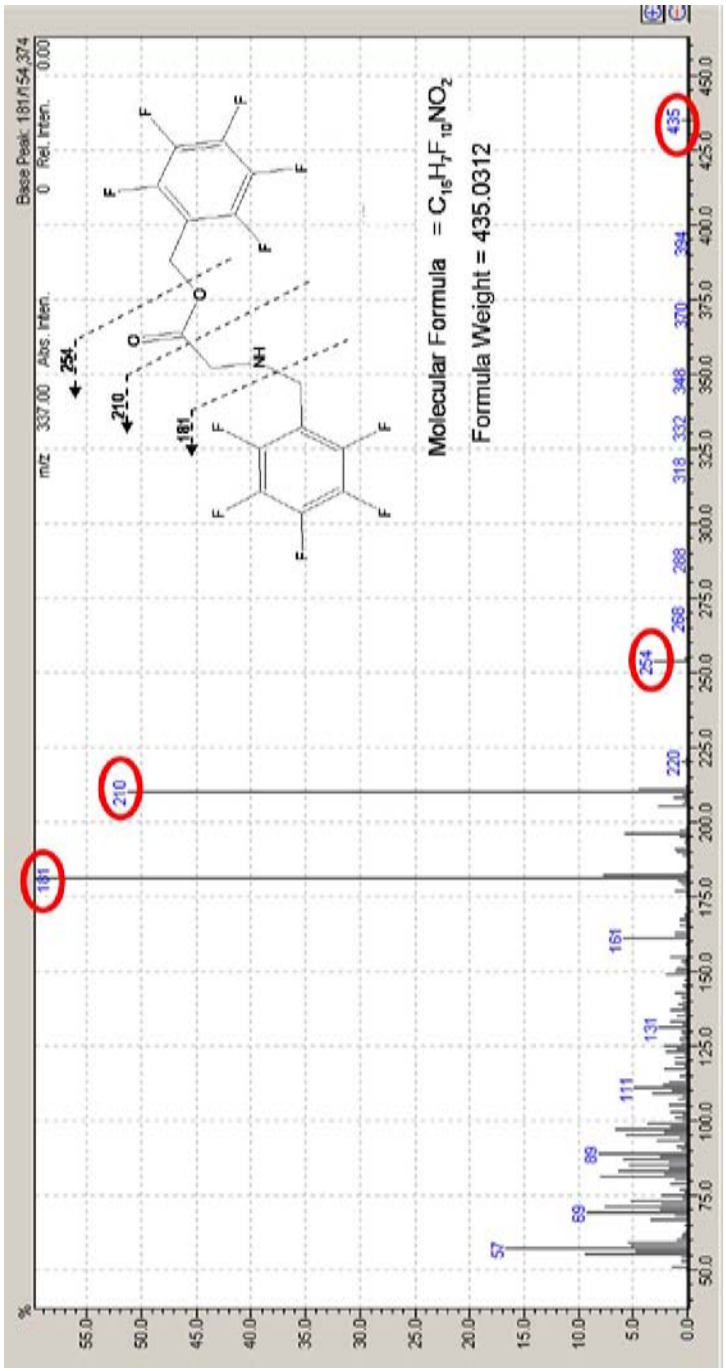

Figure 5.10: GCMS EI signal, fragmentation of the 435 m/z and 254 m/z PFB derivatized peaks, and interpretation of the EI spectrum based on the subsequent QTOF accurate mass ESI data. The di-PFB glycine ester has a parent mass of 435 m/z in EI.

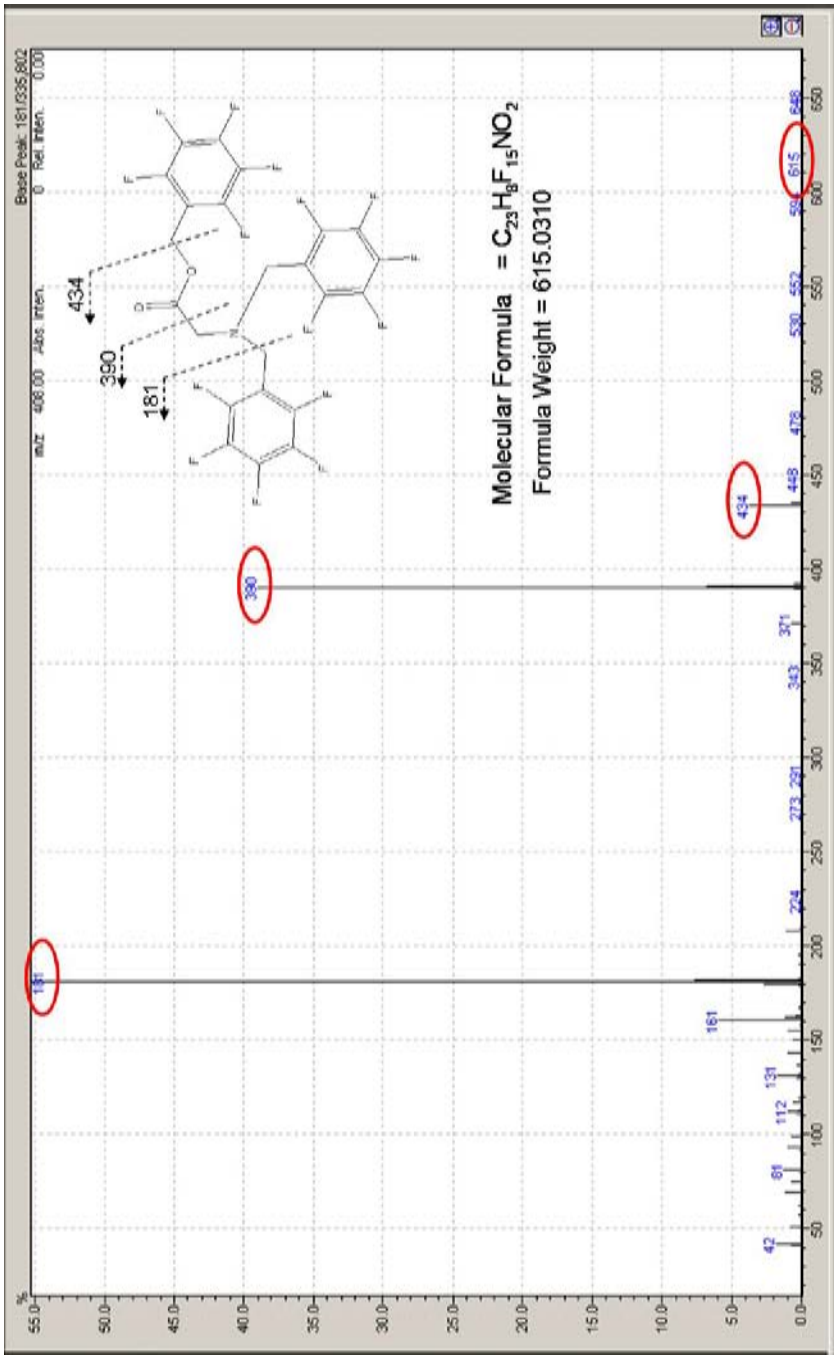

Figure 5.11: GCMS EI signal, fragmentation of the 615 m/z and 434 m/z peaks, and interpretation of the EI spectrum based on the subsequent QTOF accurate mass ESI data. The tri-PFB glycine ester has a parent mass of 615 m/z in EI.

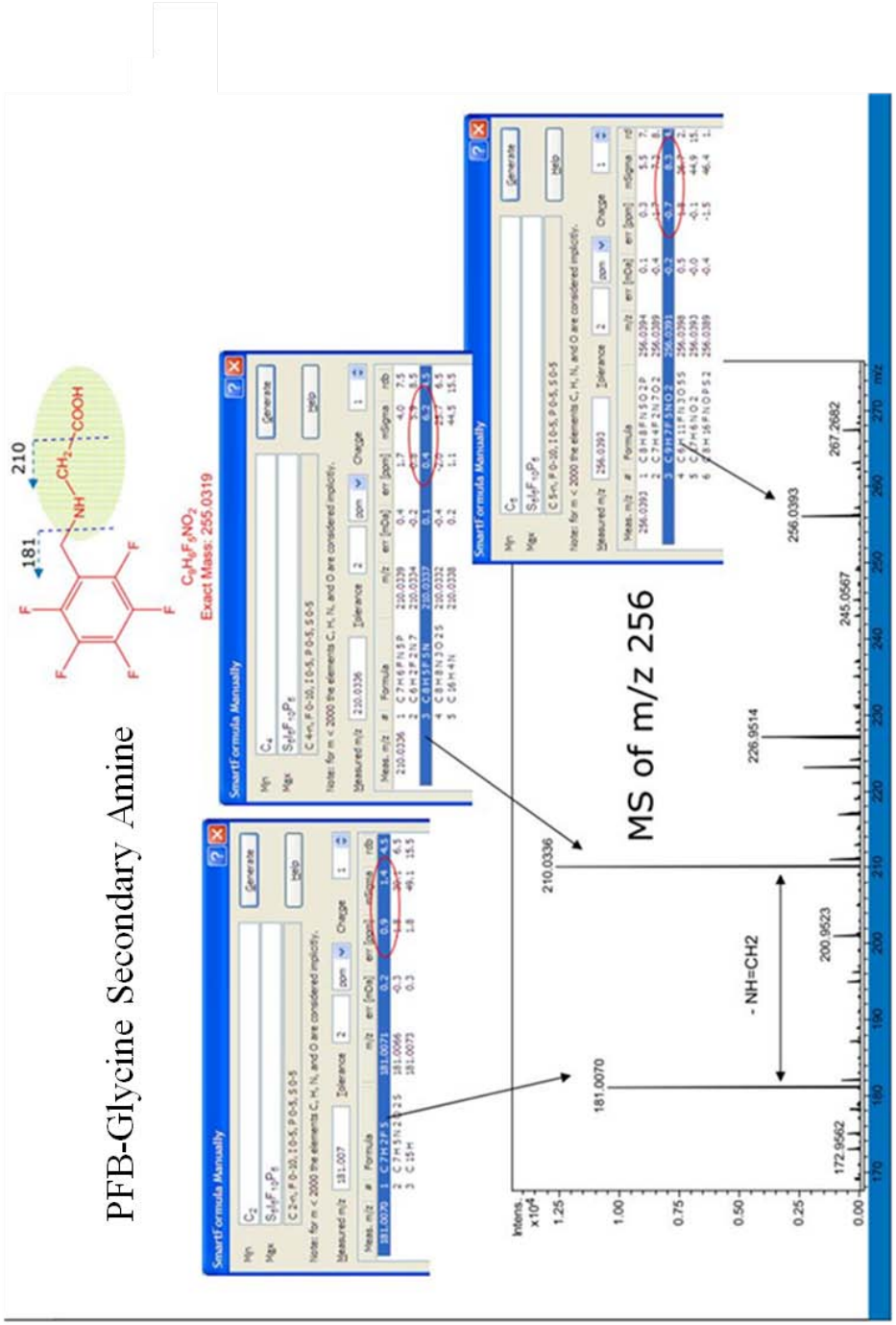

Figure 5.12: Bruker MaXis QTOF ESI fragmentation of what was later found to be Di-PFB glycine using positive mode analysis. One additional PFB was linked to the carboxylic acid as an ester, which fell off during the ESI process at the typical capillary exit voltage conditions used for this spectrum.

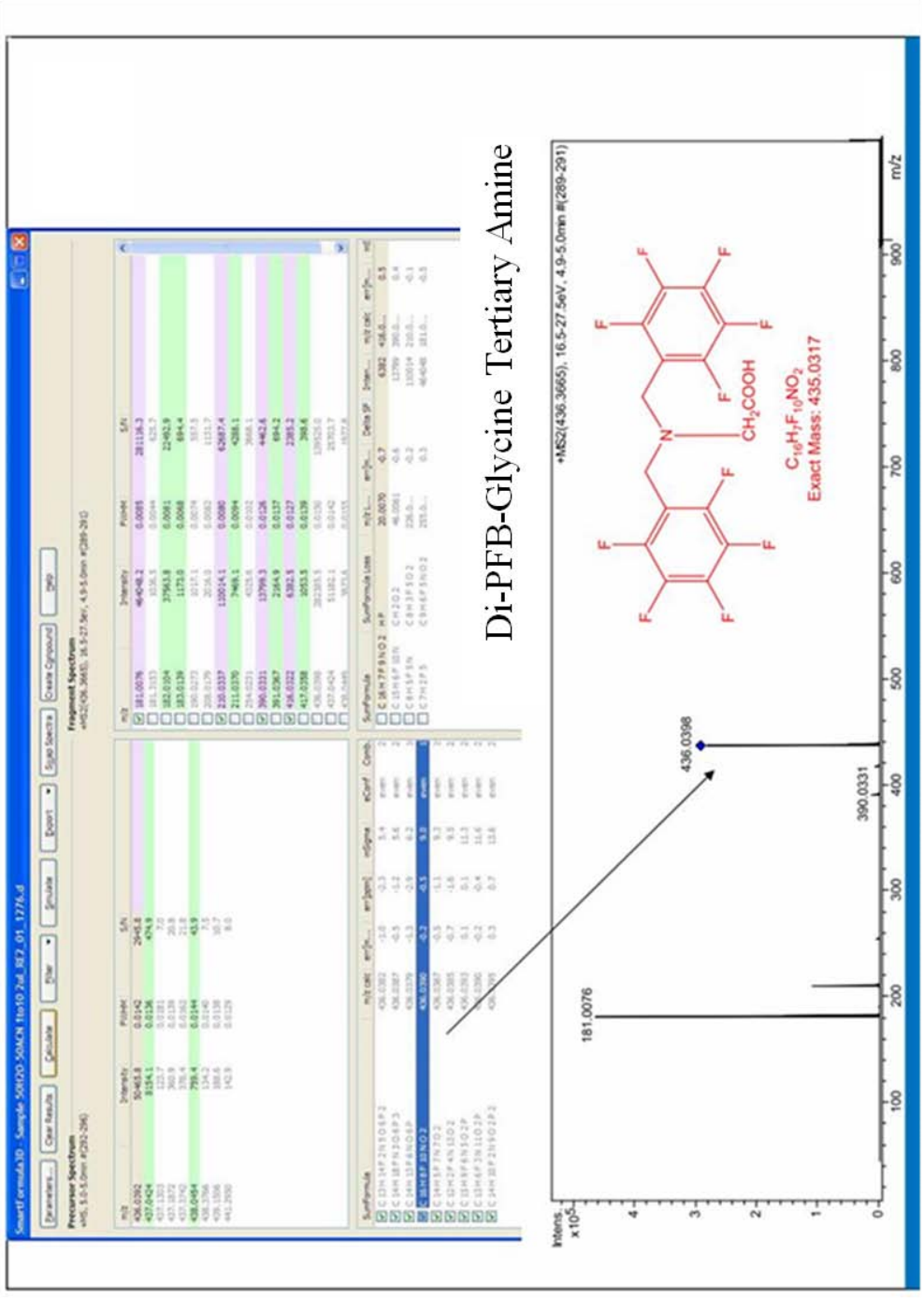

Figure 5.13: Bruker MaXis QTOF ESI fragmentation of what was later found to be Tri-PFB glycine, using positive mode analysis. One additional PFB was linked to the carboxylic acid as an ester, which fell off during the ESI process at the typical capillary exit voltage conditions used for this spectrum.

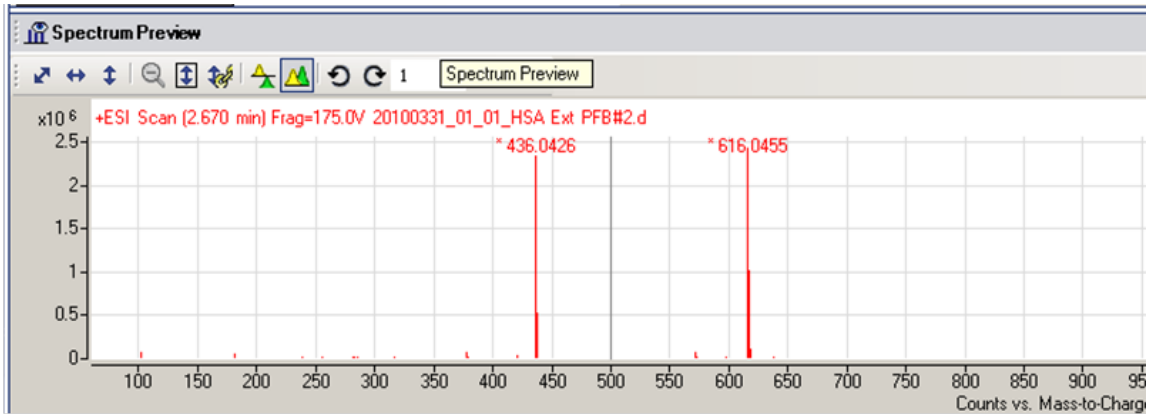

Figure 5.14: ESI spectrum of PFB Bromide reacted authentic glycine produces a di-PFB glycine M + H^+ at 436.04 m/z and tri-PFB glycine M + H^+ at 616.05 m/z species measured on an Agilent 6520 QTOF with reduced capillary exit voltage. The PFB on the carboxylic acid did not fall off during the ESI process when the capillary exit voltage was reduced to 175 volts.

To confirm the tentative identification of these PFB-glycine compounds, we reacted authentic glycine with (1/10/1000) (v/v/v) (PFB Br/ DIA/ACN) and 0.1% BHT at 60° C to form PFB glycine derivative. Accurate mass measurements were made on the Agilent 6520 QTOF with a reduced capillary exit voltage of 175 volts to retain the PFB bound to the carboxylic acid on glycine. This revealed peaks at 436.0426 m/z, corresponding to di-PFB glycine (M + H), and at 616.0455 m/z corresponding to tri-PFB glycine (M + H). GCMS in both EI and NCI modes of the PFB derivative of authentic glycine matched the mass, fragmentation and retention times for the peaks obtained from the hydrophobic extract of the abundant protein fraction in T2D and HC plasma, confirming the identification of the peaks from these abundant plasma extract.

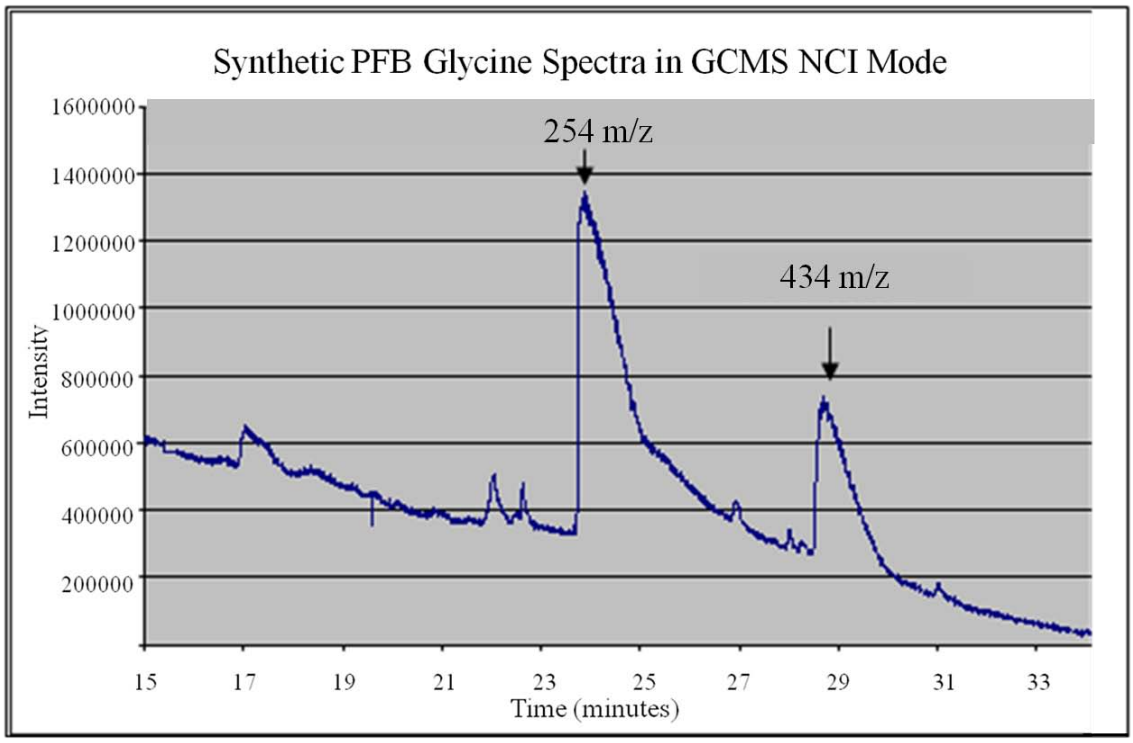

Figure 5.15: Synthetic PFB glycine derivative run in GCMS NCI confirms the identification of the previously unknown 254 m/z and 434 m/z peaks from the hydrophobic extract of the abundant protein fraction from T2D and HC. The PFB glycine showed accurate mass values on an Agilent QTOF consistent with a di and tri-PFB glycine. The GCMS in both EI and NCI modes confirmed this identification by matching mass, fragmentation and retention times for both peaks of the authentic compound to the spectra obtained from the plasma hydrophobic extracts derivatized with PFB Br.

A standard curve for the sum of the di-PFB-glycine and tri-PFB-glycine signals in GCMS from known amounts of the authentic compound (that arise from the loss of the PFB ester from the glycine carboxylic acid) was generated in the presence of an added known concentration of PFB-C15:0 internal standard. This internal standard addition allowed for a determination of the PFB-glycine concentration in the hydrophobic extract of the abundant plasma proteins from T2D and HC samples. PFB glycine species levels were found to be 1.1 nmoles/sample +/- (0.68 nmoles) for HC, and to be 2.4

nmole/sample +/- (0.9 nmoles). It was later found that there was approximately 25 nmoles of HSA in these samples.

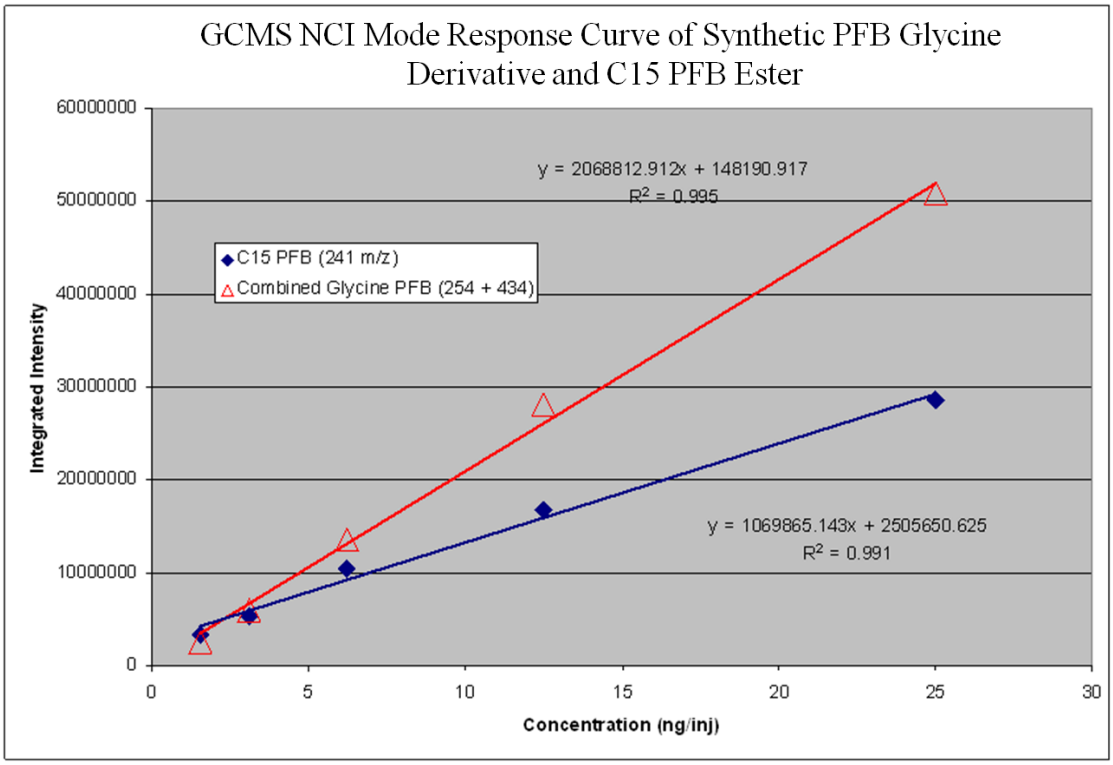

Figure 5.16: Quantification of the amount of PFB glycine species in NCI mode was carried out using a standard curve. Reaction of PFB Br with free glycine produced the same two peaks at 254 m/z and 434m/z as found in the abundant protein fraction of the human plasma, and the areas of both peaks were summed. Known amounts of the authentic PFB-glycine were mixed with known amounts of C15 PFB ester an internal standard to correlate with signal strengths in the original data set. The amounts of PFB glycine in the experimental sample could then be determined using intensity, slope, and intercept of the standard.

To determine how much of this hydrophobic PFB glycine species was bound to the HSA relative to the total abundant protein fraction we acquired an Agilent polyclonal HSA immuno-depletion column to isolate the HAS from the plasma sample. Using this Agilent polyclonal HSA immuno-depletion column, and performing a modified Folch

DCM:MeOH extraction, as previously described, three samples of HSA immuno-depleted plasma, and the corresponding HSA fractions were collected. The DCM hydrophobic extracts of both the HSA immuno-depleted plasma flow through and the hydrophobic extract of the HSA fraction from each sample were derivatized with PFB Br as previously described. GCMS analysis of these hydrophobic extracts found 95% +/- 2% of the hydrophobic glycine-containing compounds were detected in the HSA fraction. This leads us to hypothesize that this type of compound is specifically associated with HSA in plasma, and might be responsible for altering the protein binding properties of HSA inferred from the results of Laffoon (*42*). We hypothesize that these types of glycine-containing compounds may be ubiquitous in all individuals, but were not previously recognized because HSA cargos are not often probed, and PFB ester derivatization is rarely used for fatty acid analysis.

The amount of free glycine, if any, that might partition into the DCM layer along with the hydrophobic compounds when extracting the abundant plasma protein fraction was tested. We solublized a 4 mg sample of isotopically labeled 2[C13] glycine in 500 uL of plasma, and ran the spiked plasma through the Agilent HSA immuno-depletion column to obtain the HAS fraction separated from all the other proteins. We then extracted the aqueous and the hydrophobic fraction, using the same modified Folch extraction procedure that was used in the prior sample preparation steps (*184, 185*). 2[C13] glycine could not be detected in the HSA DCM layer. All of the 2[C13] glycine was accounted for in the MeOH: H_2O layer of the DCM:MeOH extraction of the anti-HSA antibody flow through. This finding leads us to conclude that the glycine we

detected in the hydrophobic extract of the abundant protein fraction of plasma is covalently bound to an unknown hydrophobic moiety or moieties bound to HSA in the plasma samples.

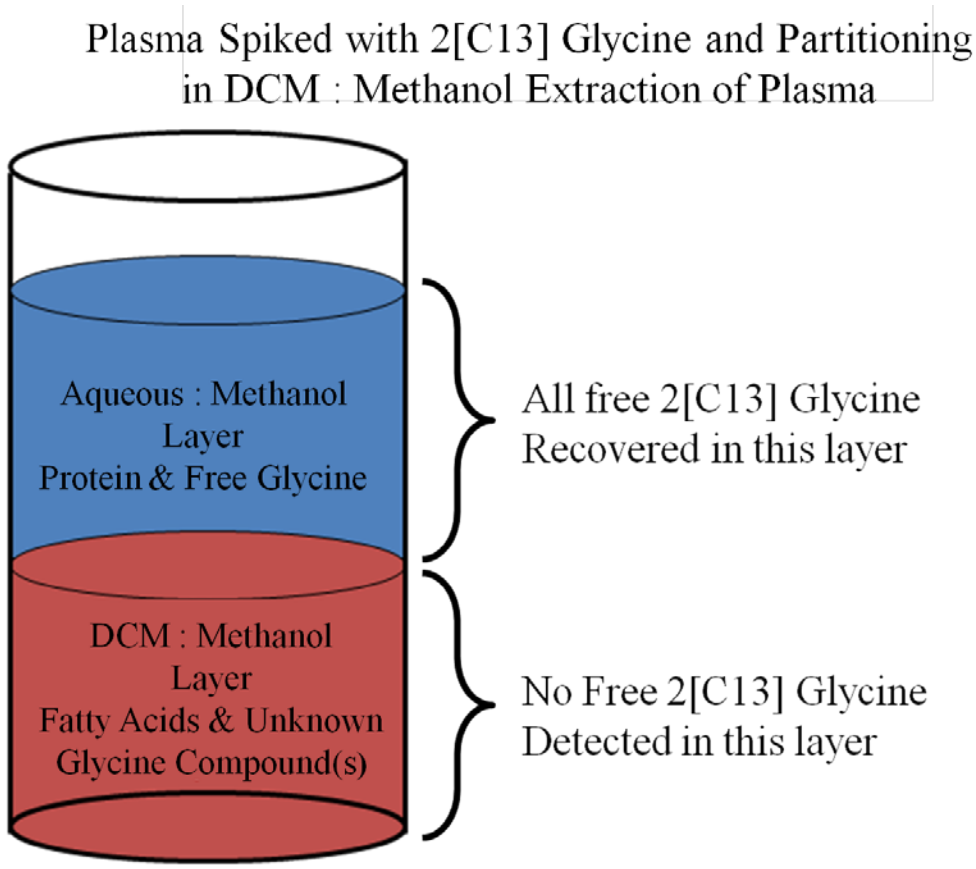

Figure 5.17: Free 2[C13] glycine spiked into plasma and separated in the HSA fraction by immuno affinity does not partition into DCM layer. The free glycine remained exclusively in the aqueous layer. To make this clear, a sample of 500 uL plasma was spiked with 4 mg isotopically labeled 2[C13] glycine, and processed through the same HAS purification extraction steps as described previously. First, the sample was run through an Agilent HSA immunodepletion column, and the flow through proteins and the HSA fraction collected. Second, both protein fractions were extracted with aqueous:MeOH and DCM:MeOH using the same modified Folch method described previously. Third, each of the four fractions were analyzed for isotopic 2[C13] glycine by LCMS. Fourth, the fractions were derivatized with PFB Br to increase detection sensitivity with PFB derivatives and analyzed by LCMS.

A.

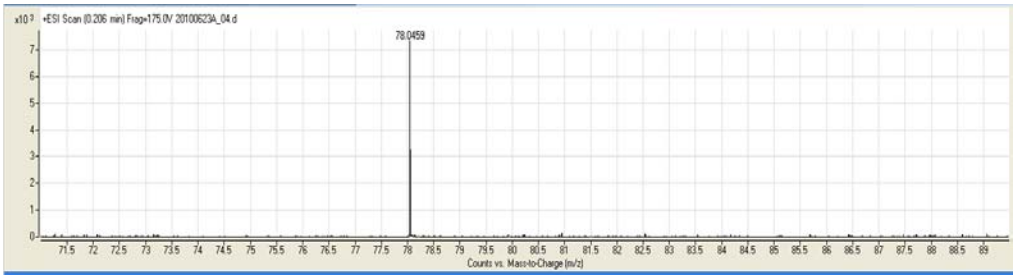

B.

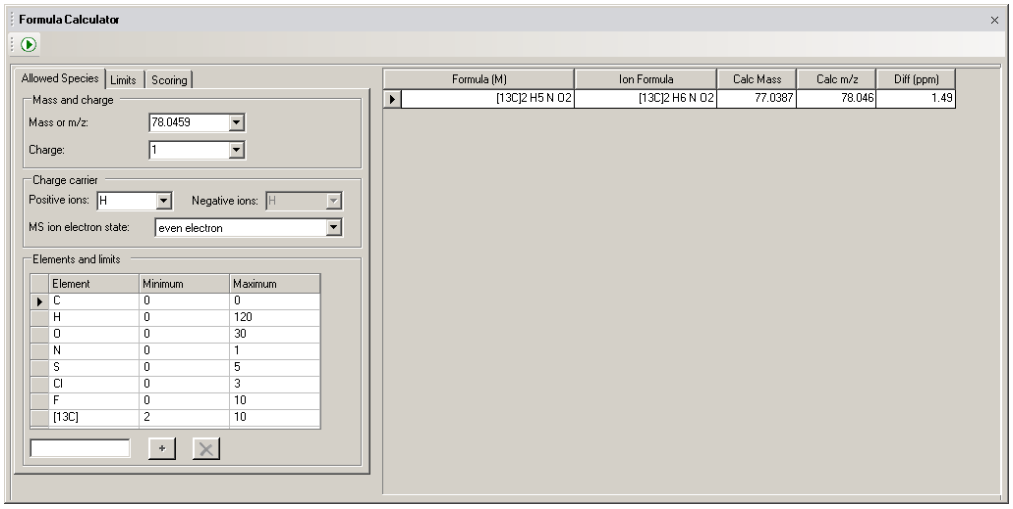

Figure 5.18: (a) LC QTOF analysis of each of the plasma protein fractions found that the aqueous extract layer of the modified Folch extraction of the flow through from the HSA immuno depletion of plasma contained all the spiked isotopic 2[13C] glycine at 78.0459 m/z. (b) The elemental formula prediction $[13C]_2H_5NO_2$ for the observed 78.0459 m/z peak was within 1.49 ppm of the calculated 78.046 m/z for isotopic 2[13] glycine, confirmed that this was the only fraction to contain the isotopic 2[13] glycine.

A.

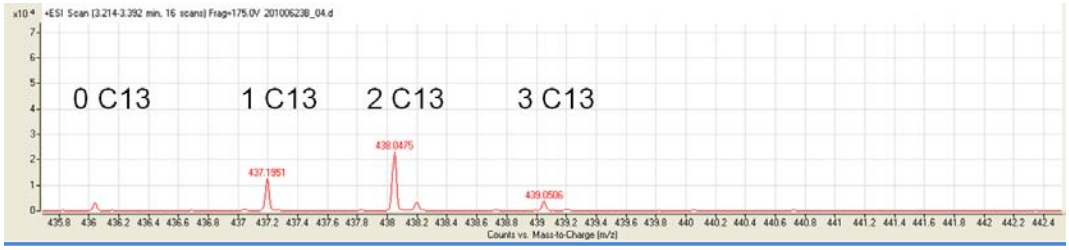

B.

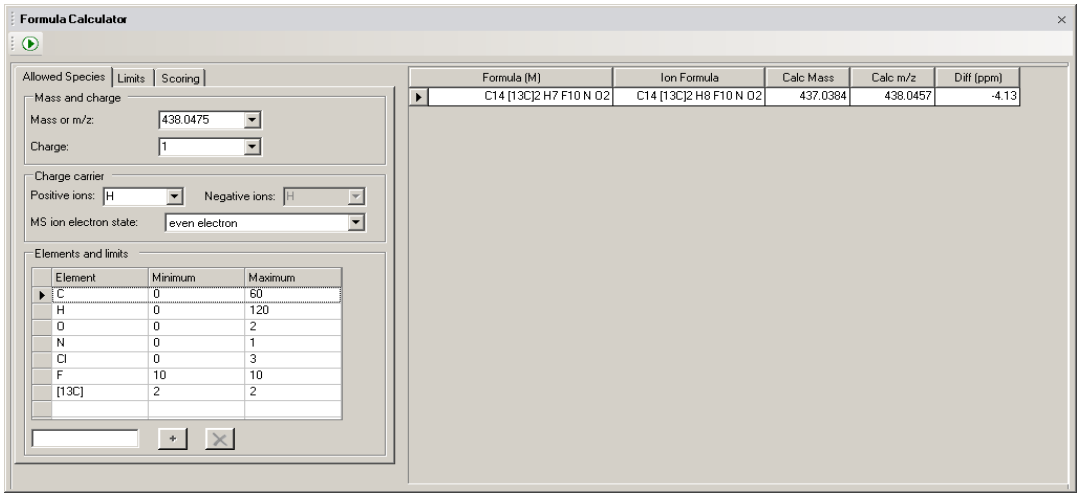

Figure 5.19: Each fraction from the modified Folch extracts of the HSA immuno depletion of the plasma that had been doped with 2[C13] glycine was derivatized with PFB Br, as previously described, and measured on the QTOF. To gain greater sensitivity and make sure that the isotopic 2[C13] glycine is not somehow now covalently trapped along with a hydrophobic compound and later released during derivatization. (a) Only the HSA immuno-depletion column flow thru fraction from plasma was found to contain the isotopic 2[C13] glycine, which had been spiked into the starting plasma sample. The isotope pattern observed corresponded to the 2[C13] enrichment of the starting 2[C13] authentic glycine. (b) The elemental formula prediction for the observed (M+H) 438.0475 m/z peak of the PFB glycine derivative was within 4.13 ppm of the calculated 438.0457 m/z for PFB 2[13] glycine with 2 PFB groups.

We investigated several hydrophobic glycine-containing molecules that were known to associate with HSA seeking to identify the unknown parent compounds we found bound to HSA and elevated in T2D. The known compounds investigated were all glycine amides, as shown in table 5.3. We had no success in cleaving the glycine amides

and forming a PFB-glycine from any of these compounds using our PFB Br reaction conditions. Several other synthetic glycine containing molecules were also tested as shown in table 5.3. Those molecules with a glycine ester bond attached to the hydrophobic moiety were susceptible to cleaving the glycine during the PFB Br reaction and reacting to form PFB esters. These results are summarized in table 5.3. The PFB glycine esters also bound one or two additional PFB's on the glycine amino groups at expected. Although we did not test glycine thioesters under PFB Br derivatization conditions, organic chemistry principals predict that glycine thioesters would also be cleaved by the basic PFB Br derivatization conditions that yield PFB-glycine esters. There are glycine amides joined to hydrophobic groups, but no known glycine ester or thioester hydrophobic compounds in the Lipid Maps database (22,500 compounds) or the Metlin (metabolite) database (25,467 compounds), which comprise the most comprehensive collection of MS data on hydrophobic compounds available to us (*186, 187*). It appears that only glycine esters or glycine thioesters and not glycine amides would yield PFB derivativatized glycine under our conditions, but no glycine ester or thioester compounds are known in biology. We are now investigating the possibility that Schiff bases of glycine formed from reactive aldehydes or ketones might be cleaved to liberate PFB esters of the glycine carboxylic acid and PFB glycine amines under the conditions we used.

Table 5.3: PFB Br derivatization reactions were performed on several compounds known to be present in plasma and bound to HSA that contain a glycine attached to a hydrophobic moiety. Compounds bound through an amide linkage to glycine were unreactive to the standard conditions (1/10/1000) (v/v/v) (PFB Br/ DIA/ACN) and 0.1% BHT at 60° C we employed in these studies. However, ester linked glycine compounds reacted under these conditions to liberate the glycine and produce PFB glycine derivatives.

Compound	Formula & (Glycine Linkage)	Aqueous: or DCM Layer	Glycine Cleaves during derivatization	Structure
Glycocholic Acid (Bile Salt)	C26H43NO6 (amide)	Not Measured	No	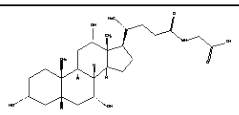
Reduced Glutathione	C10H17N3O6S (amide)	Not Measured	No	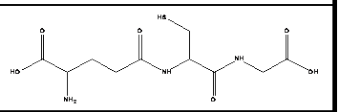
Oxidized Glutathione	C10H17N3O9S (Amide)	Not Measured	No	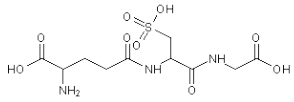
Oleolyglycine	C20H37NO3 (Amide)	DCM	No	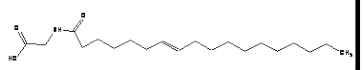
Glycine Benzyl Ester	C9H12NO2 (Ester)	Aqueous	Yes	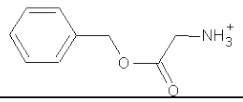
O-octadecyl glycine	C20H41NO2 (Ester)	DCM	Yes	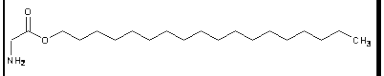

This unknown compound (or possible family of compounds) appears to be potentially extremely important, due to the strong correlation with T2D. Our desire to understand the structure and biology of these unknown glycine-containing molecules has led us to probe the unreacted plasma for this previously unknown compound, which was found at different levels in both healthy and diseased individuals. We found these two rarely used approaches extraction of hydrophobic cargo abundant plasma proteins and PFB Br derivatization that yielded unexpected results. Identification of these new

compounds has the potential to generate new mechanistic insights and diagnostic possibilities.

To better understand the hydrophobicity of these new compounds we investigated their solubility. First, samples of pooled T2D and pooled HC hydrophobic extracts were prepared. We washed the DCM: MeOH extract with water. When water is used to wash the DCM:MeOH layer much of the methanol in the DCM layer partitions into the water layer, thus giving a more hydrophobic DCM layer depleted of methanol, and a methanol rich water layer, which has different partitioning properties then the original DCM:MeOH and H_2O:MeOH solvent system. The wash layer and the residual DCM layer were treated with the PFB Br derivatization conditions. A large fraction of the PFB glycine-reactive species were observed in the aqueous wash layer of the DCM:MeOH layer from the modified Folch extract of the HSA bound immuno-depletion fraction as shown in figure 5.20. The PFB-glycine-reactive species behaved differently in the T2D and HC samples. Our hypothesis to explain this partitioning behavior is that the compounds of interest present in T2D and HC are substantially different and the bulk of the hydrophobic glycine-containing species in T2D requires a higher percentage of methanol to remain soluble in the DCM:MeOH layer. When water is added to the DCM:MeOH the MeOH is largely removed from the DCM layer, but some very abundant glycine-containing PFB Br reactive species are partitioned into the aqueous methanol wash layer. This water wash layer of the modified Folch DCM:MeOH layer is the richest source of PFB-glycine signal from the T2D samples.

There were distinct differences in the behavior of the glycine-containing PFB reactive species associated in this layer between T2D and HC sample pools, this suggests that a family of glycine-containing compounds is involved, or alternatively it is possible that the compounds have been changed due to multiple environmental manipulations. It is hypothesized that a HILAC column, which binds polar compounds in high organic solvent and elutes these polar compounds with an increasing aqueous solvent gradient, may be an excellent approach to investigate the compounds in this DCM:MeOH aqueous wash layer by QTOF MS in the future.

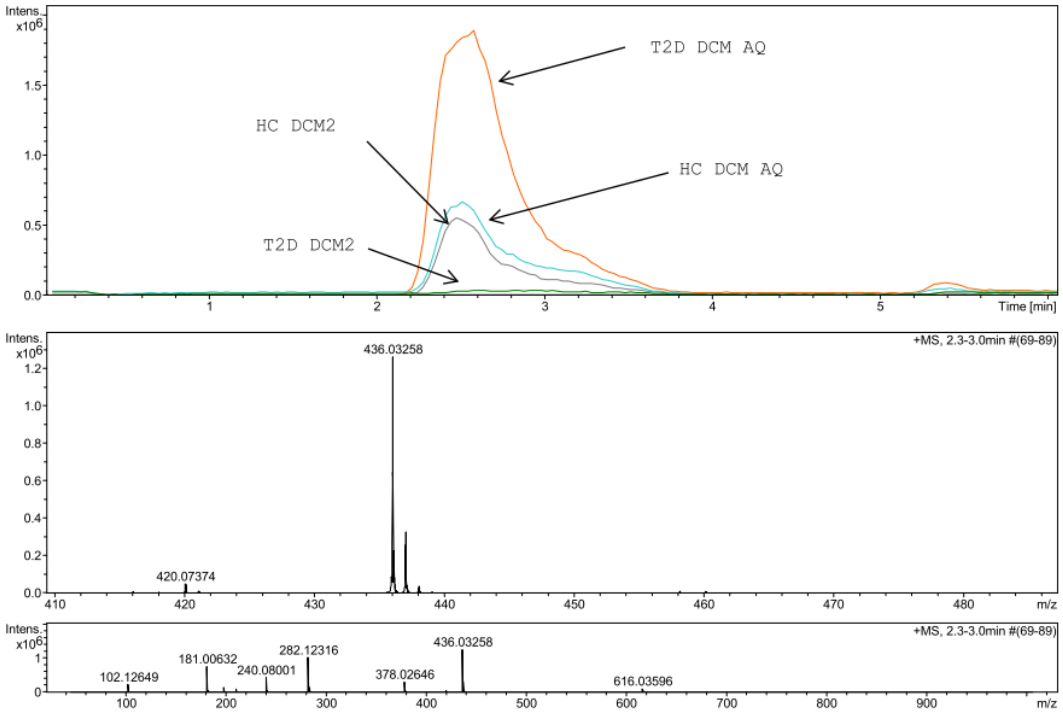

Figure 5.20: Differences in solvent partitioning of the glycine-containing compounds in the pooled T2D and HC sample extracts from HSA were observed. The DCM (DCM2) layer and DCM layer washed with water (DCM AQ) were analyzed on a Bruker MicroTof. The capillary voltage allows some 616 m/z tri-PBF glycine to appears, but the most sensitive signal is the 436 m/z using the commonly used settings on the Bruker MicroTof. The results indicated that T2D DCM wash layer was by far the richest in glycine-containing compounds. Whereas the glycine-containing compounds from the HC

Figure 5.20 (continued) partitioned almost equally between the aqueous wash of the DCM layer and the DCM2 layer suggests that a family of glycine-containing compounds are significantly different in HC and T2D.

RP Separation of the Unknown Glycine-Containing Compounds

The DCM2 layers in figure 5.20 from the T2D and HC samples, were dried and taken up in a 4% ACN and 96% water solvent, and separated using an ACN gradient on a C12 RP column on the Agilent 6520 QTOF. The gradient conditions to separate the hydrophobic compounds present in the DCM2 are shown in table 5.4. One minute fractions were collect across the entire HPLC run. Each fraction was divided into two aliquots which were both frozen, and lyophilized to dryness. One half of each fraction was reacted with the PFB Br derivatization conditions. PFB-glycine signals were detected in both T2D and HC samples prepared from the abundant protein hydrophobic extract of the MARS14 immuno-affinity column, assuring that the hydrophobic glycine containing compound(s) were eluting from a C12 RP column.

Table 5.4: The RP HPLC method used for separating and fractionating the HSA extracted hydrophobic compounds found in the DCM2 layer. A Jupiter 4u Proteo 90A, 250mm x 10mm RP C12 column was equilibrated with buffer A (0.1% TFA water) and eluted with a buffer B (0.1% TFA ACN) gradient at 0.2 mL per minute.

Time (minutes)	% Buffer B (0.1% TFA ACN)
0	4
0.5	4
8	20
14	100
20	100
20.01	4
32	4

The PFB Br derivatization-reactive glycines from T2D and the paired HC sample were found in 5 distinct peaks eluting from the C12 RP column, under the solvent gradient employed, as shown in figures 5.21. Only the first fraction at four minutes appears to contain the biomarker species associated with the newly diagnosed T2D samples (red trace in figure 5.21). Two types of healthy control samples were analyzed in this way. The HC paired with the T2D was from fasting donors (in blue) were matched to T2D samples which were from fasting donors, and the other HC was not fasting (in green). Quite different glycine-containing compounds were observed in the two HC samples by reverse phase fractionation, compared to the T2D sample as shown in figure 5.21. The second healthy control sample in green was from a non-fasting blood plasma, used in method development.

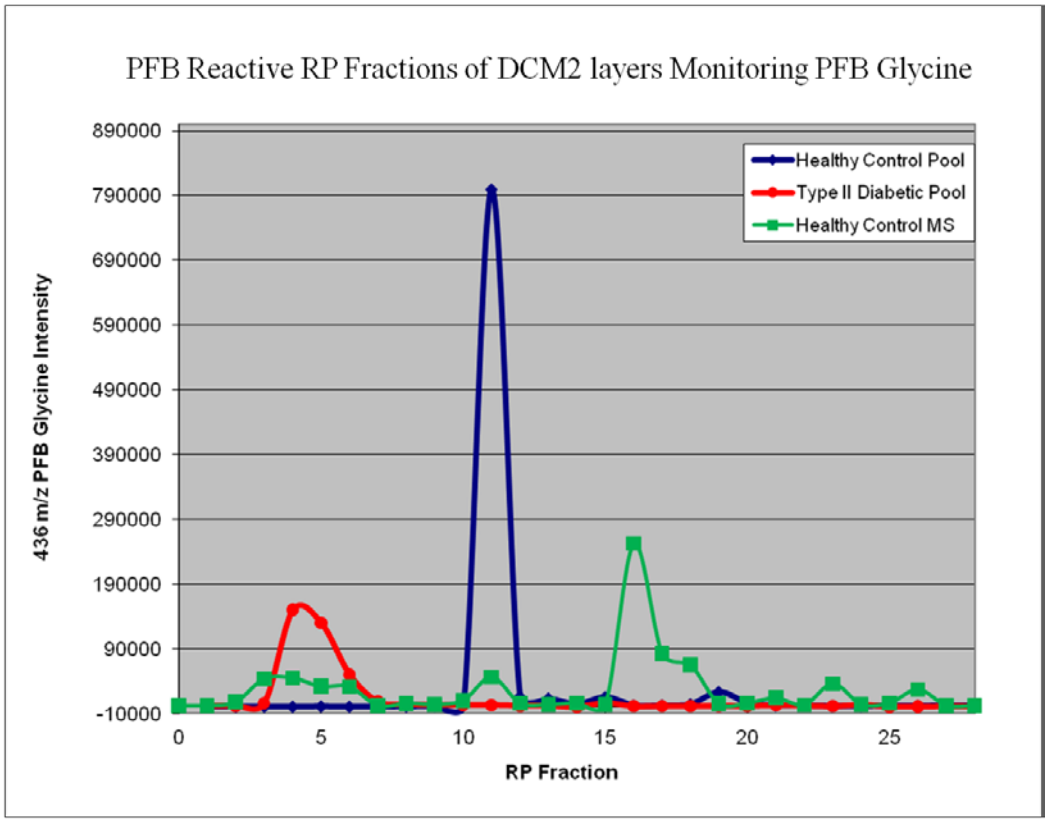

Figure 5.21: Samples of DCM2 hydrophobic extracts from the abundant protein MARS14 fraction were separated on a C12 RP. One-minute fractions were collected throughout each RP run. Each fraction was divided in half, and one half was reacted with the PFB Br to monitor glycine-containing compounds that are susceptible to PFB derivatization. Monitoring for the PFB glycine compound 436 m/z peak with the Agilent 6520 QTOF, 5 peaks at unique retention times were found to contain PFB glycine. Only the first peak at 4 minutes appears to be associated with fasting pooled diabetic sample (red). A peak at 11 minutes was associated with the fasting pooled HC (blue). Additional peaks in green were observed from a non-fasting HC.

The other un-reacted half of these fractions from the HSA hydrophobic samples were analyzed in triplicate using the Agilent QTOF 6520 to search for peaks changing significantly between the pools of T2D and HC fractions. These fractions were fragmented using auto MS/MS in both positive and negative ionization modes to search for glycine-containing compounds. Several compounds with a glycine fragment mass at

74.0248 m/z were detected in negative ionization mode in the 4 minute RP C12 T2D sample, whereas none of these fractions yielded glycine fragments in positive mode. Detection of these glycine-containing compounds in this 4 minute RP fraction does not prove that these compounds are the same compounds that were detectable after derivatization with PFB Br; however, they are strongly correlated, and this strategy is the best we were able to devise given limited sample availability. In the remaining RP C12 fractions from both T2D and HC samples in negative and positive ionization modes, there were no detectable glycine fragment ions in the MS/MS spectra, using auto MS/MS fragmentation. Since glycine-containing compounds were present in these fractions as revealed by the PFB Br derivatization, it was likely that insufficient fragmentation energy was used in auto MS/MS or that possibly the relevant peaks were not selected for fragmentation.

The parent masses, elemental compositions, and fragmentation patterns of the compounds that yielded glycine fragments are shown in figures 5.22(a-c), 5.23(a-c), and 5.24(a-c). Since the compounds in the HC are clearly different by RP then the compounds in the T2D samples it is possible that they might require higher MS/MS collision induced dissociation (*188*) energy to fragment and produce glycine, or possibly that the compounds fragments differently and do not yield a detectable glycine fragment. Higher fragmentation energies should be tried when we have been able to purify larger amounts of material and will have stronger MS signals to work with.

Each spectrum containing a fragment ion that matched the glycine molecular fragment mass was assigned an elemental formula prediction, using Agilent's Mass

Hunter software. The exact atomic masses of each element were combined in all possible ways by the software and formulas were computed to determine possible mass matches to the MS and MS/MS spectra, using the high mass accuracy data (< 1 to 2 ppm). Mass accuracy of the elemental formulas computed for compounds 2 and 3 were 10 ppm and 15 ppm respectively. This does not altogether eliminate the best fit formula generated, as the mass accuracy shift may be explained by a low ion intensity, which can distort the mass accuracy. Assuming the compound contains a glycine, we know these structures must contain carbon, hydrogen, nitrogen, and oxygen, and these elements are considered for each mass formula. We do not know if other possible elements such as sulfur, phosphate, or fluorine are present, but the possibility that they may be forces us to allow these elements in potential formulas as well. Potassium and sodium are considered by the software as possible salt adducts, however, in negative mode the possibility of observing an ion with these salts seems very slim. The software also considers the distinctive isotope ratios of elements such as sulfur and chloride, as well as nitrogen and carbon that affect the isotope pattern. Finally, these mass variables are then computed for each of the fragment ions to produce a score and a possible formula. The parent mass formula that best explains all of the fragment ions, and isotope pattern is then ranked the highest. In many cases this strategy can reduce the possible formulas to one or two.

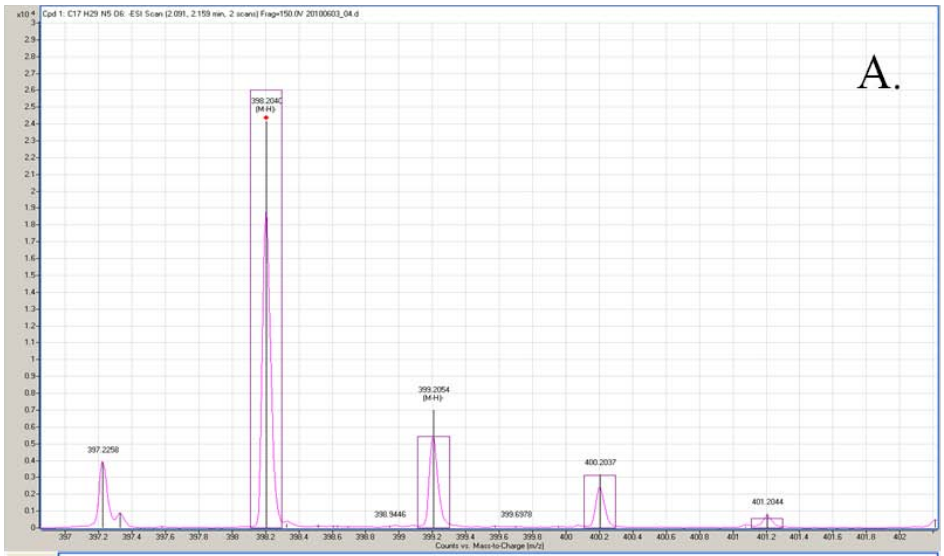

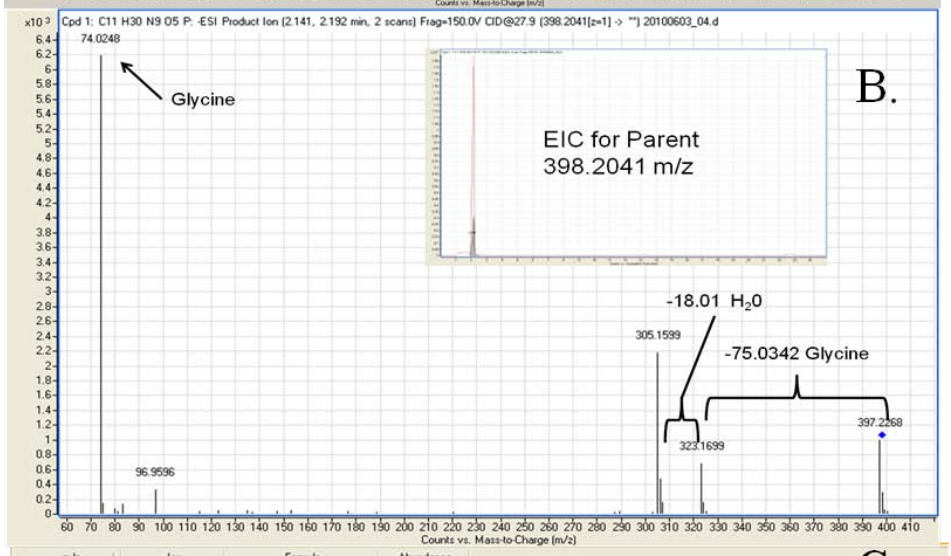

C.

m/z	Ion	Formula	Abundance
398.204	(M-H)-	C19 H33 N3 O2 P S	24141.2

Best	Formula (M)	Ion Formula	Calc m/z	Coverage	Score	Cross Score	Mass	Calc Mass	MS/MS Score
1 ☑	C19 H34 N3 O2 P...	C19 H33 N3 O2 P S	398.2037	87.72	84.89		399.2113	399.2109	79.1
2 ☐	C17 H37 N O5 S2	C17 H36 N O5 S2	398.204	90.77	84.57		399.2113	399.2113	85.33
3 ☐	C17 H29 N5 O6	C17 H28 N5 O6	398.2045	87.72	69.73		399.2112	399.2118	80.93
4 ☐	C11 H30 N9 O5 P	C11 H29 N9 O5 P	398.2035	87.72	68.1		399.2113	399.2108	81.59
5 ☐	C16 H33 N O10	C16 H32 N O10	398.2032	87.72	65.83		399.2112	399.2104	82.93

	MS/MS Score	Diff (ppm)	Abs Diff (ppm)	Abund Match	Spacing Match	Mass Match	m/z	DBE	MS Score
1	(cont) 79.1	-0.8	0.8	69.88	81.08	98.71	398.204	5	86.27
2	(cont) 85.33	0.15	0.15	68.67	72.1	99.96	398.204	0	84.39
3	(cont) 80.93	1.35	1.35	37.23	44.33	96.34	398.204	6	67.07
4	(cont) 81.59	-1.28	1.28	16.79	59.01	96.7	398.204	2	64.89
5	(cont) 82.93	-1.97	1.97	31.7	36.57	92.39	398.204	1	61.76

Figure 5.22: Compound 1 found to contain a glycine fragment using auto MS/MS with an Agilent 6520 QTOF. (A.) Parent mass (M+H) 398.2040 m/z isotope pattern profile, the pink boxes are the predicted isotope pattern for compound 2 with a sulfur included in the isotope pattern overlayed against the centroided (line) data. (B.) Compound 1 has an average parent mass of 398.2041 m/z. (C.) Elemental formula predictions are numbered 1 – 5.

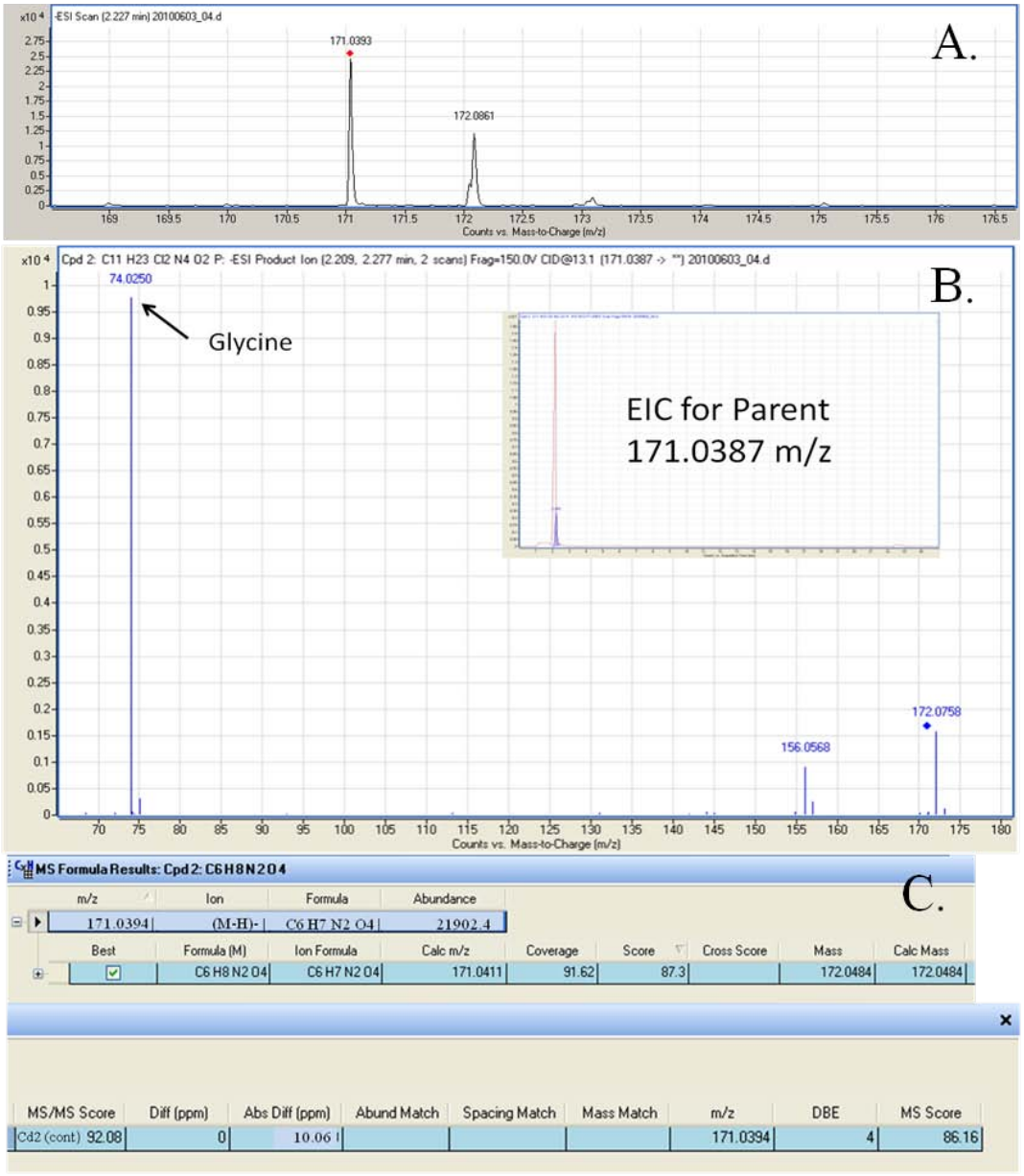

Figure 5.23: Compound 2 found to contain a glycine fragment using auto MS/MS. (A.) Parent mass (M+H) 171.0393 m/z showing the observed isotope pattern. (B.) Compound 2 has an average parent mass of 171.0387 m/z. (C.) The best predicted formula was $C_6H_8N_2O_4$. The best fitting formula was deduced using MS/MS data, high mass accuracy, and isotopic ratios from compound 2.

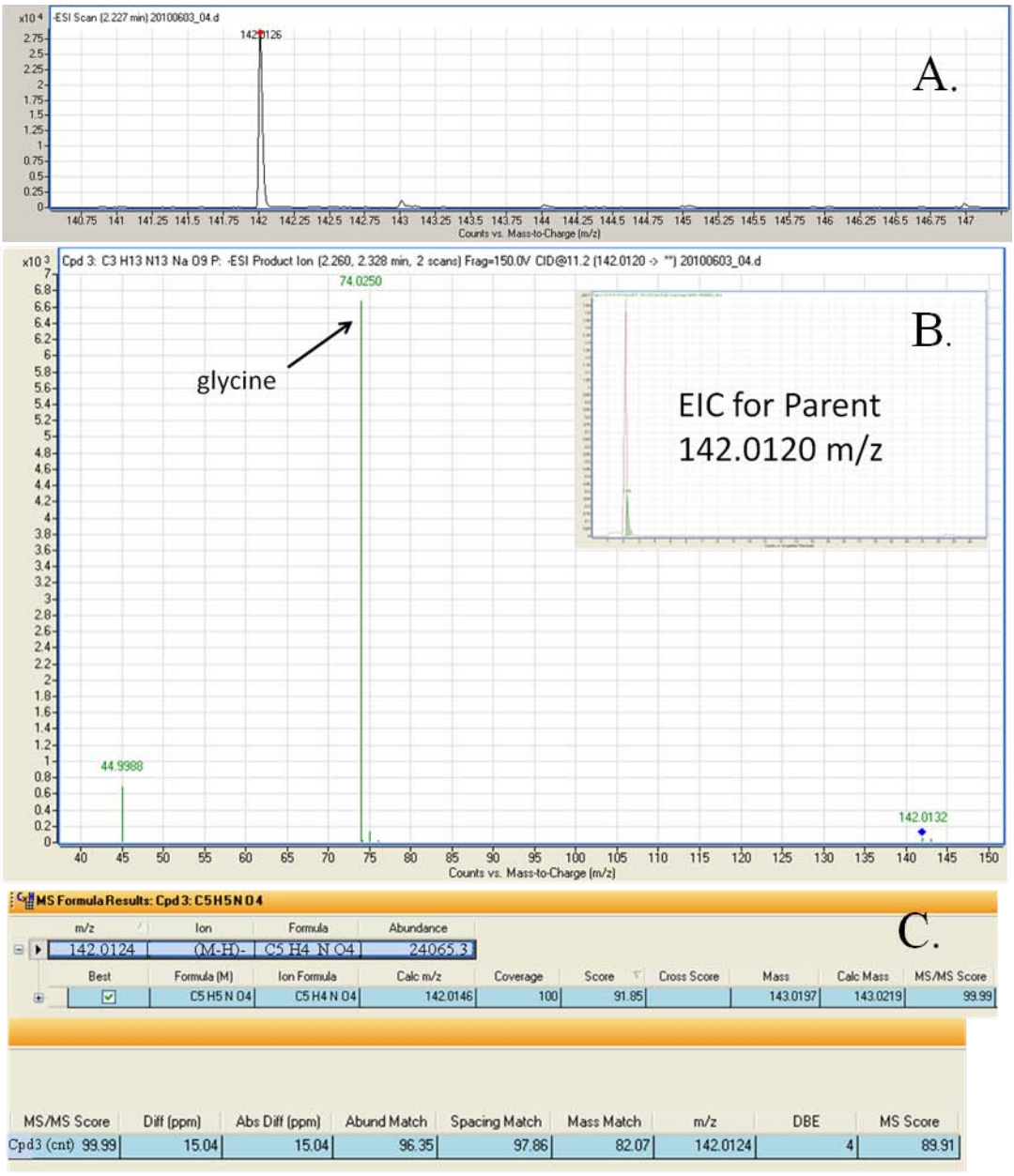

Figure 5.24: Compound 3 found to contain a glycine fragment using auto MS/MS . (A.) Parent mass (M+H) 142.0126 m/z observed isotope pattern. (B.) Compound 3 has an average parent mass of 142.0120 m/z. (C.) The best predicted formula was $C_5H_5NO_4$. The best formula was deduced using MS/MS data, high mass accuracy, and isotopic ratios from compound 3.

For Compound 1 in figure 5.22 several of the formulas generated by the Agilent Mass Hunter software are not a very likely. Formula #1 $C_{19}H_{34}N_3O_2PS$ is unlikely as it does not contain enough oxygens to make a phosphate with the P. Formula #2 $C_{17}H_{37}NO_5S_2$ is a possibility, but we are uncertain if the isotopic pattern confirms the presence of sulfur. Formula #3 $C_{17}H_{29}N_5O_6$ is a good possibility. Formula #4 $C_{11}H_{30}N_9O_5$ is unlikely as it contains too many nitrogens to make a reasonable biological compound of this molecular weight. Formula #5 $C_{16}H_{33}N0_{10}$ is unlikely as it may contain too many oxygens. So we are left with formulas 2 and 3 as the most likely possibilities. All formulas were deduced from compound 1 and scored using MS/MS fragmented data, high mass accuracy, and best fit to isotopic ratios.

The molecular formulas from these glycine-containing fragmentation results on the T2D samples obtained on an Agilent 6520 QTOF, have been reduced to the 4 most likely formulas as shown in table 5.5. It is expected that with larger amounts of samples and increased fragmentation energy, several additional glycine-containing compounds will be detected by mass spectrometry in the other RP fractions.

Table 5.5: Best fit formula predictions for 3 measured glycine containing molecules detected on RP C12 column in the 4 minute fraction from T2D plasma.

Measured M/Z	Formula Prediction	Formula Prediction – Gly adding OH	Formula Prediction - 2 Gly + 2 OH
398.2041	$C_{17}H_{29}N_5O_6$	$C_{15}H_{26}N_4O_5$	$C_{13}H_{23}N_3O_4$
398.2041	$C_{17}H_{37}NO_5S_2$	$C_{15}H_{34}O_4S_2$	$C_{13}H_{31}O_3S_2$
171.0387 m/z	$C_6H_8N_2O_4$	$C_4H_5NO_3$	
142.0120 m/z	$C_5H_5NO_4$	$C_3H_2O_3$	

These glycine-containing molecular formulas generated in fitting the auto-MS/MS data from our Agilent 6520 QTOF were searched against the structural databases Chem Spider and SciFinder. These databases generate chemical structures found in the literature based on matches to the formula. Hundreds of possible structures were generated using these formulas. None of them that we found had an ester or thioester linkage for the glycine moiety. Thus, we subtracted the glycine moiety from the formulas and added back an OH group to the resulting formula. The OH was added because we expect that the glycine was attached to the parent structure via an ester linkage (or possibly a thio ester linkage) due to the PFB-glycine esters produced by the PFB Br derivatization. For compound 1 we also subtracted 2 glycine and added 2 OH. The formulas minus a glycine moiety and with the OH added are shown in table 5.5 and then searched against Chem Spider and SciFinder. Hundreds of possible targets were again generated, especially for the higher molecular weight compound 1. Structures that resembled a plausible biological building block and contained a free OH group were filtered and the glycine moiety was added back after substracting the the H_20 group that would have been removed in the condensation reaction. Three such plausible structures were found to match the formula of compound 1 and are shown in figure 5.25 from the formula $C_{17}H_{29}N_5O_{6,}$ which was considered as having one glycine moiety. These structures are being synthesized by Dr. Trevor Rainey's group to provide authentic compounds to test QTOF fragmentation patterns, reactivity to PFB Br, retention time matching by HPLC, and hydrophobic partitioning properties in DCM: MeOH.

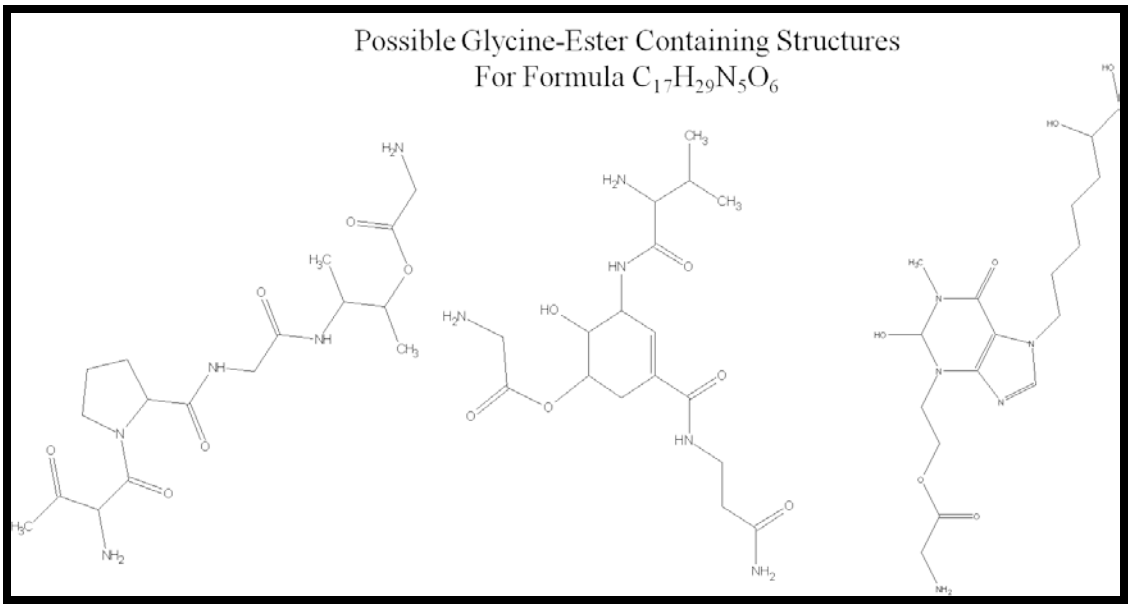

Figure 5.25: Possible glycine-ester containing molecular structures designed after searching Chem Spider and SciFinder databases for parent structures where a glycine could be attached as an ester in a condensation reaction to generate the formula $C_{17}H_{29}N_5O_6$.

Several previous studies have revealed some potentially interesting correlations between T2D and glycine (*189-191*). Evidence has been presented that relatively large oral doses of glycine (~5 grams) stimulates insulin secretion in humans (*189, 190*). Glycine receptors located in the gut have been discovered to release glucagon-like-peptide (GLP)-1, which is a directly increases the secretion of insulin from the beta cells (*191*). Metabolite studies found glycine levels in blood were down regulated in T2D prior to gastric bypass surgery and were restored to normal levels immediately following the surgery, at which time the T2D symptoms resolved (*16*). Glycine was found to be significantly decreased in other metabolomic studies of T2D (*192, 193*). Similarly, it was found that supplementing the diet with glycine in diabetic prone mouse models had a

significant effect in delaying the incidence of T2D and lowering the percentage of occurrence of T2D by 22%, compared to a normal chow diet containing casein (*194*). We have found several additional studies that report that an increase in dietary glycine may have a modest effect on prevention of T2D (*31, 189-191, 194-196*). This effect was proposed to be tied to the ability of glycine to inhibit advanced glycation product formation, and this could be consistent with aldehyde Schiff bases of glycine being amoung the compound identities to match the molecular formula we found. This decrease in glycation products could also be an indirect effect due to the blood sugar lowering effects of glycine (*189, 190, 195*).

Differential Lipidomics Study on Hydrophobic Extract of Whole Plasma by QTOF

We were curious to determine if these types of compounds might be found using a broader lipidomics approach on the hydrophobic extract of whole plasma, comparing lipid differences between T2D and HC. Sample preparation proceeded as follows:

LCMS Sample Preparation

The study began with 8 HC samples and 8 T2D samples. Because of low amounts of samples remaining, the HC and T2D samples were pooled in sets of two, resulting in 4 HC pools and 4 T2D pools. An internal standard of 0.1 ug of C15:0 was added to 70 uL of human plasma in each of the 4 pools of newly diagnosed T2D and the 4 pools of the matched HC. Extraction of hydrophobic compounds, including NEFA, used the same modified Folch extraction technique (*184, 185*) as previously described.

Thus, 1 mL of 0.88% KCl and 2 mL of 2:1 DCM: MeOH were added to each plasma pool. Extraction was allowed to proceed for 2 hours, with agitation, the DCM layer was removed and dried under a stream of nitrogen. The hydrophobic compounds were re-solublized in 100 uL of 20% ACN and 80% water. 10 uL of this sample was diluted to 100 uL with water, and injected on the LC-MS/MS spectrometer.

These samples were run in triplicate on an ultra high pressure HPLC (Agilent 1290 uHPLC) RP column on an ultra high resolution Agilent 6538 QTOF. The column was a Phenomex 1.7 u Kinetex 100 Å 150 x 2.1 mm RP C18. The triplicate analysis of each sample was performed in both positive and negative ionization modes. Initial LCMS gradient conditions for positive mode were 0.4 ml/minute flow rate of 70% buffer A [0.1% Formic Acid (FA), 100% H20] and 30% buffer B [0.1% FA, 100% ACN] with the column temperature set at 50º C. These conditions were maintained for 5 minutes, then adjusted to 95% buffer B over a 95 minute linear gradient and maintained at 95% buffer B for 5 minutes. At 105 minutes the gradient was returned to 30% buffer B. Sample data collection was completed at 120 minutes. Similar gradient conditions were used for data collection in negative ionization mode. However, buffer A in the negative ionization mode was 10mM ammonium acetate, 100% H_2O, and buffer B was 10mM ammonium acetate, 100% ACN. The ESI VCap was set at 3500 volts and 300º C with nitrogen gas pressure at 25 psi. MS survey scans were acquired over a range of 50 m/z to 1700 m/z in extended dynamic range mode. The fragmentor voltage was set at 175 volts, the skimmer at 65 volts, and the octapole 1 RF was set to 750 volts. Spectra were acquired at a rate of 6.57 spectra/second, which required 152.2 ms/spectrum, with the

targeted MS/MS collision fragmentation energy set at 2.6 volts per 100 daltons, and a slope offset of 2.7.

The initial sample injection volume was insufficient to detect the internal C15:0 spike at a level that could be easily distinguished above the background. This lack of detection applied to the majority of NEFA as well. The unknown glycine-containing compound would be expected at a similar concentration to the C15:0 spike. Therefore we increased our injection amount ten-fold by direct injection of 10uL the hydrophobic extract that had been solubilized in 100uL of 20% ACN and 80% water, without further dilution. With the increased sample volume the internal standard C15:0 could be seen with a good signal to noise, and many of the NEFA could be detected with a good signal to noise, as shown in figure 5.26. In a desire to preserve enough sample for multiple runs of targeted fragmentation and to perform triplicate MS analysis in both positive and negative ionization modes all of the remaining 70 uL of each of the 4 HC pools and 4 T2D pools were combined into a single T2D pool and single HC pool with 8 contributing individuals in each pool. Loading of these concentrated hydrophobic plasma extract was found to require extended column wash times between runs to prevent sample carryover between runs.

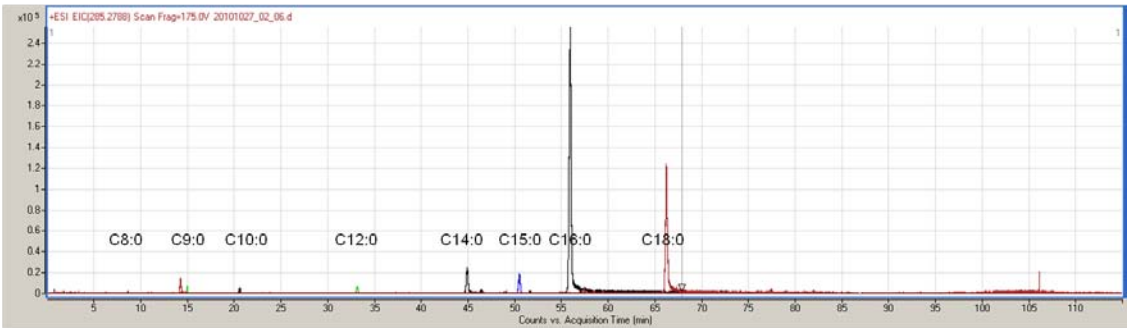

Figure 5.26: Overlay of extracted ion chromatogram of NEFA detected in the total hydrophobic fraction of the modified Folch extract of total human plasma, using the positive ionization mode on the Agilent 6538 QTOF, and a uHPLC RP Kinetix C18 column to separate over a two hour gradient. The pentadecanoic acid (C15:0) internal standard was added to each sample to normalize for variability in sample extraction and processing.

We observed an average of 2386 MS molecular species from triplicate runs of these samples in positive ionization mode using the Agilent Mass Hunter software. The base peak chromatogram is shown in figure 5.27. The mass features were extracted, and the relative levels of the MS peaks in the T2D and HC samples were compared using the Agilent Mass Profiler Professional (MPP) software package. It was observed that 216 MS peaks were found to have a two- fold or greater difference in amounts between the triplicate T2D and HC runs in positive ion mode. In the negative mode 61 MS features were observed as being different between T2D and HC. The ammonium acetate appeared to inhibit the signal strength and thus reduce the sensitivity of detection in the negative ion mode. Sensitivity reduction from ammonium acetate has previously been reported in the literature, but is usually not a problem in concentrations below 20 mM, such as we used (*197*). After processing these negative ion spectra through Agilent MPP program, 4 features had a p-value of <0.05 and a change of two- fold or greater between

T2D and HC. We hypothesized that there were fewer features in negative mode due to signal suppression because of the presence of 10 mM ammonium acetate. We could observe many of the NEFA peaks as well as our internal C15:0 spike in each of the triplicate injections from the T2D and HC pooled samples. We did not find the masses of any of our previously targeted glycine-containing molecular targets, however, using this MS profiling approach. The glycine-containing molecular targets that previously had been detected were found in the negative ion mode, thus the low detection sensitivity in the negative mode in these experiments decreased the probability that the desired compounds would be found.

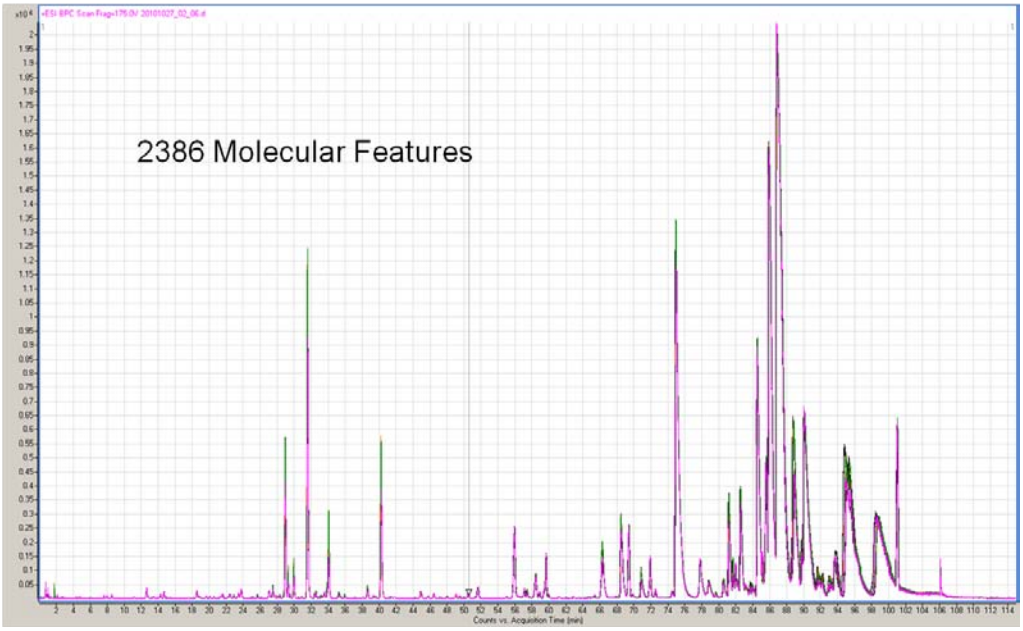

Figure 5.27: Example of a base peak chromatogram from the modified Folch hydrophobic extract of human plasma in positive ionization mode on the Agilent 6538 QTOF, using an uHPLC RP Kinetix C18 column over a two hour solvent gradient. 2386 molecular features were detected on average from triplicate runs in the T2D and HC samples examined in this study.

We then used the list of molecular species that were identified by the Agilent MPP program to differ in T2D and HC, and performed targeted fragmentation on those compounds. A collision energy of 2.6 volts per m/z, with a slope offset of 2.7, was used for all targeted fragmentation. We had previously found that this collision energy profile had been demonstrated to fragment two of our glycine ester model compounds. We were able to fragment 208 of the 277 total MPP targets and to indentify 110 of them with a high degree of confidence using both the high accuracy MS and MS/MS data. We searched the masses and MS/MS profiles or the compounds against the Lipid Maps as well as the Metlin Databases (*186, 187*). The identified compounds and the percentage changes in levels between T2D and HC are listed in figures 5.28-5.30.

Many of these compound identities match previous findings from metabolomic studies done on T2D. Of significance, are a variety of phosphatidylcholine (PC), phosphatidylethanol amines (PE), and bile acid species, which are associated with the choline pathway (*16, 198-200*). A decrease of several vitamin D3 metabolites was observed in T2D. Previous studies have seen an association of the risk of T2D increasing in ethnicities which originated in warmer climates and who have dark skin (*201*), which may be related to this correlation with low vitamin D3 metabolites. Data from the CDC suggest that risk factors of ethnicities orginating in warmer climates are much higher for T2D (*3*). Compared to non-Hispanic white adults, the risk of diagnosed diabetes was 18% higher among Asian Americans, 66% higher among Hispanics, and 77% higher among non-Hispanic blacks (*3*). Among Hispanics compared to non-Hispanic white adults, the risk of diagnosed diabetes was about the same for Cubans and for Central and

South Americans, 87% higher for Mexican Americans, and 94% higher for Puerto Ricans (*3*).

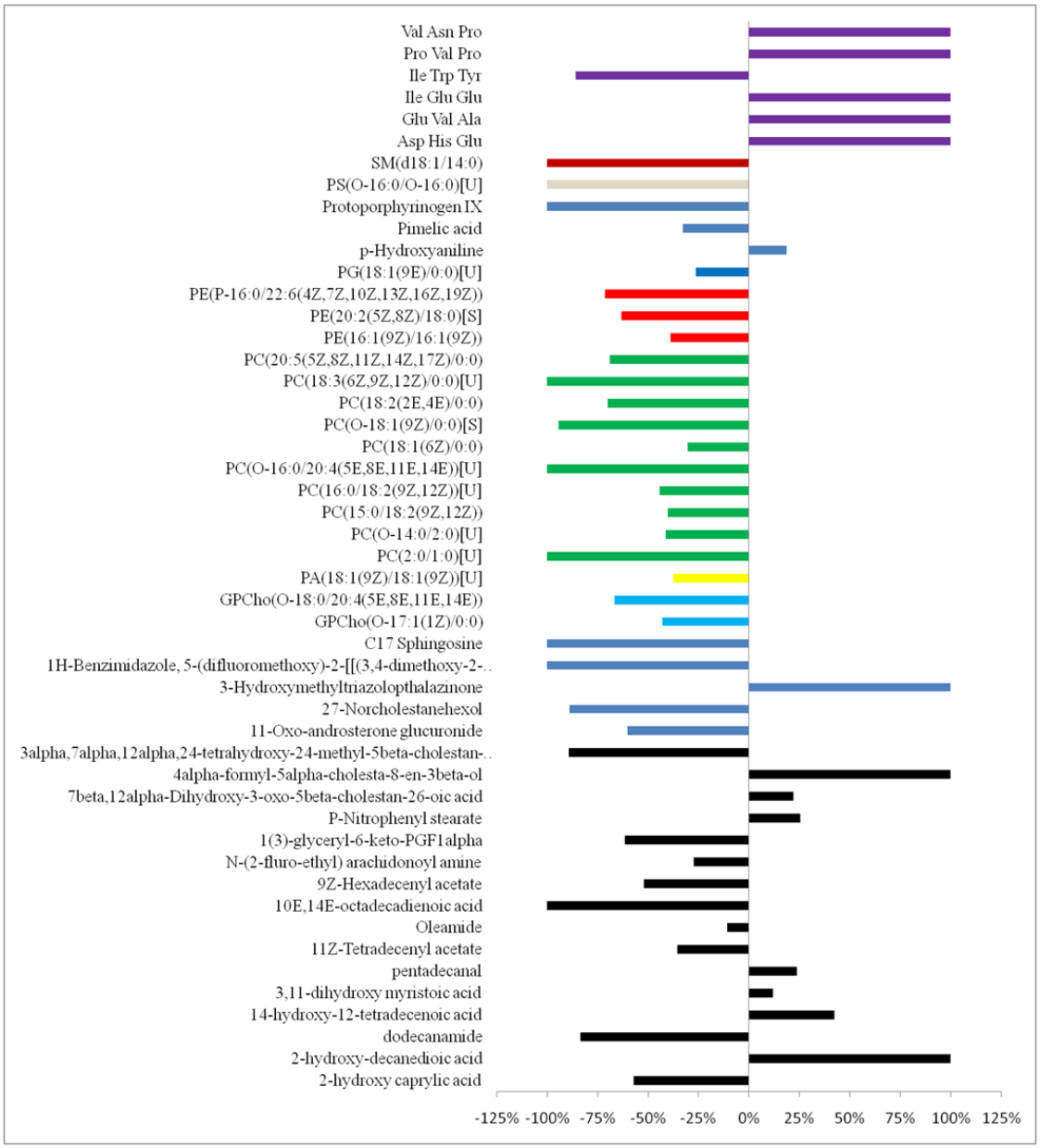

Figure 5.28: Positive mode Mass Profiler Professional targeted MS/MS features identified using the Agilent 6538 QTOF as being different between T2D pool and HC pools. Features higher in T2D are shown to the right.

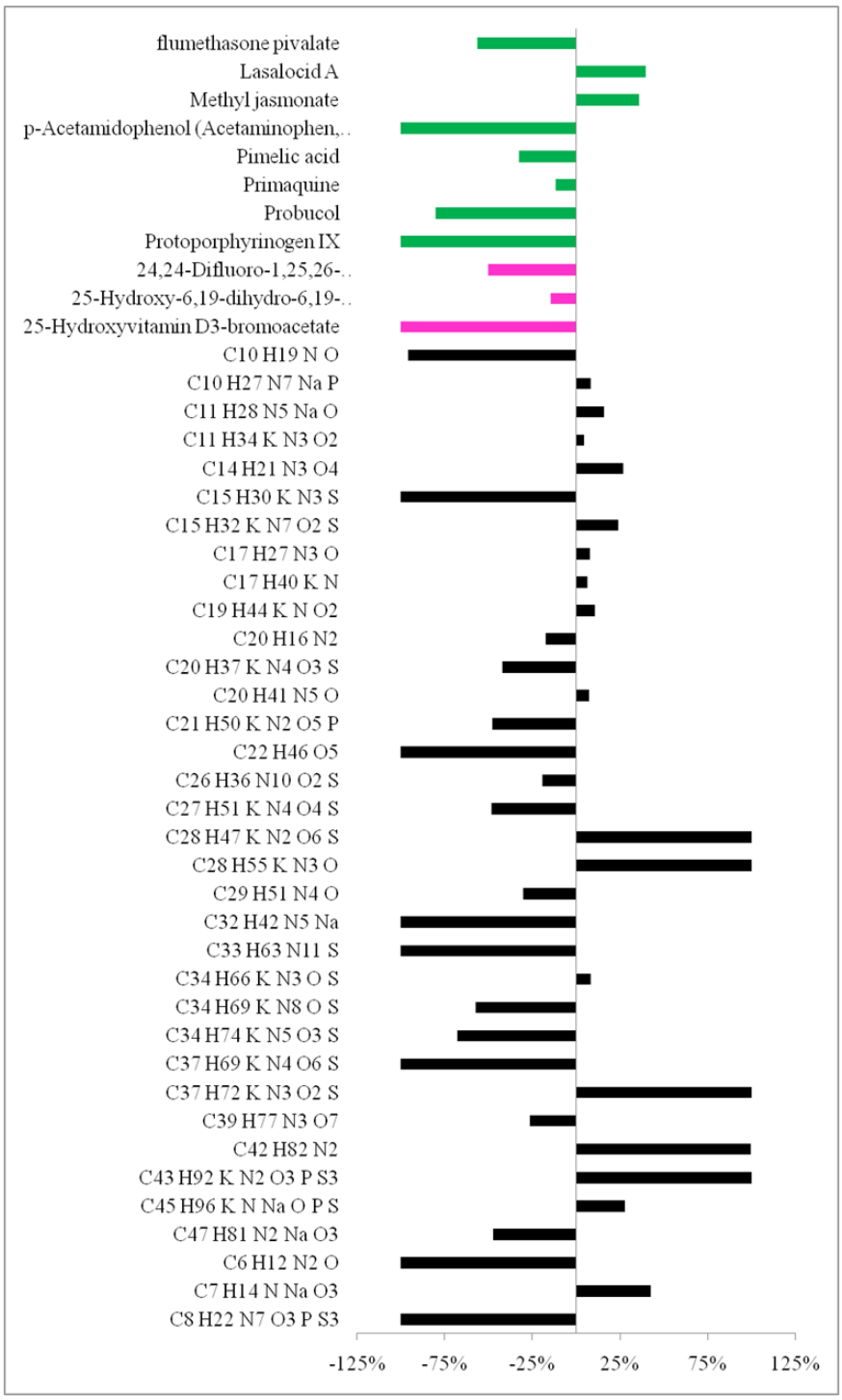

Figure 5.29: Positive mode Mass Profiler Professional targeted MS/MS features identified or the best fit formula obtained using the Agilent 6538 QTOF as being different between T2D pool and HC pools. Features higher in T2D are shown to the right.

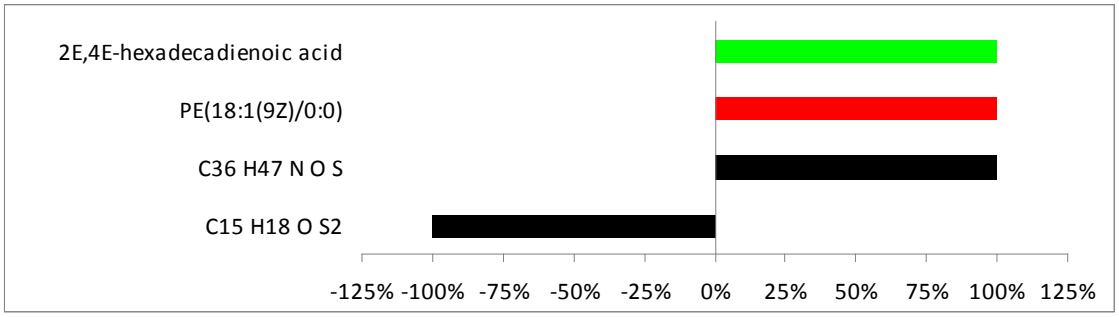

Figure 5.30: Negative mode Mass Profiler Professional targeted compounds identified using the Agilent 6538 QTOF as different between T2D and HC pools. Features higher in T2D are shown to the right.

Branched Chain Amino Acids

Up regulated tri-peptides that were observed in our metabolomic study included several peptides that contained branched chain amino acid (BCAA) species: e.g. Val-Asn-Pro, Pro-Val-Pro, Ile-Trp-Try, and Glu-Val-Ala. There was one down regulated BCAA tripeptide-containing species: Ile-Trp-Try. These findings on up regulated BCAA in T2D are consistent with other metabolomic studies (*16, 182, 192, 202*). Early recommendations even suggested that an increased consumption of protein diets with high BCAA leucine were beneficial for T2D patients (*203*). Weight loss and maintained steady state glucose levels were observed with this high leucine diet (*203*).

More recent studies have proposed that high BCAA may not be beneficial in humans (*182, 204*). BCAA levels in the blood are directly correlated with BCAA in the diet (*182, 204*). However, studies done on rats with diets consisting of a high percentage of fat and high BCAA intake, even in low caloric amounts, resulted in insulin resistance (*182*). In fact the development of insulin resistance in rats occurred even earlier than it

did in diets with high fat and greater caloric intake, but low BCAA intake (*182*). Diets high in animal proteins have been correlated with an increase risk for T2D (*204*), but this does not agree with many other studies reported in (Good Calories, Bad Calories, by Gary Taubes) (*205*). Diets high in protein (BCAA) resulted in decreased triacylglycerides (TAG) levels in the blood, increased HDL and LDL levels, and increased LDL particle size in the blood. Increased HDL is believed to be beneficial both in T2D and heart disease (*176*). Diets with increased protein also increased the amounts of carnosine, which has been shown to have benefits in decreasing protein glycation in T2D (*206*).

We purpose another hypothesis for increased BCAA in T2D that as insulin resistance develops in cytosketal muscle cells the cells cannot obtain glucose and elevated insulin also shuts off fat utilization so the cells are forced into a starvation mode (*70*). Under starvation conditions the animals are likely to revert to digesting muscle tissue, which would release BCAA into the blood. The liver does not absorb BCAA, however, which would result in an increase in BCAA in the blood (*190*).

Phosphatidylcholine (PC),
Phosphatidylethanol (PE) Amine, and Bile Acids

Two of the most prominently decreased species in our metabolomic study of T2D were the PC and PE groups, as shown in figure 5.28. Two glycerol phosphocholine species (GPCho) and two bile acid species: 27-Norcholestanehexol, and (3-alpha, 7-alpha, 12-alpha, 24-tetrahydroxy-24-methyl-5-beta-cholestan-26-oic acid) were also decreased in T2D. Another bile acid species: (7-beta, 12-alpha-dihydroxy-3-oxo-5-beta-

cholestan-26-oic acid) was increased. Our prelimary data suggest that many bile acids, such as glycocholic acid would not have been extracted into the hydrophobic fraction, using the modified Folch extraction method, as they are not soluble in DCM (*184, 185*). Thus, we did not examine the more hydrophilic bile acids. However, other studies have found that many bile acids are increased in T2D (*132*). Many bile salts are involved in the choline pathway, and are potentially related to T2D, with numerous opinions as to their contribution to the cause of T2D or as a consequence of T2D (*16, 174, 198, 199, 202, 207-210*).

Diets low in choline have been linked to fatty liver (*199*). A hypothesis to explain this is that choline deficient diets restrict PC formation, which use large amounts of FFA in assembly (*199*). PC is primarily synthesized primarily in the liver (*211*). If the system is low in choline many fats cannot be exported from the liver, which would increase the risk of fatty liver. Additionally, PC is required in the assembly of many lipoproteins, especially HDL (*211*). PC is the most abundant phospholipid in animals, and is a key building block of membrane bilayers in cells (*211, 212*). PC is the principal phospholipid in blood plasma (*211*). There are three known pathways for PC synthesis, but only two are utilized in mammals (*211-213*).

The first PC pathway was discovered by Eugene Kennedy and is called the Kennedy pathway (*211*). This pathway is used in mammals and involves three enzymes, ATP, choline, and diacylglyerol (figure 5.28) (*212*). The second PC pathway is also utilized in mammals and involves PE receiving three successive steps of methylation

from S-adenosylmethionine, as shown in figure 5.31 (*211, 212*). This latter pathway has been studied extensively in yeast (*211, 212*).

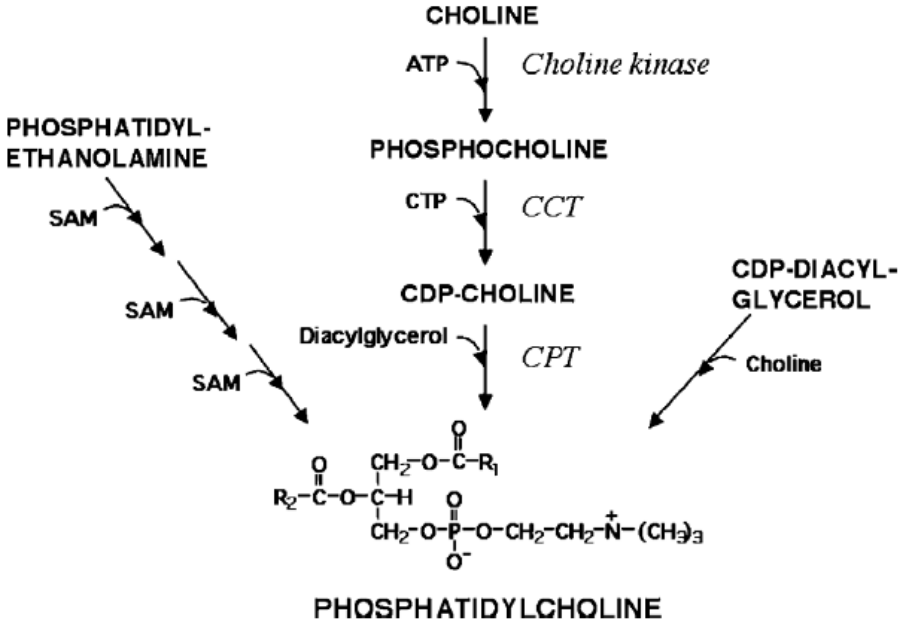

Figure 5.31: Three pathways for biological synthesis of PC. The center path is termed the Kennedy pathway, which is used in humans. The left path has three successive methylations to the amino group in PE with S-adenosylmethionine as the methyl donor. The right path is found to occur in only one bacterial species, symbiotic with plants (Sinorhizobium meliloti) (*211, 212*).

Choline for synthesis of PC enters from the diet but is not synthesized by humans (*132, 211, 212*). However, 95% of the choline is recycled (*132*). Choline is also utilized by the liver in production of bile acids, which are required for efficient fat absorption (*132*). The two most common bile acids formed in humans are cholic acid and chenodeoxycholic acid (*132*). These bile acids are commonly conjugated with either taurine, 2-amino ethane sulfonate or to glycine, which enhances the hydrophilicity of the bile acids (*132, 136*). Bile acids are used by the gut to act as biological detergents to

solublize fat (*132*). Microbial gut flora convert the most common bile acids into additional forms, such are found in our study (*132*). These initial findings suggest that changes in populations of the microbial gut flora and effects on the bile acids relevant to T2D may be an interesting area of study. The microbial gut flora in humans contributes to the bile acids we synthesize, the digestion of foods, and may be a potential risk factor for developing T2D.

Bile acid sequestrants, such as colesevelam, have been used for over 40 years to reduce blood levels of cholesterol. Observations by Garg and Grundy, 1994 (*214*), suggested new uses for bile sequestering drugs in regulating glucose and lipid metabolism in T2D (*132*). Sequestration of the bile acids may be involved in the increase of intestinal GLP-1, which gives individuals a feeling of being full and satiated (*132, 215*). It appears that altered bile acids and changing amounts of bile acids are commonly associated with T2D, and further studies on the pathways and mechanisms of bile acid synthesis and modification might well be fruitful (*216-218*).

The farnesoid X receptor (FXR) is a bile acid sensor, involved in regulating bile acid re-absorption after a meal (*132*). 95% of the bile acids are normally reabsorbed (*132*). The FXR receptor has also been found to modulate glucose absorption in the proximal intestine (*132*). Recall that glycine in the diet also led to GLP-1 secretion in the gut (*191*). Several roles for GLP-1 include increasing insulin secretion in a glucose dependent manner, decreasing glucagon secretion, and increasing insulin sensitivity of the alpha and beta cells (*215, 219*). Other benefits of drugs that cause bile acid sequestration appear to be reductions in fasting glucose and Hb A1C (*132*). These

observations are leading to new branding of established bile acid sequestrants as promising drug therapies in T2D (*132*). New branding of old drugs is becoming increasingly common in the pharmaceutical industry. To do this a drug that has already been approved for safety and toxicity by the FDA is re-named and administered for another purpose. Only the efficacy has to be demonstrated for FDA approval. This saves the drug company tens of millions of dollars, in cases where rebranding is applicable.

Our findings of decreased levels of PC, PE, and selected bile acids in T2D patients, suggest that therapies to increase the available choline in the diet may be beneficial in preventing fatty liver. Fatty liver increases overall risk of T2D. Diets high in choline would also be beneficial in increasing levels of HDL, which would likely be beneficial in lowering the risk of T2D. Additional studies of the cause of these decreases in PC, PE, and reasons for altered levels of bile acids in diabetics, may lead to a clearer understanding of metabolic pathways changed in T2D.

Vitamin D3

Vitamin D has an amazing history. Vitamin D receptors are prevalent in many cells (*220, 221*). Vitamin D has been best known for its role in calcium and phosphate trafficking, but vitamin D has many additional roles in the body, including modulation of cell growth, neuromuscular and immune function, and reduction of inflammation (*220, 221*). Prior metabolomic data indicated a decrease of vitamin D3, and its metabolites in T2D (*201, 221*), and we observed this also in a subset of vitamin D3 metabolites. The vitamin D metabolites that decrease are 25-hydroxy vitamin D3, 1,25,26 trihydroxy vitamin D3, and 25-hydroxy-6, 19-dihydro-6, 19-ethano-25-hydroxy vitamin D3. Some

background on vitamin D metabolism below will explain the metabolite conversions that must occur to obtain the active vitamin D3 that may be used by cells.

There are two major dietary forms of vitamin D: vitamin D2 (ergocalciferol) found in plants, and vitamin D3 (cholecalciferol) found in animal products (*201*). Vitamin D is found in significant amounts in certain foods like large ocean fish, eggs, beef, and mushrooms (*220*). Vitamin D is not a true vital amine (vitamin), since mammals, including humans, can manufacture their own supply if exposed to sufficient sunlight (*222*). Vitamin D is fat soluble and the normal endogenous synthesis system in humans requires UV light on the skin to convert 7-dehydrocholesterol to the active form of vitamin D (*220*).

Around 1918-1920 a British doctor, Edward Mellanby, noticed that dogs fed cod liver oil did not develop rickets (*222*). By 1921 Elmer McCollum, who had discovered vitamin A in cod liver oil, was able to isolate a second substance in cod liver oil, that he termed vitamin D, and which was found to be responsible for the curing of rickets (*222*).

By 1923 Harry Steenbock was successful in demonstrating that irradiation of certain foods activated the formation of vitamin D (*222*). This activated form of Vitamin D3 is commonly found in milk, where most individuals obtain their dietary vitamin D today (*222*). Steenbock patented this process, and by 1945, when his patent had expired, rickets has all but been eliminated in the US (*222*).

A description of this photolytic conversion that occurs in the skin and with Steenbock's light activation process is described in figure 5.33 (*223*).

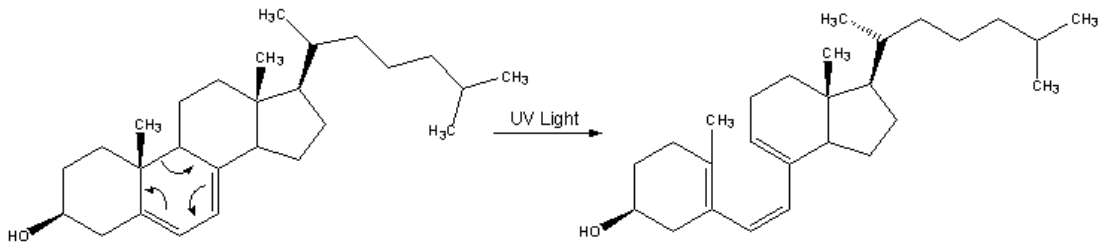

Figure 5.32: In the skin 7-dehydrocholesterol, a derivative of cholesterol, is irradiated by ultraviolet light. This end product is pre-vitamin D3.

Pre-vitamin D3 spontaneously isomerizes to Vitamin D3 (cholecalciferol). At room temperature this process takes about 12 days to complete (*223*). As shown in figure 5.34:

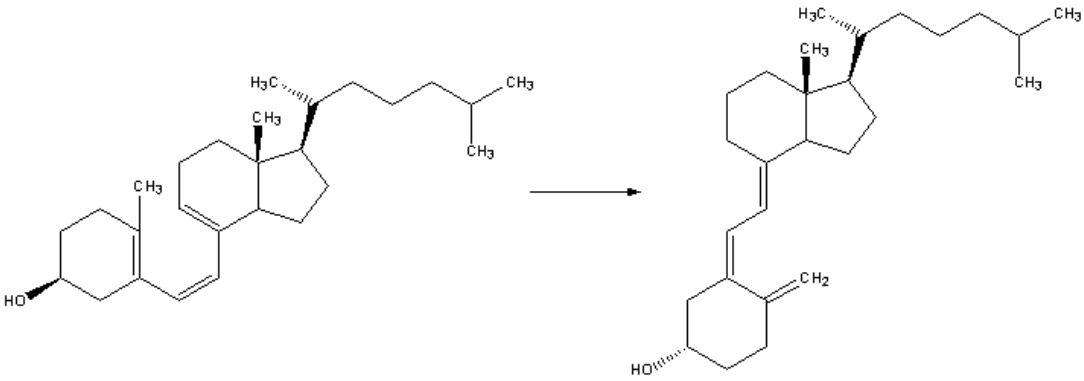

Figure 5.33: The spontaneous conversion of pre-vitamin D3 to cholecalciferol (Vitamin D3) occurs at room temperature.

Vitamin D3 can be ingested or formed in the skin. After either route the molecule undergoes two additional reactions. In the first reaction vitamin D3 is hydroxylated by vitamin D 25-hydroxylase in the liver shown in figure 5.35 (*223*). This calcidiol product

is stored in the liver hepatocytes until needed (*223*), and this 25-hydroxy D3 is one of the metabolites found down regulated in T2D in our metabolomic study.

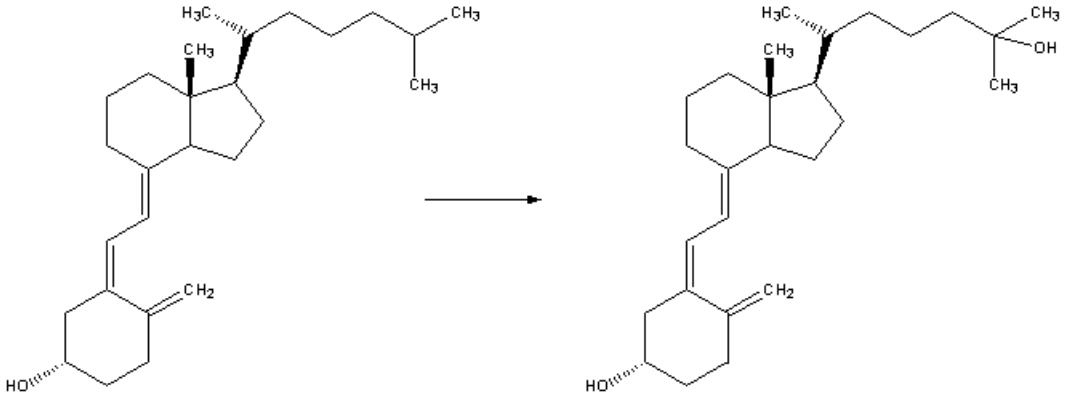

Figure 5.34: The conversion of cholecalciferol to calcidiol, 25-hydroxy D3, which is a major storage form occurs in the presence of the enzyme vitamin D 25-hydroxylase in the liver.

The second reaction occurs in the kidneys (*223*) as shown in figure 5.36. The calcidiol is hydroxylated at the 1-alpha position forming calcitriol with the enzyme 25-hydroxy vitamin D3 1-alpha hydroxylase (*223*). This final calcitriol product is transported on the vitamin D receptor (VDR), which is bound to HAS in the blood plasma (*223*). The final conversion to the active form is shown figure 5.36 is regulated by the parathyroid hormone, which is elevated by low levels of phosphate or calcium (*223*). Thus, alterations in the HSA that effect VDR binding, may also be effecting delivery of active calicitriol.

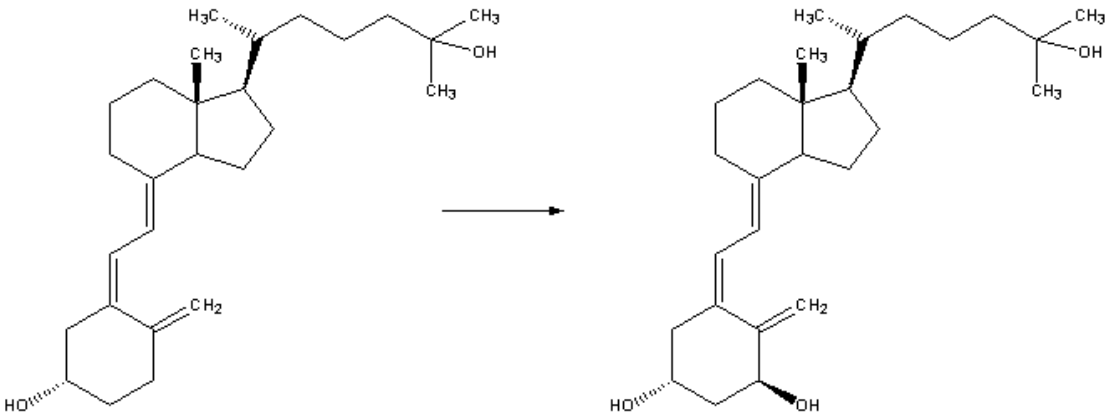

Figure 5.35: Conversion of the calcidiol to calcitriol by hydroxylating the 1-alpha position as occurs in the kidneys. The enzyme 25-hydroxy vitamin D3 1- alpha hydroxylase catalyzes the reaction.

The ability to produce vitamin D is dimished in dark skin (*201, 223*). The melanin pigmentation inhibits the penetration of UV light and reduces the photoactivation process (*223*). This is particularly of interest, as a correlative has been drawn between low vitamin D in dark skinned ethnicities and specific diseases, including T2D, autoimmune, and peripheral arterial disease (*201, 221, 224, 225*).

One rationale that supports association of low vitamin D with T2D, deals with the role of vitamin D in intercellular calcium flux (*221*) . Calcium status is intricately tied to insulin secretion, which is a calcium-dependent process. In addition, there is some evidence that the circulating, active form of vitamin D affects the insulin response to glucose stimulation (*221*). It is hypothesized that inadequate levels of vitamin D directly affect the balance of the calcium pool levels in β-cells, which may interfere with normal insulin release, especially in response to glucose loads (*221*). Futhermore, a decrease in the insulin response has been correlated with the vitamin D levels experimentally (*221*).

Vitamin D supplementation was shown to improve insulin responses in some studies (*221, 226-228*). Another beneficial role of vitamin D may lie with a reduction of inflammation, since increased inflamation has been associated with T2D (*156, 221, 229*). It is thought that elevated levels of cytokines in β-cells may result in triggering β-cell apotosis (*221*). Vitamin D is thought to have a role in modulating the generation and effect of cytokines in β-cells, which promotes β-cell survival (*221*). Despite all of these correlations, the overall impact of vitamin D and calcium supplementation, while very positive in some studies (*221, 225, 228*), has not been consistent in measurable benefit in T2D (*221, 226, 230*). This may be a result of lack of adjustment for factors such as adiposity, physical activity, and the current vitamin D and calcium status in these studies (*221*).

Vitamin D metabolites were found in our metabolomic study to be down regulated, consistent with previous findings. This provides added evidence that Vitamin D supplementation, absorbable calcium supplementation, and more UV-containing sunlight may well be beneficial to individuals at risk for T2D. Addition research into the β-cell response to the Vitamin D mediated insulin response may help unravel the role of vitamin D in T2D.

Further research on the glycine-containing molecules bound to HSA, that our work has found to be strongly associated with T2D, will include determining the structures of these compounds by NMR, determining the effects of these compounds on HSA cargo binding, and assessing the association with metabolomic syndrome and T2D in a larger group of individuals.

CONCLUSION

We found several significant changes in the cargo of HSA in T2D and SLE compared to HC. Changes in thermal stability that Garbett, et al had reported in the plasma from inflammatory disease patients were not detectable on the thermal stability of a commercial T2D sample examined by DSC (*78*). The SLE plasma DSC thermogram was consistent with Garbett, et al's findings, but the thermogram of HC did not agree with Garbett el al (*78*).

Changes in the thermal stability of HSA were also studied by monitoring the fluorescent lifetime of the single endogenous tryptophan in HSA, since the environment of the tryptophan changes during a stepwise thermal denaturation. The differences in fluorescence lifetimes that we observed between the disease states also did not agree with Garbett, et al's results (*78*). An extrinsic fluorescent probe, ANS, added to bind to HSA in whole plasma samples, showed that the cargo content of HSA in plasma from SLE, LD, and T2D patients were different from the cargo contents of HSA in plasma of a healthy control. The total fluorescence from bound ANS was measured at ambient temperatures by FRET transfer from the single HSA tryptophan to ANS. All samples (SLE, LD, T2D, and HC) were adjusted to contain equal amounts of total protein and ANS. Total fluorescent from the bound ANS at ambient temperatures was most intense in the HC plasma samples compared with less total fluorescence in ANS bound to HSA in LD, T2D, and SLE plasma samples. The decreased ANS binding to HSA in SLE, T2D, and LD samples compared to HC samples supports the concept that inflammation

diseases such as T2D may load HSA with additional hydrophobic cargo blocking access to added hydrophobic probes.

Extensive efforts were made to interrogate the LMW peptidome from human plasma, using one and two-colored fluorescent dye labeling approaches. A fluorescent dye pair was selected so that they co-eluted chromatographically, using SCX and RP separation of covalently labeled LMW peptides. The LMW peptide method of extraction with MWCO filters commonly used in the literature, as a rapid technique to obtain samples, was found to have poor recovery of a LMW peptide spike, as well poor reproducibility. A size exclusion chromatography (SEC) method, that had not previously been applied to this problem, was found to produce a higher yield of LMW peptides bound to plasma proteins then was found using the widely used MWCO filter method, as reported by Tammen et al (*99*). It was found that the yield of isolated LMW peptides from plasma could likely be increased substantially by switching from urea denaturant to guanidine HCl or sodium dodecyl sulfate (SDS) denaturants.

An approach for quantitative guanidylating of lysine groups in the LMW peptides prior to covalent fluorescence labeling the N-terminus of the peptides with fluorescent dyes using the NHS ester reaction was found to be effective. Subsequent fluorescence labeling with NHS ester fluorescent dyes in anhydrous DMF and DIPEA was found to produce consistent, 67% +/- 3% yield of labeling the peptide N-terminus only. A pair of closely co-eluting dyes on RP and SCX was discovered, ZB-Butyl and BSBIII-229, that could be excited by the same wavelength. Model peptides labeled with these Zdyes nearly co-eluted in both SCX and RP. These labeled model peptides could be detected

and identified by MALDI-TOF/TOF; however, we were unable to identify either of these fluorescent dyes covalently bound to the LMW peptides from human plasma, using MALDI TOF/TOF. ESI MS had previously been shown to cleave portions of the fluorescent tags during ESI.

The complexity of the overall LMW peptidome was found to be too great to use this fluorescent peptide methodology. Using a simplified sample of a BSA tryptic digest plus or minus BSA oxidization, it became apparent that specific species of LMW peptides were labeling differentially with the two different fluorescent dyes at a level detectable in the RP absorbance profiles. Single dye experiments using ZB-Butyl were successful in identifying multiple changes occurring between a digest of the control BSA peptides and the peptides in a digest of oxidized BSA. Identification of the modified peptides, using MALDI TOF/TOF has been unsuccessful to date.

The hydrophobic cargo of HSA investigated in T2D compared to HC revealed that fatty acid species were reduced in T2D, as measured by GCMS, using PFB Br transesterification and NCI. There was a 24% decrease of overall total fatty acids in T2D as well as a 35% decrease of nonanoic acid (C9:0). Two large additional peaks bound to HSA in plasma were identified after the PFB Br derivatization as di-PFB glycine and tri-PFB glycine. These glycine molecules were released from molecules contained in the hydrophobic cargo of HSA and were found to be up 2 fold ($p < 0.005$) in eight T2D samples compared to eight HC samples.

Free glycine was not present in the hydrophobic extract. PFB glycine could be produced from ester, thioester, or possibly Schiff base glycine species that are contained

in the HSA hydrophobic extract. The PFB glycine was cleaved from larger parent hydrophobic molecules during the PFB Br derivatization reaction. Amide linked glycine compounds do not release a PFB glycine during PFB Br derivatization. Ester and thioester glycine linkages and perhaps Schiff bases are susceptible to releasing PFB glycine during the derivatization conditions used. There are however, no previously known hydrophobic ester or thioester glycine molecules in biology. Therefore these new ester or thioester hydrophobic compounds that are increased in the HSA cargo in T2D (p value <0.005) are extremely interesting.

Efforts to identify the hydrophobic glycine ester or thioester species suggest that there were at least 5 or more glycine-containing species in the HSA hydrophobic extract in HC and T2D. One minute RP fractions shown to contain the glycine-containing species were examined by uHPLC QTOF. Three glycine containing species were detected during fragmentation from the T2D samples. The fragmentation patterns and high mass accuracy measurements predicted several candidate formulas containing glycine. The molecular formulas generated by MS and MS/MS did not match any compounds in the Lipid Maps or METLIN databases, and the atomic formulas did not reveal currently known structures in SciFinder or Chem Spider, that contained an ester or thioester linked glycine. Searching SciFinder and Chem Spider for structures after removing a glycine and substituting a hydroxyl group that would have been present prior the condensation reaction forming this parent molecule, allowed us to deduce several hypothetical structures by focusing on incorporating potential biological building blocks. Trevor Rainey's lab at MSU is synthesizing some of the most promising compounds to

test for RP retention time, MS/MS fragmentation, solubility in DCM, and ability to produce glycine during PFB Br derivatization. We are also scaling up the isolation and purification of these unknown compounds to determine their structure, using NMR spectrometry. Perhaps the identification of these new targets will provide new insights into causal mechanisms of T2D, as well as being useful for diagnostic markers for disease progression and response to treatment.

A global metabolomic study was performed on the hydrophobic extracts of T2D and HC plasma using uHPLC and high mass accuracy QTOF in positive and negative ionization modes. Analysis of 2447 total molecular features detected by positive and negative QTOF MS analysis in the plasma hydrophobic extract with Agilent MPP software found 220 molecules that differed in T2D samples compared to HC samples by MS with a greater than 2 fold change and p-value less than 0.05. These target MS differences were fragmented in subsequent MS/MS runs with high mass accuracy and examination of isotope ratios, which allowed identification of 110 of these differences in T2D with high confidence.

The hydrophobic metabolites we found to change matched several previously identified metabolite changes related to T2D. The results included decreased levels of several PC and PE species and altered levels of certain bile acids. PC, PE, and bile acids are connected through choline metabolism, which is a highly conserved pathway. Choline deficient diets have been linked to fatty liver in mouse models and fatty liver is implicated in causing insulin resistance and T2D (*199*). Our study did not measure most bile acid metabolites because they partition into the aqueous phase of the Folch

extraction, which we did not investigate. Previous data back up our findings of alterations in bile acid composition in T2D, and have previously indicated that bile acid sequestrants have benefits in improving insulin resistance in type II diabetics (*132, 214, 231*). We also found that branched chain amino acids (BCAA) were higher in T2D. Higher levels of BCAA have been correlated with T2D (*182, 204*). Diets high in BCAA (high protein diets) have been hypothesized to result in an increased risk for T2D (*182, 204*); however, cells in type II diabetics cannot efficiently obtain glucose, and high insulin suppresses fat mobilization and metabolism for energy, so proteins are digested for energy (*70*). The liver does not take up BCAA, so elevated BCAA in blood may not be a cause, but rather an effect of T2D (*190*). Several vitamin D3 metabolites were decreased in T2D, which are hypothesized to result in reduced sensitivity of the pancreatic β-cells to glucose stimulation and decreased insulin secretion. Diets with increased calcium and supplementation of Vitamin D3 are likely to prove beneficial in prevention of T2D (*221, 229*).

In summary, our efforts to search the cargo contents of HSA, the most abundant protein in blood plasma, suggest a rich area of future research to develop a more complete understanding of T2D. The new, previously unknown glycine-containing hydrophobic molecules carried on HSA that we found greatly elevated and altered in composition in T2D may be particularly important for new understanding of underlying metabolic mechanisms in T2D. These new compounds may also provide facile targets for early diagnosis of T2D and for measurement of progression or steps to prevention. The research suggests that studying the HSA cargo in other disease states may also lead

to cargo targets that will enrich our understanding of the mechanisms of adaptation that are utilized in human health and disease.

BIBLIOGRAPHY

1. Sreekumar, A., Poisson, L. M., Rajendiran, T. M., Khan, A. P., Cao, Q., Yu, J., Laxman, B., Mehra, R., Lonigro, R. J., Li, Y., Nyati, M. K., Ahsan, A., Kalyana-Sundaram, S., Han, B., Cao, X., Byun, J., Omenn, G. S., Ghosh, D., Pennathur, S., Alexander, D. C., Berger, A., Shuster, J. R., Wei, J. T., Varambally, S., Beecher, C., and Chinnaiyan, A. M. (2009) Metabolomic profiles delineate potential role for sarcosine in prostate cancer progression, *Nature 457*, 910-914.

2. Boyle, J. P., Thompson, T. J., Gregg, E. W., Barker, L. E., and Williamson, D. F. (2010) Projection of the year 2050 burden of diabetes in the US adult population: dynamic modeling of incidence, mortality, and prediabetes prevalence, *Popul Health Metr 8*, 29.

3. CDC. (2010) National Diabetes Fact Sheet United States, www.cdc.gov, Department of Health and Human Services, Centers for Disease Control and Prevention, Atlanta, GA.

4. Engelgau, M. M., Narayan, K. M., and Herman, W. H. (2000) Screening for type 2 diabetes, *Diabetes Care 23*, 1563-1580.

5. Sacks, D. B., Bruns, D. E., Goldstein, D. E., Maclaren, N. K., McDonald, J. M., and Parrott, M. (2002) Guidelines and recommendations for laboratory analysis in the diagnosis and management of diabetes mellitus, *Clin Chem 48*, 436-472.

6. Santos-Rey, K., Fernandez-Riejos, P., Mateo, J., Sanchez-Margalet, V., and Goberna, R. (2010) Glycated hemoglobin vs. the oral glucose tolerance test for the exclusion of impaired glucose tolerance in high-risk individuals, *Clin Chem Lab Med 48*, 1719-1722.

7. CDA. (2011) The History of Diabetes, www.diabetes.ca/diabetes-and-you/what/history/, Canadian Diabetes Association, Toronto, ON.

8. Notkins, A. L., and Lernmark, A. (2001) Autoimmune type 1 diabetes: resolved and unresolved issues, *J Clin Invest 108*, 1247-1252.

9. CDC. (2007) Diabetes/Data and Trend www.cdc.gov/diabetes/stastics/, Department of Health and Human Services, Center for Disease Control and Prevention, Atlanta, GA.

10. WHO. (1999) Definition, Diagnosis, and Classification of Diabetes Mellitus and its Complications, www.who.int/diabetes/currentpublications/en/, World Health

Organization Department of Noncummunicable Disease Surveillance, Geneva, Switzerland.

11. Ponting, C. (1991) *A green history of the world: The environmental and collapse of great civilizations*, Vol. Ch. 11, Penguin Books.

12. USDA. (2001-2001) Agricultural Factbook, Profiling Food Consumption in America, www.usda.gov/factbook/chapter2.html, United States Department of Agriculture, Washington, DC.

13. Ackerman, Z., Oron-Herman, M., Grozovski, M., Rosenthal, T., Pappo, O., Link, G., and Sela, B. A. (2005) Fructose-induced fatty liver disease: hepatic effects of blood pressure and plasma triglyceride reduction, *Hypertension 45*, 1012-1018.

14. Adiels, M., Taskinen, M. R., and Boren, J. (2008) Fatty liver, insulin resistance, and dyslipidemia, *Curr Diab Rep 8*, 60-64.

15. Daily, D. (2011) Famous People with Diabetes, www.diabetesdaily.com/wiki/famous_people_with_diabetes, Diabetes Daily.

16. Mutch, D. M., Fuhrmann, J. C., Rein, D., Wiemer, J. C., Bouillot, J. L., Poitou, C., and Clement, K. (2009) Metabolite profiling identifies candidate markers reflecting the clinical adaptations associated with Roux-en-Y gastric bypass surgery, *PLoS One 4*, e7905.

17. Colucci, R. A. (2011) Bariatric surgery in patients with type 2 diabetes: a viable option, *Postgrad Med 123*, 24-33.

18. Tuomilehto, J., Lindstrom, J., Eriksson, J. G., Valle, T. T., Hamalainen, H., Ilanne-Parikka, P., Keinanen-Kiukaanniemi, S., Laakso, M., Louheranta, A., Rastas, M., Salminen, V., and Uusitupa, M. (2001) Prevention of type 2 diabetes mellitus by changes in lifestyle among subjects with impaired glucose tolerance, *N Engl J Med 344*, 1343-1350.

19. Dean L, M. J. (2004) *The Genetic Landscape of Diabetes*, www.ncbi.hlm.nih.gov/books/NBK1664/.

20. Ridderstrale, M., and Groop, L. (2009) Genetic dissection of type 2 diabetes, *Mol Cell Endocrinol 297*, 10-17.

21. Song, Y., Hsu, Y. H., Niu, T., Manson, J. E., Buring, J. E., and Liu, S. (2009) Common genetic variants of the ion channel transient receptor potential

membrane melastatin 6 and 7 (TRPM6 and TRPM7), magnesium intake, and risk of type 2 diabetes in women, *BMC Med Genet 10*, 4.

22. Dupuis, J., Langenberg, C., Prokopenko, I., and al., E. (2010) New genetic loci implicated in fasting glucose homeostasis and their impact on type 2 diabetes risk, *Nat Genet 42*, 105-116.

23. Otway, D. T., Mantele, S., Bretschneider, S., Wright, J., Trayhurn, P., Skene, D. J., Robertson, M. D., and Johnston, J. D. (2011) Rhythmic Diurnal Gene Expression in Human Adipose Tissue From Individuals Who Are Lean, Overweight, and Have Type 2 Diabetes, *Diabetes*.

24. Cheng, Y. J., Gregg, E. W., Geiss, L. S., Imperatore, G., Williams, D. E., Zhang, X., Albright, A. L., Cowie, C. C., Klein, R., and Saaddine, J. B. (2009) Association of A1C and fasting plasma glucose levels with diabetic retinopathy prevalence in the U.S. population: Implications for diabetes diagnostic thresholds, *Diabetes Care 32*, 2027-2032.

25. Kerr, M. (2009) Experts Recommend that Hemoglobin A1c also be used to Diagnose Diabetes, http://www.labtestsonline.org/news/a1c090901.html, American Diabetes Association.

26. Mostafa, S. A., Davies, M. J., Srinivasan, B. T., Carey, M. E., Webb, D., and Khunti, K. (2010) Should glycated haemoglobin (HbA1c) be used to detect people with type 2 diabetes mellitus and impaired glucose regulation?, *Postgrad Med J 86*, 656-662.

27. Hu, Y., Liu, W., Chen, Y., Zhang, M., Wang, L., Zhou, H., Wu, P., Teng, X., Dong, Y., Zhou, J., Xu, H., Zheng, J., Li, S., Tao, T., and Jia, Y. (2010) Combined use of fasting plasma glucose and glycated hemoglobin A1c in the screening of diabetes and impaired glucose tolerance, *Acta Diabetol 47*, 231-236.

28. Rutten, G. (2010) Screening for type 2 diabetes--where are we now?, *Lancet 375*, 1324-1326.

29. Kuzuya, T., Nakagawa, S., Satoh, J., Kanazawa, Y., Iwamoto, Y., Kobayashi, M., Nanjo, K., Sasaki, A., Seino, Y., Ito, C., Shima, K., Nonaka, K., and Kadowaki, T. (2002) Report of the Committee on the classification and diagnostic criteria of diabetes mellitus, *Diabetes Res Clin Pract 55*, 65-85.

30. Boizel, R., Benhamou, P. Y., Lardy, B., Laporte, F., Foulon, T., and Halimi, S. (2000) Ratio of triglycerides to HDL cholesterol is an indicator of LDL particle

size in patients with type 2 diabetes and normal HDL cholesterol levels, *Diabetes Care 23*, 1679-1685.

31. Gougeon, R., Pencharz, P. B., and Sigal, R. J. (1997) Effect of glycemic control on the kinetics of whole-body protein metabolism in obese subjects with non-insulin-dependent diabetes mellitus during iso- and hypoenergetic feeding, *Am J Clin Nutr 65*, 861-870.

32. Morishita, R., Nakamura, S., Nakamura, Y., Aoki, M., Moriguchi, A., Kida, I., Yo, Y., Matsumoto, K., Nakamura, T., Higaki, J., and Ogihara, T. (1997) Potential role of an endothelium-specific growth factor, hepatocyte growth factor, on endothelial damage in diabetes, *Diabetes 46*, 138-142.

33. Robertson, R. P., Harmon, J., Tran, P. O., and Poitout, V. (2004) Beta-cell glucose toxicity, lipotoxicity, and chronic oxidative stress in type 2 diabetes, *Diabetes 53 Suppl 1*, S119-124.

34. Zhang, Z., Liew, C. W., Handy, D. E., Zhang, Y., Leopold, J. A., Hu, J., Guo, L., Kulkarni, R. N., Loscalzo, J., and Stanton, R. C. (2010) High glucose inhibits glucose-6-phosphate dehydrogenase, leading to increased oxidative stress and beta-cell apoptosis, *FASEB J 24*, 1497-1505.

35. ADA. (2011) Diabetes, www.diabetes.org, American Diabetes Association.

36. Bressler, P., Bailey, S. R., Matsuda, M., and DeFronzo, R. A. (1996) Insulin resistance and coronary artery disease, *Diabetologia 39*, 1345-1350.

37. Becker, K. L. (2001) *Principles and Practices of Endocrinology and Metabolism*, Lippincott Wialliams & Wilkins.

38. Harnett, J. D., Foley, R. N., Kent, G. M., Barre, P. E., Murray, D., and Parfrey, P. S. (1995) Congestive heart failure in dialysis patients: prevalence, incidence, prognosis and risk factors, *Kidney Int 47*, 884-890.

39. Liu, J., Sempos, C., Donahue, R. P., Dorn, J., Trevisan, M., and Grundy, S. M. (2005) Joint distribution of non-HDL and LDL cholesterol and coronary heart disease risk prediction among individuals with and without diabetes, *Diabetes Care 28*, 1916-1921.

40. Byrne, C. D., Maison, P., Halsall, D., Martensz, N., Hales, C. N., and Wareham, N. J. (1999) Cross-sectional but not longitudinal associations between non-esterified fatty acid levels and glucose intolerance and other features of the metabolic syndrome, *Diabet Med 16*, 1007-1015.

41. ADA. (2010) ADA Endorses HbA1c for Diabetes Diagnosis, www.aacc.org/publications/cln/2010/February/Pages/newsbrief0210.aspx, American Diabetes Association.

42. Laffoon, S. (2010) Type 2 Diabetes and Innate Immunity: Connections revealed by multi-dimensional fractionation of blood plasma, In *Ph.D Defense*, pp 1-362, Montana State University, Bozeman.

43. Peters, T., Jr. (1996) *All about Albumin Biochemistry, Genetics, and Medical Applications*, Academic Press.

44. Peters, T., Jr. (1985) Serum albumin, *Adv Protein Chem 37*, 161-245.

45. Varshney, A., Sen, P., Ahmad, E., Rehan, M., Subbarao, N., and Khan, R. H. (2010) Ligand binding strategies of human serum albumin: how can the cargo be utilized?, *Chirality 22*, 77-87.

46. Varshney, A., Rehan, M., Subbarao, N., Rabbani, G., and Khan, R. H. (2011) Elimination of endogenous toxin, creatinine from blood plasma depends on albumin conformation: site specific uremic toxicity & impaired drug binding, *PLoS One 6*, e17230.

47. Cohn, E. J., Hughes, W. L., Jr., and Weare, J. H. (1947) Preparation and properties of serum and plasma proteins; crystallization of serum albumins from ethanol water mixtures, *J Am Chem Soc 69*, 1753-1761.

48. Sugio, S., Kashima, A., Mochizuki, S., Noda, M., and Kobayashi, K. (1999) Crystal structure of human serum albumin at 2.5 A resolution, *Protein Eng 12*, 439-446.

49. Spector, A. A. (1975) Fatty acid binding to plasma albumin, *J Lipid Res 16*, 165-179.

50. Sadler, P. J., and Viles, J. H. (1996) 1H and (113)Cd NMR Investigations of Cd(2+) and Zn(2+) Binding Sites on Serum Albumin: Competition with Ca(2+), Ni(2+), Cu(2+), and Zn(2+), *Inorg Chem 35*, 4490-4496.

51. Beaven, G., Alebis, A., Gratzer, W. . (1972) The interaction of bilirubing with human serum albumin, *Eur. J. Biochem. 33*, 500-510.

52. Fanali, G., Bocedi, A., Ascenzi, P., and Fasano, M. (2007) Modulation of heme and myristate binding to human serum albumin by anti-HIV drugs. An optical and NMR spectroscopic study, *Febs J 274*, 4491-4502.

53. Lopez, M. F., Mikulskis, A., Kuzdzal, S., Golenko, E., Petricoin, E. F., 3rd, Liotta, L. A., Patton, W. F., Whiteley, G. R., Rosenblatt, K., Gurnani, P., Nandi, A., Neill, S., Cullen, S., O'Gorman, M., Sarracino, D., Lynch, C., Johnson, A., McKenzie, W., and Fishman, D. (2007) A novel, high-throughput workflow for discovery and identification of serum carrier protein-bound peptide biomarker candidates in ovarian cancer samples, *Clin Chem 53*, 1067-1074.

54. Gundry, R. L., Fu, Q., Jelinek, C. A., Van Eyk, J. E., and Cotter, R. J. (2007) Investigation of an albumin-enriched fraction of human serum and its albuminome, *Proteomics Clin Appl 1*, 73-88.

55. Lundsgaard-Hansen, P. (1986) Physiology and pathophysiology of colloid osmotic pressure and albumin metabolism, *Curr Stud Hematol Blood Transfus*, 1-17.

56. Dockal, M., Chang, M., Carter, D. C., and Ruker, F. (2000) Five recombinant fragments of human serum albumin-tools for the characterization of the warfarin binding site, *Protein Sci 9*, 1455-1465.

57. Bree, F., Urien, S., Nguyen, P., Riant, P., Albengres, E., and Tillement, J. P. (1990) A re-evaluation of the HSA-piroxicam interaction, *Eur J Drug Metab Pharmacokinet 15*, 303-307.

58. Gulyassy, P. F., and Depner, T. A. (1983) Impaired binding of drugs and endogenous ligands in renal diseases, *Am J Kidney Dis 2*, 578-601.

59. Simard, J. R., Zunszain, P. A., Hamilton, J. A., and Curry, S. (2006) Location of high and low affinity fatty acid binding sites on human serum albumin revealed by NMR drug-competition analysis, *J Mol Biol 361*, 336-351.

60. Meijers, B. K., Bammens, B., Verbeke, K., and Evenepoel, P. (2008) A review of albumin binding in CKD, *Am J Kidney Dis 51*, 839-850.

61. Holt, L. J., Basran, A., Jones, K., Chorlton, J., Jespers, L. S., Brewis, N. D., and Tomlinson, I. M. (2008) Anti-serum albumin domain antibodies for extending the half-lives of short lived drugs, *Protein Eng Des Sel 21*, 283-288.

62. Ruiz-Cabello, F., and Erill, S. (1984) Abnormal serum protein binding of acidic drugs in diabetes mellitus, *Clin Pharmacol Ther 36*, 691-695.

63. Arredondo, G., Suarez, E., Calvo, R., Vazquez, J. A., Garcia-Sanchez, J., and Martinez-Jorda, R. (1999) Serum protein binding of itraconazole and fluconazole in patients with diabetes mellitus, *J Antimicrob Chemother 43*, 305-307.

64. Leal, N., Calvo, R., Agrad, F. Z., Lukas, J. C., de la Fuente, L., and Suarez, E. (2005) Altered dose-to-effect of propofol due to pharmacokinetics in rats with experimental diabetes mellitus, *J Pharm Pharmacol 57*, 317-325.

65. Buttar, D., Colclough, N., Gerhardt, S., MacFaul, P. A., Phillips, S. D., Plowright, A., Whittamore, P., Tam, K., Maskos, K., Steinbacher, S., and Steuber, H. (2010) A combined spectroscopic and crystallographic approach to probing drug-human serum albumin interactions, *Bioorg Med Chem 18*, 7486-7496.

66. Hein, K. L., Kragh-Hansen, U., Morth, J. P., Jeppesen, M. D., Otzen, D., Moller, J. V., and Nissen, P. (2010) Crystallographic analysis reveals a unique lidocaine binding site on human serum albumin, *J Struct Biol 171*, 353-360.

67. Curry, S., Mandelkow, H., Brick, P., and Franks, N. (1998) Crystal structure of human serum albumin complexed with fatty acid reveals an asymmetric distribution of binding sites, *Nat Struct Biol 5*, 827-835.

68. Saifer, A., and Goldman, L. (1961) Free Fatty Acids Bound to Human Serum Albumin, *Journal of Lipid Research 2*, 268-&.

69. Simard, J. R., Zunszain, P. A., Ha, C. E., Yang, J. S., Bhagavan, N. V., Petitpas, I., Curry, S., and Hamilton, J. A. (2005) Locating high-affinity fatty acid-binding sites on albumin by x-ray crystallography and NMR spectroscopy, *Proc Natl Acad Sci U S A 102*, 17958-17963.

70. Saltiel, A. R., and Kahn, C. R. (2001) Insulin signalling and the regulation of glucose and lipid metabolism, *Nature 414*, 799-806.

71. Paolisso, G., and Giugliano, D. (1996) Oxidative stress and insulin action: is there a relationship?, *Diabetologia 39*, 357-363.

72. Togashi, D. M., and Ryder, A. G. (2008) A fluorescence analysis of ANS bound to bovine serum albumin: binding properties revisited by using energy transfer, *J Fluoresc 18*, 519-526.

73. Santos, E. C., and Spector, A. A. (1974) Effects of fatty acids on the interaction of 1-anilino-8-naphthalenesulfonate with human plasma albumin, *Mol Pharmacol 10*, 519-528.

74. Flora, K., Brennan, J. D., Baker, G. A., Doody, M. A., and Bright, F. V. (1998) Unfolding of acrylodan-labeled human serum albumin probed by steady-state and time-resolved fluorescence methods, *Biophys J 75*, 1084-1096.

75. Pepe, I. M. (1971) Electron spin resonance studies of ultraviolet irradiation effects on some proteins, *Biophysik 7*, 115-119.

76. Medline. (2011) Albumin - Serum, www.nlm.nih.gov/medlineplus/ency/article/003480.htm, Medline Plus - National Institute of Health, Bethesda, MD

77. Clarke, C. S., and Bannon, F. J. (2005) Serum albumin in Down Syndrome with and without Alzheimer's Disease, *Ir J Med Sci 174*, 4-8.

78. Garbett, N. C., Miller, J. J., Jenson, A. B., and Chaires, J. B. (2008) Calorimetry outside the box: a new window into the plasma proteome, *Biophys J 94*, 1377-1383.

79. Han, X., Abendschein, D. R., Kelley, J. G., and Gross, R. W. (2000) Diabetes-induced changes in specific lipid molecular species in rat myocardium, *Biochem J 352 Pt 1*, 79-89.

80. Ku, T., Lu, P., Chan, C., Wang, T., Lai, S., Lyu, P., and Hsiao, N. (2009) Predicting melting temperature directly from protein sequences, *Comput Biol Chem 33*, 445-450.

81. Rodkey, F. L. (1965) Direct Spectrophotometric Determination of Albumin in Human Serum, *Clin Chem 11*, 478-487.

82. Dandona, P., Aljada, A., Chaudhuri, A., Mohanty, P., and Garg, R. (2005) Metabolic syndrome: a comprehensive perspective based on interactions between obesity, diabetes, and inflammation, *Circulation 111*, 1448-1454.

83. Ahmad, N., and Qasim, M. A. (1995) Fatty acid binding to bovine serum albumin prevents formation of intermediate during denaturation, *Eur J Biochem 227*, 563-565.

84. Shrake, A., and Ross, P. D. (1990) Ligand-induced biphasic protein denaturation, *J Biol Chem 265*, 5055-5059.

85. Shrake, A., and Ross, P. D. (1988) Biphasic denaturation of human albumin due to ligand redistribution during unfolding, *J Biol Chem 263*, 15392-15399.

86. Zolotarjova, N., Mrozinski, P., Chen, H., and Martosella, J. (2008) Combination of affinity depletion of abundant proteins and reversed-phase fractionation in proteomic analysis of human plasma/serum, *J Chromatogr A 1189*, 332-338.

87. Sidaway, J. E., Davidson, R. G., McTaggart, F., Orton, T. C., Scott, R. C., Smith, G. J., and Brunskill, N. J. (2004) Inhibitors of 3-hydroxy-3-methylglutaryl-CoA reductase reduce receptor-mediated endocytosis in opossum kidney cells, *J Am Soc Nephrol 15*, 2258-2265.

88. Faure, P., Wiernsperger, N., Polge, C., Favier, A., and Halimi, S. (2008) Impairment of the antioxidant properties of serum albumin in patients with diabetes: protective effects of metformin, *Clin Sci (Lond) 114*, 251-256.

89. Strickler, S. J., Berg, Robert A. (1962) Relationship between Absorption Intensity and Fluorescence Lifetime of Molecules, *The Journal of Chemical Physics 17*, 814-822.

90. Yvon, J. (2011) A guide to recording fluorescence quantum yields, www.horiba.com/us/en/scientific/products/fluorescence-spectroscopy/application-notes/quantum-yields/, Jobin Yvon, Edison New Jersey, NJ.

91. Bal, W., Christodoulou, J., Sadler, P. J., and Tucker, A. (1998) Multi-metal binding site of serum albumin, *J Inorg Biochem 70*, 33-39.

92. Mothes, E., and Faller, P. (2007) Evidence that the principal CoII-binding site in human serum albumin is not at the N-terminus: implication on the albumin cobalt binding test for detecting myocardial ischemia, *Biochemistry 46*, 2267-2274.

93. Stewart, A. J., Blindauer, C. A., Berezenko, S., Sleep, D., and Sadler, P. J. (2003) Interdomain zinc site on human albumin, *Proc Natl Acad Sci U S A 100*, 3701-3706.

94. Chausmer, A. B. (1998) Zinc, insulin and diabetes, *J Am Coll Nutr 17*, 109-115.

95. Agilent. (2007) Agilent Technologies Introduces High-Capacity Human-14 Protein Removal System for Proteomic Biomarker Discovery www.agilent.com/about/newsroom/presrel/2007/2004jun-ca07031.html, Agilent.

96. Aguilar, M. V., Saavedra, P., Arrieta, F. J., Mateos, C. J., Gonzalez, M. J., Meseguer, I., and Martinez-Para, M. C. (2007) Plasma mineral content in type-2 diabetic patients and their association with the metabolic syndrome, *Ann Nutr Metab 51*, 402-406.

97. Keowmaneechai, E., and McClements, D. J. (2002) Influence of EDTA and citrate on physicochemical properties of whey protein-stabilized oil-in-water emulsions containing CaCl2, *J Agric Food Chem 50*, 7145-7153.

98. Tammen, H., Hess, R., Rose, H., Wienen, W., and Jost, M. (2008) Peptidomic analysis of blood plasma after in vivo treatment with protease inhibitors - A proof of concept study, *Peptides 29*, 2188-2195.

99. Tammen, H., Hess, R., Schulte, I., Kellmann, M., Appel, A., Budde, P., Zucht, H. D., and Schulz-Knappe, P. (2005) Prerequisites for peptidomic analysis of blood samples: II. Analysis of human plasma after oral glucose challenge -- a proof of concept, *Comb Chem High Throughput Screen 8*, 735-741.

100. Tammen, H. (2008) Specimen collection and handling: standardization of blood sample collection, *Methods Mol Biol 428*, 35-42.

101. Tammen, H., Hess, R., Rose, H., Wienen, W., and Jost, M. (2008) Peptidomic analysis of blood plasma after in vivo treatment with protease inhibitors--a proof of concept study, *Peptides 29*, 2188-2195.

102. Tammen, H., Schulte, I., Hess, R., Menzel, C., Kellmann, M., Mohring, T., and Schulz-Knappe, P. (2005) Peptidomic analysis of human blood specimens: comparison between plasma specimens and serum by differential peptide display, *Proteomics 5*, 3414-3422.

103. Tammen, H., Schulte, I., Hess, R., Menzel, C., Kellmann, M., and Schulz-Knappe, P. (2005) Prerequisites for peptidomic analysis of blood samples: I. Evaluation of blood specimen qualities and determination of technical performance characteristics, *Comb Chem High Throughput Screen 8*, 725-733.

104. Villanueva, J., Philip, J., Entenberg, D., Chaparro, C. A., Tanwar, M. K., Holland, E. C., and Tempst, P. (2004) Serum peptide profiling by magnetic particle-assisted, automated sample processing and MALDI-TOF mass spectrometry, *Anal Chem 76*, 1560-1570.

105. Villanueva, J., Shaffer, D. R., Philip, J., Chaparro, C. A., Erdjument-Bromage, H., Olshen, A. B., Fleisher, M., Lilja, H., Brogi, E., Boyd, J., Sanchez-Carbayo, M., Holland, E. C., Cordon-Cardo, C., Scher, H. I., and Tempst, P. (2006) Differential exoprotease activities confer tumor-specific serum peptidome patterns, *J Clin Invest 116*, 271-284.

106. Lopez, M. F., Mikulskis, A., Kuzdzal, S., Bennett, D. A., Kelly, J., Golenko, E., DiCesare, J., Denoyer, E., Patton, W. F., Ediger, R., Sapp, L., Ziegert, T., Lynch, C., Kramer, S., Whiteley, G. R., Wall, M. R., Mannion, D. P., Della Cioppa, G., Rakitan, J. S., and Wolfe, G. M. (2005) High-resolution serum proteomic profiling of Alzheimer disease samples reveals disease-specific, carrier-protein-bound mass signatures, *Clin Chem 51*, 1946-1954.

107. Aristoteli, L. P., Molloy, M. P., and Baker, M. S. (2007) Evaluation of endogenous plasma peptide extraction methods for mass spectrometric biomarker discovery, *J Proteome Res 6*, 571-581.

108. Geho, D. H., Liotta, L. A., Petricoin, E. F., Zhao, W., and Araujo, R. P. (2006) The amplified peptidome: the new treasure chest of candidate biomarkers, *Curr Opin Chem Biol 10*, 50-55.

109. Budde, P., Schulte, I., Appel, A., Neitz, S., Kellmann, M., Tammen, H., Hess, R., and Rose, H. (2005) Peptidomics biomarker discovery in mouse models of obesity and type 2 diabetes, *Comb Chem High Throughput Screen 8*, 775-781.

110. Falth, M., Svensson, M., Nilsson, A., Skold, K., Fenyo, D., and Andren, P. E. (2008) Validation of endogenous peptide identifications using a database of tandem mass spectra, *J Proteome Res 7*, 3049-3053.

111. Gaspari, M., Ming-Cheng Cheng, M., Terracciano, R., Liu, X., Nijdam, A. J., Vaccari, L., di Fabrizio, E., Petricoin, E. F., Liotta, L. A., Cuda, G., Venuta, S., and Ferrari, M. (2006) Nanoporous surfaces as harvesting agents for mass spectrometric analysis of peptides in human plasma, *J Proteome Res 5*, 1261-1266.

112. Harper, R. G., Workman, S. R., Schuetzner, S., Timperman, A. T., and Sutton, J. N. (2004) Low-molecular-weight human serum proteome using ultrafiltration, isoelectric focusing, and mass spectrometry, *Electrophoresis 25*, 1299-1306.

113. Li, X., Xu, S., Pan, C., Zhou, H., Jiang, X., Zhang, Y., Ye, M., and Zou, H. (2007) Enrichment of peptides from plasma for peptidome analysis using multiwalled carbon nanotubes, *J Sep Sci 30*, 930-943.

114. Liotta, L. A., and Petricoin, E. F. (2006) Serum peptidome for cancer detection: spinning biologic trash into diagnostic gold, *J Clin Invest 116*, 26-30.

115. Lowenthal, M. S., Mehta, A. I., Frogale, K., Bandle, R. W., Araujo, R. P., Hood, B. L., Veenstra, T. D., Conrads, T. P., Goldsmith, P., Fishman, D., Petricoin, E. F., 3rd, and Liotta, L. A. (2005) Analysis of albumin-associated peptides and proteins from ovarian cancer patients, *Clin Chem 51*, 1933-1945.

116. Orvisky, E., Drake, S. K., Martin, B. M., Abdel-Hamid, M., Ressom, H. W., Varghese, R. S., An, Y., Saha, D., Hortin, G. L., Loffredo, C. A., and Goldman, R. (2006) Enrichment of low molecular weight fraction of serum for MS analysis of peptides associated with hepatocellular carcinoma, *Proteomics 6*, 2895-2902.

117. Robbins, R. J., Villanueva, J., and Tempst, P. (2005) Distilling cancer biomarkers from the serum peptidome: high technology reading of tea leaves or an insight to clinical systems biology?, *J Clin Oncol 23*, 4835-4837.

118. Schrader, M., and Selle, H. (2006) The process chain for peptidomic biomarker discovery, *Dis Markers 22*, 27-37.

119. Scully, M. F. (2006) Plasma peptidome: A new approach for assessing thrombotic risk?, *Thromb Haemost 96*, 697.

120. Tian, R., Ye, M., Hu, L., Li, X., and Zou, H. (2007) Selective extraction of peptides in acidic human plasma by porous silica nanoparticles for peptidome analysis with 2-D LC-MS/MS, *J Sep Sci 30*, 2204-2209.

121. Tian, R., Zhang, H., Ye, M., Jiang, X., Hu, L., Li, X., Bao, X., and Zou, H. (2007) Selective extraction of peptides from human plasma by highly ordered mesoporous silica particles for peptidome analysis, *Angew Chem Int Ed Engl 46*, 962-965.

122. Tirumalai, R. S., Chan, K. C., Prieto, D. A., Issaq, H. J., Conrads, T. P., and Veenstra, T. D. (2003) Characterization of the low molecular weight human serum proteome, *Mol Cell Proteomics 2*, 1096-1103.

123. Yewdell, J. W. (2003) Immunology. Hide and seek in the peptidome, *Science 301*, 1334-1335.

124. Zheng, X., Baker, H., and Hancock, W. S. (2006) Analysis of the low molecular weight serum peptidome using ultrafiltration and a hybrid ion trap-Fourier transform mass spectrometer, *J Chromatogr A 1120*, 173-184.

125. Yates, N. A., Deyanova, Ekaterina G., Geissler, Wayne, Wiener, Matthew C., Sachs, Jeffrey R., Wong, Kenny K., Thornberry, Nancy A., Roy, Ranabir Sinha, Settlage, Robert E., Hendrickson, Ronald C. (2007) Indentification of peptidase substrates in human plasma by FTMS based differential mass spectrometry, *International Journal of Mass Spectrometry 259*, 174-183.

126. Pieper, R., Gatlin, C. L., McGrath, A. M., Makusky, A. J., Mondal, M., Seonarain, M., Field, E., Schatz, C. R., Estock, M. A., Ahmed, N., Anderson, N. G., and Steiner, S. (2004) Characterization of the human urinary proteome: a method for high-resolution display of urinary proteins on two-dimensional electrophoresis gels with a yield of nearly 1400 distinct protein spots, *Proteomics 4*, 1159-1174.

127. Granger, J., Siddiqui, J., Copeland, S., and Remick, D. (2005) Albumin depletion of human plasma also removes low abundance proteins including the cytokines, *Proteomics 5*, 4713-4718.

128. Zeng, X.-H., Huang, He-Qing, Chen, Dong-Shi, Jin, Hong-Wei, Huang, Hui-Ying. (2007) Proteomic study of serum using gel chromatography and MALDI-TOF MS reveals diagnostic biomarkers in male patients with liver-cancer, *International Journal of Mass Spectrometry 261*, 108-114.

129. Merrell, K., Southwick, K., Graves, S. W., Esplin, M. S., Lewis, N. E., and Thulin, C. D. (2004) Analysis of low-abundance, low-molecular-weight serum proteins using mass spectrometry, *J Biomol Tech 15*, 238-248.

130. Millipore. (2010) Fast and Easy Protein Prepartion, www.millipore.com/proteinprep, Billerica, MA.

131. Tanaka, Y., Akiyama, H., Kuroda, T., Jung, G., Tanahashi, K., Sugaya, H., Utsumi, J., Kawasaki, H., and Hirano, H. (2006) A novel approach and protocol for discovering extremely low-abundance proteins in serum, *Proteomics 6*, 4845-4855.

132. Staels, B., and Fonseca, V. A. (2009) Bile acids and metabolic regulation: mechanisms and clinical responses to bile acid sequestration, *Diabetes Care 32 Suppl 2*, S237-245.

133. Horn, A., Kreusch, S., Bublitz, R., Hoppe, H., Cumme, G. A., Schulze, M., Moore, T., Ditze, G., and Rhode, H. (2006) Multidimensional proteomics of human serum using parallel chromatography of native constituents and microplate technology, *Proteomics 6*, 559-570.

134. Cazes, J. (2005) *Encyclopedia of Chromatography Second Edition* Vol. 2.

135. The University of Adelaide, A.-D. o. C. (2010) Size Exclusion Chromatography (SEC), www.chemphys.adeladie.edu.au, The University of Adelaid, Australia - Department of Chemistry.

136. Kramer, W., Wess, G., Schubert, G., Bickel, M., Girbig, F., Gutjahr, U., Kowalewski, S., Baringhaus, K. H., Enhsen, A., Glombik, H., and et al. (1992) Liver-specific drug targeting by coupling to bile acids, *J Biol Chem 267*, 18598-18604.

137. Thompson, A., Schafer, J., Kuhn, K., Kienle, S., Schwarz, J., Schmidt, G., Neumann, T., Johnstone, R., Mohammed, A. K., and Hamon, C. (2003) Tandem

mass tags: a novel quantification strategy for comparative analysis of complex protein mixtures by MS/MS, *Anal Chem 75*, 1895-1904.

138. Hsu, J. L., Huang, S. Y., Chow, N. H., and Chen, S. H. (2003) Stable-isotope dimethyl labeling for quantitative proteomics, *Anal Chem 75*, 6843-6852.

139. Brancia, F. L., Oliver, S. G., and Gaskell, S. J. (2000) Improved matrix-assisted laser desorption/ionization mass spectrometric analysis of tryptic hydrolysates of proteins following guanidination of lysine-containing peptides, *Rapid Commun Mass Spectrom 14*, 2070-2073.

140. Brancia, F. L., Openshaw, M. E., and Kumashiro, S. (2002) Investigation of the electrospray response of lysine-, arginine-, and homoarginine-terminal peptide mixtures by liquid chromatography/mass spectrometry, *Rapid Commun Mass Spectrom 16*, 2255-2259.

141. Boersema, P. J., Raijmakers, R., Lemeer, S., Mohammed, S., and Heck, A. J. (2009) Multiplex peptide stable isotope dimethyl labeling for quantitative proteomics, *Nat Protoc 4*, 484-494.

142. Crimmins, D. L. (1995) Peptide Analysis Protocols, *Methods in Molecular Biology 36*, 53-64.

143. Saimaru, H., Yasui, E., Takamura, N., and Imai, K. (2006) Synthesis and evaluation of fluorogenic reagents for simultaneous detection of peptides and proteins by HPLC in two different samples, *Biomed Chromatogr 20*, 576-584.

144. McCarthy, J., Hopwood, F., Oxley, D., Laver, M., Castagna, A., Righetti, P. G., Williams, K., and Herbert, B. (2003) Carbamylation of proteins in 2-D electrophoresis--myth or reality?, *J Proteome Res 2*, 239-242.

145. Scientific, T. (2008) Pierce BCA Protein Assay Kit, www.piercenet.com/files/1296as1298.pdf, Thermo Scientific, Rockford, IL.

146. Zor, T., and Selinger, Z. (1996) Linearization of the Bradford protein assay increases its sensitivity: theoretical and experimental studies, *Anal Biochem 236*, 302-308.

147. Dieckmann-Schuppert, A., and Schnittler, H. J. (1997) A simple assay for quantification of protein in tissue sections, cell cultures, and cell homogenates, and of protein immobilized on solid surfaces, *Cell Tissue Res 288*, 119-126.

148. Adkins, J. N., Varnum, S. M., Auberry, K. J., Moore, R. J., Angell, N. H., Smith, R. D., Springer, D. L., and Pounds, J. G. (2002) Toward a human blood serum proteome: analysis by multidimensional separation coupled with mass spectrometry, *Mol Cell Proteomics 1*, 947-955.

149. Richter, R., Schulz-Knappe, P., Schrader, M., Standker, L., Jurgens, M., Tammen, H., and Forssmann, W. G. (1999) Composition of the peptide fraction in human blood plasma: database of circulating human peptides, *J Chromatogr B Biomed Sci Appl 726*, 25-35.

150. Ostrowski, W. (1968) Michael S. Tswett--inventor of column chromatography. (On the occasion of 65th anniversary of his lecture on the column chromatography technique), *Folia Biol (Krakow) 16*, 429-448.

151. Snyder, L. R. (2000) HPLC: past and present, *Anal Chem 72*, 412A-420A.

152. Touchstone, J. C. (1993) History of Chromatography, *Journal of Liquid Chromatography 16*, 1647-1665.

153. Wu, N., Lippert, J. A., and Lee, M. L. (2001) Practical aspects of ultrahigh pressure capillary liquid chromatography, *J Chromatogr A 911*, 1-12.

154. Shen, Y., Lee, Milton. (1998) General Equation for Peak Capacity in Column Chromatography, *Anal Chem 70*, 3853-3856.

155. Nagele, E., Vollmer, M., Horth, P., and Vad, C. (2004) 2D-LC/MS techniques for the identification of proteins in highly complex mixtures, *Expert Rev Proteomics 1*, 37-46.

156. Devaraj, S., Dasu, M. R., and Jialal, I. (2010) Diabetes is a proinflammatory state: a translational perspective, *Expert Rev Endocrinol Metab 5*, 19-28.

157. Pandey, K. B., Mishra, N., and Rizvi, S. I. (2010) Protein oxidation biomarkers in plasma of type 2 diabetic patients, *Clinical biochemistry 43*, 508-511.

158. Oettl, K., and Stauber, R. E. (2007) Physiological and pathological changes in the redox state of human serum albumin critically influence its binding properties, *Br J Pharmacol 151*, 580-590.

159. ExPASY. (2011) ExPASY Proteomics Server - Peptide Mass, http://expasy.org/tools/peptide-mass.html, Swiss Insitute of Bioinformatics, Lausanne, Switzerland.

160. Boisvert, M. R., Koski, K. G., and Skinner, C. D. (2010) Increased oxidative modifications of amniotic fluid albumin in pregnancies associated with gestational diabetes mellitus, *Analytical Chemistry 82*, 1133-1137.

161. Koyama, H., Sugioka, N., Uno, A., Mori, S., and Nakajima, K. (1997) Effects of glycosylation of hypoglycaemic drug binding to serum albumin, *Biopharm Drug Dispos 18*, 791-801.

162. Takabayashi, K., Imada, T., Saito, Y., and Inada, Y. (1983) Coupling between fatty acid binding and sulfhydryl oxidation in bovine serum albumin, *Eur J Biochem 136*, 291-295.

163. Singh, R., Barden, A., Mori, T., and Beilin, L. (2001) Advanced glycation end-products: a review, *Diabetologia 44*, 129-146.

164. Berlett, B. S., and Stadtman, E. R. (1997) Protein oxidation in aging, disease, and oxidative stress, *J Biol Chem 272*, 20313-20316.

165. Stadtman, E. R. (2006) Protein oxidation and aging, *Free Radic Res 40*, 1250-1258.

166. Science, M. (2011) Mascot http://www.matrixscience.com/, Matrix Science, Boston, MA.

167. Charbonneau, D., Beauregard, M., and Tajmir-Riahi, H. A. (2009) Structural analysis of human serum albumin complexes with cationic lipids, *J Phys Chem B 113*, 1777-1784.

168. Djousse, L., Gaziano, J. M., Buring, J. E., and Lee, I. M. (2011) Dietary omega-3 fatty acids and fish consumption and risk of type 2 diabetes, *Am J Clin Nutr 93*, 143-150.

169. Kaushik, M., Mozaffarian, D., Spiegelman, D., Manson, J. E., Willett, W. C., and Hu, F. B. (2009) Long-chain omega-3 fatty acids, fish intake, and the risk of type 2 diabetes mellitus, *Am J Clin Nutr 90*, 613-620.

170. Griffin, M. E., Marcucci, M. J., Cline, G. W., Bell, K., Barucci, N., Lee, D., Goodyear, L. J., Kraegen, E. W., White, M. F., and Shulman, G. I. (1999) Free fatty acid-induced insulin resistance is associated with activation of protein kinase C theta and alterations in the insulin signaling cascade, *Diabetes 48*, 1270-1274.

171. Storlien, L. H., Jenkins, A. B., Chisholm, D. J., Pascoe, W. S., Khouri, S., and Kraegen, E. W. (1991) Influence of dietary fat composition on development of

insulin resistance in rats. Relationship to muscle triglyceride and omega-3 fatty acids in muscle phospholipid, *Diabetes 40*, 280-289.

172. Kelley, D. E., He, J., Menshikova, E. V., and Ritov, V. B. (2002) Dysfunction of mitochondria in human skeletal muscle in type 2 diabetes, *Diabetes 51*, 2944-2950.

173. van Doorn, M., Vogels, J., Tas, A., van Hoogdalem, E. J., Burggraaf, J., Cohen, A., and van der Greef, J. (2007) Evaluation of metabolite profiles as biomarkers for the pharmacological effects of thiazolidinediones in Type 2 diabetes mellitus patients and healthy volunteers, *Br J Clin Pharmacol 63*, 562-574.

174. Zhao, X., Peter, A., Fritsche, J., Elcnerova, M., Fritsche, A., Haring, H. U., Schleicher, E. D., Xu, G., and Lehmann, R. (2009) Changes of the plasma metabolome during an oral glucose tolerance test: is there more than glucose to look at?, *Am J Physiol Endocrinol Metab 296*, E384-393.

175. Gorska, M., Dobrzyn, A., and Baranowski, M. (2005) Concentrations of sphingosine and sphinganine in plasma of patients with type 2 diabetes, *Med Sci Monit 11*, CR35-38.

176. Layman, D. K., Clifton, P., Gannon, M. C., Krauss, R. M., and Nuttall, F. Q. (2008) Protein in optimal health: heart disease and type 2 diabetes, *Am J Clin Nutr 87*, 1571S-1575S.

177. Sakac, V., and Sakac, M. (2000) [Free oxygen radiacals and kidney diseases--part I], *Med Pregl 53*, 463-474.

178. German, J. B. (1999) Food processing and lipid oxidation, *Adv Exp Med Biol 459*, 23-50.

179. Duncombe, W. G., and Rising, T. J. (1973) Quantitative extraction and determination of nonesterified fatty acids in plasma, *J Lipid Res 14*, 258-261.

180. Wako. (2009) HR Series NEFA-HR (2) ACS - ACOD method, www.wakodiagnostics.com, WAKO, Richmond, VA.

181. Nijtmans, L. G. J., de Jong, J., Sanz, M.A., Coates, P.J., et al. (2000) Prohibitins act as a membrane-bound chaperone for the stabilization of mitochondrial proteins, *The EMBO Journal 19*, 2444-2451.

182. Newgard, C. B., An, J., Bain, J. R., Muehlbauer, M. J., Stevens, R. D., Lien, L. F., Haqq, A. M., Shah, S. H., Arlotto, M., Slentz, C. A., Rochon, J., Gallup, D.,

Ilkayeva, O., Wenner, B. R., Yancy, W. S., Jr., Eisenson, H., Musante, G., Surwit, R. S., Millington, D. S., Butler, M. D., and Svetkey, L. P. (2009) A branched-chain amino acid-related metabolic signature that differentiates obese and lean humans and contributes to insulin resistance, *Cell Metab 9*, 311-326.

183. Pawlosky, R. J., Sprecher, H. W., and Salem, N., Jr. (1992) High sensitivity negative ion GC-MS method for detection of desaturated and chain-elongated products of deuterated linoleic and linolenic acids, *J Lipid Res 33*, 1711-1717.

184. Van Kuuk, F. J. G. M., Thomas, David W., Stephens, Robert J., Dratz, Edward A. (1985) Gas Chromatography-Mass Spectrometry Method for Determination of Phospholipid Peroxides; II. Transesterification to form pentafluorobenzyl esters and detection with picogram sensitivity, *Journal of Free Radicals in Biology & Medicine 1*, 387-393.

185. Folch, J., Lees, M., and Stanley, G. H. S. (1957) A Simple Method for the Isolation and Purification of Total Lipides from Animal Tissues, *Journal of Biological Chemistry 226*, 497-509.

186. Smith, C. A., O'Maille, G., Want, E. J., Qin, C., Trauger, S. A., Brandon, T. R., Custodio, D. E., Abagyan, R., and Siuzdak, G. (2005) METLIN: a metabolite mass spectral database, *Ther Drug Monit 27*, 747-751.

187. Sud, M., Fahy, E., Cotter, D., Brown, A., Dennis, E. A., Glass, C. K., Merrill, A. H., Jr., Murphy, R. C., Raetz, C. R., Russell, D. W., and Subramaniam, S. (2007) LMSD: LIPID MAPS structure database, *Nucleic Acids Res 35*, D527-532.

188. Lucidi, P., Rossetti, P., Porcellati, F., Pampanelli, S., Candeloro, P., Andreoli, A. M., Perriello, G., Bolli, G. B., and Fanelli, C. G. (2010) Mechanisms of insulin resistance after insulin-induced hypoglycemia in humans: the role of lipolysis, *Diabetes 59*, 1349-1357.

189. Gannon, M. C., Nuttall, J. A., and Nuttall, F. Q. (2002) The metabolic response to ingested glycine, *Am J Clin Nutr 76*, 1302-1307.

190. Anuradha, C. V. (2009) Aminoacid support in the prevention of diabetes and diabetic complications, *Curr Protein Pept Sci 10*, 8-17.

191. Gameiro, A., Reimann, F., Habib, A. M., O'Malley, D., Williams, L., Simpson, A. K., and Gribble, F. M. (2005) The neurotransmitters glycine and GABA stimulate glucagon-like peptide-1 release from the GLUTag cell line, *J Physiol 569*, 761-772.

192. Bain, J. R., Stevens, R. D., Wenner, B. R., Ilkayeva, O., Muoio, D. M., and Newgard, C. B. (2009) Metabolomics applied to diabetes research: moving from information to knowledge, *Diabetes 58*, 2429-2443.

193. Menge, B. A., Schrader, H., Ritter, P. R., Ellrichmann, M., Uhl, W., Schmidt, W. E., and Meier, J. J. (2010) Selective amino acid deficiency in patients with impaired glucose tolerance and type 2 diabetes, *Regul Pept 160*, 75-80.

194. Elliott, R. B., Reddy, S. N., Bibby, N. J., and Kida, K. (1988) Dietary prevention of diabetes in the non-obese diabetic mouse, *Diabetologia 31*, 62-64.

195. Munoz-Carlin Mde, L., Rodriguez-Moctezuma, J. R., Gomez Latorre, J. G., Montes-Castillo, M. L., and Juarez-Adauta, S. (2011) [Effects of glycine on auditory evoked potentials among diabetic patients with auditory pathway neuropathy], *Rev Med Chil 138*, 1246-1252.

196. McCarty, M. F., Barroso-Aranda, J., and Contreras, F. (2009) The hyperpolarizing impact of glycine on endothelial cells may be anti-atherogenic, *Med Hypotheses 73*, 263-264.

197. Iavarone, A. T., Udekwu, O. A., and Williams, E. R. (2004) Buffer loading for counteracting metal salt-induced signal suppression in electrospray ionization, *Anal Chem 76*, 3944-3950.

198. Nijjar, M. S., Khangura, B. S., and Juravsky, L. I. (1984) The effect of maternal diabetes on the synthesis and secretion of phosphatidylcholine in fetal and maternal rat lungs in vitro, *Diabetologia 27*, 219-224.

199. Raubenheimer, P. J., Nyirenda, M. J., and Walker, B. R. (2006) A choline-deficient diet exacerbates fatty liver but attenuates insulin resistance and glucose intolerance in mice fed a high-fat diet, *Diabetes 55*, 2015-2020.

200. Suhre, K., Meisinger, C., Doring, A., Altmaier, E., Belcredi, P., Gieger, C., Chang, D., Milburn, M. V., Gall, W. E., Weinberger, K. M., Mewes, H. W., Hrabe de Angelis, M., Wichmann, H. E., Kronenberg, F., Adamski, J., and Illig, T. Metabolic footprint of diabetes: a multiplatform metabolomics study in an epidemiological setting, *PLoS One 5*, e13953.

201. Scragg, R. (2008) Vitamin D and type 2 diabetes: are we ready for a prevention trial?, *Diabetes 57*, 2565-2566.

202. Suhre, K., Meisinger, C., Doring, A., Altmaier, E., Belcredi, P., Gieger, C., Chang, D., Milburn, M. V., Gall, W. E., Weinberger, K. M., Mewes, H. W.,

Hrabe de Angelis, M., Wichmann, H. E., Kronenberg, F., Adamski, J., and Illig, T. (2010) Metabolic footprint of diabetes: a multiplatform metabolomics study in an epidemiological setting, *PLoS One 5*, e13953.

203. Layman, D. K., and Walker, D. A. (2006) Potential importance of leucine in treatment of obesity and the metabolic syndrome, *J Nutr 136*, 319S-323S.

204. Sluijs, I., Beulens, J. W., van der, A. D., Spijkerman, A. M., Grobbee, D. E., and van der Schouw, Y. T. (2010) Dietary intake of total, animal, and vegetable protein and risk of type 2 diabetes in the European Prospective Investigation into Cancer and Nutrition (EPIC)-NL study, *Diabetes Care 33*, 43-48.

205. Taubes, G. (2007) *Good Calories, Bad Calories*, Alfred A. Knopf, New York.

206. Hipkiss, A. R. (2005) Glycation, ageing and carnosine: are carnivorous diets beneficial?, *Mech Ageing Dev 126*, 1034-1039.

207. Lankinen, M., Schwab, U., Erkkila, A., Seppanen-Laakso, T., Hannila, M. L., Mussalo, H., Lehto, S., Uusitupa, M., Gylling, H., and Oresic, M. (2009) Fatty fish intake decreases lipids related to inflammation and insulin signaling--a lipidomics approach, *PLoS One 4*, e5258.

208. Graessler, J., Schwudke, D., Schwarz, P. E., Herzog, R., Shevchenko, A., and Bornstein, S. R. (2009) Top-down lipidomics reveals ether lipid deficiency in blood plasma of hypertensive patients, *PLoS One 4*, e6261.

209. Zhao, X., Fritsche, J., Wang, J., Chen, J., Rittig, K., Schmitt-Kopplin, P., Fritsche, A., Haring, H. U., Schleicher, E. D., Xu, G., and Lehmann, R. (2010) Metabonomic fingerprints of fasting plasma and spot urine reveal human pre-diabetic metabolic traits, *Metabolomics 6*, 362-374.

210. Lucio, M., Fekete, A., Weigert, C., Wagele, B., Zhao, X., Chen, J., Fritsche, A., Haring, H. U., Schleicher, E. D., Xu, G., Schmitt-Kopplin, P., and Lehmann, R. (2010) Insulin sensitivity is reflected by characteristic metabolic fingerprints--a Fourier transform mass spectrometric non-targeted metabolomics approach, *PLoS One 5*, e13317.

211. Christie, W. W. (2010) Phosphatidylcholine and related lipids, Structure, Occurence, Biochemistry, and Analysis, In *Lipidlibrary.AOCS*, http://lipidlibrary.aocs.org/Lipids/pc/index.htm, Dundee, Scotland.

212. Kent, C. (2005) Regulatory enzymes of phosphatidylcholine biosynthesis: a personal perspective, *Biochim Biophys Acta 1733*, 53-66.

213. Vance, D. E., Li, Z., and Jacobs, R. L. (2007) Hepatic phosphatidylethanolamine N-methyltransferase, unexpected roles in animal biochemistry and physiology, *J Biol Chem 282*, 33237-33241.

214. Garg, A., and Grundy, S. M. (1994) Cholestyramine therapy for dyslipidemia in non-insulin-dependent diabetes mellitus. A short-term, double-blind, crossover trial, *Ann Intern Med 121*, 416-422.

215. Toft-Nielsen, M. B., Madsbad, S., and Holst, J. J. (2001) Determinants of the effectiveness of glucagon-like peptide-1 in type 2 diabetes, *J Clin Endocrinol Metab 86*, 3853-3860.

216. Greiner, T., and Backhed, F. (2011) Effects of the gut microbiota on obesity and glucose homeostasis, *Trends in endocrinology and metabolism: TEM*.

217. Nandagopal, R., Brown, R. J., and Rother, K. I. (2010) Resolution of type 2 diabetes following bariatric surgery: implications for adults and adolescents, *Diabetes Technol Ther 12*, 671-677.

218. Sekirov, I., Russell, S. L., Antunes, L. C., and Finlay, B. B. (2010) Gut microbiota in health and disease, *Physiological reviews 90*, 859-904.

219. Meier, J. J., Weyhe, D., Michaely, M., Senkal, M., Zumtobel, V., Nauck, M. A., Holst, J. J., Schmidt, W. E., and Gallwitz, B. (2004) Intravenous glucagon-like peptide 1 normalizes blood glucose after major surgery in patients with type 2 diabetes, *Crit Care Med 32*, 848-851.

220. NIH. (2011) Dietary Supplement Fact Sheet Vitamin D, http://ods.od.nih.gov/factsheets/vitamind/, National Institute of Health Office of Dietary Supplements, Bethesda, MD.

221. Pittas, A. G., Lau, J., Hu, F. B., and Dawson-Hughes, B. (2007) The role of vitamin D and calcium in type 2 diabetes. A systematic review and meta-analysis, *J Clin Endocrinol Metab 92*, 2017-2029.

222. Rajakumar, K. (2003) Vitamin D, cod-liver oil, sunlight, and rickets: a historical perspective, *Pediatrics 112*, e132-135.

223. Joshi, D., Center, Jacqueline R., Eisman, John A. (2010) Vitamin D deficiency in adults, *Autralian Prescriber 33*, 103-106.

224. Melamed, M. L., Muntner, P., Michos, E. D., Uribarri, J., Weber, C., Sharma, J., and Raggi, P. (2008) Serum 25-hydroxyvitamin D levels and the prevalence of

peripheral arterial disease: results from NHANES 2001 to 2004, *Arterioscler Thromb Vasc Biol 28*, 1179-1185.

225. Holick, M. F. (2004) Sunlight and vitamin D for bone health and prevention of autoimmune diseases, cancers, and cardiovascular disease, *Am J Clin Nutr 80*, 1678S-1688S.

226. Mathieu, C. (2010) Vitamin D and diabetes: the devil is in the D-tails, *Diabetologia 53*, 1545-1548.

227. Song, Y., Manson, JoAnn E. (2010) Vitamin D, Insulin Resistance, and Type 2 Diabetes, *Curr Cardio Risk Rep 4*, 40-47.

228. Harris, S. S. (2011) Does vitamin D deficiency contribute to increased rates of cardiovascular disease and type 2 diabetes in African Americans?, *The American journal of clinical nutrition*.

229. Goldfine, A. B., Fonseca, V., and Shoelson, S. E. (2011) Therapeutic approaches to target inflammation in type 2 diabetes, *Clinical chemistry 57*, 162-167.

230. Patel, P., Poretsky, L., and Liao, E. (2010) Lack of effect of subtherapeutic vitamin D treatment on glycemic and lipid parameters in Type 2 diabetes: A pilot prospective randomized trial, *J Diabetes 2*, 36-40.

231. Grundy, S. M., Benjamin, I. J., Burke, G. L., Chait, A., Eckel, R. H., Howard, B. V., Mitch, W., Smith, S. C., Jr., and Sowers, J. R. (1999) Diabetes and cardiovascular disease: a statement for healthcare professionals from the American Heart Association, *Circulation 100*, 1134-1146.